The role of mTORC1 in mesenchymal stem cell fate determination, osteoblast differentiation and skeletal development

Mary Patricia Matthews

Myeloma Research Laboratory
Adelaide Medical School
Faculty of Health and Medical Sciences
University of Adelaide, Adelaide, Australia
&
Cancer Theme
South Australian Health and Medical Research Institute
Adelaide, Australia

A thesis submitted to the University of Adelaide
for the degree of Doctor of Philosophy
October 2017

Table of Contents

List of Figures

List of Tables

Abstract

As we age, skeletal integrity becomes compromised due to a decrease in bone mineral density. Bone formation is mediated by osteoblast (OB) cells which originate from mesenchymal stem cells (MSC). MSCs, a rare stem cell population within the bone marrow, possess self-renewal and multi-lineage differentiation potential. In aging or diseased states, such as osteoporosis, there is a reduction in osteoblastic differentiation potential of MSCs in favour of differentiation toward fat storing adipocytes (AdC). Several signalling pathways have been shown to regulate osteogenic commitment of MSCs as well as the subsequent processes of osteoblast differentiation and skeletal formation. The mammalian target of rapamycin complex 1 (mTORC1) has been implicated as a master regulator of cell metabolism that integrates signals which control MSC commitment and OB function. However, the direct role of this complex in these functions remains to be determined. To definitively address the role of mTORC1 in MSC fate determination, OB differentiation and bone accrual, this project utilised the Cre-*loxP* system of targeted transgenesis, which enabled the tissue-specific and temporal inactivation of *Rptor*, the gene encoding for the mTORC1 complex-specific protein raptor.

In this study *Rptor*-deficient MSCs cultured under osteogenic and adipogenic-inductive conditions displayed a reduced capacity to form lipid-laden AdCs and an increased capacity to form a mineralised matrix. Consistent with the increased osteogenic differentiation, deletion of *Rptor* in MSC resulted in an up-regulation in the expression of the osteogenic growth factor BMP2, a known inducer of RUNX2 expression, OB maturation and mineral formation.

To examine the role of raptor in skeletal development, *Rptor* was deleted in pre-osteoblastic cells marked by their expression of the osterix (*Osx*) gene, by crossing $Rptor^{fl/fl}$ mice with Osx-cre transgenic mice. Deletion of *Rptor* lead to a reduction in limb length at birth and post-natally and was associated with smaller epiphyseal growth plates. Deletion of *Rptor* caused a marked reduction in pre- and post-natal bone acquisition in both

intramembranous and endochondral ossification leading to skeletal fragility. The decrease in bone acquisition was not due to a reduction in OB numbers but a reduction in OB function. *In vitro*, primary OBs from knockout animals failed to respond to extracellular factors that promote bone formation including insulin and BMP2 and assessment of bone development markers in *Rptor* knockout OBs revealed a transcriptional profile consistent with an immature OB phenotype suggesting that OB differentiation was hindered early in osteogenic development. These findings demonstrate that mTORC1 plays an important role in skeletal development by controlling OB differentiation and hence function.

Taken together, these studies show that mTORC1 plays an important role in MSC fate determination and bone accrual. Notably, deletion of raptor in pre-osteoblasts blocked osteoblast differentiation causing defective intramembranous and endochondral ossification resulting in a low bone mass phenotype and skeletal fragility.

Declaration

I certify that this work contains no material which has been accepted for the award of any other degree or diploma in my name, in any university or other tertiary institution and, to the best of my knowledge and belief, contains no material previously published or written by another person, except where due reference has been made in the text. In addition, I certify that no part of this work will, in the future, be used in a submission in my name, for any other degree or diploma in any university or other tertiary institution without the prior approval of the University of Adelaide and where applicable, any partner institution responsible for the joint-award of this degree. I give consent to this copy of my thesis when deposited in the University Library, being made available for loan and photocopying, subject to the provisions of the Copyright Act 1968. I acknowledge that copyright of published works contained within this thesis resides with the copyright holder(s) of those works. I also give permission for the digital version of my thesis to be made available on the web, via the University's digital research repository, the Library Search and also through web search engines, unless permission has been granted by the University to restrict access for a period of time.

Signed

Mary Patricia Matthews

Acknowledgements

First I would like to thank my supervisors. Professor Andrew Zannettino, Dr Stephen Fitter, Dr Sally Martin and Professor Stan Gronthos. This has been both an amazing and difficult experience for me and I cannot express in words how much gratitude and respect I have for you all. You have been alongside me through blood, sweat and tears and have stood next to me and fought with me through this long journey. I am so proud of what we have achieved together, there is no doubt that this final product is reflective of the hours/years of effort you have invested in me. Thank you Andrew for your continued support during this project and for the incredible experience of having a brilliant scientist as a mentor. I have learnt so much from you and I believe (and hope) I am a better person due to this journey. Thank you so much, your success and drive is truly inspirational. To Steve and Sal, I am so honoured to have spent so much time with you both. Thank you Stephen for the daily support in the lab, with the thesis, for guiding me with your knowledge and being a rad dude. Sally, I have learnt so much from you being able to ask stupid questions thanks for being incredibly understanding, caring and fun to work with. Your effort in teaching me in the lab and bringing so much enjoyment to the icky or mundane experiments will stay with me forever. The work you have put into this thesis is beyond words. Steve and Sal, this is for you. Stan, thanks for always cheering for me, for your support and for having a laugh. To all four of you, my admiration of the intelligence, dedication and endurance you have will be my inspiration with everything I strive for in the future. My love and respect for you all is eternal.

So much support from this project has come from my colleagues at the Cancer Theme Laboratories for being teachers, friends, colleagues and immense amounts of support. Vicki Wilczek for helping out in so many ways, particularly for the thousands of genotyping PCRs. Sharon Paton for keeping the lab running. Dr Kate Vandyke, thank you for being an amazing friend and for inspiring me constantly. Dr Sarah Hemming for supporting me through the laughs and the tears. Thank you to all members of the lab over the years who have been there through this journey; Duncan Hewitt, Lachlan Cooper, Kim Hynes, Thao Nugyen, Danijela Menicannin, Agnes Arthur, Jim Cakouros, Peter Diamond, Sharon Williams, Krzysztof Mrozik, Ankit Dutta, Chee Man Cheong, Romana Panagopoulos, Bill Panagopolous, Jacqueline Noll, Melissa Masters and Maya Tong.

Thank you to the following people for their help developing protocols in the various experiments for this thesis; Bec and Kate at the Detmold Facility for all their time and effort with FACS. Ruth and Agatha at Adelaide Microscopy. Natalie Sims at St Vincent's Institute. John Codrington in the School of Engineering. All staff Veterinary Services, IMVS, especially Kelly, Chris and Nichola for their work with the huge mouse colonies we produced.

To my team; Dr Joe Latham, Dr Lachlan Cooper and Claire Chivell thank you for listening and supporting me at my worst. To Joe for being on the other end of the phone listening to all my stressed out ramblings and the well needed messages of love and support. To Locky for dinners, hugs, hikes, chats and the constant source of insight and perspective. To CC, my oldest friend, thank you for sticking by me, making my life richer as we grow older and for including me in the family with Y-Diddy and Lil-S.

An extra special mention must go to the amazing David Waldie for his artistic input into this project as well as being one of the best mates there is.

Thanks to the Andos. My beautiful sister Jane, you are an amazing woman and I love you very much. My nephews Max and Will, you are a constant source of joy and love and have helped me more than you will ever know. To my brother in law Joe for all the chats and advice over the years and always welcoming me in your home.

To my parents and two of my best friends, Shelagh and Neil. Everything I have gone through in this journey, you have been there every step of the way. There is no doubt that I would not have reached this point without you. Thank you for inspiring and supporting me to do my best. For picking me up when I am down. For housing and feeding me. For allowing me to grow as an adult while providing me with so much support. We did it. I love you.

Publications

Scientific Manuscripts

Fitter, S., **Matthews, M. P.**, Martin, S. K., Xie, J., Ooi, S. S., Walkley, C. R., Codrington, J. D., Ruegg, M. A., Hall, M. N., Proud, C. G., Gronthos, S., Zannettino, A. C. (2017). mTORC1 Plays an Important Role in Skeletal Development by Controlling Preosteoblast Differentiation. *Molecular and Cellular Biology*, 37(7)

Martin, S. K., Fitter, S., Dutta, A. K., **Matthews, M. P.**, Walkley, C. R., Hall, M. N., Ruegg, M. A., Gronthos, S., Zannettino, A. C. (2015). Brief report: the differential roles of mTORC1 and mTORC2 in mesenchymal stem cell differentiation. *Stem Cells*, 33(4):1359-1365

Conference Proceedings

Matthews, M. P., Zannettino, A. C., Fitter, S., Martin, S. K. The effect of mTORC1 on postnatal skeletal development. *European Calcified Tissue Society Congress 2013*, Lisbon, Portugal, May 2013.

Matthews, M. P., Zannettino, A. C., Fitter, S., Martin, S. K. The effect of mTORC1 on postnatal skeletal development. *Australian Bone Mineral Society Meeting*, Adelaide, Australia 2012.

Abbreviations

α-MEM	α-modified Eaglees medium
4E-BP1	eukaryotic initiation factor binding protein1
7-AAD	7-aminoactinomycin D
ATF4	Activating Transcription Factor 4
Alpl	alkaline phosphatase
AMPK	adenosine monophosphate-activated protein kinase
ANCOVA	analysis of covariance
ANOVA	analysis of variance
ATP	adenosine triphosphate
BFR	bone formation rate
BM	bone marrow
BMC	bone marrow stromal cell
BMD	bone mineral density
BMP	bone morphogenetic protein
B.Pm	bone perimeter
BrdU	bromodeoxturidine
BS	bone surface
BSA	bovine serum albumin
BV	bone volume
C/EBP	CCAAT/enhancer binding protein
CFU-F	colony forming units - fibroblast
Col1a1	Type I collagen
Col2a1	Type II collagen
CsA	cyclosporine A

Ct.Th	cortical thickness
CTX-1	C-terminal collagen crosslinks
DTT	Dithiothreitol
E	embryonic day
ECM	extracellular matrix
EDTA	ethylenediaminetetraacetic acid
eIF	eukaryotic initiation factor
ELISA	enzyme-linked immunosorbent assay
ERK	extracellular signal-regulated kinase
ES	embryonic stem cells
FCS	foetal calf serum
FACS	fluorescence activated cell sorting
FGF	fibroblast growth factor
FKBP	FK506-binding protein
Fl	floxed
Floxed	flanked by lox-P
Flp	Flippase
FRB	FKBP12-rapamycing binding
FRT	Flp recombination target
FOXO	forkhead box class O
GAG	glycosaminoglycan
GDP	guanosine diphosphate
GFP	green fluorescent protein
GP	growth plate
Grb	growth factor receptor-bound protein
GSK	Glycogen synthase kinase

GTP	Guanosine triphosphate
HBSS	Hanks buffered saline solution
HCl	hydrochloric acid
HEPES	N-2-hydroxyethylpiperazine-N'-2-ethanesulfonic acid
HZ	hypertrophic zone
Ibsp	integrin-binding saloprotein
Ig	immunoglobulin
IGF	insulin-like growth factor
IGF-R	insulin like growth factor receptor
Ihh	Indian hedgehog
Inhba	inhibinβ A chain
Inhbe	inhibinβ E chain
IRS	insulin receptor substrate
KLF	Krüppel-like factors
KO	knockout
LKB	liver kinase B
LRP	low density lipoprotein receptor-related protein
MAPK	mitogen-activated protein kinase
MAR	mineral apposition rate
μ-CT	micro-computed tomography
mRNA	messenger ribonucleic acid
MSC	mesenchymal stem cell
mTOR	mammalian target of rapamycin
mTORC1	mammalian target of rapamycin complex 1
mTROC2	mammalian target of rapamycin complex 2

NBF	neutral buffered formalin
N.Ob	number of osteoblasts
N.Oc	number of osteoclasts
Nog	Noggin
OB	osteoblast
Ob.S	osteoblast surface
OC	osteoclast
OCN	osteocalcin
Oc.S	osteoclast surface
OPG	osteoprotegerin
OPN	osteopontin
Osx	Osterix
P1NP	pro-collagen type I amino-terminal propeptide
PBS	phosphate buffered saline
PDGF	platelet-derived growth factor
PDGFR	platelet-derived growth factor receptor
PDK1	phosphoinositide dependent protein kinase-1
PEG	polyethylene glycol
PI3K	phosphoinositide-3-kinase
PPARγ	peroxisome proliferator-activated receptor γ
Pten	
PTH	parathyroid hormone
PTHrP	parathyroid hormone-related protein
PVDF	polyvinylidene difluoride
PZ	proliferative zone

Rag	RagA family of small GTPases
RANK	receptor activator of nuclear factor-□B
RANKL	receptor activator of nuclear factor-□B ligand
Raptor	Regulartory-associated protein of TOR
Rheb	ras homolog enriched in brain
REDD	regulation of DNA damage response 1
Rictor	Rapamycin insensitive component of TOR
ROI	region of interest
Runx2	runt-related transcription factor 2
RZ	resting zone
S6K	p70-S6 kinase
SD	standard deviation
SDS	sodium dodecyl sulphate
SDS-PAGE	sodium dodecyl sulphate polyacrylamide gel electrophoresis
SEM	standard error of the mean
SMAD	mothers against decapentaplegic homologues
SMI	structure model index
Sox	sex determining region Y box
Sparc	osteonectin
Spp1	*osteopontin*
TAM	tamoxifen
Tb.N	trabecular number
Tb.Pf	trabecular pattern factor
TBS	Tris-buffered saline
Tb.Sp	trabecular spacing

TBS-Tween	Tris-buffered saline with 1% Tween 20
Tb.Th	trabecular thickness
TEMED	N,N,N,N-tetramethylethylenediamine
TGF-β	transforming growth factor-β
TOR	target of rapamycin
TRAP	tartrate-resistant acid phosphatase 5
TSC	tuberous sclerosis complex
TV	total volume
ULK1	Unc-51-like kinase 1
UV	ultraviolet
Wnt	wingless-type integration
WST1	4-[3-(4-iodophenyl)-2-(4-nitrophenyl)-2H-5-tetrazolio]-1,3-benzene disulphonate
Wt	wildtype
YFP	yellow fluorescent protein

Chapter 1 - Introduction

1.1 Overview

Skeletal diseases associated with excessive bone loss and skeletal fragility, such as osteoporosis and osteopenia, are currently estimated to affect 66% of Australians over the age of 50 years [1]. In 2012, osteoporosis, osteopenia and bone fractures in older Australians cost the Australian Health System an estimated $2.75 billion per annum, with this figure projected to rise to $3.84 billion per annum by 2022[1]. Alarmingly, studies have shown that in recent years, little progress has been made in preventing and managing osteoporosis in Australia. With an increasingly aging population, the prevalence of this disease is expected to increase exponentially in coming decades, highlighting the necessity for research into new therapeutics.

Osteoporosis is associated with a decrease in bone mineral density and an increase in intramedullary adiposity [2]. Adipocytes (fat cells) and osteoblasts (bone cells) are derived from a common mesenchymal stem cell (MSC) progenitor, and the differentiation toward either lineage is a mutually exclusive and transcriptionally controlled process governed by transcriptional cues. It has been hypothesised that the shift in the osteoblast (OB) to adipocyte (AdC) ratio observed in osteoporosis arises from increased adipogenic differentiation at the expense of osteoblastic differentiation in osteoporotic individuals [3, 4].

While the mechanisms underlying these changes in MSC behaviour remain to be determined, it is possible that as we age, key signalling pathways responsible for determining MSC fate become aberrantly regulated in this cell population. To date, several signalling pathways including Wnt/β-catenin [5, 6], BMP/SMAD [7, 8], Indian hedgehog (IHH) [9-11], MAPK [12, 13] and insulin/IGF1 [14, 15] have been implicated to play a role in MSC fate determination. Furthermore, recent studies have also implicated mammalian target of rapamycin (mTOR) as being important in MSC fate determination, with inhibition of mTOR promoting OB differentiation [13, 16-18] and suppressing AdC differentiation [19-23]. However, contradictory

studies have shown that inhibition of mTOR inhibits OB differentiation [24-29], and therefore the precise role of mTOR in MSC lineage determination and skeletal development remains unclear.

The following introduction presents a brief overview of the literature regarding (i) the process of skeletal development and bone accrual, (ii) MSC commitment and differentiation, (iii) the role of mTORC1 in MSC commitment and (iv) the role of mTORC1 in skeletal development and bone accrual.

1.2 Bone structure and composition

Bone is the main support structure of vertebrate animals and serves several important functions. Structurally, the skeleton serves as a protective cage for vital organs such as the brain, lungs and heart, provides mechanical support to soft tissues and aids movement by acting as a lever in muscle action. Bones also house and protect the bone marrow, responsible for the production of red and white blood cells and serve as a reservoir for calcium and phosphate for the maintenance of mineral homeostasis [30-33].

Bones consist of both organic and inorganic elements. The inorganic mineral component, composed mostly of calcium and phosphate in the form of hydroxyapatite [$Ca_{10}(PO_4)_6(OH)_2$], provides stiffness and structure and serves as a metabolic reserve for mineral homeostasis. The organic component is formed of collagen, proteoglycans, matrix proteins, cytokines, growth factors and bone cells, which collectively maintain skeletal integrity and provide tensile strength and elasticity [31, 34]. Structurally, there are two types of bone tissue: cortical bone and trabecular bone. These tissues are biologically identical, however as described in detail below, the different arrangements of their respective microstructures mean that they perform vastly different functions.

1.2.2 Cortical bone

Most bones consist of a dense outer layer known as cortical bone. Also known as compact bone, cortical bone is made up of densely-packed mineral covered by a vascular layer of connective tissue containing progenitor cells capable of maturing into bone forming cells. The outer bone surface connective tissue layer is termed the periosteum and the inner surface layer adjacent to the medullary cavity is the endosteum. Cortical bone tissue provides strength and hardness to the bone and contributes approximately 80% of the weight of a human skeleton. Structurally cortical bone facilitates many of the skeleton's main functions: to support the body, protect organs, provide levers for movement and store and release chemicals. Canals in the compact mineral allow for nerves, blood vessels and lymph vessels to interact with the marrow cavity and periosteum [31] (Figure 1.1).

1.2.3 Trabecular bone

Trabecular or cancellous bone accounts for approximately 20% of the human skeleton and provides structural support and flexibility to the skeleton without the weight of cortical bone. It exists in a three dimensional, lattice-like formation (Figure 1.1), which gives it a much higher surface area to mass ratio and softer, weaker and more flexible characteristics than the dense cortical bone. Trabecular bone makes up much of the enlarged ends (epiphyses) of the long bones, and is a major component of the ribs, skull, shoulder blades and various other short, flat bones that comprise the skeleton. Depending on the need for strength or flexibility, different bones contain varying proportions of space relative to bone within their trabecular region. The open structure of trabecular bone also enables it to dampen sudden stresses, and its greater surface area facilitates metabolic activity (e.g. exchange of calcium and phosphate for mineral homeostasis). As it is more highly involved in the elasticity of the bone structure, trabecular bone constantly requires repair and maintenance.

Figure 1.1 - Trabecular and cortical bone: Cross sectional image of bone illustrating the cortical and trabecular bone structure. Adapted from Junqueira's Basic Hisology: Text and Atlas, by A.L. Mescher, 12th edition, Copyright© by "The McGraw-Hill Companies, Inc".

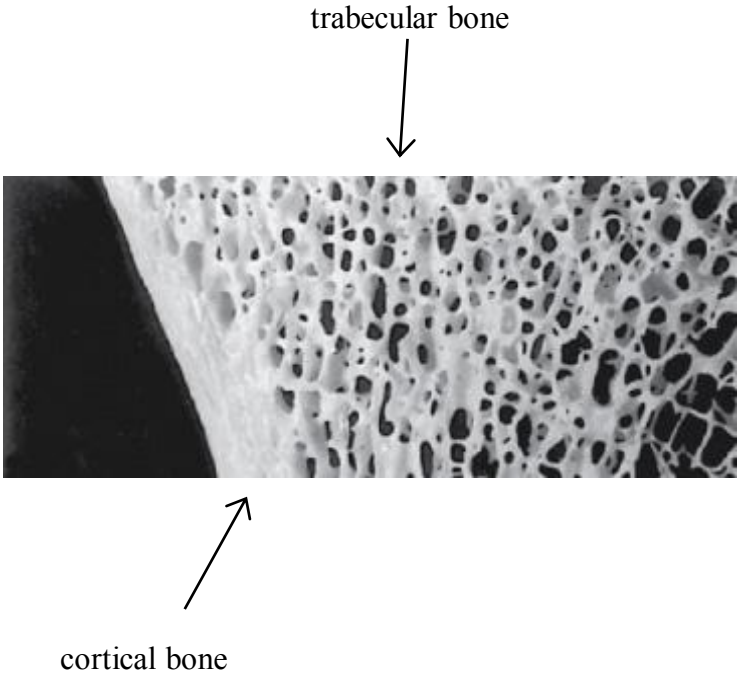
trabecular bone
cortical bone

1.3 Bone development

Bone development occurs via two distinct processes termed intramembranous ossification and endochondral ossification. Intramembranous ossification is responsible for the formation of most of the craniofacial skeleton and flat bones, whereas endochondral ossification is responsible for the formation of the long bones, ribs and vertebrae of the appendicular and axial skeleton (reviewed by [35]). In both processes, osteoblasts (OBs), the bone forming cells of the skeleton, play an essential role.

1.3.1 Intramembranous ossification

During embryonic development, intramembranous ossification begins with proliferation of embryological mesenchymal stem cells (MSCs) that condense to form a sheet of connective tissue termed the mesenchyme. These MSCs then differentiate into bone-forming OBs which secrete osteoid, an extracellular matrix composed primarily of type-I collagen fibrils which provide the initial scaffold for mineralised bone formation. Following osteoid synthesis, OBs deposit hydroxyapatite crystals forming woven bone matrices in small mineral masses of bone called spicules. OBs continue the synthesis of osteoid and mineral lengthening, connecting adjacent spicules to form the lattice-like network. Some OBs become embedded within the matrix and undergo terminal differentiation to become osteocytes, creating a signalling network within the bone and to the bone surface. New bone is invaded by blood vessels enabling the formation of the haematopoietic bone marrow. The periosteum is then formed around the trabeculae which consist structurally of an inner layer of bone lining OB precursors held together by an outer layer of fibroblasts. Osteogenic precursors from the periosteum mature into OBs leading to the further deposition of osteoid and mineral, creating layer upon layer of ossified bone. This mineral layering occurs until an optimal density is achieved, forming the cortical bone in a process known as appositional bone formation (Figure 1.2) [36].

Figure 1.2 - Intramembranous ossification: A) Ossification centres appear within a sheet of dense fibrous connective tissue when clusters of mesenchymal stem cells begin differentiating into osteoblasts and start secreting osteoid. B) Osteoblasts mature and synthesise calcified bone matrix to replace the fibrous membrane in small masses called spicules. During the ossification process, osteoblastic cells trapped within the matrix form osteocytes. C) Spicules expand until they fuse in a lattice-like structure, known as the trabeculae, around blood vessels. The layer of mesenchyme condenses on the external surface leading to the formation of the periosteum. D) As the structure matures, trabeculae near the periosteum thicken forming an outer later of compact bone with spongy bone in the interior.

A

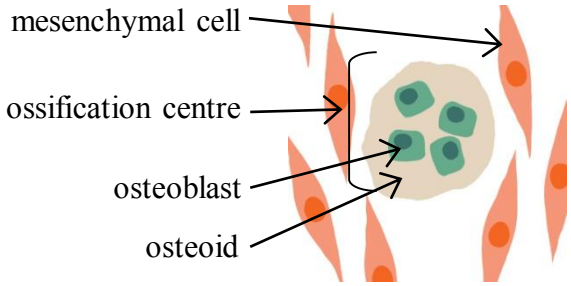
mesenchymal cell
ossification centre
osteoblast
osteoid

B

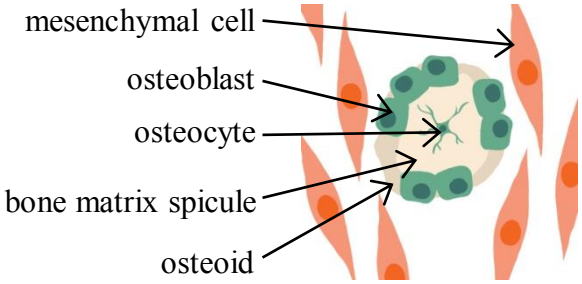
mesenchymal cell
osteoblast
osteocyte
bone matrix spicule
osteoid

C

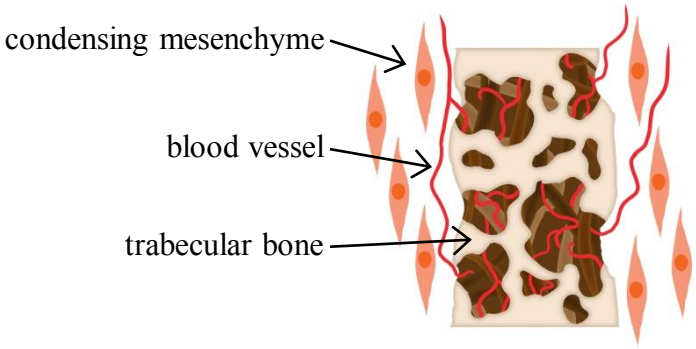
condensing mesenchyme
blood vessel
trabecular bone

D

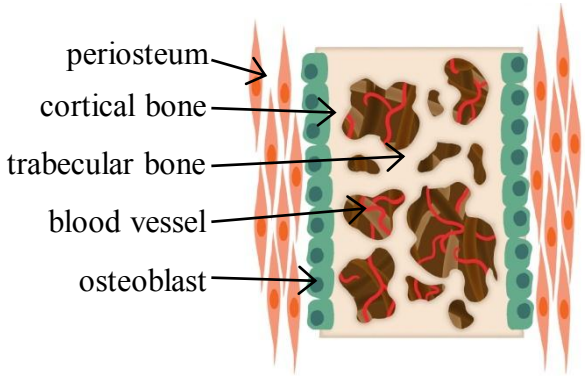
periosteum
cortical bone
trabecular bone
blood vessel
osteoblast

1.3.2 Endochondral Ossification

Unlike intramembranous ossification, endochondral ossification is preceded by the formation of a cartilage structure [37, 38]. As outlined in Figure 1.3, endochondral ossification begins with the condensation and differentiation of MSCs into chondrocytes which produce a cartilaginous matrix scaffold, or anlage, composed predominantly of type II collagen and chondroitin sulphate proteoglycan (aggrecan) aggregates [39, 40]. The anlage acts as a template for the subsequent formation of the bony elements of the skeleton and is covered by the perichondrium, a fibrous dense layer of tissue which, once vascularised, becomes the periosteum. Ossification centres appear first in the centre of the anlage followed by the extremities. In these centres, the chondrocytes enlarge and mature, coinciding with an increase in intracellular calcium concentrations. Then, as chondrocyte apoptosis occurs, a calcified scaffold appears. Simultaneously, neo-vascularisation of the perichondrium leads to the formation of the periosteum which delivers the OB progenitors. Capillaries and osteogenic cells then invade the calcified scaffold, initiating the deposition of the osteoid that is subsequently ossified by mature osteoblasts to form mineralised bone [30, 37, 41].

1.3.2.1 Chondrogenesis and the growth plate

During skeletal growth, long bone elongation occurs in specialised regions known as growth plates. At the cellular level, the growth plate is organised into three layers of morphologically and actively distinct chondrocytes termed the resting-, proliferative- and hypertrophic zones [42-45] (Figure 1.4).

The rate of longitudinal bone growth is primarily dictated by the rate of chondrocyte proliferation and hypertrophy [45, 46]. During childhood and adolescence, growth plate activity is at its peak velocity which progressively declines following sexual maturation and ceases in adulthood. The decline in activity is accompanied by a steady reduction in growth plate width.

Figure 1.3 - Endochondral ossification: A) Endochondral ossification begins with the condensation of MSCs into chondrocytes which produce a cartilaginous scaffold or anlage for subsequent mineral formation. B) MSCs within the perichondrium undergo OB differentiation and synthesise a collar of bone around the anlage. C) Chondrocytes within the anlage proliferate and hypertrophy. Invading blood vessels deliver OBs which replace the cartilaginous scaffold with bone mineral. D) Chondrocytes at the epiphyses continue to proliferate and hypertrophy and the scaffold is replaced by mineralised bone facilitating bone elongation.

A

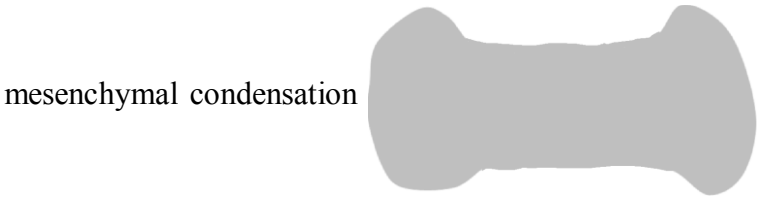
mesenchymal condensation

B

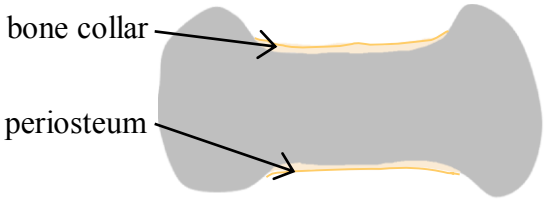
bone collar
periosteum

C

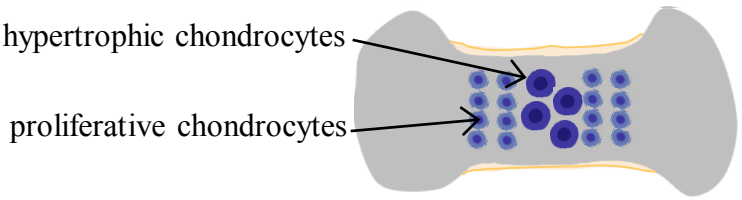
hypertrophic chondrocytes
proliferative chondrocytes

D

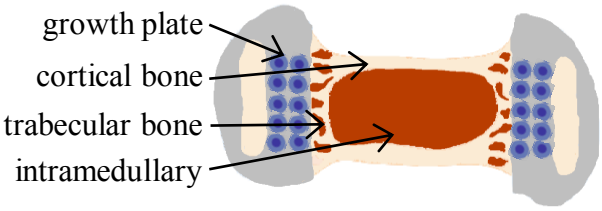
growth plate
cortical bone
trabecular bone
intramedullary

Figure 1.4 - The growth plate: Longitudinal bone growth is dependent upon the activity of the growth plates located in the epiphyses of long bones. Chondroblasts form the resting zone and function as a reserve for proliferative clones. Resting chondrocytes, located near the metaphases mature and enter the proliferative-zone where they align in column, parallel to the axes of the bone and synthesise a cartilaginous matrix. Farthest from the epiphyses, in the hypertrophic zone, chondrocytes cease proliferation and increase in size which increases the width of the cartilage scaffold. Hypertrophic chondrocytes then undergo apoptosis and the remaining cartilage scaffold is vascularised. OBs and OCs are recruited to the scaffold which function co-ordinately to form the primary spongiosa.

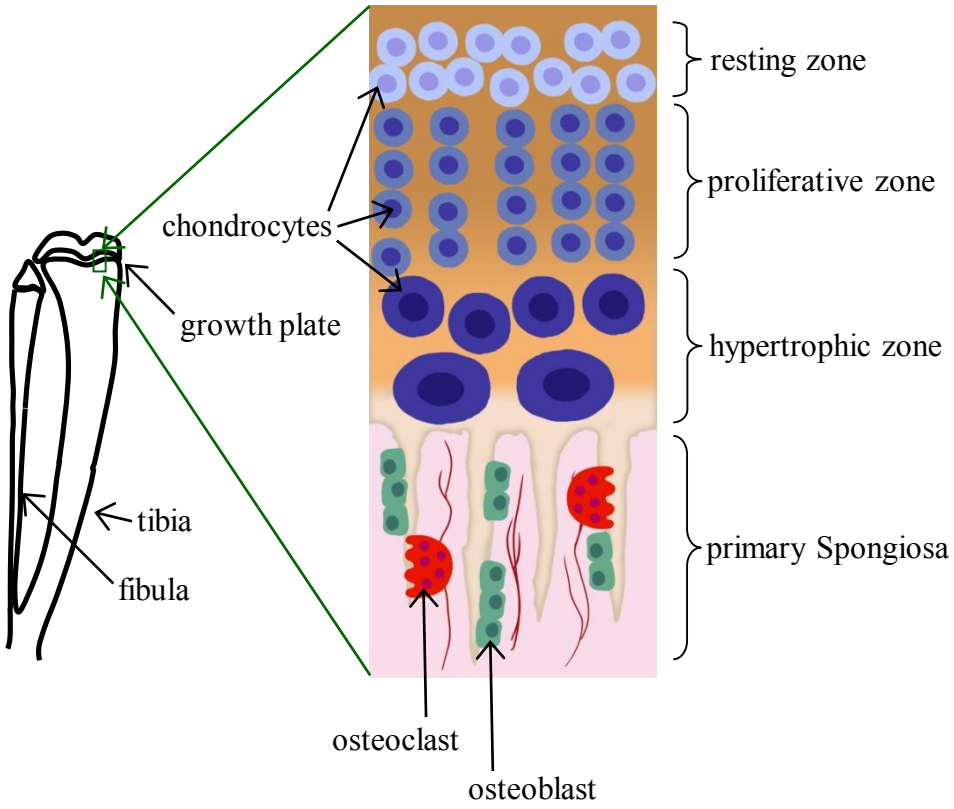
resting zone
proliferative zone
chondrocytes
growth plate
hypertrophic zone
tibia
fibula
primary Spongiosa
osteoclast
osteoblast

In adult humans, the active cellular components of the growth plate are replaced by inorganic mineral, which stops further long bone growth [47, 48].

The resting zone, positioned nearest the epiphyses, is formed of closely grouped and irregularly arranged chondroblasts which rarely divide and function as a reserve of stem-like cells capable of generating proliferative clones[44, 45]. Chondroblasts located near the metaphyses mature and begin the formation of the proliferative zone. Here chondrocytes flatten and align into columns parallel to axes of the bone. Chondrocyte proliferation within the columns facilitates organised elongation of the growth plate. Simultaneously, proliferative zone chondrocytes begin anlage synthesis [42-45, 49]. Farthest from the epiphyses is the hypertroic zone,where proliferative chondrocytes cease dividing and increase in size via both dry mass and fluid accumulation [50]. It is the proliferation and hypertrophy of the chondrocytes which increases the width of the cartilage scaffold. The enlarged hypertrophic chondrocytes undergo apoptosis creating crevasses within the anlage.

Concurrent to chondrocyte hypertrophy, surrounding perichondrial MSCs differentiate into OBs and begin the initial stages of mineral deposition. Crevasses are invaded by blood vessels in the formation of the medullary cavity[42, 51]. The cartilage scaffold is digested and replaced with mineral in the initial formation of the epiphyseal trabecular bone (spongiosa). The spongiosa is digested and reformed in the process termed bone remodelling.

1.4 Bone remodelling

Bone remodelling is the homeostatic process required to build and maintain skeletal integrity. Remodelling is orchestrated by the actions of two cell types, namely the bone-forming OBs and bone-resorbing osteoclasts (OCs) [30, 52]. Bone remodelling alters the microarchitecture of the skeleton to form an optimal structure, repairs micro-fracture-related damage, changes bone density and facilitates the management of systemic calcium and phosphate levels.

In the healthy adult skeleton, bone remodelling is tightly-coupled in time and space, with OC activity and OB activity maintained in equilibrium. As outlined in Figure 1.5, bone remodelling is a cyclical process beginning on a quiescent bone surface covered in bone lining cells. In response to signals, usually originating from osteocytes, bone lining cells retract and expose the bone surface [53]. Haematopoietic precursors are recruited to the exposed bone surface and mature into bone-resorbing OCs. OCs fuse to the bone surface and secrete proteolytic enzymes and acids which digest bone mineral through the breakdown of hydroxyapatite and organic components. This process increases cytosolic Ca^{2+} signalling, which in turn signals OCs to detach from the mineral matrix and expose the resorbed surface [54]. During resorption, factors sequestered within the mineralised bone, such as transforming growth factor β (TGFβ), platelet derived growth factors (PDGFs), insulin-like growth factor (IGF1) and bone morphogenic proteins (BMPs), are released and signal the recruitment of OBs. OBs assemble on the resorbed bone surface and initiate the synthesis of new mineralised bone matrix (Figure1.5) [55-58].

Uncoupling of normal bone remodelling results in pathological changes to the skeleton. In diseases such as osteoporosis, there is a reduction in the number and bone forming capacity of OBs. This results in an imbalance between the rate of resorption and the rate of formation, resulting in reduced bone mineral density [3, 4]. In Paget's disease, abnormal bone growth occurs as a result of increased bone resorption due to increased OC numbers [55, 59]. The increase in OC activity increases bone activating factors which, in turn, signal the limited numbers of OBs to rapidly form bone and as a result, this bone is of poor structural integrity and lacks the strength and shape of normal bone [59].

Figure 1.5 - Bone remodelling: In the resting state, the bone surface is covered by bone lining cells which retract at activated sites. Osteoclasts are recruited to active sites to digest mineral matrices in the process of resorption. Resorption of bone releases factors that lead to the chemotaxis of osteoprogenitors to the site of the resorption pits. The osteoprogenitors differentiate into the osteoblasts, which form the osteoid matrix that is subsequently mineralized. The osteoblasts trapped in the matrix from osteocytes and osteoblasts become bone lining cells in a resting state completing this cycle.

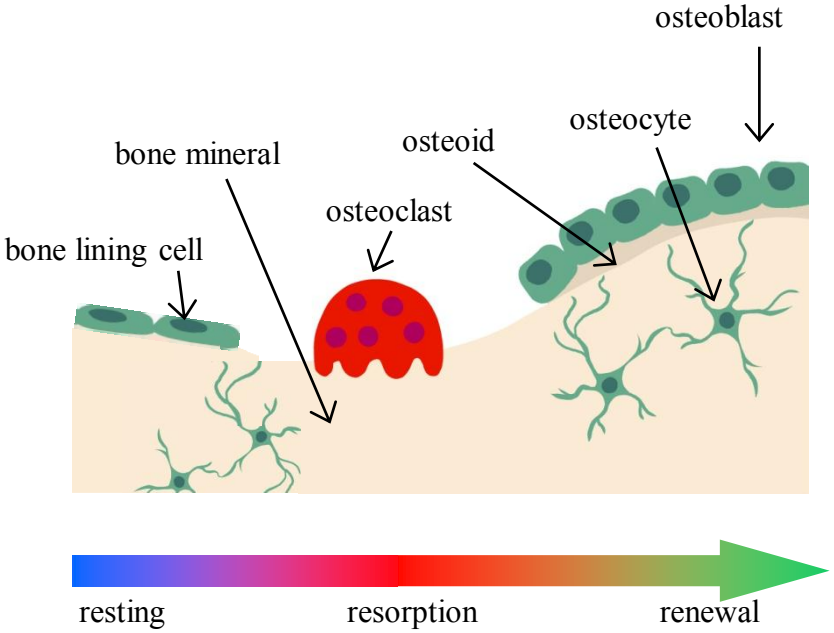
osteoblast
osteocyte
osteoid
bone mineral
osteoclast
bone lining cell
resting
resorption
renewal

1.4.1 Osteoblasts

OBs are mature, non-proliferative cuboidal cells with a single nucleus, an intensely basophilic cytoplasm and a prominent golgi apparatus. Derived from multipotent MSCs in response to a variety of stimuli (described in detail in section 1.5), they are responsible for the synthesis of an uncalcified osteoid matrix consisting of Type I collagen, osteonectin, osteopontin, bone sialoprotein and serum-derived globular proteins [55]. The osteoid matrix is then mineralised by OBs through the deposition of hydroxyapatite crystals which are composed of calcium and phosphate [60]. At the bone surface, OBs facilitate active transport of Ca^{2+} ions to the bone formation space through nucleated vesicles and increase phosphate levels at the mineralisation front via the enzymatic cleavage of phosphate ions. Hydroxyapatite crystal nuclei are synthesised from which further mineral deposition is founded.

1.4.2 Osteocytes

Osteocytes are terminally differentiated, non-proliferative cells derived from mature OBs that become embedded in lacunae of the bone matrix during bone formation. They act as a mechanosensory network deep within the bone by forming a syncytium with other osteocytes, OBs and bone lining cells via the canalicular network and intercellular gap junctions [51, 61]. In

response to extracellular events such mechanical strain, fluid flow and micro-fracture damage, osteocytes produce factors such as IGF-1 and nitric oxide, which act as signalling molecules to influence bone remodelling[62-65].

1.4.3 Osteoclasts

OCs arise from mononucleated precursors of haemopoietic origin [51, 66-68]. OCs are recruited to the bone surface through the recognition of binding matrix proteins which

facilitate OC adhesion to the bone surface via the formation of an actin ring sealing zone [51, 69, 70]. Adhesion of OCs to the bone surface is mediated predominantly via integrins [71]. Following adhesion to the bone surface, OCs polarize and undergo cytoskeletal organisation, allowing them to spread along the bone surface. Fusion occurs via a process involving the formation of a ruffled membrane which fuses to the bone surface facilitating the transport of intracellular microtubules and vesicles containing proteases and protons to the bone surface [51, 70, 72-76]. Proton pumps along the ruffled membrane, within the sealing zone, reduce the pH and solubilise the mineral component of bone [76, 77]. Enzymes such as cathepsin K are then released to solubilise the collagen matrix [78]. Both the solubilised mineral and collagen type I fragments are released into the systemic circulation and the OC unseals before undergoing apoptosis or are recruited to bone remodelling sites by signals generated from osteocytes[79, 80].

1.5 Mesenchymal Stem Cells

OBs originate from a pool of precursor stem cells, MSCs which have a capacity for self-renewal and multi-lineage differentiation. MSCs are the precursor for a number of cell types including, but not limited to OBs, adipocyes (AdCs), chondrocytes and myocytes for the regeneration of bone, cartilage, tendons, muscle, ligaments, adipose and stroma [81-83]. MSCs have been identified in numerous adult tissue including bone marrow [81], adipose tissue [84], dental pulp [85] and muscle [86]. Isolated MSCs can be cultured ex vivo without significant changes in their general properties making them ideal for tissue regenerative therapies.

As the precursor of OBs, MSCs are essential for the development and homeostasis of bone. In aging and diseased states, MSCs undergo behavioural changes often resulting in a reduction in their self-renewal and differentiation capacities. For example, osteoporosis is characterised by both a decline in MSC pools and a reduction in their osteogenic capacity [3, 4]. Initial commitment of MSC to each lineage is a tightly-regulated process governed by extracellular cues driving intracellular signalling cascades which promote the commitment

and multistep maturation stages. During the differentiation process, MSCs progress through developmental stages both morphologically and functionally, which can be identified by the expression of functional markers specific to each lineage [87, 88].

1.5.1 Osteoblast differentiation

OB differentiation is the process by which MSC mature into bone forming OBs. This is a linear process which can be simplified into three stages of development, namely; the formation of OB progenitors, pre-OBs and OBs. Each step is characterised by the temporal-spatial expression of OB gene markers required for their maturation and function.

OB differentiation is regulated by two primary transcription factors; Runt-related transcription factor 2 (Runx2) and Osterix (Osx). Both transcription factors are essential for OB differentiation, as mice lacking Runx2 or Osx are devoid of a mineralised skeleton due to complete absence of mature OBs[87, 89]. Runx2 regulates the expression of OB genes including osterix (Sp7) [90], integrin-binding saloprotein (Ibsp), osteopontin (Spp1), osteonectin (Sparc) and osteocalcin (Bglap) [91, 92]. Together, Runx2 and Osx regulate the expression for OB genes encoding collagen type I (COL1A1), and alkaline phosphatase (ALPL)[34].

The expression of Runx2, Osx and other OB genes occurs in a stage-dependant manner which is commonly utilised in the quantification of the differentiation process. Widely considered to be the master regulator of osteogenesis, Runx2 signifies the differentiation of multipotent MSCs into the precursors of both OBs and chondroctyes (osteochondroprogenitors) [93]. Runx2 is a central mediator in bone morphogenic protein (BMP) and Wingless-related integration site (Wnt) signalling, which function to promote cell lineage commitment and osteogenesis.

Progenitor cells are morphologically indistinct from their MSC predecessors and expansion and maturation of progenitor cells are regulated by both fibroblast growth factors (FGF) and parathyroid hormone (PTH/PTHrP) [94]. Both the expression of Osx and canonical Wnt signalling activation mark the end of the proliferative precursor stage and are essential

for progression into the subsequent developmental stage of a pre-OBs. Wnt proteins, BMPs and transforming growth factor beta (TGFβ) families are involved in early skeletal development and act as mitogenic factors for MSC proliferation. At this time, cellular morphology shifts into the cuboidal shape of the mature OB cell, and pre-OBs begin synthesising extracellular matrix (ECM) proteins. Composed primarily of collagen type I (COL1A1), the synthesis of ECM by pre-OBs requires the expression of the COL1A1 and BSP proteins [95]. Progression into the mature OB stage is marked by decreased levels of Runx2 and increased levels of alkaline phosphatase (ALP). At this stage, OBs continue the synthesis of ECM and initiate mineralisation with upregulation of osteopontin (OPN) and osteocalcin (OCN). Mature stage mineralisation is facilitated by the OB-specific protein OCN, which binds the calcium and phosphate components of hydroxyapatite crystals [95].

1.5.2 Chondrocyte differentiation

Chondrocytes, also arising from MSCs, are responsible for the production of cartilaginous matrices during endochondral ossification (as outlined in section 1.3.2), for the synthesis of on the epiphyseal surfaces of long bones and the intervertebral discs of the spine, and form structural components of the rib cage, ear, nose and bronchial tubes [96].

Chondrogenic differentiation is facilitated by the expression of key transcription factors Runx2 and sex determining region Y box 9 (Sox9) [35]. As mentioned in section 1.5.2, chondrogenic differentiation begins with the initial expression of Runx2 in MSCs, which drives the initial stages of commitment to the osteochondroprogenitor lineage. Secondary to Runx2 upregulation and in the absence of Osx, commitment to the chondrocyte lineage is facilitated by the expression of Sox9. Expression of Sox9 and its downstream targets Sox5 and Sox6 stimulates the expression of genes encoding cartilaginous extracellular matrix proteins including collagens II, IX and XI and aggrecan [97-99]. Unlike osteogenesis, where Runx2 expression decreases in mature osteoblasts, Runx2 is expressed in mature pre-hypertrophic and hypertrophic chondrocytes and promotes hypertrophic differentiation. The

necessity of Runx2 in these later stages is evidenced by a decrease in the number of hypertrophic chondrocytes in Runx2 null mice [89, 100-102].

1.5.3 Adipocyte differentiation

AdCs, also arising from MSCs, control the systemic balance of energy and lipid homeostasis through the storage and expenditure of energy via lipid accumulation and release and the production of adipokines [103].

The main transcription factors involved in the commitment and maturation of AdCs from multipotent cells are the nuclear hormone receptor, peroxisome proliferator-activated receptor γ (PPARγ) and the CCAAT/enhancer binding protein α, C/EBPα [104]. PPARγ is the master regulator of adipogenesis [88] and is required during both the initial commitment and in the maintenance of an adipogenic state as its expression can be detected throughout the lifespan of the AdC [105]. PPARγ promotes the expression of CAAT-enhancer binding proteins (C/EBP) including C/EBPα, C/EBPβ and C/EBPδ, which are also essential in adipogenesis [106, 107]. Like PPARγ, C/EBPα expression is maintained throughout the lifespan of an AdC [108]. Together, their expression is essential for both the regulation of early adipogenesis and the expression of adipogenic genes such as insulin-responsive glucose transporter (GLUT4), Stearoyl-CoA desaturase–1 (SCD1) and leptin [109]. PPARγ and C/EBPα then form a positive feedback loop to maintain and enhance their expression and activate adipogenic genes required for function and maintenance of differentiated AdCs and accumulation of triglycerides [108, 110].

1.6 Inverse relationship between adipocytes and osteoblasts

The aging skeleton is characterized by a reduction in bone mineral density and an increase in intramedullary adiposity [3, 111]. At the cellular level, these age-related changes are associated with an increase in bone marrow AdCs and a decrease in bone-forming OBs [2]. At the cessation of longitudinal bone growth, the requirement for bone development is limited to

micro- and macro-damage repair resulting in a reduction in MSC proliferation and a decrease osteogenic capacity.

As AdCs and OBs originate from a common MSC progenitor [112-115], the shift in the AdC:OB ratio is thought to occur in response to increased AdC differentiation at the expense of OB differentiation [116, 117]. This is associated with a decrease in response to bone stimulating factors favouring the upregulation of genes involved in adipogenesis [118, 119]. In support of this, functional comparisons of MSCs isolated from osteoporotic and healthy individuals show that while similar in morphology, size and cell surface antigen expression, MSCs from osteoporotic individuals exhibit a reduced propensity for osteogenic differentiation [3, 4].

Key transcription factors for each lineage not only promote lineage commitment but prevent commitment to the opposing lineage. Runx2, the master regulator of osteogenesis, has been shown to inhibit PPARγ expression and AdC differentiation [120]. Conversely, PPARγ, has been shown to inhibit Runx2 expression and OB differentiation [108, 121-123].

1.6.1 Signalling pathways governing OB and AdC differentiation

The balance between OB and AdC differentiation requires the coordinated communication of extracellular stimuli activating complex intracellular signalling cascades. Activation of these cascades regulats the expression of lineage-specific genes. Specific to the AdC:OB ratio, several signalling pathways, including Wnt/β-catenin, BMP/SMAD, Indian hedgehog (IHH) and Insulin/IGF1 have been shown to direct MSC to either or both lineages[33, 124-127].

1.6.1.1 Insulin

The role of insulin and insulin-like growth factor-1 (IGF-1) in MSC differentiation has been well documented, with both shown to have both pro-osteogenic and pro-adipogenic effects. In most tissues, IGF-1 functions in an endocrine/paracrine and autocrine manner [124].

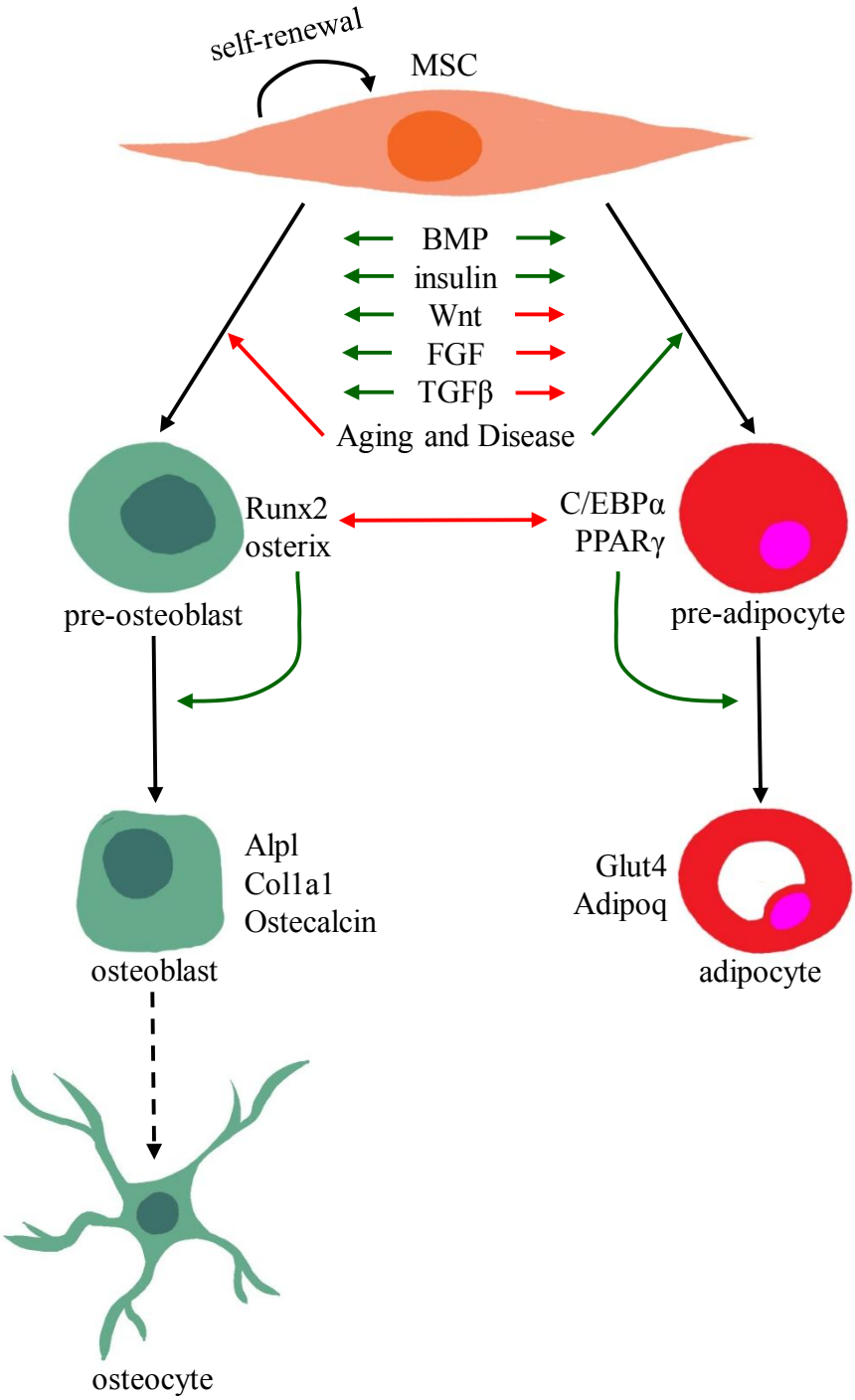
self-renewal
MSC
BMP
insulin
Wnt
FGF
TGFβ
Aging and Disease
Runx2
osterix
C/EBPα
PPARγ
pre-osteoblast
pre-adipocyte
Alpl
Col1a1
Ostecalcin
Glut4
Adipoq
osteoblast
adipocyte
osteocyte

Figure 1.6 - Osteogenic and adipogenic MSC Differentiation: Activation of signalling pathways drive the initial commitment of MSCs to lineage precursors by promoting the transcription of genes essential in cell maturation and function. (Green arrows = stimulate; red arrows = inhibit)

The binding of IGF-1 to the IGF1-R receptor activates insulin receptor substrate (IRS) proteins and mediates OB maturation via upregulating Osx expression in pre-OBs. Furthermore, bone formation has been shown to be mediated by IGF-1 signalling as it mediates OCN transcription [124]. Insulin and IGF-1 indirectly regulate Runx2 to promote post-natal bone accrual. Insulin down-regulates Twist1 and Twist2 expression [124] which inhibit Runx2 activity [124]. IGF-1 and Insulin also inhibit Foxo1-mediated suppression of Runx2 activity by promoting Foxo1 phosphorylation and nuclear exclusion [128]. IGF-1 signalling is also necessary for the proliferation of pre-AdCs and essential for expression of PPARγ and C/EBP and the activation of the adipogenic cascade[129, 130].

1.6.1.2 Wnt Signalling

Wnt/β-Catenin signalling is crucial for bone formation and is involved in pre-OB replication, induction of OB differentiation [131] and inhibition of OB apoptosis [132, 133]. Wnt signalling is activated following the binding of ligands such as Wnt1, Wnt3a and Wnt8 to membrane receptor complexes composed of Frizzled and LRP5/6 (low density lipoprotein receptor-related protein 5 and 6) [134]. Activation results in the stabilisation and translocation of β-catenin to the nucleus where it regulates gene expression [135]. In vitro studies show that Wnt signalling is significantly upregulated during OB differentiation and enhances OB differentiation at the pre-OB stage through the upregulation of Runx2 [33, 125, 136]. Studies also show that Wnt signalling suppresses AdC differentiation by downregulating C/EBPα and PPARγ whilst increasing Osx and Runx2 expression [137].

1.6.1.3 BMP Signalling

BMPs are part of the TGFβ superfamily and play a crucial role in the formation of cartilage and bone as well as postnatal bone formation. BMPs have been found to play important roles in both embryonic development and adult tissue homeostasis [138-141]. Notably,

BMP-2 expression is involved in both osteogenic MSC differentiation [142] and induces OCN expression in mature OBs [143]. During osteogenic MSC differentiation, BMPs bind to type I and type II BMP receptors and form a multimeric receptor-ligand complex [144]. This leads to the phosphorylation and translocation of SMADs to the nucleus [145]. SMADs then induce Runx2 expression, directing MSCs to differentiate towards the OB lineage. BMP-2 is known to promote OB differentiation by inducing the expression of both Runx2 and Osx [146, 147]

1.7 The mammalian target of rapamycin (mTOR) pathway

The mTOR pathway is a key nutrient-sensing pathway that controls cell growth and metabolism. Mammalian target of rapamycin (mTOR) functions as a nutrient sensing checkpoint integrating several environmental cues including energy levels, growth factors, amino acids and cellular stress [148-152]. Compared to other effectors, mTOR has only recently become recognised as a regulator of MSC differentiation and bone development. The target of rapamycin (TOR) gene was first identified in yeast as recently as 1991 by collaborators of this project at the Biozentrum, Basel, Switzerland [153]. The mammalian ortholog, mTOR, was identified several years later in 1994 [148] has since been recognised as the primary protein kinase in two multiprotein complexes; mTOR complex 1 an 2 (mTORC1 and mTORC2) [154-156]. mTORC1 and mTORC2 are structurally distinct and both complexes localise to different subcellular compartments with differing effectors and downstream targets [157]. mTORC1 consists of Raptor (regulatory associated protein of mTOR), PRAS40, mLST8 and mTOR, and controls protein synthesis, ribosome biogenesis and nutrient transport [150, 158]. mTORC2 consists of Rictor (rapamycin insensitive companion of mTOR), mSIN1, mLST8 and mTOR and is involved in cytoskeletal organisation [156].

The distinct mTOR complexes were originally distinguished by their sensitivity to mTOR kinase inhibition by the macrolide, rapamycin. Notably, rapamycin readily inhibits mTORC1 activity but only inhibits mTORC2 activity following prolonged exposure and

mediates its inhibitory effect on mTORC1 by blocking substrate recruitment. Rapamycin forms a complex with cytosolic 12kDa FK506-binding protein (FKB12) which binds directly to mTORC1 via the FKBP12-rapamycin binding (FRB) domain [159, 160]. It is thought that by binding to the FRB domain, the FKRBP12-rapamycin complex exerts an allosteric influence on substrate alignment to mTOR[159, 161]. Conversely, while the FKBP12-rapamycin complex readily binds to mTORC1, it cannot bind to pre-formed mTORC2 [155, 157]. However, it does bind to free mTOR, destabilising both mTORC1 and mTORC2 formation [150, 162].

Rapamycin studies, both *in vivo* and *in vitro*, have identified mTORC1 as being a key regulator in MSC lineage commitment and skeletal development. As detailed in section 1.7, both complex-specific studies and studies targeting mTORC1-effectors have provided further evidence that mTORC1 is a mediator in these processes. For these reasons, the focus of this study is to better define role of mTORC1 independently of mTORC2 in these processes. (Figure 1.7).

1.7.1 mTORC1

mTORC1 is ubiquitously expressed in all cell types and has been established as a master regulator of cell growth, metabolism and proliferation by activating translation of proteins [163]. The mTORC1 signalling network is activated by growth factors including IGF-1, Wnt signaling, energy status, oxygen and amino acids (Figure 1.7).

1.7.1.1 Upstream activators of mTORC1

Activation of mTORC1 is mediated primarily through the ras homolog enriched in brain (Rheb) which is modulated via TSC1/2 complex activity. Other direct effectors of mTORC1 include RagA family of small GTPases (Rag) and mitogen-activated protein kinase (MAPK), AMPK. Extra-cellular factors that control skeletal development and bone accrual activate mTORC1 (Figure 1.6).

Figure 1.7 - Simplified schematic representation of the mammalian target of rapamycin (mTOR) signalling pathway. (Green arrows = activate; red arrows=inhibit)

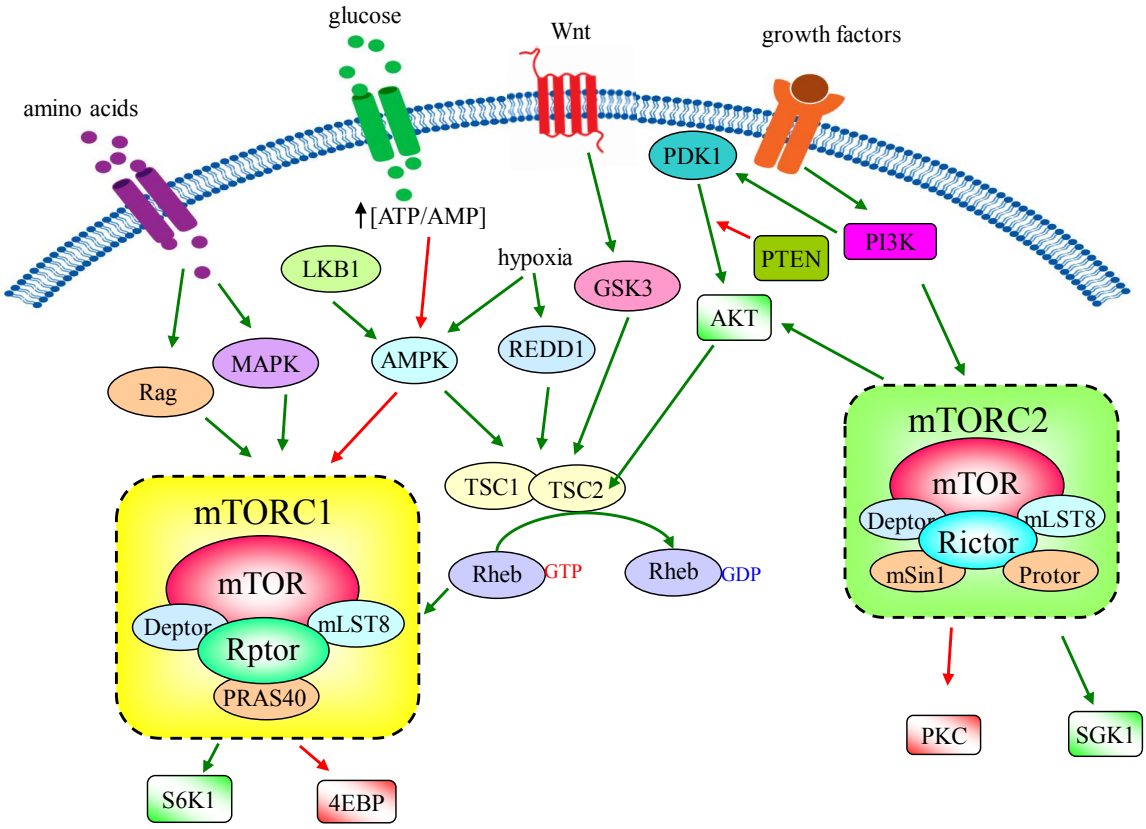
glucose
Wnt
growth factors
amino acids
PDK1
[ATP/AMP]
PTEN
PI3K
LKB1
hypoxia
GSK3
AKT
MAPK
AMPK
REDD1
Rag
mTORC2
mTOR
Deptor
mLST8
Rictor
mSin1
Protor
TSC1
TSC2
mTORC1
mTOR
Deptor
mLST8
Rptor
PRAS40
Rheb
GTP
Rheb
GDP
PKC
SGK1
S6K1
4EBP

Growth factors including insulin and IGF-1 activate mTORC1 through stimulation of the PI3K/Akt signalling cascade. Binding of insulin to its receptor promotes the recruitment of IRS1 causing the subsequent activation of PI3K and recruitment of AKT to the plasma membrane. This leads to suppression of the negative regulator of mTORC1, TSC1/2, which is a GTPase activating protein for Rheb, a small GTPase. In its GTP-bound state, Rheb binds to and activates mTORC1 [152, 164, 165].

mTORC1 is also activated by Wnt ligands. Wnt proteins activate mTORC1 via Akt-mediated suppression of GSK-3β. In the absence of Wnt signalling, GSK-3β phosphorylates and enhances the activity of TSC2 promoting the conversion of Rheb-GTP to Rheb-GDP thereby inhibiting mTORC1 function [166, 167].

Cellular energy status regulates mTORC1 activity via AMP-activated protein kinase (AMPK) to modulate cellular proliferation and function in at least three separate ways. Firstly, AMPK is activated under low glucose influx, causing the phosphorylation and activation of TSC2 and the inhibition of mTORC1 activity [168]. Secondly, activation of AMPK also directly inhibits mTORC1 through the phosphorylation of Raptor [169]. Thirdly, recent studies have shown that AMPK is involved in the regulation of Rheb, which binds to and activates mTORC1 in its GDP-bound form.

Reduced cellular oxygen levels modulate mTORC1 activity through multiple channels to decrease mitochondrial function and cellular apoptosis [170]. Hypoxic conditions (i.e. conditions of reduced oxygen availability) reduce cellular ATP, which activates AMPK and decreases mTORC1 activity [171, 172]. TSC1/2 is also activated in response to low oxygen levels through transcriptional regulation of the DNA damage response 1 (REDD1) protein [173].

Finally, sufficient amino acid availability is required for mTORC1 activity which is independent of its association with TSC1/2 [163]. Evidence suggests that amino acid signalling regulates mTORC1 activity through the RagA family of small GTPases and mitogen-

activated protein kinase 3 (MAPK) [174, 175]. While the mechanisms by which this occurs are yet to be fully elucidated, studies show that amino acid availability is essential for the re-localisation of cytoplasmic mTORC1 to a perinuclear region in order for it to associate with the coactivator, Rheb [152, 176].

1.7.1.2 Downstream of effectors of mTORC1

The two best characterised targets of mTORC1 are p70-S6 Kinase 1 (S6K) and the eukaryotic initiation factor 4E binding protein 1 (4E-BP1) [177](Figure 1.6). mTORC1 phosphorylates at least two residues of S6K including threonine T389, which stimulates subsequent phosphorylation of S6K by PDK1. Once activated, S6K is known to mediate several roles in the regulation of cellular processes including translation initiation, ribosomal biogenesis [178] and in a positive feedback loop activates mTOR translation [179].

4E-BP1, also a direct target of mTORC1, controls cap-dependent translation initiation together with S6K1. Phosphorylation of 4E-BP1 causes its dissociation from eukaryotic initiation factor 4E (eIF4E) allowing for its subsequent association with the eIF4G complex [177, 180]. Simultaneously, S6K1 acts on the formation of the eIF4G complex through the activation of eIF4B[181]. This complex binds to the 5' cap of mRNA and once assembled, facilitates cap-dependant translation and elongation, mRNA biogenesis and the translation of ribosomal proteins [182, 183].

mTORC1 regulates starvation-induced autophagy via direct interaction with unc-51-like kinase 1 (ULK1). Active mTORC1, phosphorylates and inactivates ULK1. In response to decreased amino acid levels, mTORC1 activity is reduced, and ULK1 is activated. [161, 184-187]. While the mechanisms by which mTORC1 inhibits autophagy remain unclear, studies show that ULK1 activation regulates the formation of autophagosomes for the degradation of intracellular proteins and organelles [188].

mTORC1 also has a central role in homeostatic regulation of protein synthesis via feedback loops whereby downstream effectors of mTORC1 also act as upstream regulators. For example, growth factor initiated Akt/mTORC1 signalling is negatively regulated by the phosphorylation IRS-1 by S6K. Activated S6K interacts directly with IRS-1, promoting its degradation, thereby inhibiting its sensitivity to insulin and subsequently inactivating PI3K/Akt signalling [183, 189-191]. Additionally, S6K also participates in a positive feedback loop by phosphorylating mTOR resulting in the stimulation of mTOR activity [179, 192]. Additionally, growth factor receptor-bound protein (Grb10), a negative regulator of IGF-1 signalling, has been identified as a direct target of mTOR leading to the inhibition of mTORC1 activity via interaction with both the insulin receptor and Raptor [193, 194].

1.7.1.3 Raptor is an essential component of mTORC1

Raptor is essential in mTORC1 activity as it integrates both upstream and downstream signalling events. Raptor is a scaffold protein which recruits phosphorylation targets of mTORC1 including S6K and 4EBP1 [186, 195-198]. This is facilitated by the direct binding of Raptor to a short amino-acid sequence referred to as the TOS (mTOR signaling) motif present in both S6K and 4EBP1 [197, 199, 200]. Raptor also works as a signal receiver via interaction with upstream regulators of mTORC1. Multiple phosphorylation domains have been recognised on Raptor which interact directly with Rheb[201], RagA[152] and MAPK activated ribosomal protein S6 kinase (RSK) [174] to stimulate mTORC1 activity. Conversely, during cellular energy stress, activation of AMPK results in the direct phosphorylation and inactivation of Raptor inhibiting mTORC1 activity[169]. Raptor has been identified as both a unique component of mTORC1 [189] and an essential in mTORC1 function[202]. It is for these reasons that Raptor is the target of functional studies of mTORC1.

1.8 Evidence for a role of mTORC1 in MSC lineage commitment

Established *in vitro* protocols have identified mTORC1 as a mediator of lineage specific gene expression during MSC differentiation. As mentioned previously (Section 1.5.5.1), activation of insulin signalling is required for adipogenesis. Constitutive activation of mTORC1 through loss of TSC1/2 function increases mRNA and protein expression of PPARγ which, in turn, leads to increased triglyceride levels in pre-adipocyte cells[23]. Additionally, inhibition of mTORC1 via rapamycin results in reduced AdC differentiation and lipid accumulation by mature AdC. Inhibition of mTOR decreases expression of most adipogenic genes including PPARγ, adipsin and ADD1/SREP1c, stalling adipogenic MSC differentiation resulting in reduced lipid accumulation [20-22, 203, 204].

Observations indicate that mTORC1 signalling is required in the proliferative stages of OB differentiation with rapamycin inhibition reducing the proliferative capacity of osteogenic mouse cell lines, primary mouse bone marrow cells [25] and human embryonic stem cells [205]. However *in vitro* inhibitor studies investigating the role of mTOR in differentiation and bone formation have produced conflicting evidence depending largely on cell type and inhibitory method used. In differentiating OBs, OB-like cells and primary bone marrow stromal cells (BMCs) display reduced OB differentiation in response to rapamycin administration[25]. Rapamycin treatment blocks the expression of osteoblastic gene expression and mineral matrix production in rat BMCs [24] and osteogenic protein-1-induced ALP activity in primary rat calvarial OBs [27].

However, studies have also indicated that rapamycin treatment increases expression of osteoblastic genes during differentiation of MSC to bone forming OBs [18, 205] and in differentiated OBs [27]. Rapamycin promotes osteogenic differentiation of hESCs by blocking proliferation and stimulating BMP signalling resulting in increased expression in Rux2, OCN, BMP2, osteonectin and osteoprotegerin [205]. Rapamycin increases mRNA expression of

osteopontin and osteocalcin in terminally differentiated osteosarcoma cell line resulting in increased mineral matrix deposition [17]. Inhibition of both PI3K and mTOR using the compound, BEZ235, also promoted the differentiation of hMSC by upregulating the expression of osteogenic markers including BMP2, ALPL, and BGLA and increasing mineral matrix production. BEZ235 also enhanced de novo bone formation in calvarial cultures. Knockdown of mTOR in OB like cells also promoted osteogenesis by increasing the expression of osteogenic markers including BMP2, ALPL, and BGLA [18].

1.9 Evidence for an *in vivo* skeletal role for mTORC1: clinical observations in humans

Although limited in nature, clinical observations provide evidence for a role for mTORC1 in the regulation of bone density and development in humans. To this end, a recent meta-analyses of genome-wide association studies have identified a link between mTOR signalling and heritability for adult height [206]. It has also been established that several upstream effectors of mTORC1 are associated with skeletal disorders. For example, the low bone mass phenotype of patients with Osteoporosis Pseudoglioma syndrome is associated with loss of function mutations in the Wnt co-receptor LRP-5 [207]. Conversely, a high bone mass phenotype is presented in humans harbouring gain of function mutations in LRP5 [208, 209]. Humans with tubercular sclerosis exhibit loss of function mutations in upstream effector TSC1 and/or TSC2 and present with scelrotic and lytic bone changes [210]. Additionally, systemic deficiency of IGF-1 is common in several conditions which are associated with low bone mass including osteoporosis [211, 212], diabetes type 1 [213, 214] and anorexia nervosa [215, 216].

Rapamycin and analogues thereof, have been used clinically as immunosuppressants to prevent organ rejection following transplant [217-222] as well as preventing mTORC1-mediated cancer cell proliferation [223-230]. Rapamycin is used clinically as bone-sparing alternative to commonly administered immunosuppressant cyclosporin A (CsA) for

suppression of T-cell and B-cell activation in graft-versus-host-disease. While CsA administration is associated with rapid bone loss resulting in severe osteopenia, clinical evidence has indicated that rapamycin administration preserves bone mass while still maintaining immunosuppressive activity [231-235]. Furthermore, rapamycin has also been identified as a bone sparing agent for patients suffering from osteoporosis and/or bone loss which is exacerbated as a result of chemotherapy [236, 237].

While these observations highlight a potential role mTORC1 signalling in human skeletal development and bone accrual, knowledge of what aspects of bone formation that it regulates remains largely unknown.

1.10 Evidence for an *in vivo* skeletal role for mTORC1: knockout mouse models

Early studies targeting mTORC1 *in vivo*, were limited by their use of traditional global KOs of mTOR which revealed that *Rptor* KO confered embryonic lethality shortly after implantation [202, 238, 239] due to cellular degeneration and vascularisation defects [202]. To minimise the unintended consequences of traditional KO strategies, conditional KO models, which make use of the Cre-loxP system, have been developed[202]. The Cre-loxP system provides a means to "knock-out" and "knock-in" genes in a tissue-targeted manner and as described below, has enabled the effects of tissue-specific ablation of *Rptor* to be assessed. To this end, the function of mTORC1, has been investigated in mice with conditional deletion of *Rptor* in adipose tissue [240], skeletal muscle [241], liver [242], neural cells [243], oligodendrocytes [244], T-cells [245], oocytes [246], intestinal epithelial cells [247] and haematopoietic cells [248]. Notably, the adipose-specific KO of *Rptor* resulted in a substantial reduction in adipose tissue,[240] supporting *in vitro* evidence that mTORC1 is essential in adipogenesis [20-22, 203, 204]. However, prior to this study, bone-specific conditional targeting of *Rptor* had not been reported.

Numerous Cre-transgenic lines have been generated for skeletal tissue-specific knockout of genes including; The PRX1-Cre line, utilised in the targeting of mesenchymal cells with recombination occurring in chondrocytes, osteoblasts, periosteal, and perichondrial cells[249]. The OSX-Cre line, targeting committed OB progenitors [33] and the OCN-Cre line, targeting mature, differentiated osteoblasts [250]. As described below, for this study, the OSX-Cre line was selected to investigate the role of mTORC1 in OB maturation and function.

1.10.1 mTORC1-related knockout models

Some insight into the role of mTORC1 in skeletal development has been revealed in studies where genes encoding for proteins that utilise the mTORC1 pathway have been either deleted globally or in OBs.

Homozygous deletion of genes encoding *IGF1*, *IGF2* or the IGF receptor (*IGF1R*) all conferred abnormal embryonic skeletal development resulting in dwarfism [251-253]. While postnatal survival of *IGF1*-/- mice was reduced, progeny were infertile and exhibited delayed bone development [251]. Furthermore, heterozygous deletion of IGF-1 resulted in reduced cortical bone mineral density [254]. *IGF1r-/-* embryos showed delayed ossification that was thought to be due to a failure of *Igflr* null OBs to fully differentiate into mature osteocalcin-positive cells [251].

Bone-specific IGF-1 knockout mice, in which IGF-1 deletion was restricted to mature Col1a2-expressing OBs, displayed reduced bone formation and decreased bone mass [255]. Furthermore, IGF-R ablation via OCN-Cre also caused decreased bone formation at 6 weeks of age, due to an impairment of OB activity [256]. In contrast, over-expression of IGF-1 in Col1a1-expressing cells increased thickness of cortical bone [257]. Taken together, these studies highlight the importance of IGF signalling, which occurs upstream of mTORC1, in bone formation.

Downstream of IGF signalling, mice harbouring a global knockout of *Akt1* developed an osteopenic phenotype at 8 weeks of age, as a result of suppressed OB differentiation and

function [258]. In addition, mice lacking both *Akt1* and *Akt2* showed neonatal lethality, dwarfism [259] and delayed bone ossification [166, 260]

The role of the negative regulator of PI3K/Akt/mTOR signalling, PTEN, on skeletal development was investigated in conditional knockout mice. *Pten* deletion in mature OBs, driven by Col2a1:Cre, resulted in increased skeletal formation and an increase in both AKT and mTOR activity [261]. In other studies, mice lacking *Pten* in mature OBs via OCN-Cre also displayed a progressive increase in bone mineral density, attributed to decreased OB apoptosis and increased mTOR activity [262].

1.11 Summary and project aims

Recently, a growing body of evidence has emerged suggesting that mTORC1 signalling is critical for the regulation of both the differentiation of MSCs and accrual of bone mass. While overwhelming evidence suggests mTORC1 is an essential mediator of adipogenic MSC differentiation [19-23], conflicting observations have been made in relation to its role in OB differentiation and function [13, 16-18, 24-29]. The differences in the results of previous studies may be attributed to the types of cell used and/or their stage of differentiation. The results of inhibitor studies are also confounded by a lack of specificity making it difficult to attribute function to mTORC1 or mTORC2. Therefore, the role of mTORC1 in MSC differentiation remains unclear. Furthermore, while both clinical and animal studies have suggested a role for mTORC1 in bone formation, no definitive studies that target bone-specific mTORC1 have been performed.

To address the limitations of previous studies, the Cre-LoxP system of targeted transgenesis was utilized to target *Rptor*, an essential component of mTORC1, in mice. To examine the role of mTORC1 in MSC fate determination, primary multipotential MSCs deficient of *Rptor* were generated for *in vitro* differentiation assays. Additionally, to examine the role of mTORC1 in skeletal development, pre-OB specific deletion of *Rptor* was achieved through Cre-mediated targeted deletion in osterix-expressing cells.

The studies presented in this thesis were designed to address the following aims:

Aim 1: To determine the role of mTORC1 in MSC fate determination.

Aim 2: To determine the role of mTORC1 in embryonic and postnatal skeletal development.

Chapter 2 - Materials and methods

2.1 Commonly used reagents

Table 2.1: Reagents and Suppliers

Reagent	Supplier	Catalogue Number
α-Modified Eagle's medium (α-MEM)	SAFC Biosciences,Lenexa, USA	51451C
Acetic acid	Merck	6.10001.2500
Acetone	Ajax Finechem, Taren Point, NSW	6-2.5L
Acrylamide (30% bis solution)	BioRad, Gladesville, NSW	161-0148
Agarose	Sigma-Aldrich	A9539
Alcian blue	Sigma-Aldrich	A5268
Alizarin red	Sigma-Aldrich	A5533
Calcein	Sigma-Aldrich	C0875
Calcium chloride	Sigma-Aldrich	C1016
Chromium (III) potassium sulphate dodecahydrate	Sigma-Aldrich	243361
Citric acid, powder	Sigma-Aldrich	C1909

Table 2.1: Reagents and Suppliers

Reagent	Supplier	Catalogue Number
Citric acid solution	Sigma-Aldrich	91-S
Dexamethasone	Sigma-Aldrich	D4902
D-glucose	Sigma-Aldrich	G8270
Dimethyl sulphoxide (DMSO)	Ajax Finechem	225-2.5L
Dithiothreitol (DTT)	Invitrogen, Mulgrave, VIC	P2325
Eosin Y	Merck	1.15935.0025
Ethylenediaminetetraacetic acid (EDTA)	Chem Supply, Gilman, SA	EA023
Ethanol (analytical grade)	Merck	6.10107.2511
Fast green	Sigma-Aldrich	F7252
Foetal calf serum (FCS)	SAFC	12003C
Formaldehyde, 40% (w/v)	Merck	10113
Gelatine	Sigma-Aldrich	G9391
Glycerol	Ajax Finechem	242-25L

Table 2.1: Reagents and Suppliers

Reagent	Supplier	Catalogue Number
Haematoxylin	ProSciTech, Thuringowa Central, QLD	C1071
Hanks buffered saline solution (HBSS)	SAFC	55021C
Indomethacin	Sigma-Aldrich	I7378
Isoporopanol	Ajax Finechem, Taren Point, NSW, Australia	ACR327272500
L-ascorbate-2-phosphate	Wako Pure Chemical Industries, Osaka, Japan	013-12061
L-glutamine, 200 mM	SAFC	59202C
Hoescht 33258	Sigma-Aldrich	B61405
Hydrochloric acid (HCl), 35%	Merck	6.10307.2511
Methanol	Chem Supply	MA004-P
Methyl green	Sigma-Aldrich	M8884
Methylmethacrylate	Merck	8.00590.1000

Table 2.1: Reagents and Suppliers

Reagent	Supplier	Catalogue Number
Neutral buffered formalin (NBF, 10%)	Fronine Laboratory Supplies, Riverstone, NSW	JJ01810
Oil Red O	MP Biomedicals, Solon, OH	215598425
Paraformaldehyde	Merck	296474L
Penicillin 5000 U/mL, streptomycin 5mg/mL	Sigma-Aldrich	P4458
Perkadox	16 AkzoNobel, Tullamarine, VIC	1552-11-3
Phosphate buffered saline (PBS)	20x Media Production Unit IMVS	N/A
Polyethylene glycol 300 (PEG 300)	Sigma-Aldrich	81162
Proteinase K	Invitrogen	25530-015
Safranin O	Sigma-Aldrich	S8884
Salmon sperm DNA	Sigma-Aldrich	31149
Sodium acetate	Sigma-Aldrich	236500

Table 2.1: Reagents and Suppliers

Reagent	Supplier	Catalogue Number
Sodium bicarbonate	McKenziees, Altona, VIC	N/A
Sodium carbonate	Merck	10240
Sodium chloride	Sigma-Aldrich	S9625
Sodium dodecyl sulphate (SDS)	Merck	444464T
Sodium hydroxide, pellets	Merck	567530
Sodium hypochlorite (12.5% w/v)	ACE Chemical Company	F386
Sodium iodate	Sigma-Aldrich	S4007
Sodium-L-tartrate	Sigma-Aldrich	228729
Sodium nitrite solution	Sigma-Aldrich	91-4
Sodium phosphate	Sigma-Aldrich	S342483
Sodium pyrophosphate	Sigma-Aldrich	S9515
Sodium pyruvate	Sigma-Aldrich	P5280
Sodium thiosulfate	Sigma-Aldrich	S7143

Table 2.1: Reagents and Suppliers

Reagent	Supplier	Catalogue Number
Tartrate solution	Sigma-Aldrich	387-3
Toluidine blue	Sigma-Aldrich	T3260
Tris	Roche	1185-53-1
TRIzol	Invitrogen	15596-018
Trypan blue (0.4%)	Sigma-Aldrich	T8154
Trypsin-EDTA (0.5%)	Gibco	15400-054
Tween-20	Sigma-Aldrich	P9416
Type I collagenase (400U/mL)	Worthington Biochem, Lakewood, NJ, USA	LS0004196
WST-1	Tanaka, Madison, USA	11644807601
Xylene	Ajax Finechem	577-102

2.2 Antibodies

Table 2.2: Antibodies

Antibody	Supplier	Catalogue Number
B220 Biotin	BioLegend	103204
CD11b Biotin	eBioscience	13-0112-82
CD3 Biotin	BioLegend	100304
CD31 PerCP/Cy5.5	BioLegend	102420
CD4 Biotin	BioLegend	100404
CD45 APC-eFlour 780	eBioscience	47-0451-82
CD51 PE	eBioscience	12-0512
Gr1 Biotin	BioLegend	17-5931-82
Sca-1 PECy7	BD Bioscience	561021
Ter119 Biotin	BioLegend	116204

2.3 Real time PCR primers

Table 2.3: Real time PCR primers

Gene	Forward Primer (5'-3')	Reverse Primer (5'-3')
b-actin	TTGCTGACAGGATGCAGAAG	AAGGGTGTAAAACGCAGCTC
C/ebpa	CAAGAACAGCAACGAGTACCG	GTCACTGGTCAACTCCAGCAC'
Adipoq	TGTTCCTCTTAATCCTGCCCA	CCAACCTGCACAAGTTCCCTT
Alpl	GCCTTACCAACTCTTTTGTGC	GGCTACATTGGTGTTGAGCTT
Bmp2	GGGACCCGCTGTCTTCTAGT	TCAACTCAAATTCGCTGAGGAC
Col10a1	CATCTCCCAGCACCAGAATC	GCTAGCAAGTGGGCCCTTTA'
Col2a1(II)	GCGACCGGGAGCATATAACT	GCCCTAATTTTCGGGCATCC
Ibsp	CAGTCCAGGGAGGCAGTG	GGAAAGTGTGGCGTTCTCTG
Inhba	TGAATGAACTCATGGAGCAGACC	AGCTGGCTGGTCCTCACAG
Inhbe	TACCTGAGGATCTTCCGTTGC	TCCAGTTGGAGTTTCACGACG
Mmp13	AGCAGTTCCAAAGGCTACAACT	CCTCGGAGACTGGTAATGGC
Noggin	CGAGCGAGATCAAAGGGCT	TCCTCCTCAGCTTCTTGCTCA

Table 2.3: Real time PCR primers

Gene	Forward Primer (5'-3')	Reverse Primer (5'-3')
Rptor	TGGGTCTTCAACAAGAACTAC ACT	TCTGGGCAAGTGGATGGTTT'
Runx2	ATGATGACACTGCCACCTCTG	ATGAAATGCTTGGGAACTGC
Sp7	ATGGCGTCCTCTCTGCTTG	GTCCATTGGTGCTTGAGAAGG
Spp1	AGCAAGAAACTCTTCCAAGC AA	GATTCGTCAGATTCATCCGAGT'
Sparc	ACTACATCGGACCATGCAAAT AC	CGTACAAGGTGACCAGGACAT

2.4 Animals

2.4.1 Housing

All mice were bred and housed at the SA Pathology Animal Care Facility and studies were performed with Institutional Ethics approval (SA Pathology Animal Ethics Committee approval Project #63/10). *Rptor*$^{fl/fl}$ mice [241], Osx1-GFP::cre mice [33] and R26-stop-EYFP mice [263] were used in this study.

2.4.2 Genotyping

Routine genotying was performed on DNA isolated from tail biopsies. Briefly, genomic DNA was isolated by placing the tail biopsy into 300µL lysis buffer and 4µL proteinase K and incubating overnight at 56ºC with agitation. Samples were subsequently incubated at 95ºC for 10mins and centrifuged at 16,000g for 10 mins. Supernatant, containing the genomic DNA was isolated and PCR was performed using the following primers; *Rptor*$^{fl/fl}$, 5'-ATGGTAGCAGGCACACTCTTCATG-3' and 5'-GCTAAACATTCAGTCCCTAATC-3'; *Osx1-GFP::cre*, 5'-CGCGGTCTGGCAGTAAAAACTATC-3' and 5'-CCCACCGTCAGTACGTGAGATATC-3'; *R26-stop-EYFP*, 5'-AAAGTCGCTCTGAGTTGTTAT-3' and 5'-GCGAAGAGTTTGTCCTCAACC-3'. Detection of *Rptor* gene deletion was performed using 5'-ATGGTAGCAGGCACACTCTTCATG-3' and 5'-CTCAGAGAACTGCAGTGCTGAAGG-3'.

2.5 Cell culture solutions, buffers and media

2.5.1 Adipogenic media

α-MEM was supplemented with 10%FCS, 10mM 2mM L-glutamine, 1mM sodium pyruvate, 15mM HEPES, 50U/mL penicillin and 50μg/mL streptomycin, 60μM indomethacin and 1μM dexamethasone. Media was stored at 4°C until use.

2.5.2 Complete α-MEM/20%FCS for murine MSC culture

α-MEM was supplemented with 20% FCS, 2mM L-glutamine, 1mM sodium pyruvate, 15mM HEPES, 50U/mL penicillin and 50μg/mL streptomycin, 100μM ascorbate-2-phosphate and filter-sterilised using a 0.2μm syringe filter. Media was stored at 4°C for up to two weeks.

2.5.3 Osteogenic Media

α-MEM was supplemented 2%FCS, 2mM L-glutamine, 1mM sodium pyruvate, 15mM HEPES, 50U/mL penicillin and 50μg/mL streptomycin, 10^{-7}M dexamethasone and 1.8mM KH_2PO_4. Media was stored at 4°C until use.

2.5.4 Trypsin, 0.05%

0.5% Trypsin-EDTA (1mL) was thawed at 37°C and mixed with 9mL HBSS and was stored for up to one week at 4°C.

2.5.5 Type I Collagenase DNase

A Type I collagenase(400U/ml)/DNase (50U/ml) solution was made by dissolving type I collagenase in PBS

2.5.6 EDTA, 0.5M

EDTA solution (0.5M, pH 8) was made by dissolving EDTA in RO water and the pH was adjusted to 8.0 by the addition of sodium hydroxide pellets. Solution was stored at room temperature.

2.6 *In vitro* techniques

2.6.1 Cell counts and viability staining

Trypan blue staining was used to obtain viable cell counts. Cells in suspension were diluted in 0.4% (w/v) trypan blue and cells were incubated at room temperature for 3-10mins. Cells were then loaded onto a haemocytometer (Weber Scientific International, Teddington, England) in duplicate. Viable cells were counted using a light microscope (Olympus BX40, Tokyo, Japan) and cell concentration and viability were calculated.

2.6.2 Standard culture conditions.

All tissue culture techniques were performed in a Class II Biological Safety Cabinet (Top Safe 1.2, Bio Air, Siziano, Italy). Cell lines were maintained in a humidified environment at 37°C in hypoxic invitro cabinet (Coy Laboratory Products). All media was warmed to 37°C before use. All tissue culture plates were obtained from BD Biosciences (North Ryde, NSW).

2.6.3 Trypsinisation of adherent cells lines

Cells were washed with pre-warmed HBSS and treated with 0.05% trypsin-EDTA for 3-5mins. Cells were dislodged by agitation of the flask. The trypsin was inactivated by the addition of culture media containing FCS. Cells were pelleted by centrifugation at 800g for 5mins at 4°C in an Eppendorf 5810 centrifuge (Eppendorf South Pacific, North Ryde, NSW). Supernatant was aspirated and cells were vigorously agitated to produce a single cell suspension

in an appropriate volume of culture media. Cells were transferred at an appropriate density into a new tissue culture flask.

2.6.4 Cryopreservation and storage of cells

Cells were preserved in FCS containing 10% DMSO and stored long term in liquid nitrogen storage (-196°C). The cell suspension was pelleted by centrifugation at 800g for 5mins in an Eppendorf 5810R centrifuge. Supernatant was aspirated and the pellet was resuspended in FCS (1mL) filter-sterilised using a 0.2μm syringe filter. FCS containing 20% DMSO (1mL) was added to the cell suspension. 1mL volumes containing 5-10 x 10^6 cells were aliquoted into cryovials (Greiner, Kremsmuester, Germany) and cryovials were transferred to a 4°C cryopreservation freezing container (Mr Frosty; Nalgene, USA) catalogue number 5100-0001) and were cooled to -80°C for at least 3 hours before being transferred to liquid nitrogen storage tanks.

2.6.5 Thawing of Cryopreserved Cells

Cell suspensions were thawed rapidly from liquid nitrogen in a 37°C water bath. Cells were rapidly transferred to a 14mL round-bottom polypropylene tube. Pre-warmed culture media (1mL) was added dropwise to thawed cell suspension and incubated at room temperature for 5mins. The cell suspension was topped up to 10mL with pre-warmed culture media and cells were pelleted by centrifugation at 800g for 5mins in an Eppendorf 5810R centrifuge and the supernatant discarded. Cells were resuspended in 10mL culture media and seeded in a 75cm^2 culture flask. Cells were passaged at least once before use in experiments.

2.6.6 Compact bone digestion for long bone and calvarial MSC isolation

Compact bone isolation of MSCs was conducted as previously described[264]. Briefly, mice were humanly killed by CO_2 asphyxiation and cervical dislocation and for long bone compact bone isolation, tibiae and femora were recovered. For calvarial cell isolation, calvarial

plates were recovered. All bones were excised from the animals and cleaned thoroughly to remove excess muscles and tendons. Bones were gently cracked open with a mortar and pestle and washed in ice cold PBS/2% FCS/2mM EDTA to remove marrow. Bones were digested in PBS containing 3mg/mL collagenase/50units/mL DNase for 45mins at 37°C with gentle agitation.

Following digestion, bone chips were left to settle in ice cold PBS / 2% FCS / 2mM EDTA for 5mins. Supernatant was removed, strained using a 70µm cell strainer and transferred to a 14mL round-bottom polypropylene tubes. This was repeated and the supernatant centrifuged at 400 x g for 10mins at 4°C. Supernatants were then aspirated and cells were resuspended and combined in a 5mL polypropylene tube. Cell number and viability was assessed by trypan blue staining and haemocytometer assessment as described above. Cells were resuspended at 2 x 10^7 viable cells/mL in PBS/2% FCS/2mM EDTA.

2.6.7 Isolation of R26eYFP-*Rptor*$^{fl/fl}$ MSCs

Cells obtained following compact bone digestion (described in section 2.6.6) were incubated with mouse gamma globulin at 1:1000 and the cell suspension incubated on ice for 30mins in the dark. Cells were washed twice with PBS/2% FCS/2mM EDTA. Cells were pelleted at 400g for 10mins and supernatant was aspirated. Cells were resuspended at 2 x 10^7 cells/mL in the antibody cocktail comprised of biotinylated lineage (Lin) antibodies (CD3, CD5, B220, CD11b, Gr-1, Ter119, CD4, CD8) and streptavidin-APC, CD45, CD31, CD51 and Sca1. FloroGold was used to distinguish between dead and living cells. Cells were incubated with the antibody cocktail for 30mins on ice, in the dark. Cells were washed twice with PBS/2% FCS/2mM EDTA as described above. Cells were resuspended in 300µL PBS/2% FCS and sorted by fluorescence activate cell sorting (FACS) using Epics Altra HyPer Sort FACS machine (Beckman Coulter, Miami, Florida, USA). MSCs were identified as $Lin^-CD51^-CD45^-CD31^-Sca1^{+264}$.

2.6.8 Isolation of eYFP+ cells

Compact bone isolated MSCs in PBS/2% FCS/2mM EDTA cells were isolated based on eYFP+ expression by fluorescence activate cell sorting (FACS) using Epics Altra HyPer Sort FACS machine (Beckman Coulter, Miami, Florida, USA).

2.6.9 Generation of RapKO cells

In order to generate primary MSC populations, devoid of raptor, compact bone isolated cells were infected with a lentivirus harbouring a tamoxifen-inducible self-deleting Cre recombinase (LEGO-CreERT2-iG2), or vector control (LEGO-iG2) in the presence of 4μg/mL polybrene as previously described [265].

Briefly, HEK239-T cells were grown to confluence before being transfected with the lentiviral vector as previously described [266, 267]. Successful transfection was assessed by examining the cells for green fluorescence protein using a UV fluorescent microscope (Olympus, Tokyo, Japan.) as previously described [268].

Once transfection was verified, supernatant containing viral particles was removed from HEK293-T cells and the supernatant diluted with 1:1 with α-MEM + additives supplemented with Polybrene (4μg/mL; Sigma Aldrich, Castle Hill, Australia). This mixture was then added drop wise to the target MSC population which were then cultured in the presence of the viral particles for 48hrs. After infection, GFP expression was verified using a UV microscope. Cells were reinfected in the same manner described above to increase the number of infected cells. After a further 48hrs the viral supernatant was removed and replaced with appropriate growth media, α-MEM + additives.

Infected MSCs were cell sorted based on GFP expression using an Epics Altra HyPer Sort FACS machine (Beckman Coulter, Miami, Florida, USA). The brightest 30% of cells in the positive fraction were selected using Expo 32 Multi-comp software (Software version 1.2B). This selected portion of the population was collected and cultured as previously

described. Following *in vitro* expansion, cells were treated with 0.5mM 4-hydroxytamoxifen (4-OHT, Sigma-Aldrich) or vehicle (0.05% ethanol) for 8 days.

2.6.10 BrdU Assay

Cells (1.25x104/cm2) were seeded into 24-well plates in growth media, allowed to adhere overnight then incubated with 5-bromo-2'-deoxyuridine (BrdU) for 16 hours. Incorporated BrdU was detected using a colourimetric assay according to the manufacturer's instructions (Roche, NSW, Australia).

2.6.11 Cell Proliferation WST-1 Assay

Cells were seeded at $4x10^3$ cells per well in a 96-well flat bottom plate in 100µL of the appropriate media and cultured in a humidified environment at 37°C in the presence of 5% CO_2. The relative number of viable cells in each well was determined at days 1, 3, 5 and 7 using the colorimetric assay reagent WST-1 (4-[3-(4-Iodophenyl)-2-(4-nitrophenyl)-2H-5-tetrazolio]-1,3-benzene disulphonate, Roche, USA) according to manufacturers' instructions. Briefly, 10µl of WST-1 was added to each well (and to wells containing medium alone, to enable background subtraction) and incubated for 90 minutes at 37oC. The optical density of the dye solution was measured with a plate reader (Bio-Rad Model 3550, USA) at 450nm wavelength.

2.6.12 7AAD/Annexin V assay

The Annexin V-PE Apoptosis Detection Kit I (BD Biosciences, San Diego, CA, USA) was used to analyse apoptosis in cell populations. Briefly, cells were resuspended in binding buffer (10 mM HEPES pH 7.4, 140 mM NaCl, 2.5 mM CaCl2) and incubated in the presence of Annexin V-PE and 7-AAD in the dark at room temperature for 15 mins. Cells were subsequently resuspended in binding buffer and analysed by flow cytometry using Epics Altra HyPer Sort FACS machine (Beckman Coulter, Miami, Florida, USA). Percentages of viable,

apoptotic and dead cells were defined by their distribution in a fluorescence Annexin/7-AAD dot plot.

2.6.13 Assessment of adipogenic differentiation potential

Adipogenesis assays were performed as previously described [81, 269]. MSCs were seeded at $8x10^3$ per cm^2 in 24 well plates and cultured for 28 days in the presence of adipogenic media with media changes twice a week. At 28 days, the wells were washed 3 times with 1xPBS and cells fixed in 10% NBF for 1 hour at room temperature. Oil Red O staining solution and further diluted 3:20 in RO water. Formation of lipid-laden fat cells was determined by Oil Red O staining.

2.6.14 Assessment of osteogenic differentiation potential

In vitro mineralization assays were performed as previously described [269]. Briefly, MSCs were seeded at $8x10^3$ cells per cm^2 in 96 well plates and cultured in mineralization induction media for 28 days with media change twice weekly. At 28 days, the wells were washed three times with 1x PBS and the mineralized matrix dissolved in 100µL of 0.6M HCl for 1 hour at room temperature. The dissolved mineral solution was then transferred to 96-well microtitre plates and calcium levels were quantitated by the Cresophthalein Complexone assay (Thermo Electron Corporation, Melbourne, VIC, Australia). Briefly, 5µL of each supernatant was transferred to a single well of a fresh microtitre plate. A calcium chloride standard curve was also established in triplicate. Equal volumes of reagent A (cresophthalein complexone 0.10mmol/L, 8-hydroxyquinoline 5.2mmol/L, polyinlpyrolidine 0.07 mmol/L) and reagent B (2-amino-1-methylpropanol 260mmol/L) were mixed and 200µL was added per well. The plates were incubated at room temperature for 2 mins and the absorbance was read at 540nm on a microplate reader (EL808 Ultra, BIO-TEK Instruments, Winooski, VT, USA).

Following dissolution of the mineral with HCl, the wells were washed with 1x PBS and the cells were digested with 100µL of proteinase K for 2 hours at room temperature or overnight at 4°C. The cells were then mixed thoroughly to ensure complete disruption and 50µL volumes were transferred to a while 96-well microtitre plate (Costar, Corning, New York, NY, USA). DNA content per well was then quantified using the Picogreen assay.

2.6.15 Osteogenic potential of isolated MSCs

Assessment of osteogenic potential was conducted on cavarial MSCs isolated as previously described in section 2.6.6. Osteogenic assays were conducted for 21 days and mineral quantified described in section 2.6.14.

2.6.16 Insulin stimulation response

Assessment for response to insulin stimulation was assessed on isolated calvarial cells. The assessment of osteogenic potential was conducted (as previously described 2.6.14) for 14 days in the presence or absence of 10mM insulin. Mineral quantitation was conducted as described in section 2.6.14.

2.6.17 CFUF

Mice were humanely euthanized using CO_2 gas followed by cervical dislocation. The tibiae were surgically removed and cleared of soft tissue in a Class II laminar flow hood (Top Safe 1.2, Bio Air Siziano, Italy), using sterile instruments. The distal and proximal ends of each femur were removed using sterile forceps and a surgical blade (#22). A 10mL syringe attached to a 21-gauge needle was then inserted into either end of the bone with a screw motion. The bone marrow was flushed then stored on ice in a 50mL Falcon tube, before being transferred to a 6cm culture dish with enough complete α-MEM media to cover the bones (~500µL). The bone was then crushed into small pieces with a sterile scalpel blade and transferred to a 10mL yellow capped tube with 1mL collagenase solution. The crushed bone was then incubated for

45mins-1hr at 37°C with shaking at 200rpm. Once digested, 10mL complete α-MEM media was added to the bone chips. The digested bone chips were then strained through a 70μm cell strainer and combined with the flushed bone marrow. The filtered bone chip/marrow solution was then centrifuged at 800g at 4°C for 10 mins. Once centrifuged, cells were counted in white cell fluid and diluted to concentrations of 9, 18 and 36 x 105 cells per well (3mL per well) and plated in duplicate in 6 well plates. Both plates were then incubated for 9 days in a hypoxic in vitro cabinet (Coy Laboratory Products) at 37oC before staining for CFU-F colonies with 0.1% (w/v) toluidine blue in 1% paraformaldehyde as previously described [269]. Aggregates of >50 cells were scored as CFU-F-derived colonies and aggregates of >10 and <50 cells were scored as clusters.

2.6.18 BMP2 assay

Calvarial bone organ cultures established from 4 day-old mice were cultured in the presence of rhBMP-2 (50ng/mL) or media alone for 10 days as previously described [18]. Calvariae were then fixed in formalin for 24 hours, decalcified overnight (14% EDTA, pH 7.2) and embedded in paraffin. Sections (5μm) were cut 1200μm into the specimen parallel to the midline suture and stained with Haematoxylin and Eosin. The average width of new bone formed relative to the length of calvarial bone specimen analysed was quantitated using the Osteomeasure XP system (OsteoMetrics Inc.)

2.7 Molecular Biology Buffers and Reagents

2.7.1 DNA Standards for cDNA quantitatioin

A 1mg/ml stock solution was made by dissolving salmon sperm DNA in RO water overnight at 4°C. Aliquots of 100μL were stored at -20°C. Salmon sperm DNA was diluted in a 4M sodium chloride, 0.1M sodium phosphate solution for a final DNA concentration of 1.56-100μg/mL.

2.7.2 Calcium standards

Calcium chloride (11.098g) was dissolved in RO water (100mL) and stored at room temperature. A standard curve for the Cresolphthalein Complexone assay was prepared by diluting calcium stock solution from 2.5-0.25mM in RO water.

2.7.3 EDTA, 0.5M

EDTA (93.05g) was dissolved in RO water (500mL) and sodium hydroxide pellets were used to adjust the pH to 8.0. The solution was stored at room temperature.

2.7.4 Flow cytometry fixative (FACS Fix)

1xPBS was supplemented with 1% (v/v) formalin, 2% (w/v) D-glucose, and 0.02% (w/v) sodium azide and stored at 4°C.

2.7.5 Proteinase K 0.01%(w/v)

Proteinase K solution 1%(w/v) was made by dissolving proteinase K in RO water. 500µL aliquots were stored at -20°C.

2.7.6 Lysis buffer

Lysis buffer was comprised of 1% Nonidet P40, 20mM Tris, 150mM sodium chloride, 1mM ethylenediaminetetraacetic acid, 25mM sodium fluoride, 10mM sodium phosphate, 2mM vanadate and 0.5mM phenylmethylsulfonyl fluoride supplemented with complete protease inhibitors in RO water. Solution was stored at -20ºC for up to 3 months.

2.7.7 Blocking buffer

Blocking buffer was comprised of 5% Amersham block (Amersham Biosciences UK Limited, Little Chalfont, UK) in TBS / 0.1% Tween 20.

2.7.8 TBS /Tween

Tween 20 (1% v/v) was added to TBS and stored at room temperature.

2.8 Molecular Biology Techniques

2.8.1 Preparation of protein lysate

Whole cell lysates were prepared on ice from 3 x 10^6 MSC. Cells were washed once with 10mL of ice cold PBS before 300µL of lysis buffer was added and cells were scraped off the dish using a cell scraper and the cells transferred to an eppendorf tube and vortexed. This preparation was incubated on ice for approximately 30 minutes and cells were lysed by sonication for 10 seconds at 3 watts using a probe sonicator (XL2007, Misonix Inc., Farmingale, NY, USA). Cell lysate was then centrifuged for 30 minutes at 16,000*g* at 4°C. Centrifugation was sufficient to separate out the nuclear proteins and other cellular debris which formed a pellet at the bottom of the tube. The supernatant was transferred to a new tube from which an aliquot was taken and protein concentration quantitated using the RC/DC protein assay kit (Bio-Rad Laboratories, Hercules, CA, USA) according to the manufacturer's instructions.

Once protein concentrations were determined, 50µg of protein per lane was loaded onto a 12% polyacrylamide gel and electrophoresed at 15mA and 30mA through the stacking and separating gels, respectively. Gels were transferred to a Hybond-P 0.45µm PVDF membrane (Amesham Bioscience UK Limited, Little Chalfont, UK)using the SEMI-PHOR^{TM} Hoefer Semi Dry blotter (Hoefer Scienific Instruments, San Fransisco, USA) and blocked with 50mL blocking buffer overnight at 4°C. After blocking, the membranes were washed three times using TBS/Tween to remove any residual blocking buffer solids.

The membrane was submerged in this solution of primary antibody and probed overnight at 4°C on a rocker. The membrane was washed three times in TBS/Tween. Following the final wash, the membrane was probed with a secondary antibody (goat anti-mouse Ig

affinity isolated alkaline phosphatase conjugated, P326A, Chemicon Australia Pty. Ltd., Melbourne, Australia) diluted 1 in 2000 into % BSA TBS/Tween. The secondary antibody was incubated with the membrane for 1 hour at room temperature on a rocker. The membrane was washed a further three times with TBS/Tween, rinsed three times with TBS, developed using ECF substrate and visualized using a Typhoon 9410 variable model imager (GE Healthcare, Europa Bio Producs, RPN5785).

2.8.2 Preparation of total RNA

Total cellular RNA was prepared using TRIzol (Life Technologies, Carlsbad, Canada). Up to 1 x 10^6 MSC were lysed in 1mL TRIzol. Chloroform (200µL per mL) was added to this solution and tubes were shaken vigorously for 15 seconds before a 3min incubation at 30°C. The mixture was centrifuged at 12,000g for 15 mins at 2°C and resulted in phase separation. The lower two layers contained protein and DNA while RNA remained in the upper aqueous phase. This aqueous phase was transferred to a fresh tube and total RNA was precipitated using isopropanol (500µL per mL) and glycogen (1µL per mL; Sigma Aldrich, Castle Hill, Australia). This preparation was incubated for 1hr on ice to ensure maximum RNA precipitation. RNA was pelleted by centrifugation at 12,000g for 10 mins at room temperature. Supernatant was removed and the pellets washed in 1mL of 75% ethanol before being centrifuged at 7,500g for 5 minutes at 4°C. Ethanol was removed and the RNA was air dried for approximately 10 minutes. The dried RNA was then dissolved in RNAse free water at room temperature for 10 minutes before being quantitated using NanoDrop Mass spectrometer (NanoDrop ND-1000 Spectrophotometer, Biolabgroup, Clayton, Victoria, Australia) and stored at -20°C.

2.8.3 Quantification and purity analysis of RNA

The NanoDrop mass spectrometer was used for the quantification and purity analysis of RNA samples. Samples were diluted 1:1 with buffer TE before 1.5µL was added to the stage

of the NanoDrop. Absorbance at 260nm was measured to determine the quantity of the RNA and purity was measured by the ratio of A260:A280. Ratios between 1.85 and 1.95 were commonly obtained. Samples with values within this range were considered of high purity and were either used immediately to generate cDNA or stored at -20°C for future use.

2.8.4 Complementary DNA (cDNA) synthesis

Complementary cDNA was generated using the SuperScript III Reverse Transcriptase kit (Invitrogen, Carlsbad, Canada. Briefly, 1μL oligo(dT), 1-5μg total RNA, 1μL dNTP mix and distilled water to a total volume of 13μL was added to each microcentrifuge tube. This mixture was heated to 70°C for 5 minutes and then incubated on ice for 1min to denature the RNA. The tube was then briefly centrifuged before 4μL 5x first-strand buffer, 2μL 0.1M DTT and 1μL of SuperScript III RT (200 units / μL) was added. This solution was mixed with gentle pipetting before being incubated at 42°C for 1hr to allow for primer extension and first strand synthesis. The reaction was stopped by incubation at 70°C for 15 minutes leading to deactivation of the reverse transcriptase enzyme. RNAse free water was added to a volume of 50x the number of μg template RNA added originally. The resulting cDNA was used as a template for PCR reactions and stored a -20°C.

2.8.5 Real-time PCR

Real-time PCR was used to assess the levels of RNA expression for genes of interest. Beta-actin (β-actin) was used as a housekeeping control gene and samples were normalized against this control. A reaction mixture containing 2μL of sample cDNA, 7.5μL cyber green (Jomar Diagnostics, Adelaide, Australia), 0.75μL (10μM) mixed primer pairs and 4.75μL DEPEC water was mixed to generate a 15μL reaction. Iterative amplifications were performed on a Rotor Gene RG-6000 PCR machine (Corbett Research, Sydney, Australia).

2.8.6 Confirmation of osteoblast specific *Rptor* deletion

Genomic DNA was isolated from multiple tissues (bone, liver, spleen, heart, kidney, lung) and PCR used to amplify a product generated by Cre-mediated recombination of the *Rptor* gene as described in section 0.

Compact bone cells were isolated as described in section 2.6.6. RNA was isolated and quantification of changes in gene expression were conducted (described in section 2.10.7.). Amplified products were resolved on 2% agarose gels stained with Gel Red.

2.8.7 Serum biochemistry

Animals were anaesthetised with isoflurane and blood was collected by cardiac puncture, prior to sacrifice by CO_2 overdose. Cardiac blood samples were collected, spun at 800g for 15 minutes and the collected sera were stored at -20°C until analysis. The serum levels of osteocalcin, P1NP and TRAcP5 were measured by ELISA in accordance to the manufacturer's instructions (Biomedical Technologies).

2.9 Histological stains and buffers

2.9.1 Acetate-tartrate buffer

On the day of use, sodium acetate and sodium tartrate were dissolved in RO water and the pH was adjusted to 5.2 with 1.2% acetic acid final concentration of 200mM sodium acetate and 100mM sodium tartrate.

2.9.2 Acid Alcohol

A 70% (v/v) ethanol, 0.3% (v/v) hydrochloric acid solution was made by mixing RO water, ethanol and hydrochloric acid and stored at room temperature. The solution was used to differentiate Haematoxylin staining.

2.9.3 Alizarin red stain *2% (w/v)*

Alizarin Red S was dissolved in RO water for a final concentration of 2% (w/v) and pH was adjusted to 4.1-4.3 using 0.5% ammonium hydroxide. Solution was stored at room and pH adjusted prior to use.

2.9.4 Citrate/acetone/formaldehyde fixative

On day of use, citric acid solution, acetone, and formaldehyde were mixed thoroughly for a final concentration of 4.6M citric acid, 66.3% (v/v) acetone and 3.3% (v/v) formaldehyde solution.

2.9.5 Decalcification Buffer

Decalcification buffer was made to a final concentration of 0.5M EDTA and paraformaldehyde 5% (w/v) in PBS. Sodium hydroxide pellets were added as required to adjust the pH to 8.0. Solution was stored at 4°C for up to 1 month.

2.9.6 Eosin

An 11% (w/v) eosin, 1.1% (w/v) phloxine and 83% (v/v) ethanol solution was made by combining RO water, ethanol, eosin Y, phloxine and acetic acid. The solution was stored at 4°C until use.

2.9.7 Fast green stain 0.2% (w/v)

Fast green 0.2% (w/v) solution was made by dissolving fast green in RO water. The solution was stored at room temperature until use.

2.9.8 Gelatin/chromic potassium sulphate solution

A gelatine 1% (w/v), chromic potassium sulphate 0.05% (w/v) solution was made by dissolving gelatine RO water by heated stirrer. After cooling, chromium (III) phosphate

dodecahydrate was added and stirred until dissolved. The solution was stored at room temperature until use.

2.9.9 Mayer's haematoxylin

A 5% (w/v) aluminium ammonium sulphate, 0.5% (w/v) haemotoxylin, 1% (v/v) ethanol, 0.1% (w/v) sodium iodate, 2% (v/v) acetic acid and 30% (v/v) glycerol solution was made by dissolving aluminium ammonium sulphate in RO water on a heated stirrer. The solution was cooled and haematoxylin, ethanol, sodium iodate, acetic acid and glycerol were added. The solution was stored at room temperature until use.

2.9.10 Methacrylate embedding mixture

On day of use, methacrylate embedding mixture was made by mixing methyl methacrylate and polyethylene glycol (PEG) at a 10:1 ratio.

2.9.11 Oil red O 0.5%(w/v)

Oil Red O 0.5%(w/v) staining solution was prepared by dissolving Oil Red O in of isopropanol.

2.9.12 Safranin O stain, 0.1% (w/v)

Safranin O 0.1% (w/v) stained was made by dissolving Safranin O in RO water. Solution was stored at room temperature until use.

2.9.13 Sodium carbonate, 5% (w/v)

Sodium carbonate 5% (w/v) was dissolved in RO water and the solution was stored at room temperature until use.

2.9.14 Sodium thiosulphate, 5% (w/v)

Sodium thiosulfate 5% (w/v) was dissolved in mL RO water and the solution was stored at room temperature until use. The solution was used neat or was diluted 1:1 in RO water prior to use.

2.9.15 Sodium bicarbonate, 0.1% (w/v)

Sodium bicarbonate 0.1% (w/v) was dissolved in RO water on the day of use. Solution was used as a blueing agent for haematoxylin staining.

2.9.16 Sodium phosphate/citrate buffer

Citric acid and sodium phosphate were dissolved in RO water for a final concentration of 8.22mM citric acid and 4.575mM sodium phosphate. The pH was adjusted to 3.7 and the solution stored at room temperature until use.

2.9.17 Toluidine blue stain, 2% (w/v)

Toluidine blue 2% (w/v) was dissolved in sodium phosphate/citrate buffer. The pH was adjusted to 3.7, and the solution was filtered through a 0.45µm syringe filter. The solution was stored at room temperature until use.

2.10 Histomophometric techniques

2.10.1 Methacrylate processing

Samples were fixed in 10% NBF for four days at 4°C before being transferred to PBS at 4°C. Tissue was trimmed from one side of the excised tibia to ensure correct orientation. Samples were transferred to 25mL polypropylene tubes and filled with 70% acetone at 4°C for 1hr. The samples were sequentially transferred into 90% acetone for 1hr, 100% acetone for 1hr hour and 100% acetone for an additional hour. At this stage, the samples were fully dehydrated and acetone was replaced with 11mL methacrylate embedding mixture.

Samples were placed with lid loosened under vacuum for one week to allow for complete infiltration of the embedding mixture. Following complete infiltration, the embedding mixture was transferred to a waste container and replaced with 11mL methacrylate embedding mixture with Perkadox (0.04g/11mL). With lids tightened, samples were places into a glass tray containing ~3cm water and kept in an incubator at 37°C until completely polymerized. Tubes were cut open with a band-saw to remove the plastic block, which was sanded and attached to an aluminium block using Araldite® epoxy resin.

Using a Leica SM2500 motorised sledge microtome (Leica Microsytems), 5µm sections were taken from each block and attached to gelatine-coated slides using spreading solution. Slides were clamped together overnight and incubated at 42ºC to dry. Sections were deplasticised in 100% acetone for 15mins prior to staining.

2.10.2 Paraffin Processing

Excised tibiae were fixed in 10% NBF for four days at 4°C before being transferred to PBS and stored at 4°C. Samples were transferred to decalcification buffer and stored at 4°C. Samples were considered decalcified by the absence of X-Ray-detectable mineralised bone material. Once completely decalcified, samples were processed overnight for paraffin infiltration in the Neuropathology Laboratory (Hanson Institute, South Australia). Infiltrated samples were embedded into paraffin blocks using a Leica embedding station (Leica, North Ryde, NSW, Australia) and embedding cassettes (Techno-Pls, St Marys, South Australia). Longitudinal sections (5µm) were cut and were mounted on Snowcoat X-tra slides (Surgipath, Richmond, USA). Sections were dewaxed through xylene and rehydrated through 100% ethanol and H_2O prior to staining.

2.10.3 Haematoxylin and Eosin Staining

Slides were stained in haematoxylin for 5 mins. Once stained, slides were rinsed in running tap water, immersed in bicarbonate solution for 10 second differentiated in 0.3% acid alcohol for 5 seconds, rinsed in running tap water, immersed in bicarbonate solution for 10 seconds and rinsed in running tap water. Slides were counterstained with eosin for two minutes before being dehydrated in three ethanol washes and two xylene washes. Slides were then cover-slipped.

2.10.4 Safranin O Staining

Slides were rinsed twice in dH_2O and stained with Fast Green for 5 minutes. Following staining, slides were immersed once in 1% acetic acid before being counter-stained in Safranin O for 3 minutes. Slides were immersed in 1% acetic acid and thoroughly blotted on both sides before being differentiated and dehydrated by transferring quickly through three changes of ethanol and two changes of xylene. Slides were then cover-slipped.

2.10.5 Toluidine Blue Staining

Slides were rinsed twice in dH_2O and stained with 2% toluidine blue stain for 3 minutes. Following staining, slides were dipped twice in sodium thiosulphate and thoroughly blotted on both sides before being differentiated and dehydrated by transferring quickly through three changes of ethanol and two changes of xylene. Slides were then cover-slipped.

2.10.6 Imaging slides

Digital images of stained slides were generated using the NanoZoomer 2.0-HT scanner (Hamamatsu, Shizuoka, Japan). Briefly, slides were wiped clean with 70% ethanol and loaded into NanoZoomer trays. Focal points were selected manually for each slide and each slide was imaged with 20x magnification.

2.10.7 Histomorphometric analyses of osteoblasts and osteoclasts

Histomorphometric analyses were conducted in duplicate on blind-coded slides using OsteoMeasure XP (OsteoMetrics, Decatur, USA). Analyses of osteoblast numbers (N.Ob/B.Pm), osteoblast-occupied bone surface (Ob.S/BS), osteoclast numbers (N.Oc/B.Pm) and osteoclast-occupied bone surface (Oc.S/BS) in the proximal mouse tibiae were performed on toluidine blue-stained slides (described in section 2.10.5) in a designated region of primary and secondary spongiosa distal to the growth plate.

2.10.8 Growth plate analysis

Assessment of the width of the resting-, proliferating- and hypertrophic-zones were performed on safranin O/fast green-stained methacrylate sections (as described in section 2.10.4) along a central 2.32 mm region of the proximal tibial growth plate. Analyses were conducted in duplicate on blind-coded slides using OsteoMeasure XP (OsteoMetrics, Decatur, USA).

2.10.9 Histological analyses of intramedullary adipose

Histomorphometric analyses were conducted in duplicate on blind-coded slides using OsteoMeasure XP (OsteoMetrics, Decatur, USA). Histomorphometric analysis of intramedullary adipose in mouse tibiae was performed on toluidine blue- stained slides (as described in section 2.10.5) in region of the proximal trabecular region of the bone excluding cortical bone.

2.10.10Immunohistochemistry

Paraffin-imbedded sections (5μm) (described in section 2.10.2) were subjected to antigen retrieval (10mM citrate buffer (pH6.0), 95°C) for 10 min then cooled to room temperature. Endogenous peroxidase was quenched with 0.5% H_2O_2 (v/v) in methanol for 30 minutes and sections were blocked in 3% normal horse serum in PBS then incubated with the

primary antibody at 4°C overnight. Sections were washed in PBS then incubated with species-specific biotinylated secondary antibodies (anti-goat (BA-5000) and anti-rabbit (BA-1000) (Vector Laboratories, CA, USA) for 1 hr at room temperature followed by a 30-minute incubation with streptavidin-HRP (Vector Laboratories). Antibody binding was visualized using DAB as per the manufacturer's instructions (Vector Laboratories). Antibodies used for IHC: osterix (ab22552; Abcam, Cambridge, UK); eGFP (A600-101-215; Rockland, PA, USA); eYFP (A600-401-215; Rockland); osteocalcin (sc-18319; Santa Cruz Biotechnology, TX, USA) and PCNA (sc-7907; Santa Cruz Biotechnology).

2.10.11Immunofluorescence staining

For immunofluorescence staining, paraffin embedded sections were antigen retrieved (as described in section 0), incubated in blocking buffer then incubated with primary antibodies overnight at 4°C. Sections were washed with ice cold PBS then incubated with fluorescently tagged species-specific secondary antibodies (anti-chicken (Alexa Fluor488 (ab150173; Abcam) and anti-rabbit (Alexa Fluor647) (ab150067; Abcam)) at room temperature for 1 hour. Sections were washed then briefly fixed for 10 minutes (0.1% formalin in PBS) and nuclei labelled with DAPI (300nM in PBS) for 5 minutes. Sections were mounted with ProLong Gold Anti-fade reagent (Invitrogen).

Fluorescent labelling was detected using a LSM400 confocal microscope (Zeiss, Oberkochen, Germany). Antibodies used for IF: eYFP (ab13970; Abcam); perilipin (9349; Cell Signaling, MA, USA).

2.11 Calcein labelling

To measure bone formation *in vivo*, mice were subcutaneously injected with calcein at 20μg per gram of body weight then injected again after a 3-day interval. Twenty-four hours

after the second injection, tibiaes were collected, fixed in 10% NBF then embedded in methyl methacrylate as previously described [270].

Unstained, deplasticised sections of mouse tibiae were cover-slipped and used for dynamic measurements of bone formation. Mineral apposition rate (MAR) was evaluated as the mean distance between the double calcein- labelled mineralised surface (MS) and the edge the bone (BS), divided by 3 days (the interval between labelling and the death of the animals). Bone formation rate (BFR) was derived using the formula: BFR = MAR × MS/BS × 365/100.

2.12 Gross phenotype analyses

Total body weight was recorded immediately prior to culling the mouse. Tibial measurements were calculated as an average of three measurements take from the proximal tibial head to the fibular notch using electronic calipers. For spinal length, the distance from cervical 1 (C1) to lumbar 5 (L5) was measured in whole body x-ray (Faxitron LX-60, Faxitron, IL, USA) and quantitated using ImageJ. The liver, spleen, heart, kidney and lungs were isolated from mice and weighed. Weights were normalised to specimen body weight.

2.13 *μ*CT

Micro architecture of whole tibiae were analysed using μ-CT (SkyScan 1076, X-ray Microtomograph, Bruker). Bones were scanned at 50kV/100 *m*A with an isometric resolution of 8.65 μm/pixel with a 0.5mm aluminium filter, 2 frame averaging at a magnification of 6.5 μm. Scanned data was reconstructed using NRecon (SkyScan).

2.13.1 Trabecular analysis by *μ*CT

For trabecular bone, the region of analysis was determined as an area of 150 microtomographic slices, commencing 20 slices distal to the primary spogiosa for an 11mm tibia. Tibial length was used to normalise the region of analysis for individual specimens.

Regions of interest (ROI) were manually defined to exclude the cortex. Quantification of bone volume fraction (BV/TV), bone surface fraction (BS/BV), trabecular thickness (Tb.Th.), trabecular number (Tb.N), trabecular spacing (Tb.Sp), structure model index (SMI) and trabecular pattern factor (Tb.Pf) were calculated using CTAn (SkyScan).

2.13.2 Cortical analysis by μCT

For cortical bone, the region of analysis was determined as the first, middle and last microtomographic slices utilised in the trabecular analysis (section 2.13.1). Measurements of cortical thickness (Ct.Th) were calculated as the average of measurement in the lateral, medial, caudal and cranial orientation of the three microtomographic slices. Intramedullary thickness was calculated as the average of measurements in the lateral-medial and caudal-cranial orientation of the three microtomographic slices.

2.13.3 Growth plate analysis by μCT

For measurement of the growth plate width, 3-dimensional (3D) re-constructions of the μCT data were generated using DataViewer (SkyScan). Growth plate width was calculated by taking an average measurement at 20 equidistant points across the central section of the proximal growth plate.

2.13.4 Assessment of longitudinal growth

Assessment of longitudinal growth was conducted on calcien-labelled sections as described in section 0. The rate of longitudinal growth per day, was determined by measuring the average width of the newly-formed primary and secondary spongiosa identified as unstained mineral, distal to the growth plate. Analyses were conducted in duplicate on blind-coded slides using OsteoMeasure XP (OsteoMetrics, Decatur, USA).

2.13.5 Skeletal staining and analysis of newborn mice

Alizarin red and alcian blue staining of new born mice was performed as previously described [271]. Briefly, newborn pup (P0) were euthanized by CO_2 for 30mins. Pups were scalded in hot tap water (65ºC-70ºC) for 30 seconds. Skin and viscera was removed with forceps and pups were fixed in 95% ethanol overnight. Pups were transferred to acetone and incubated overnight at room temperature. Specimens were rinsed in dH_2O, covered with alcian blue stain and incubated for 24hrs. Specimen were washed 7 times in 70% ethanol for 1hr. Specimens were transferred to 1% potassium hydroxide and incubated at room temperature until visibly cleared. Specimens were counterstained in alizarin red stain overnight. Specimens were cleared in 1%potassium hydroxide/20% glycerol until appropriately cleared. Specimens were stored in glycerol:ethanol (1:1) at room temperature. The percentage of the bone (humerus and tibia) that was mineralised was calculated by dividing the length of the mineralised (alizarin red) region of the bone by the total length of the bone using Image J [272]. Images were acquired using bright field optics.

2.14 Mechanical Testing

Isolated femora were subjected to three-point bend test conducted to failure using a materials testing machine (Model 800LE4; Test Resources Inc., Shakopee MN, USA) based on previously published protocols [273] The lower span width was 5.0mm. Both the upper and lower contact anvils had a radius of 1.0mm. Femurs were positioned posterior side down on the support anvils to cause bending about the medial-lateral axis (posterior side in tension). The bones were centred on the supports to ideally induce failure at the mid-point along the diaphysis on the tension (posterior) side. A pre-load of 1N was applies and then a consistent cross-head displacement rate of 0.017mm/s for the bend test to failure. Compliance in the load-line and bend fixtures was removed from the displacement measurement by using a correction factor obtained from tests with an aluminium calibration specimen. The bend tests were conducted in

tap water at room temperature (22-24°C) and before testing, bones were kept in PBS soaked gauze at room temperature for 1hr. Loading displacement curves were analysed using standard Euler-Bernoulli theory for linear-elastic beams to obtain the flexural rigidity and the ultimate moment. Flexural rigidity was calculated by multiplying the measured displacement by $6/(3aL-4a^2)$ where L is the lower span with and is half the difference between the lower and upper span widths. The ultimate moment was calculated by multiplying the ultimate force by the value at failure. No correction for shear deformation was made.

2.15 Calvarial imaging

Calvariae were scanned by μCT as described previously in section 0. Images were acquired using Avizo® Fire (FEI Visualization Science Croup, MA, USA).

2.16 Statistical Significance

All data were graphed as mean±standard deviation (SD). Statistical analyses were performed using one-way or two-way ANOVA with the Dunnet's post-hoc test or an unpaired Students t-test using GraphPad Prism (GraphPad Software Inc, CA, USA). In all cases, $p<0.05$ was considered statistically significant.

Chapter 3 - The role of mTORC1 in osteogenic and adipogenic MSC differentiation *in vitro*

3.1 Introduction

The ageing skeleton is characterized by a reduction in bone mineral density and an increase in intramedullary adiposity [3, 111]. At the cellular level, these age-related changes are associated with an increase in bone marrow AdCs and a decrease in bone-forming OBs [2]. As AdCs and OBs originate from a common multi-potent MSC progenitor [112-115], it has been postulated that the shift in the AdC:OB ratio occurs in response to increased AdC differentiation at the expense of OB differentiation [116, 117]. In support of this, functional comparisons of MSCs isolated from osteoporotic and healthy individuals show that whilst they are similar in morphology, size and cell surface antigen expression, MSCs from osteoporotic individuals exhibit a reduced propensity for osteogenic differentiation [3, 4].

In response to extracellular factors, MSCs differentiate into a range of cell types including AdCs, OBs, chondrocytes and myocytes [81, 112, 274, 275]. MSC differentiation towards each cell lineage is a tightly-regulated process governed by extracellular and environmental cues. Osteogenic MSC differentiation is regulated by a variety of local and systemic factors, and proceeds through a series of distinct developmental stages that are characterised by the expression of specific molecular and functional markers [30, 81]. BMPs, TGFβ and Wnt molecules all play an important role in OB development and function [33, 276]. BMPs stimulate bone formation *in vitro* and *in vivo* by activating a complex network of signalling molecules including SMADs, ERK1/2 and p38, culminating in the transcriptional up-regulation of key OB genes *RUNX2* and *SP7* [277, 278]. RUNX2 is the obligate OB transcription factor that regulates, and is in turn regulated by, a number of factors to control the expression of genes involved in OB differentiation and function.

Similarly, adipogenic MSC differentiation is regulated by a variety of local and systemic factors which guide cells through a series of distinct developmental stages. Members of the C/EBP family, C/EBPβ and C/EBPδ, are expressed in pre-adipocytes and subsequently activate

expression of PPARγ and C/EBPα [108, 110]. PPARγ and C/EBPα then form a positive feedback loop to maintain and enhance their expression and activate adipogenic genes required for function and maintenance of differentiated adipocytes and accumulation of triglycerides.

In recent years, considerable effort has been directed toward defining the molecular mechanisms and signalling pathways associated with MSC commitment to both the osteogenic and adipogenic lineages. Several signalling pathways, including Wnt/β-catenin, BMP/SMAD, IHH, MAPK and Insulin/IGF1 have been shown to be involved [33, 124-127].

Previous studies have shown that the mTOR signalling pathway plays an important role in the adipogenic program, as rapamycin, an allosteric mTOR inhibitor, inhibits adipogenesis [19-23] whilst deletion of TSC2, a negative regulator of mTOR, promotes adipogenesis [23]. The role of mTOR in osteogenic MSC commitment, however, is less clear as rapamycin-mediated mTOR inhibition has been shown to have both inhibitory [24-29] and stimulatory [13, 16-18] effects on osteogenesis, a disparity which may reflect the nature of the cell types and treatment conditions used in each study. Furthermore, rapamycin sequesters FKBP12 [279], a negative regulator of TGFβ1 signalling, and thus the pro-osteogenic effects of rapamycin may be the indirect result of TGFβ1 activation.

As outlined in Chapter 1, mTOR exists in two distinct multi-protein complexes, termed mTORC1 and mTORC2, which can be distinguished by their unique adaptor proteins, raptor and rictor, respectively. As there are currently no commercially available mTORC1- or mTORC2- specific inhibitors, studies are now utilising genetic approaches to delineate the roles of these complexes in various biological contexts. In this chapter, primary multipotent MSC populations were isolated from the long bones of R26eYFP-*Rptor*$^{fl/fl}$ mice and the Cre-loxP system was used to delete the mTORC1-specific protein raptor in these cells. The effect of *Rptor* deletion on osteogenic and adipogenic MSC differentiation was then examined using lineage-specific culture conditions to promote MSC differentiation into mineralised matrix-producing OBs or lipid-laden AdCs respectively.

3.2 Results

3.2.1 Generation of primary *Rptor* knockout (RapKO) MSCs.

As outlined in Figure 3.1, primary compact bone-derived MSCs were isolated from the humeri, femora, tibiae and iliac crests of R26eYFP-*Rptor*$^{fl/fl}$ mice (n≥6 mice per harvest), according to established protocols[264]. Following collagenase digestion, mature haematopoietic cells were removed from this heterogeneous cell suspension by targeting the haematopoietic cell antigens B220, Gr-1, CD3, CD4, CD5, CD8, CD11b and Ter-119. Following this lineage depletion, multipotent Lin-CD51-CD45-CD31-Sca1+ R26eYFP-*Rptor*$^{fl/fl}$ MSCs were isolated by fluorescence-activated cell sorting (FACS).

Following *in vitro* expansion of the Lin-CD51-CD45-CD31-Sca1+ R26eYFP-*Rptor*$^{fl/fl}$ MSC population, these cells were infected with a lentivirus encoding a tamoxifen (TAM)-inducible self-deleting Cre recombinase (CreER^{T2}) or empty vector control. Infected cells harbouring stable integration of CreER^{T2} or empty vector control were subsequently isolated based on eGFP expression using FACS. As CreER^{T2} remains inactive in the cytoplasm until exposed to TAM [280], CreER^{T2}-infected R26eYFP-*Rptor*$^{fl/fl}$ MSCs were cultured in the presence of TAM to induce *Rptor* deletion (herein referred to as "RapKO" MSCs). To control for any off-target effects related to TAM treatment in these cells, separate populations of CreER^{T2}-infected R26eYFP-*Rptor*$^{fl/fl}$ MSCs were treated with vehicle alone (herein referred to as "Cre-TAM" MSCs). Furthermore, to control for off-target effects related to CreER^{T2} expression, R26eYFP-*Rptor*$^{fl/fl}$ vector control MSCs were also treated with TAM (herein referred to as "vector+TAM") or vehicle alone (herein referred to as "vector-TAM"), and used as additional control cell populations in the studies outlined below.

Figure 3.1 - Generation of primary RapKO MSC populations: (A) Compact bone MSCs were isolated from the fore- and hind-limbs of 6-7 week old *Rptor*$^{fl/fl}$ mice (n≥6 per harvest) following collagenase digestion. (B) Multipotent Lin-CD51-CD45-CD31-Sca1+ *Rptor*$^{fl/fl}$ MSCs were isolated from the heterogenous bone cell population via FACS and expanded *in vitro* (orange cells). (C) Multipotent R26eYFP- *Rptor*$^{fl/fl}$ MSCs were infected with a lentivirus encoding a tamoxifen (TAM)-inducible Cre recombinase (CreERT2) or empty vector control. The Lentiviral vector (LEGO-iG2) also contains a floxed eGFP cassette. (D) GFP+ MSCs harbouring Cre recombinase or vector control were isolated using FACS (green cells) and expanded *in vitro*. (E) Transduced GFP+ *Rptor*$^{fl/fl}$ cells were treated with TAM to induce Cre-mediated deletion of *Rptor* (RapKO MSCs, blue cells). To produce control MSC cultures containing normal *Rptor* expression, CreERT2-infected cells were cultured in the absence of TAM (Cre –TAM) and vector control cells cultured in either the presence or absence of TAM (vector +TAM and vector –TAM) were used.

A

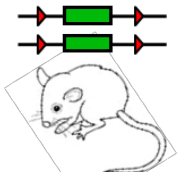

Bone lining cells were isolated from the long bones of *Rptor*$^{fl/fl}$ mice via collagenase digestion.

B

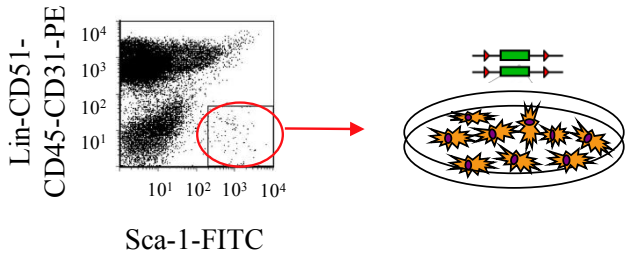

FACS was used to isolate multipotent Lin-CD51-CD45-CD31-Sca1+ MSCs.

C

Multipotent *Rptor*$^{fl/fl}$ MSCs were infected with lentivirus encoding a self-deleting tamoxifen (TAM)-inducible Cre recombinase (CreER^{T2}).

D

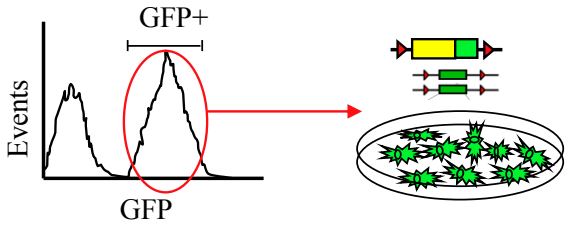

FACS was used to isolate GFP+ MSCs with stable integration of CreER^{T2} or vector control.

E

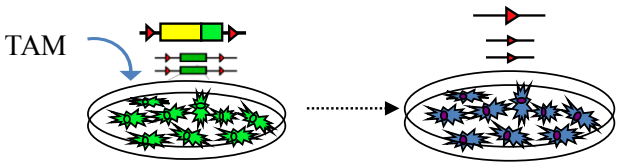

Transduced GFP+ MSCs were treated with tamoxifen (TAM) to induce Cre-mediated *Rptor* deletion to generate *Rptor* knockout (RapKO) MSCs.

3.2.2 Confirmation of *Rptor* knockout in transduced MSCs.

To confirm TAM-induced nuclear translocation of CreER^{T2} and subsequent Cre recombinase activity in transduced cells, GFP expression was monitored using flow cytometry. This was facilitated by the presence of a floxed GFP cassette within the CreER^{T2} vector, which upon induction of Cre activity, resulted in the loss of GFP expression. As outlined in Figure3.2A, GFP expression was analysed after 0, 2, 6 and 8 days of 0.5μM TAM treatment in CreER^{T2}-infected RapKO MSCs, to determine the optimal length of TAM-treatment required for complete gene deletion. Over the 8 days of TAM treatment, a progressive decrease in GFP expression was observed, with a complete loss of GFP expression observed after 8 days (Figure 3.2A). Based on this information, 8 days of TAM treatment was used to induce Cre-mediated gene deletion for all subsequent studies.

To confirm successful *Rptor* deletion in RapKO MSCs, CreER^{T2}-infected MSCs and vector control MSCs were treated for 8 days with TAM, and whole cell lysates were prepared. Western blot analyses were then performed using antibodies directed against raptor, rictor and mTOR, and downstream effectors of the mTOR signalling pathways (P-S6K$_{T389}$, P-Akt$_{S473}$, P-Akt$_{T308}$, P-IRS1$_{S636/639}$, P-FOXO1/3a$_{T24/32}$). As shown in Figure 3.2B, there was a significant reduction in levels of raptor protein expression in RapKO cells and *Rptor* deletion resulted in a decrease in the activation status of the primary mTORC1 substrate S6K. Furthermore, deletion of *Rptor* resulted in the hyperphosphorylation of Akt$_{Thr308}$, IRS-1 and FOXO1/3a signifying loss of mTORC1 mediated feedback regulation of PI3K/Akt and insulin signalling. No changes in the levels of mTOR or rictor protein, nor downstream mTORC2 targets (e.g. Akt$_{S473}$), were observed in RapKO MSCs (Figure 3.2B).

3.2.3 Proliferative capacity is reduced in RapKO MSCs.

As mTORC1 is known to regulate cell growth and proliferation, the effect of *Rptor* knockout on MSC proliferation was examined. In these studies, equal numbers of RapKO and

Figure 3.2 - Verification of *Rptor* deletion in MSC *in vitro*: Multipotent Lin-CD51-CD45-CD31-Sca1+ R26eYFP- *Rptor*$^{fl/fl}$ MSCs stably infected with a lentivirus encoding a TAM-inducible Cre recombinase were treated with TAM for 8 days to induce the translocation of CreERT2 to the nucleus. (A) Flow cytometry was used to monitor the loss of GFP expression, a surrogate marker of Cre activity, over the 8 days of TAM treatment. A representative histogram of GFP expression following 0, 2, 6 and 8 days of TAM treatment is shown relative to control (Cre-TAM). (B) Lysates were prepared from control (vehicle-treated CreERT2-infected cells) and RapKO MSCs. Western blot analyses were performed using antibodies directed against the proteins indicated to confirm the deletion of *Rptor* and determine the effect of *Rptor* deletion on downstream mTOR signalling pathways. Membranes were probed with an anti-HSP90 antibody to confirm equal protein loading.

A

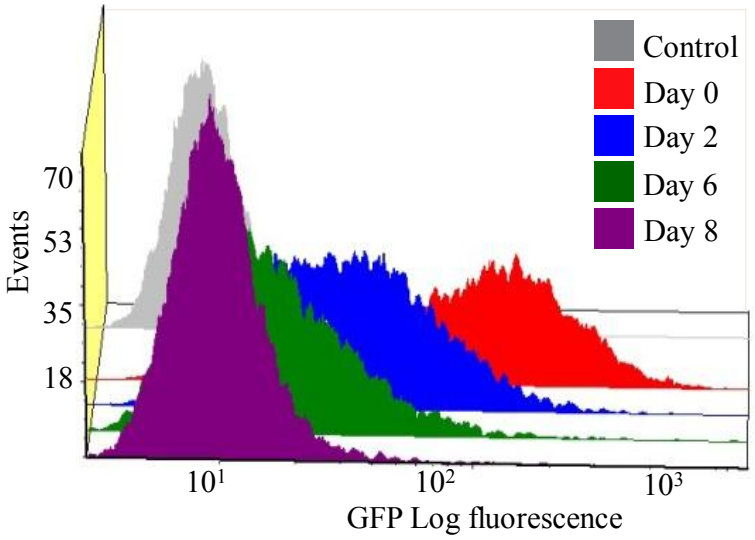
Control
Day 0
Day 2
Day 6
Day 8
Events
70
53
35
18
10^1
10^2
10^3
GFP Log fluorescence

B

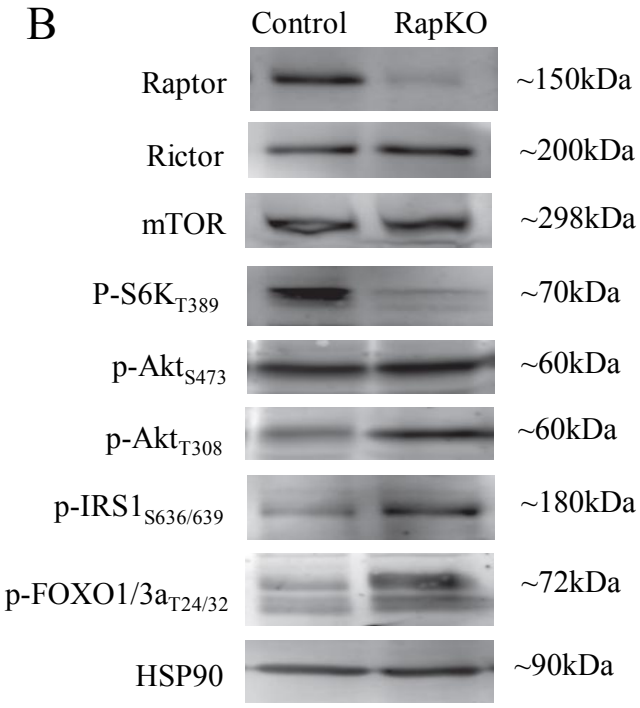
Control
RapKO
Raptor
~150kDa
Rictor
~200kDa
mTOR
~298kDa
P-S6K$_{T389}$
~70kDa
p-Akt$_{S473}$
~60kDa
p-Akt$_{T308}$
~60kDa
p-IRS1$_{S636/639}$
~180kDa
p-FOXO1/3a$_{T24/32}$
~72kDa
HSP90
~90kDa

control cells were seeded into 96-well plates and the relative number of metabolically active cells present after 1, 3, 5, and 7 days of culture was assessed using the colorimetric WST-1 assay. As outlined in Figure 3.3A, a significant decrease in the number of viable cells was observed in RapKO MSCs compared to controls after 3, 5 and 7 days of culture (Figure 3.3A).

The proliferative activity of RapKO and control cells was also examined using bromodeoxyuridine (BrdU), a synthetic nucleoside analogue of thymidine, that is incorporated into the newly-synthesised DNA of replicating cells[281]. In these studies, equal numbers of RapKO and control cells were seeded into 96 well plates and BrdU was added after 3 and 5 days of culture to label replicating cells. As shown in Figure 3.3B, RapKO cells displayed a significant decrease in proliferative activity compared to controls after 3 days (RapKO: 0.12±0.023 units *vs* control: 0.57±0.061 units) and 5 days (RapKO: 0.26±0.051 units *vs* control: 0.57±0.093 units) of culture.

3.2.4 The reduced proliferation of RapKO MSCs is not associated with apoptosis.

To determine whether the reduction in proliferation in RapKO MSCs was attributable to an increase in the rate of apoptosis and necrosis, RapKO and control MSCs were stained with Annexin V and 7-aminoactinomycin D (7-AAD), markers of early- and late-stage cell death, respectively. These markers enable the analysis of 4 distinct cell populations: viable cells (AnnV-/7AAD-), cells undergoing early apoptosis (AnnV+/7AAD-), cells in late apoptosis (AnnV-/7AAD+) and dead cells (AnnV+/7AAD+). As shown in Figure 3.4, whilst no significant difference in Annexin V labelling was observed (RapKO: 9.49% *vs* control: 11.04%), a 2.7-fold increase in 7-AAD incorporation was evident in RapKO MSCs (16.95%) compared to controls (6.36%).

Figure 3.3 - The effect of *Rptor* deletion on MSC proliferation *in vitro*: RapKO and control MSCs were cultured for 7 days and proliferation assessed using WST-1 and BrdU assays. (A) Cumulative data from WST-1 analysis showing the number of metabolically active cells following 1, 3, 5 and 7 days of culture. (B) BrdU incorporation by proliferating cells following 3 days (top) and 5 days (bottom) of culture. Data are expressed as mean ± SD of quintuplicate wells of a representative experiment of three. **p<0.005, ***p<0.001, ****p<0.0001, One-way ANOVA with Tukey's Post-Hoc test.

A

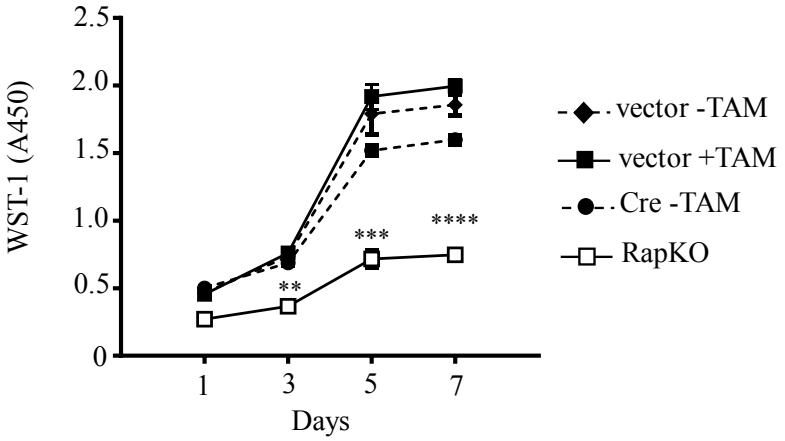
2.5
2.0
1.5
1.0
0.5
0
WST-1 (A450)
1
3
5
7
Days
**
***
****
vector -TAM
vector +TAM
Cre -TAM
RapKO

B

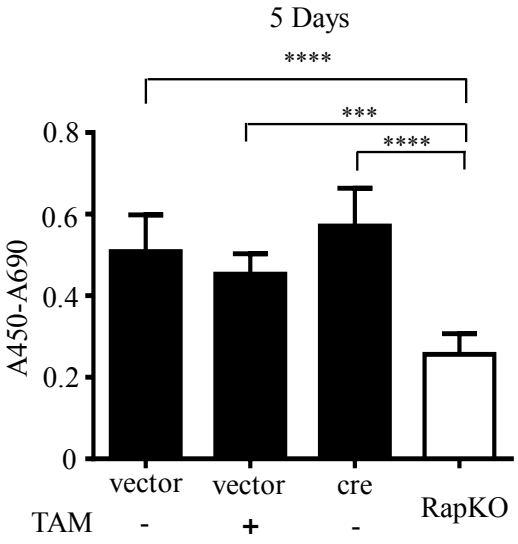
5 Days
****
***
****
0.8
0.6
0.4
0.2
0
A450-A690
vector
vector
cre
RapKO
TAM
-
+
-

Figure 3.4 - The effect of *Rptor* deletion on MSC apoptosis *in vitro*: RapKO and control MSCs were stained with Annexin V (marker of early apoptosis) and 7-AAD (marker of necrotic cells) for 15 minutes and analysed immediately by flow cytometry. Representative dot plots illustrating the percentage and distribution of Annexin V and 7-AAD labelled cells are shown for RapKO MSCs (bottom right) and control MSCs.

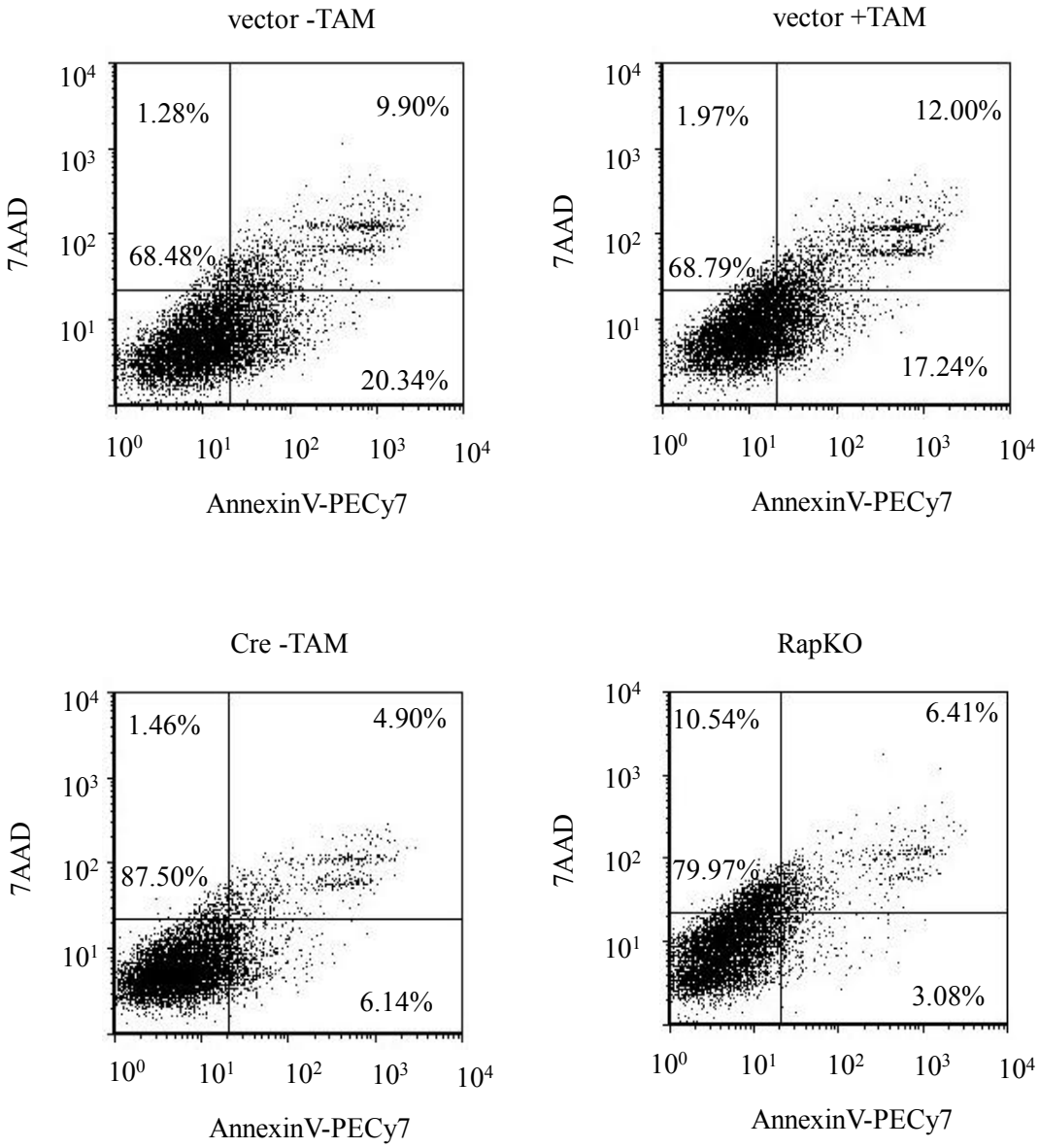
vector -TAM
1.28%
9.90%
68.48%
20.34%
7AAD
AnnexinV-PECy7
vector +TAM
1.97%
12.00%
68.79%
17.24%
7AAD
AnnexinV-PECy7
Cre -TAM
1.46%
4.90%
87.50%
6.14%
7AAD
AnnexinV-PECy7
RapKO
10.54%
6.41%
79.97%
3.08%
7AAD
AnnexinV-PECy7

3.2.5 Increased osteogenic MSC differentiation in RapKO MSCs.

To examine the role of mTORC1 in osteogenic MSC differentiation, the ability of RapKO MSCs and control MSCs to differentiate into bone-forming OBs was examined *in vitro*. In these studies, RapKO and control cells from three separate MSC harvests were cultured under osteoinductive conditions (ie. under hypoxic culture conditions [5% O_2, 10% CO_2, 85% N_2] in the presence of 20% FCS, 10^{-8}M dexamethasone, 100μM ascorbate, 4mM KH_2PO_4) for 22 days and the mineral content of cultures was visualised using Alizarin Red staining. As shown in Figure 3.5, RapKO MSCs produced a visible increase in mineralised matrix deposition compared to control MSCs. In order to quantitate the amount of mineral produced, the mineralised matrix in replicate wells was dissolved using hydrochloric acid and the calcium content quantified using the cresolphthalein complexone assay. Calcium levels were normalised to DNA content, to correct for differences in cell numbers between MSC populations. Following 22 days of osteoinductive culture, a significant increase in mineral matrix deposition was seen in RapKO MSCs compared to all controls. Notably, when quantitated, RapKO cells showed a 5-fold increase in mineralised matrix production (10.79±0.77 mM/μg DNA) compared Cre-TAM controls (1.93±0.36 mM/μg DNA).

As previously discussed, osteogenic differentiation can be characterized by the expression of key transcription factors and proteins which mark the various stages from initial osteogenic commitment through to mature OBs. To gain insight into the molecular mechanisms by which *Rptor* deletion promotes osteogenic MSC differentiation, temporal gene expression analyses were performed. For these studies, RapKO and control MSCs were cultured under osteogenic conditions for 22 days and total RNA was harvested at 0, 4, 7, 11, 14, 18 and 22 day time points. The mRNA levels of osteogenic genes were then examined by real time PCR and the data were normalized to β-actin. In these analyses, RapKO cells displayed a strong up-regulation of genes involved in OB differentiation including the osteogenic transcription factors

Figure 3.5 - The effect of *Rptor* deletion on osteogenic MSC differentiation *in vitro*: RapKO and control MSCs were cultured under osteoinductive culture conditions for 22 days, with media changed twice-weekly. After 22 days, the amount of acid-solubilised calcium was quantitated and normalised to cell number. Replicate wells were stained with Alizarin Red. Data are expressed as the mean ± SD of quadruplicate wells from a representative experiment of three. ****$p<0.0001$, one-way ANOVA with Tukey's Post-Hoc test.

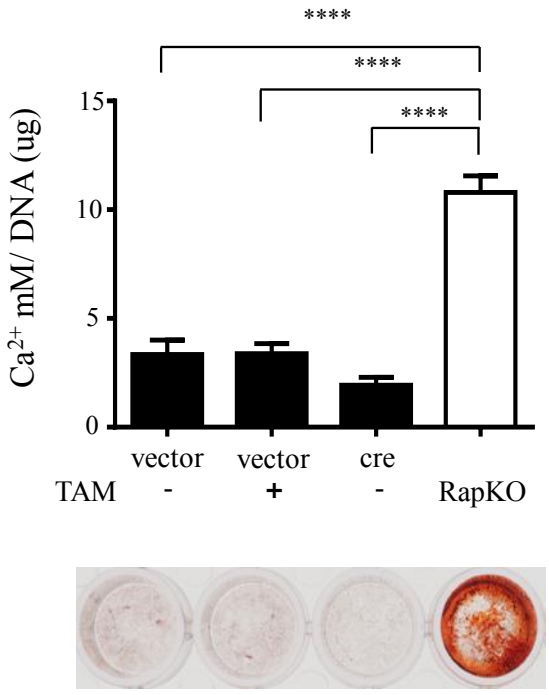
****
****
****
15
10
5
0
Ca2+ mM/ DNA (ug)
vector
vector
cre
TAM
-
+
-
RapKO

Cbfa-1 (*Runx2*) and osterix (*Sp7*), and the marker of OB function, alkaline phosphatase (*Alpl*) when compared to controls (Figure 3.6). RapKO cells also exhibited an increase in the expression of BMP-2 and other osteogenic TGFβ superfamily members such as inhibinβ A chain (*Inhba*) and inhibinβ E chain (*Inhbe*) compared with controls (Figure 3.6). In contrast, expression of integrin binding sialoprotein (*Ibsp*) was strongly down-regulated in RapKO cultures compared to controls, as was the expression of noggin (*Nog*), a negative regulator of BMP signalling (Figure 3.7).

3.2.6 Decreased adipogenic MSC differentiation in RapKO MSC

To determine the effects of mTORC1 activity on adipogenesis, the ability of MSCs to differentiate into functional AdCs was examined. RapKO and control cells were cultured under adipogenic culture conditions (ie. under hypoxic culture conditions [5% O_2, 10% CO_2, 85% N_2] in the presence of 20% FCS, 10^{-6}M dexamethasone, 60μM indomethacin, 1μg/mL insulin) for MSCs exhibited a marked decrease in lipid accumulation compared to all controls. When the number of lipid-laden, Nile Red-stained cells was quantitated and normalised to total cell number (as determined by enumeration of DAPI-stained cell nuclei), a 1.8-fold decrease in AdC formation was observed in RapKO MSCs (0.14±0.06 AdCs/total cells) compared to Cre-TAM controls (0.24±0.05 AdCs/total cells) (Figure 3.8B).

To gain an insight into the molecular mechanisms by which *Rptor* deletion inhibits adipogenic MSC differentiation, temporal gene expression analyses were performed. RapKO and control cells were cultured under adipogenic culture conditions for 8 days and RNA was harvested at 0, 2, 4, 6 and 8 day time points. The mRNA levels of adipogenic genes were examined by real-time PCR and data were normalized to β-actin. Consistent with the marked inhibition of AdC formation in RapKO MSCs, the expression of *Cebpa* and *Pparg*, transcription factors essential for adipogenesis, and *Adipoq*, an adipokine, was significantly down-regulated in RapKO MSCs compared to controls at all time points examined (Figure 3.9).

Figure 3.6 - The effect of *Rptor* deletion on osteogenic gene expression *in vitro*: RapKO and control MSCs (Cre-TAM) were cultured under osteoinductive culture conditions for 22 days and RNA was harvested at twice-weekly time points. The mRNA levels of osteogenic genes was examined by real time PCR and data were normalized to β-actin. Data are expressed as the mean ± SD of quadruplicate wells from a representative experiment of three. *$p<0.05$, **$p<0.005$, ***$p<0.001$, ****$p<0.0001$, t-test.

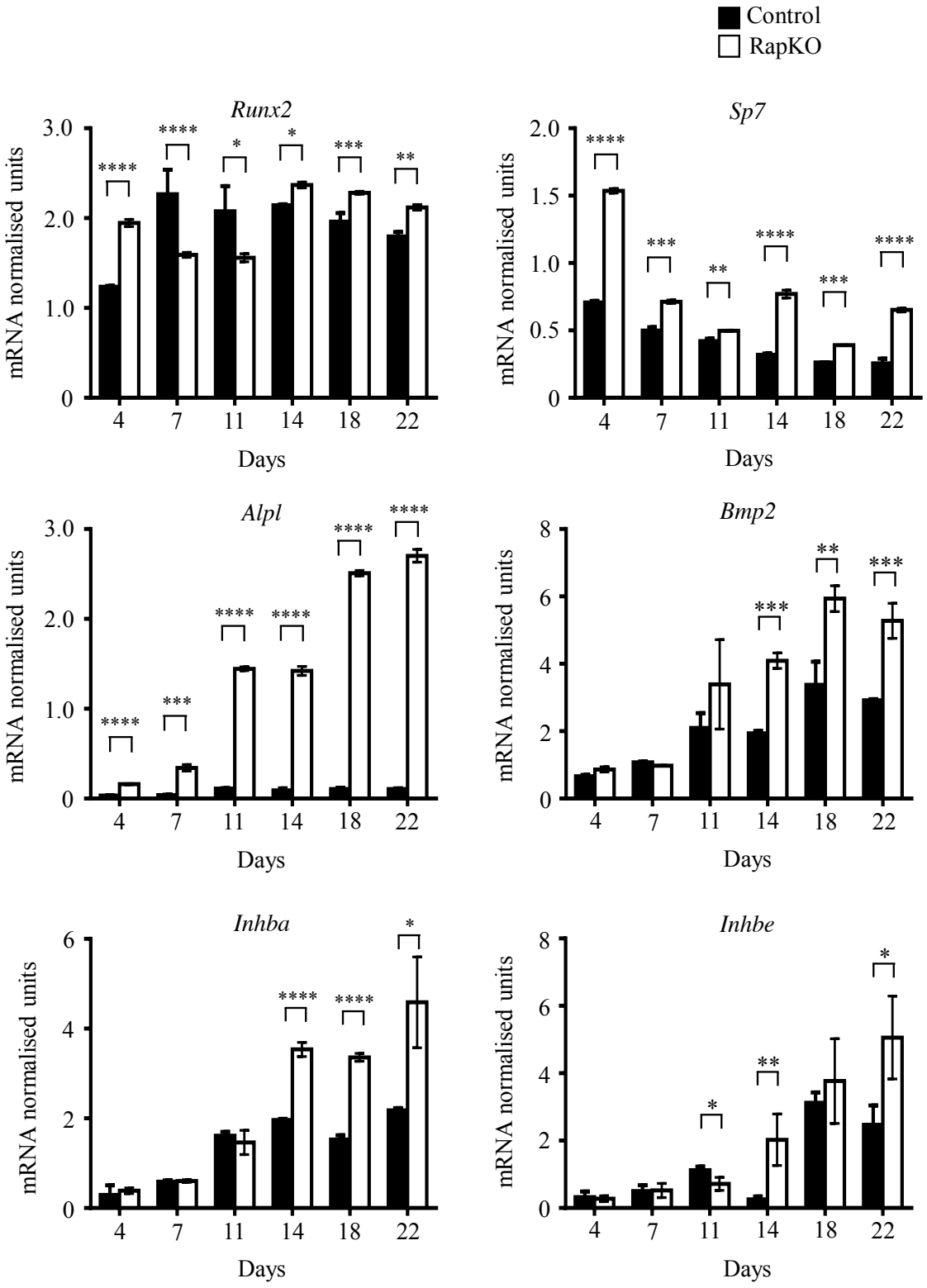
Control
RapKO
Runx2
Sp7
Alpl
Bmp2
Inhba
Inhbe
mRNA normalised units
Days
4
7
11
14
18
22

Figure 3.7 - The effect of *Rptor* deletion on the expression of osteogenic genes *in vitro*: RapKO and control MSCs were cultured under osteoinductive culture conditions for 22 days and RNA was harvested at twice-weekly time points. The mRNA levels of osteogenic genes was examined by real time PCR and data were normalized to β-actin. Data are expressed as the mean ± SD of quadruplicate wells from a representative experiment of three. *$p<0.05$ ***$p<0.001$, ****$p<0.0001$, t-test.

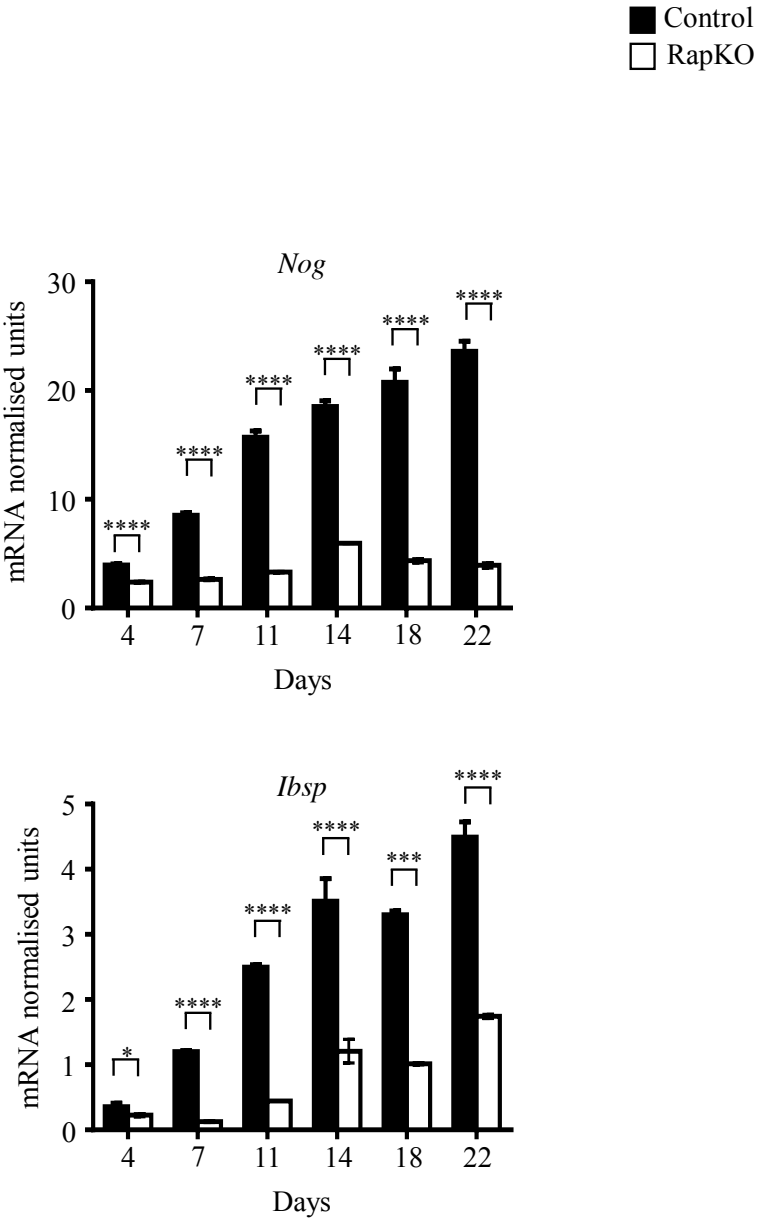
Control
RapKO
Nog
mRNA normalised units
30
20
10
0
****
4
7
11
14
18
22
Days
Ibsp
mRNA normalised units
5
4
3
2
1
0
*
***
4
7
11
14
18
22
Days

Figure 3.8 - The effect of *Rptor* deletion on adipogenic MSC differentiation *in vitro*: RapKO and control MSCs were cultured under adipogenic culture conditions for 8 days. (A) Adipocytes were visualised using Nile Red, a fluorescent stain for intracellular lipid droplets. (B) The number of adipocytes was quantitated using ImageJ and normalised to cell number (quantitated from the number of DAPI-stained cell nuclei present). Data are expressed as the mean ± SD of a representative experiment of three. *$p<0.05$, **$p<0.01$, One-way ANOVA with Tukey's post-hoc test.

A

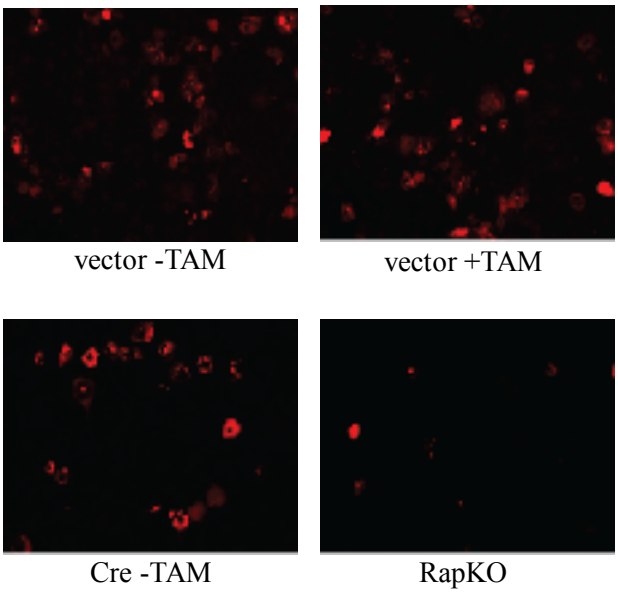
vector -TAM
vector +TAM
Cre -TAM
RapKO

B

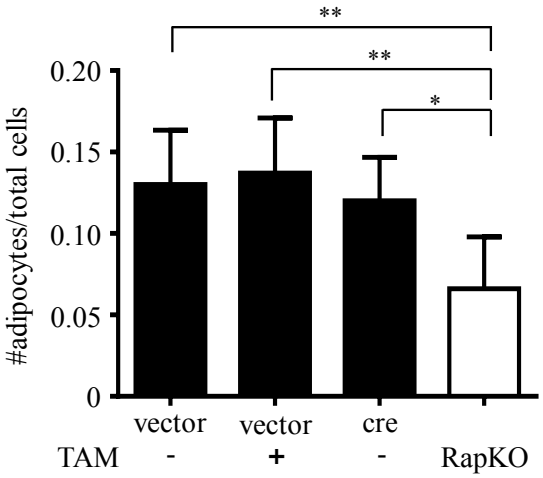
**
**
*
0.20
0.15
0.10
0.05
0
#adipocytes/total cells
vector
vector
cre
RapKO
TAM
-
+
-

Figure 3.9 - The effect of *Rptor* deletion on adipogenic gene expression *in vitro*:

RapKO and control (Cre-TAM) MSCs were cultured under adipogenic culture conditions for 8 days and RNA was harvested at stated time points. The mRNA level of adipogenic genes was examined by real-time PCR and data were normalised to β-actin. Data are expressed as the mean ± SD of quadruplicate wells from a representative experiment of three. **p<0.005, ***p<0.001, ****p<0.0001, t-test.

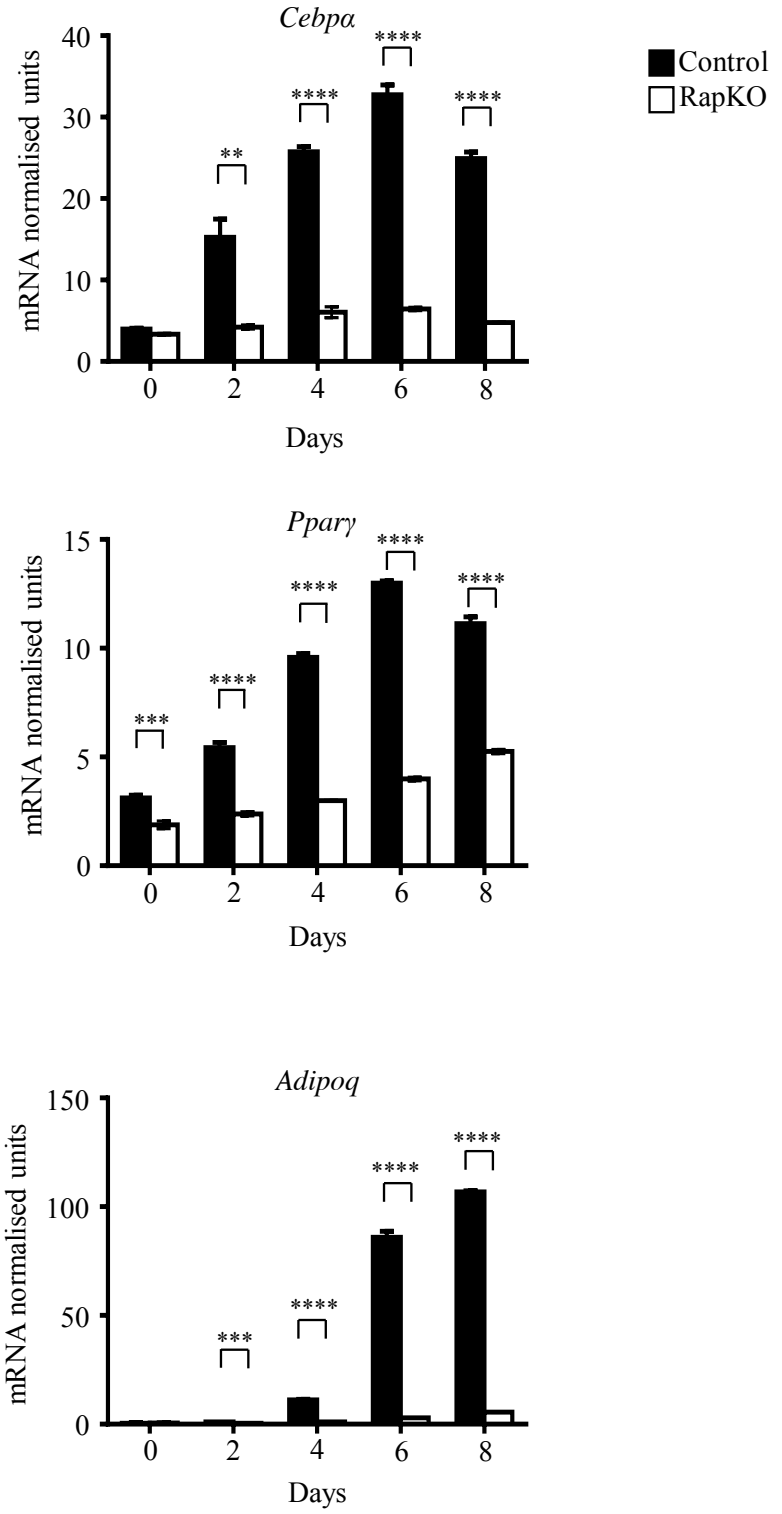
Cebpα
mRNA normalised units
40
30
20
10
0
**
****
****
****
0
2
4
6
8
Days
Control
RapKO
Pparγ
mRNA normalised units
15
10
5
0
***
****
****
****
0
2
4
6
8
Days
Adipoq
mRNA normalised units
150
100
50
0
***
****
****
****
0
2
4
6
8
Days

3.3 Discussion

The mTOR signalling pathway is a fundamental nutrient-sensing pathway in mammalian cells. Numerous studies have demonstrated a role for mTOR in directing MSC lineage commitment, however, many of these studies have utilised rapamycin and related analogues which, while they primarily target mTORC1, also target mTORC2 [154]. Furthermore, these studies have yielded conflicting results regarding the role of mTOR in osteogenesis [13, 16-18, 24-27] and adipogenesis[23, 203, 240, 282]. These conflicting results are likely attributable to variations in cell types and stages of lineage maturity as well as culture conditions used. [162, 283]. Therefore, to circumvent these issues, a genetic approach was employed in this study to specifically disrupt mTORC1 in primary murine MSCs and thus investigate the role of mTORC1 in MSC differentiation.

In this study, primary MSC populations which lacked raptor were generated via Cre-mediated deletion of exon 6 of the *Rptor* gene. Western blot analysis confirmed a significant reduction in raptor protein levels in RapKO cells, however as has been previously reported in other studies, low levels of residual raptor protein expression were observed [284-287]. These Western blot analyses also confirmed a decrease in the phosphorylation of downstream targets of mTORC1 such as S6K, and the hyperphosphorylation of Akt_{Thr308}, IRS-1 and FOXO1/3a. Importantly, deletion of *Rptor* had no effect on the protein levels of mTOR or rictor, the unique component of mTORC2. Furthermore, the activity of mTORC2 was not affected by *Rptor* deletion, as evidenced by the phosphorylation of downstream target of mTORC2, Akt_{Ser473}. Whilst RapKO MSCs were viable, there was a significant reduction in their proliferative capacity, consistent with previous reports in other cell types including human embryonic stem cells [205] and murine derived pre-osteoblast cell lines[25].

The loss of mTORC1 activity in primary murine MSCs caused an increase in the osteogenic potential of these cells, as demonstrated by a significant increase in the production of mineralised matrix compared to controls. Furthermore, there was a strong up-regulation of

genes involved in OB differentiation such as the osteogenic transcription factors *Runx2* and osterix (*Sp7*), and the marker of OB function, alkaline phosphatase (*Alpl*) observed in RapKO MSCs compared to controls. This was supported by an up-regulation in the expression of the *Bmp2*, which is known to be an important inducer of RUNX2 expression, OB maturation and mineral formation. Similar differences in osteogenic gene expression have also been noted in studies examining the pro-osteogenic properties of rapamycin *in vitro* [17, 18, 205, 288]. In addition to BMP-2, mRNA levels of other osteogenic TGFβ superfamily members such as inhibin beta A chain (*Inhba*) and inhibin beta E chain (*Inhbe*) were also elevated after 14-22 days of osteogenic culture, which coincides with the onset of mineralised matrix production.

The expression of Noggin, a potent BMP antagonist that inhibits osteogenesis *in vitro* and is associated with decreased bone formation *in vivo* [289], was also strongly down-regulated in RapKO cells, consistent with a BMP-mediated induction of osteogenesis. While further studies are required to characterise the precise mechanisms by which mTORC1 inhibition promotes osteogenesis, the up-regulation of multiple TGFβ superfamily members in RapKO MSCs suggests that it likely occurs through autocrine and/or paracrine mechanism(s) involving BMPs and TGFβ/activin signalling. While the role of BMPs in promoting osteogenesis is well-established, their roles are complex and dependent on dose and receptor subtype [290].

In this study, RapKO MSCs also displayed a decreased capacity for adipogenic differentiation and lipid accumulation. A significant reduction was observed in the mRNA expression of the adipogenic transcription factors PPARγ and C/EBPα, and the mature AdC marker, adiponectin, in RapKO MSCs compared to controls. The anti-adipogenic effect *Rptor* deletion in MSCs is consistent with observations in previous *in vitro* studies targeting mTOR through rapamycin administration in both mouse and human pre-AdCs [19, 20, 22, 291]. It has been shown that insulin signalling is essential for proper induction of PPARγ [292], with further observations indicating downstream mTORC1 activity is required for expression of PPARγ and C/EBPs leading to activation of the adipogenic cascade [21, 23, 203, 293].

Collectively, the data presented in this chapter demonstrates that mTORC1 activity is involved in directing MSC fate towards the osteogenic and adipogenic lineages. Given that PI3K/Akt/mTOR signalling is the primary nutrient-sensing pathway in mammalian cells, it is possible that mTORC1 signalling, induced by high environmental nutrient availability, guides MSC differentiation towards the adipogenic lineage in order to prevent lipotoxicity in other cells[294]. Conversely, when nutrient levels fall, suppression of mTORC1 signalling promotes MSC differentiation towards the osteogenic lineage by down-regulating adipogenic transcription factors and inducing the expression of osteogenic transcription factors.

While *in vitro* models provide important insight into biological processes, they provide limited understanding of the effects of gene deletion in the context of pre-natal and post-natal mammalian development. To address these limitations, transgenic mouse models have been developed in order to gain insight into the physiological and pathophysiological role of candidate genes of interest. In relation to the mTORC1 pathway, global knockout of *Rptor* results in embryonic lethality [202], necessitating the use of the Cre-loxP system of targeted transgenesis to investigate the role of mTORC1 in the development and function of specific tissues such as fat [202] skeletal muscle [241], haematopoetic stem cells [295], oocytes [246] and embryonic mesenchyme[286], among others. In the following chapters, the role of mTORC1 in skeletal development and homeostasis was examined in conditional knockout mice in which *Rptor* is specifically deleted in Osx-expressing pre-OB cells.

Chapter 4 - The phenotypic characterisation of osteoblast-specific *Rptor* knockout mice

4.1 Introduction

In Chapter 3, deletion of *Rptor* in compact bone derived MSCs was shown to promote osteogenesis and inhibit adipogenesis, suggesting that mTORC1 plays an important role in directing MSC fate determination. These findings are consistent with a number of previous *in vitro* studies which suggest that mTORC1 can regulate MSC differentiation [13, 16-18].

The pro-osteogenic effects of suppressing mTORC1 function in MSCs raises the possibility of utilising mTORC1 inhibitors to promote bone *in vivo*. Rapamycin, a potent inhibitor of mTORC1, is used clinically as an immunosuppressant in graft-versus-host-disease [217-222]. Pre-clinical studies in animals have shown that rapamycin analogues decrease bone resorption [296, 297]. Rapamycin is also used clinically in preventing mTORC1-mediated cancer cell proliferation with $p70^{S6K}$ and 4EBP1, direct downstream targets of mTORC1, identified as being over-expressed and/or constitutively activated in several cancer types [223-230]. Within these clinical contexts, rapamycin and related analogues have been shown to have protective effects on the skeleton. For example, while rapamycin preserves bone mass, commonly-used immunosuppressive drugs, including cyclosporine A (CsA), are associated with rapid turnover of bone resulting in severe osteopenia [231-235]. Additionally, rapamycin reduces bone loss in patients suffering from both osteoporosis and exacerbated bone loss as a result of chemotherapy [236, 237]. While these studies indicate a bone-sparing effect of rapamycin, these are largely due to reduced resorption as opposed to increased mineralisation.

In contrast to clinical studies indicating rapamycin has bone-sparing properties, loss of function studies in mice suggest the PI3K/Akt/mTOR pathway is activated during skeletal development and bone accrual. Factors which promote bone accrual, such as insulin and IGF-1, are known to activate PI3K/Akt/mTOR signalling [298]. Insulin signaling activates mTORC1 via inhibition of the TSC1/TSC2 complex. Homozygous mutation of genes encoding insulin-like growth factor 1 (*IGF1*), *IGF2* or the IGF receptor (*IGF1R*) all confer abnormal embryonic skeletal development, resulting in dwarfism [251-253]. Mice in which the Igf1r is deleted in OBs,

using *Osx-cre*, also have a low bone mass phenotype [299]. mTORC1 activity is elevated in mice harbouring *Pten* [262] or *TSC2* [300] disruption localized to mature OBs with both models conferring a high bone mass phenotype. Additionally, mice lacking both *Akt1* and *Akt2* showed neonatal lethality, dwarfism [259] and delayed bone ossification [166, 260].

Considering the findings in Chapter 3 and results from genetic studies in mice, the role of mTORC1 in *in vivo* osteogenesis remains unclear. This uncertainty is exacerbated by recent evidence suggesting that long-term treatment with rapamycin inhibits both mTORC1 and mTORC2 [162]. Investigation of the biological importance of mTORC1 and mTORC2 *in vivo* has been limited by the finding that global deletion of either mTOR, *Rptor* or *Rictor* is embryonically lethal. Of note, both $mTOR^{-/-}$ and $Rptor^{-/-}$ mice die shortly after implantation (E5.5 and E9.5 respectively), reflecting the absolute necessity for mTORC1 signalling during embryonic development [202, 238, 239].

To overcome these issues, a conditional knockout approach utilising the Cre-loxP system has been developed to facilitate tissue-specific deletion of genes of interest. In recent years, conditional tissue-specific *Rptor* knockout models have been used to characterise the role of mTORC1 in multiple tissues including mature adipocytes [240], skeletal muscle [241] and mesenchyme [286]. These studies have shown that the deletion of *Rptor* in adipose tissue caused leanness in mice due to an elevated energy expenditure caused by mitochondrial uncoupling [202]. Similarly, Benzinger et al (2008) reported that mice harbouring a skeletal muscle-specific deletion of *Rptor* have decreased muscle formation and a down-regulation of genes involved in mitochondrial biogenesis. Numerous other studies have utilised this model to assess the role or mTORC1 in tissues including but not limited to; neural cells [243], oligodendrocytes [244], T-cells [245], oocytes [246], intestinal epithelial cells [247] and red blood cells [248].

While conditional knockout models have been used to characterise the role of mTORC1 in many other tissues, to date, the role of mTORC1 signalling in skeletal development has yet to be examined. To address this, the studies outlined in this chapter describe the phenotypic characterisation of a bone-specific *Rptor* knockout mouse model, using the pre-OB-specific

promoter Osterix to drive Cre recombinase expression. Numerous other Cre transgenic lines have been utilised in the analysis of bone related genes such as markers of osteo-chondroprogenitors including Prx1 [249], Sox9 [301] and mature OBs including osteocalcin [250] and Col1A1 [302]. While the commitment of MSCs to the osteogenic lineage is marked by the expression of key transcription factors Runx2 and Osterix, Runx2 is also expressed in chondrogenic progenitors. Therefore, the Osterix-Cre line was utilized in this study as it allows for gene deletion in committed OB progenitors in both endochondral and intramembranous-derived bones [33] prior to maturation.

4.2 Results

4.2.1 Generation of OB-specific Rptor knockout mice

To examine the role of mTORC1 in skeletal development *in vivo*, conditional KO mice in which either one or both *Rptor* alleles were deleted in Osx-expressing cells were generated. To achieve this, three strains of mice were utilised: (1) *Osx1-GFP::cre* mice (herein referred to as Osx:Cre), in which Cre expression is driven by the OB-specific Osx promoter [33]; (2) *Rptor* floxed ($Rptor^{fl/fl}$) mice, in which loxP sites have been inserted to flank exon 6 of the *Rptor* gene [241]; and (3) Rosa26eYFP mice, whereby eYFP expression is activated in Cre expressing cells via deletion of an upstream floxed STOP cassette [303].

As outlined in Figure 4.1A, the breeding strategy used to generate heterozygous ($Rptor_{ob}^{-/+}$) and homozygous ($Rptor_{ob}^{-/-}$) OB-specific knockout mice was a multistep process. Firstly, Osx:Cre animals were mated with $Rptor^{fl/fl}$ mice to produce heterozygous $Rptor^{fl/+}$ offspring (in which one allele of *Rptor* is disabled in osterix expressing cells, herein referred to as $Rptor_{ob}^{-/+}$). From this mating, $Rptor_{ob}^{-/+}$ were then backcrossed with $Rptor^{fl/fl}$ mice to produce progeny of three different genotypes:(i) *Osx1-GFP::cre* transgene negative $Rptor^{fl/fl}$ or $Rptor^{fl/wt}$ (herein referred to as Wt), (ii) heterozygous $Rptor_{ob}^{-/+}$ mice and (iii) Osx-Cre-raptor$^{fl/fl}$ (homozygous OB-specific *Rptor* knockout mice, herein referred to as $Rptor_{ob}^{-/-}$).

For studies examining gene expression, ROSA26*eYFP* reporter mice were introduced into the breeding strategy to facilitate lineage tracing of MSC-derived cells or for the isolation of the cells harbouring Osx:Cre-mediated gene deletion. To achieve this, $Rptor^{fl/fl}$ mice were bred to homozygosity with Rosa26$eYFP^{fl/fl}$ mice, generating $R26eYFP^{fl/fl}$-$Rptor^{fl/fl}$ mice (herein referred to as eYFP-$Rptor^{fl/fl}$), which were mated with Osx:Cre mice in the breeding strategy as described above. From this breeding strategy, progeny with the following genotypes were generated (i) eYFP-$Rptor^{fl/wt}$ or eYFP-$Rptor^{fl/fl}$ mice (herein referred to as Wt), (ii) Osx-Cre-R26eYFP-$Rptor^{fl/wt}$ (herein referred to as eYFP-$Rptor_{ob}^{-/+}$) and (iii) Osx-Cre-R26eYFP-$Raptor^{fl/fl}$ (herein referred to as eYFP-$Rptor_{ob}^{-/-}$).

All progeny generated from this breeding strategy were genotyped in tail biopsies using PCR primers that were designed to detect (i) the presence of the Osx:Cre transgene, and (ii) the presence or absence of LoxP sites within the *Rptor* gene (Fig. 4.1B).

4.2.2 Postnatal survival is reduced in $Rptor_{ob}^{-/-}$ mice

As outlined in Figure 4.2A, animals generated from this breeding strategy were born at the expected Mendelian frequencies (i.e. approximately 50% Wt, 25% $Rptor_{ob}^{-/+}$ and 25% $Rptor_{ob}^{-/-}$). Postnatal survival was monitored over a 52 week period, and as shown in Figure 4.2B, the survival of both $Rptor_{ob}^{-/-}$ and $Rptor_{ob}^{-/+}$ mice was significantly reduced compared to Wt littermates after 52 weeks (68%, 72% and 97% survival respectively) (Fig. 4.2 B).

4.2.3 Osx:Cre mice have a distinct skeletal phenotype

To identify whether Wt littermates or Osx:Cre transgenic mice were the more suitable controls to use when characterising the skeletal phenotype of our $Rptor_{ob}^{-/+}$ and $Rptor_{ob}^{-/-}$ mice, we performed a comparative analysis of Osx:Cre animals and Wt littermate controls at 4, 8 and 12 weeks of age. As gender contributes to measurable differences in skeletal development [304, 305], this study was performed on male mice only.

At all time points examined, Osx:Cre animals were visibly smaller than Wt littermate controls (Fig. 4.3A), and had a significantly lower body weight than Wt controls at 4, 8 and 12 weeks (% reduction 34.2±8.2%, 28.2±6.4% and 18.3±4%, respectively) (Fig. 4.3B, Table 4.1). At 4 weeks of age mice were x-rayed and spinal lengths (defined by the distance from C1 to L5 vertebrae) quantitated using ImageJ. While no significant difference in spinal length was observed at any of the time points examined (Fig. 4.3C; Table 4.1), Osx:Cre animals were found to have significantly shorter tibial bones at 12 weeks of age, compared to Wt controls (mean decrease 6.3%±2.3) as measured by electronic calipers from the proximal tibial head to the fibular notch (Fig. 4.3D; Table 4.1).

Figure 4.1 - Generation of OB-specific *Rptor* KO mice: (A) The multi-step breeding strategy used to generate mice with an OB-specific *Rptor* deletion. Osx:Cre animals were mated with mice harbouring two floxed *Rptor* alleles ($Rptor^{fl/fl}$). Heterozygous Osx:Cre positive animals from this mating ($Rptor_{ob}^{-/+}$, in which one allele of *Rptor* has been deleted in pre-OBs) were then backcrossed with $Rptor^{fl/fl}$ animals to produce: (i) Osx:Cre negative animals (Wt), (ii) heterozygous OB-specific *Rptor* knockouts ($Rptor_{ob}^{-/+}$), and (iii) homozygous OB-specific *Rptor* knockouts ($Rptor_{ob}^{-/-}$). For some studies a Rosa26eYFP reporter line was utilised for identification of Cre activity. The floxed "stop" cassette in R26eYFP- $Rptor^{fl/fl}$ mice becomes excised upon exposure to Cre recombinase, thus labelling the OB-specific *Rptor* knockout cells eYFP+. (B) PCR was used to detect the presence of the Osx:Cre transgene and the presence or absence of floxed *Rptor* alleles to ascertain the genotype of all breeding progeny. M=100 base pair ladder.

A

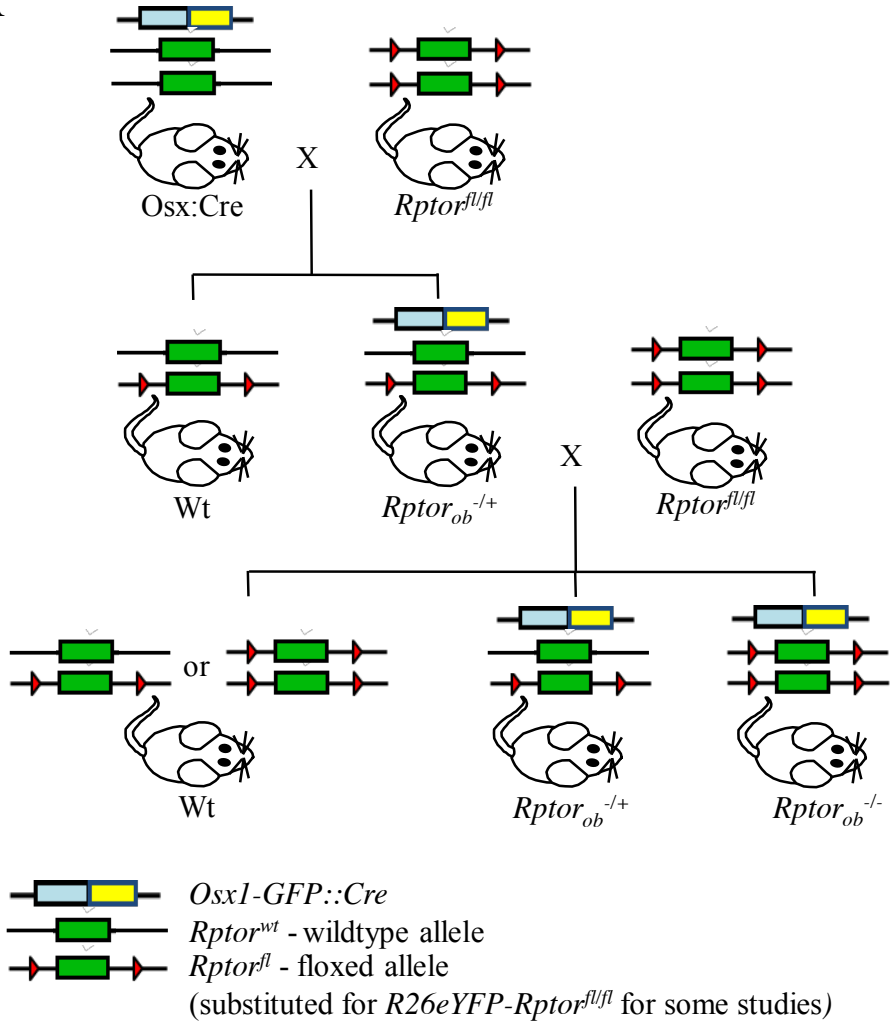
Osx:Cre
X
Rptor fl/fl
Wt
Rptor ob -/+
X
Rptor fl/fl
or
Wt
Rptor ob -/+
Rptor ob -/-
Osx1-GFP::Cre
Rptor wt - wildtype allele
Rptor fl - floxed allele
(substituted for R26eYFP-Rptor fl/fl for some studies)

B

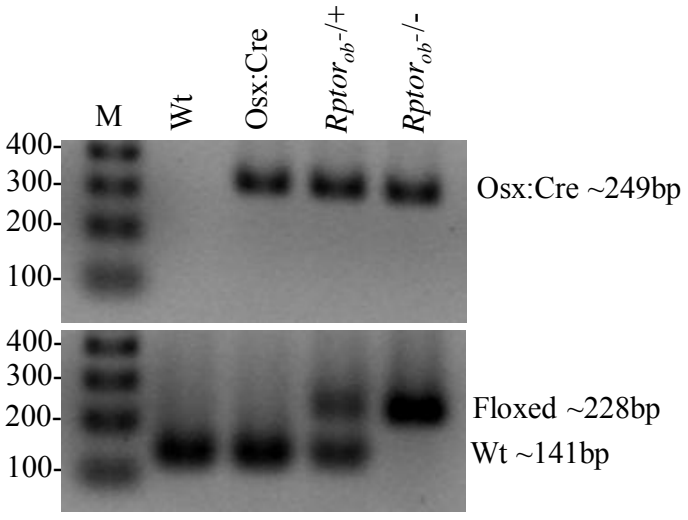
M
Wt
Osx:Cre
Rptor ob -/+
Rptor ob -/-
400
300
200
100
Osx:Cre ~249bp
Floxed ~228bp
Wt ~141bp

Figure 4.2 - Frequency and survival rates of OB-specific *Rptor* knockout mice: (A) The observed frequency of wild type, heterozygous ($Rptor_{ob}^{-/-}$) and homozygous ($Rptor_{ob}^{-/-}$) OB-specific *Rptor* knockout animals generated by our breeding strategy was consistent with expected Mendelian ratios (n>100 per group). (B) Kaplan-Meier survival curves were generated for Wt, $Rptor_{ob}^{-/+}$ and $Rptor_{ob}^{-/-}$ animals (n≥60 per group). *p < 0.05, **p < 0.01, Kaplan-Meier with Mantel-Cox test.

A

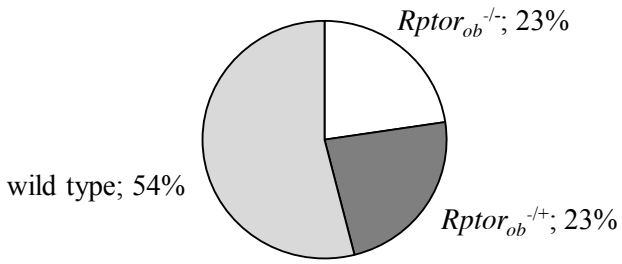
Rptor_ob-/-; 23%
wild type; 54%
Rptor_ob-/+; 23%

B

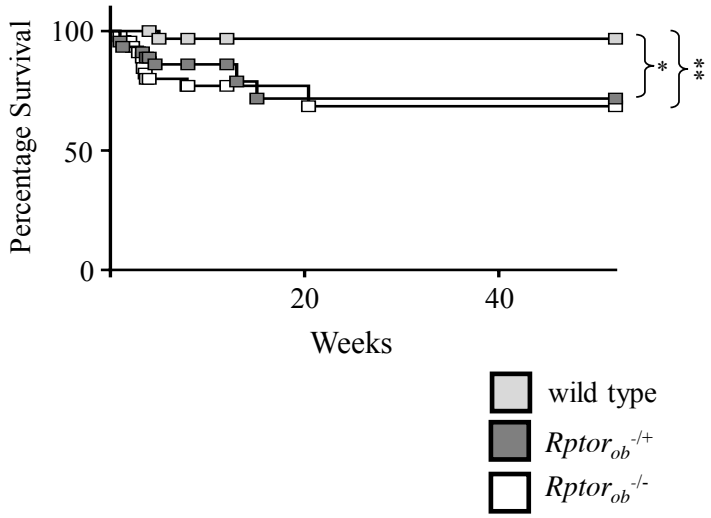
Percentage Survival
100
50
0
20
40
Weeks
*
**
wild type
Rptor_ob-/+
Rptor_ob-/-

Figure 4.3 - Osx:Cre mice display a stunted phenotype compared to Wt controls: (A) Representative images of male Wt and Osx:Cre animals at 4, 8 and 12 weeks of age. Bar = 10mm. (B) Animals were weighed at 4, 8 and 12 weeks of age. (C) Animals were x-rayed at 4, 8 and 12 weeks of age and spinal lengths (defined by the distance from C1 to L5 vertebrae) were quantitated using ImageJ. (D) Electronic callipers were used to measure the length of the tibia (from the proximal head to the fibular notch) in animals at 4, 8 and 12 weeks of age. (E) mCT analysis was performed on tibiae from animals at 4, 8 and 12 weeks of age, to measure bone volume (BV/TV) in a region of trabecular bone distal to the growth plate. (F) mCT analysis was performed on tibiae from animals at 4, 8 and 12 weeks of age, to measure the average cortical thickness (Ct.Th) in a region of trabecular bone distal to the growth plate. In all graphs, data are expressed as mean ± S.D, $n \geq 8$ per group. *$p<0.05$, **$p<0.001$ and ****$p<0.0001$, one-way ANOVA with Tukey's post-hoc test.

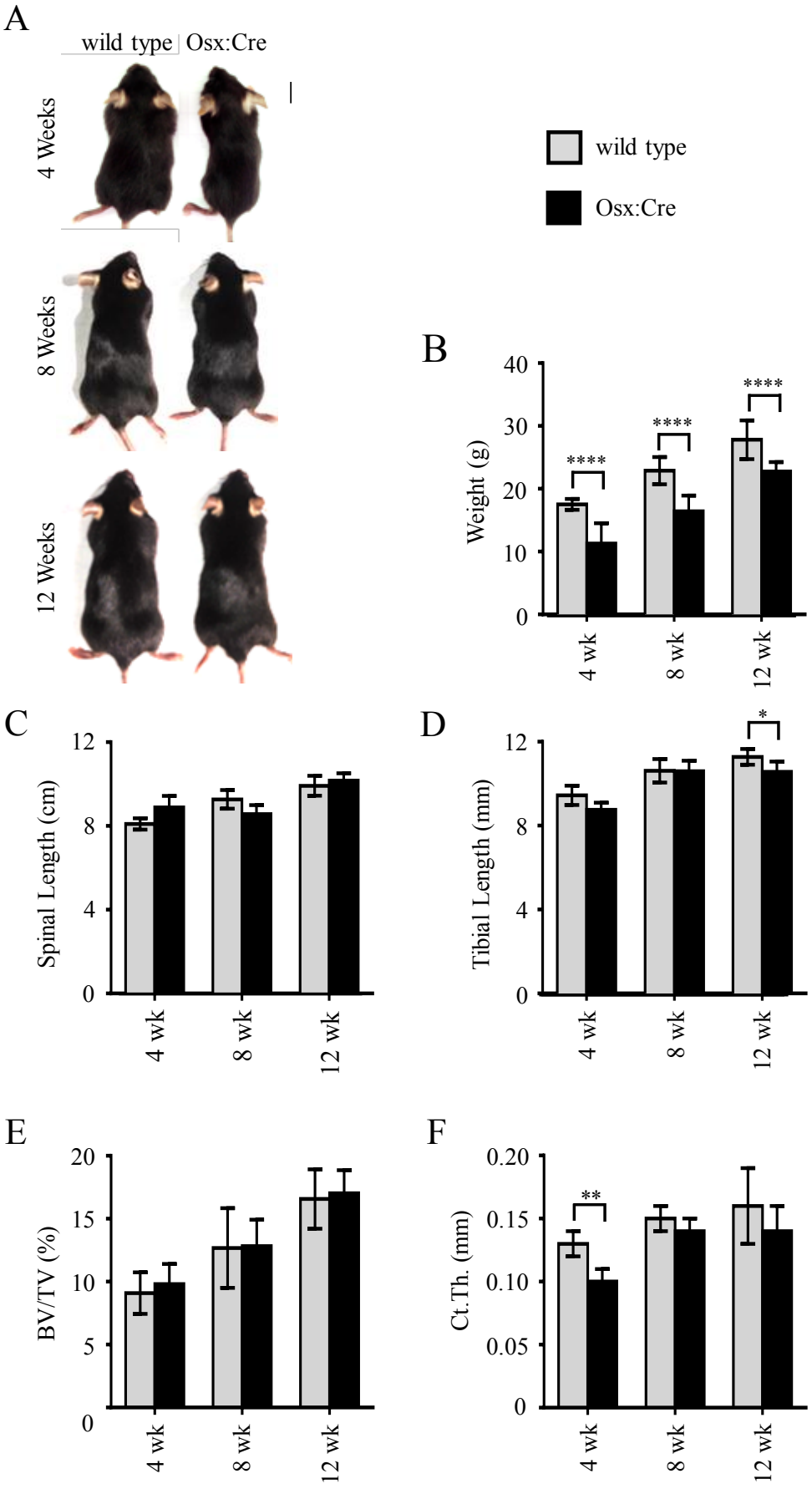
A
wild type
Osx:Cre
4 Weeks
8 Weeks
12 Weeks
wild type
Osx:Cre
B
Weight (g)
40
30
20
10
0
****
****
****
4 wk
8 wk
12 wk
C
Spinal Length (cm)
12
8
4
0
4 wk
8 wk
12 wk
D
Tibial Length (mm)
12
8
4
0
*
4 wk
8 wk
12 wk
E
BV/TV (%)
20
15
10
5
0
4 wk
8 wk
12 wk
F
Ct.Th. (mm)
0.20
0.15
0.10
0.05
0
**
4 wk
8 wk
12 wk

Table 4.1 Wildtype vs Osx:cre comparison

	Wt		Osx:Cre		Wt vs Osx:Cre	
	Mean	**St Dev[1]**	**Mean**	**St Dev**	**Sig.[2]**	**P value[3]**
Weight (g)						
4 weeks	17.52	±0.88	11.52	±3.23	****	< 0.0001
8 weeks	22.87	±2.16	16.43	±2.47	***	0.00010
12 weeks	27.80	±3.07	22.76	±1.47	****	< 0.0001
Spinal Length (cm)						
4 weeks	7.73	±0.86	8.88	±0.55	ns[4]	0.07
8 weeks	9.27	±0.44	8.57	±0.43	ns	0.2
12 weeks	9.92	±0.47	10.17	±0.35	ns	0.37
Tibial Length (mm)						
4 weeks	9.44	±0.46	9.04	±0.50	**	0.003
8 weeks	10.62	±0.56	10.60	±0.50	ns	0.95
12 weeks	11.28	±0.38	10.57	±0.49	**	0.0013
BV/TV[5] (%)						
4 wk	9.09	±1.65	9.81	±1.60	ns	0.94
8 wk	12.67	±3.17	12.83	±2.10	ns	0.9991
12 wk	16.57	±2.36	17.03	±1.83	ns	0.59
Ct.Th[6] (mm)						
4 wk	0.13	±0.01	0.10	±0.01	**	0.0030
8 wk	0.15	±0.01	0.14	±0.01	ns	0.94
12 wk	0.16	±0.03	0.14	±0.02	ns	0.45

[1]St Dev = Standard deviation
[2]Sig. = Significance
[3]P value = Values determined using ANOVA with Tukey's post hoc test
[4]ns = No significance
[5]BV/TV = Percentage of total volume comprising bone
[6]Ct.Th = Cortical bone thickness

To examine the bone microstructure in Osx:Cre and Wt animals, high-resolution micro-computed tomography (mCT) analyses were performed on the proximal tibiae. No significant difference in the percentage of trabecular bone volume to total volume (BV/TV) was observed at 4 and 8 weeks and 12 weeks in Osx:Cre mice compared to Wt mice (Fig. 4.3E; Table 4.1). Furthermore, mCT analysis of a region of trabecular bone distal to the tibial growth plate revealed that Osx:Cre mice have significantly thinner cortical bone compared to Wt controls at 4 weeks of age (mean decarese 23.1±3.9%) (Fig. 4.3F; Table 4.1).

4.2.4 Confirmation of OB-specific Rptor deletion

To confirm the bone-specific deletion of *Rptor* in this mouse model, genomic DNA was isolated from multiple tissues (bone, liver, spleen, heart, kidney, lung) of control and knockout animals and PCR used to amplify a product generated by Cre-mediated recombination of the *Rptor* gene [241]. A deletion-specific product was amplified from genomic DNA isolated from cells of the long bones of $Rptor_{ob}^{-/+}$ and $Rptor_{ob}^{-/-}$ mice but was absent in liver, spleen, heart, kidney and lung samples, thus confirming that the deletion of *Rptor* was bone-specific in these mice (Fig. 4.4A).

Further confirmation of OB-specific *Rptor* gene deletion was sought at the transcriptional level. Due to the low incidence of Osterix expressing cells harbouring the *Rptor* deletion, relative to the total cell population of the bone (which contains a heterogeneous mix of cells including osteoclasts, adipocytes, haematopoetic cells and bone marrow stromal cells), a purified population of Osterix-expressing cells was isolated from each animal cohort to confirm OB-specific *Rptor* deletion. To achieve this, the ROSA26*eYFP* reporter was utilised which, as described earlier, labels cells eYFP+ upon exposure to the Cre recombinase. Using this reporter, eYFP+ cells were isolated from eYFP-Osx:cre (ROSA26*eYFP* x Osx:Cre) and eYFP-$Rptor_{ob}^{-/-}$ mice using fluorescence activated cell sorting (FACS) and lysed for RNA. Using *Rptor*-specific primers, RT-PCR analysis of these RNA samples showed a significant reduction in *Rptor* transcript in eYFP+ cells isolated from heterozygous (eYFP-$Rptor_{ob}^{-/+}$) and

Figure 4.4 - Confirmation of tissue specific *Rptor* deletion: (A) Genomic DNA was isolated from the indicated tissues of 4-week old Osx:Cre, $Rptor_{ob}^{-/+}$ and $Rptor_{ob}^{-/-}$ animals and PCR was used to determine the genotype (upper panel) and the presence of a *Rptor* gene deletion product (lower panel). fl, floxed; wt, wildtype; del, deletion. (B and C) qPCR was performed on RNA extracted from eYFP+ cells isolated from eYFP-Osx:cre (control), eYFP- $Rptor_{ob}^{-/+}$ and eYFP- $Rptor_{ob}^{-/-}$ mice (n=10 per genotype) using *Rptor* exon 6-specific and b-actin primers. Amplified products were resolved on 2% agarose gels stained with Gel Red. *Rptor* transcript levels were quantitated using real-time PCR, and normalised to β-actin. Data are presented as mean ± S.D of quadruplicate samples. *$p<0.05$, **$p<0.01$, one-way ANOVA with Tukey's post-hoc test.

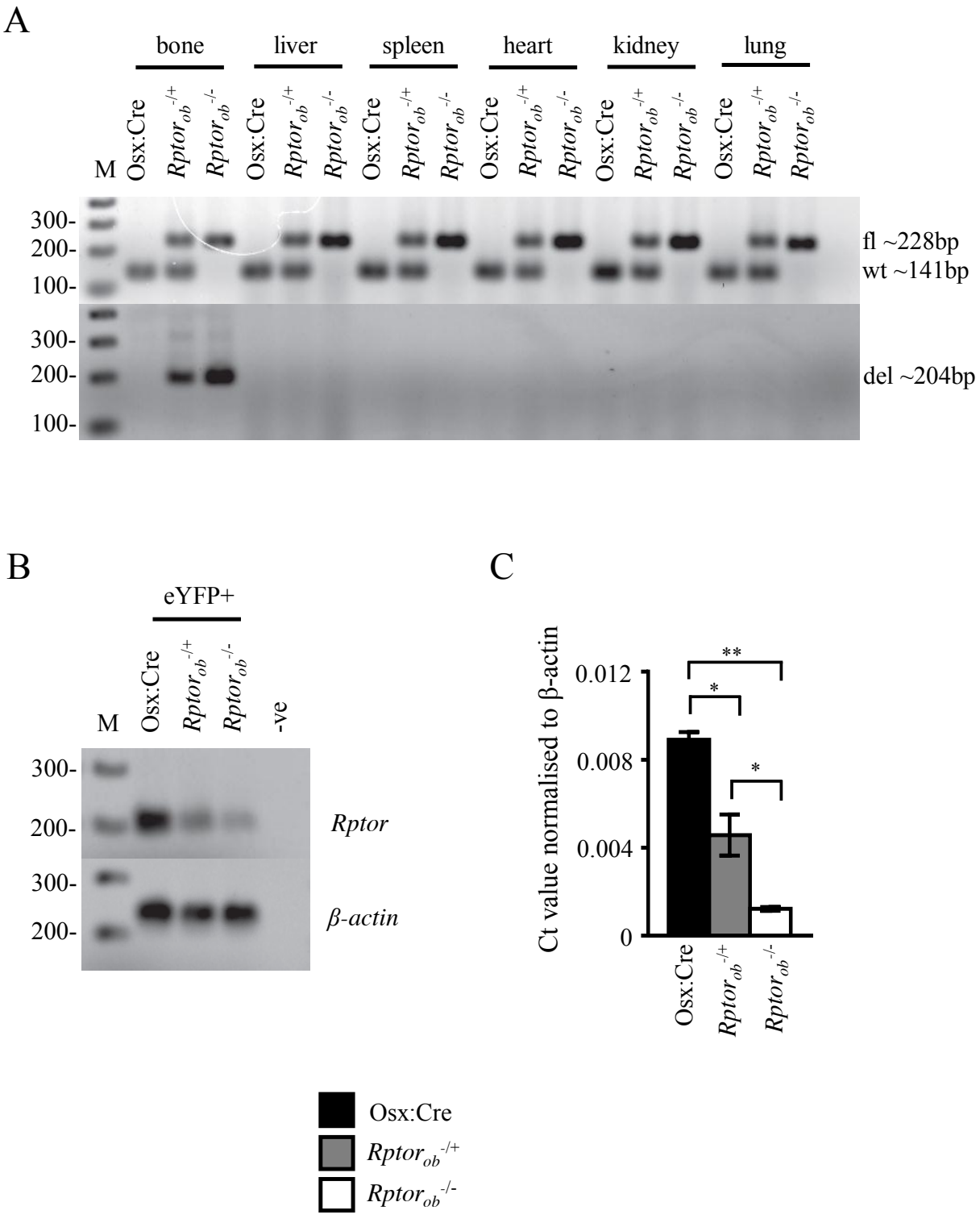
A
bone
liver
spleen
heart
kidney
lung
M
Osx:Cre
Rptor_ob -/+
Rptor_ob -/-
300-
200-
100-
fl ~228bp
wt ~141bp
del ~204bp
B
eYFP+
-ve
Rptor
β-actin
C
Ct value normalised to β-actin
0.012
0.008
0.004
0
**
*
*
Osx:Cre
Rptor_ob -/+
Rptor_ob -/-

homozygous (eYFP-*Rptor*$_{ob}^{-/-}$) knockout mice relative to eYFP-Osx:Cre controls (mean decrease 48.6±7.4% and 86.3±0.7% respectively) (Fig. 4.4B and 4.4C).

4.2.5 Prenatal skeletal phenotype in *Rptor*$_{ob}^{-/-}$ mice

To determine the effect of *Rptor* deletion on prenatal skeletal development, examinations were performed on newborn (P0) Osx:Cre and *Rptor*$_{ob}^{-/-}$ mice. As shown in Figure 4.5A, Osx:Cre and *Rptor*$_{ob}^{-/-}$ mice were phenotypically indistinguishable at birth. To investigate the effect of *Rptor* gene deletion on prenatal skeletal development, the skeletons of newborn (P0) Osx:Cre and *Rptor*$_{ob}^{-/-}$ mice were stained to assess the level of mineralised bone and cartilage using Alizarin Red and Alcian Blue, respectively. As shown in Figure 4.5B, bones of the pelvic cage such as the ilium, ischium and pubic bones were visibly less mineralised in *Rptor*$_{ob}^{-/-}$ mice compared to Osx:Cre controls. Similarly, staining of the skulls indicated that *Rptor*$_{ob}^{-/-}$ mice have narrower skulls and decreased mineralisation of the calvarial plates compared to Osx:Cre controls (Fig. 4.5C). A decrease in Alizarin Red staining was also observed in the mandibles of *Rptor*$_{ob}^{-/-}$ mice (Fig. 4.5D).

Analysis of prenatal long bone development was also performed on newborn Alizarin Red and Alcian Blue-stained Osx:Cre and *Rptor*$_{ob}^{-/-}$ mice (Fig. 4.6A and 4.6C). As shown in Figure 4.6, long bones of the hind and fore limbs (ie. the femur and humerus, respectively) were significantly shorter in newborn *Rptor*$_{ob}^{-/-}$ mice compared to Osx:Cre controls (mean decrease 8.5±1% for both bones), and the percentage of mineralised bone was also significantly reduced in newborn *Rptor*$_{ob}^{-/-}$ mice (mean decrease 17.4±2.2% for both bones) (Fig. 4.6 B and D).

4.2.6 *Rptor*$_{ob}^{-/-}$ mice have a stunted phenotype and reduced body weight

To characterise the effect of conditional deletion of *Rptor* in pre-OBs on postnatal skeletal development, male Osx:Cre, *Rptor*$_{ob}^{-/+}$ and *Rptor*$_{ob}^{-/-}$ animals were examined at 4, 8 and 12 weeks of age. These time points were selected on the basis that they represent the early, mid and later phases of long-bone growth in mice [306]. As shown in Figure 4.7A, *Rptor*$_{ob}^{-/+}$ and *Rptor*$_{ob}^{-/-}$ mice were visibly smaller than Osx:Cre control mice at 4, 8 and 12 weeks of age. At

Figure 4.5 - *Rptor*$_{ob}^{-/-}$ mice display altered prenatal skeletal mineralisation: Newborn mice (P0) were stained with Alizarin Red and Alcian Blue to visualise mineralised bone (red) and cartilage (blue), respectively. (A) Representative images of newborn (P0) Osx:Cre and *Rptor*$_{ob}^{-/-}$ animals prior to staining are shown. Bar = 10mm. (B) Schematic of the basic anatomy of the pelvic cage (left) and representative images of Alizarin Red and Alcian Blue staining of the pelvic cage of newborn Osx:Cre and *Rptor*$_{ob}^{-/-}$ animals (right). Bar = 5mm. (C) Schematic of the basic anatomy of the skull (superior view, left) and representative images of Alizarin Red and Alcian Blue staining of the skull of newborn Osx:Cre and *Rptor*$_{ob}^{-/-}$ animals (right). Bar = 5mm. (D) Schematic of the basic anatomy of the skull (lateral view, left) and representative images of Alizarin Red and Alcian Blue staining of the skull of newborn Osx:Cre and *Rptor*$_{ob}^{-/-}$ animals (right). Bar = 5mm.

A


Osx:Cre
Rptor$_{ob}^{-/-}$

B


Ilium
Pubic bone
Ischium
Osx:Cre
Rptor$_{ob}$-/-

C

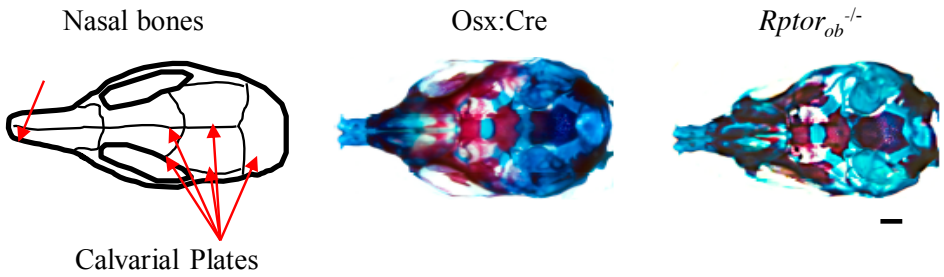
Nasal bones
Calvarial Plates
Osx:Cre
Rptor$_{ob}^{-/-}$

D


Calvarial Plates
Mandible
Osx:Cre
Rptor$_{ob}^{-/-}$

Figure 4.6 - *Rptor*$_{ob}^{-/-}$ animals display reduced prenatal long bone length and mineralisation: Newborn mice (P0) were stained with Alizarin Red and Alcian Blue to visualise mineralised bone (red) and cartilage (blue), respectively. (A) Representative images of Alizarin Red and Alcian Blue staining of the forelimbs of newborn Osx:Cre and *Rptor*$_{ob}^{-/-}$ mice. (B) The length of the humerus (left) and the percentage of the humerus that is mineralised (right) were measured using ImageJ. (C) Representative images of Alizarin Red and Alcian Blue staining of hind-limbs of newborn Osx:Cre and *Rptor*$_{ob}^{-/-}$ mice. (D) The length of the femur (left) and the percentage of the femur that is mineralised (right) were measured using ImageJ. Bar = 5mm. Data are presented as mean ± SD, n≥8 per group. **p<0.01 and ***p<0.001 t-test.

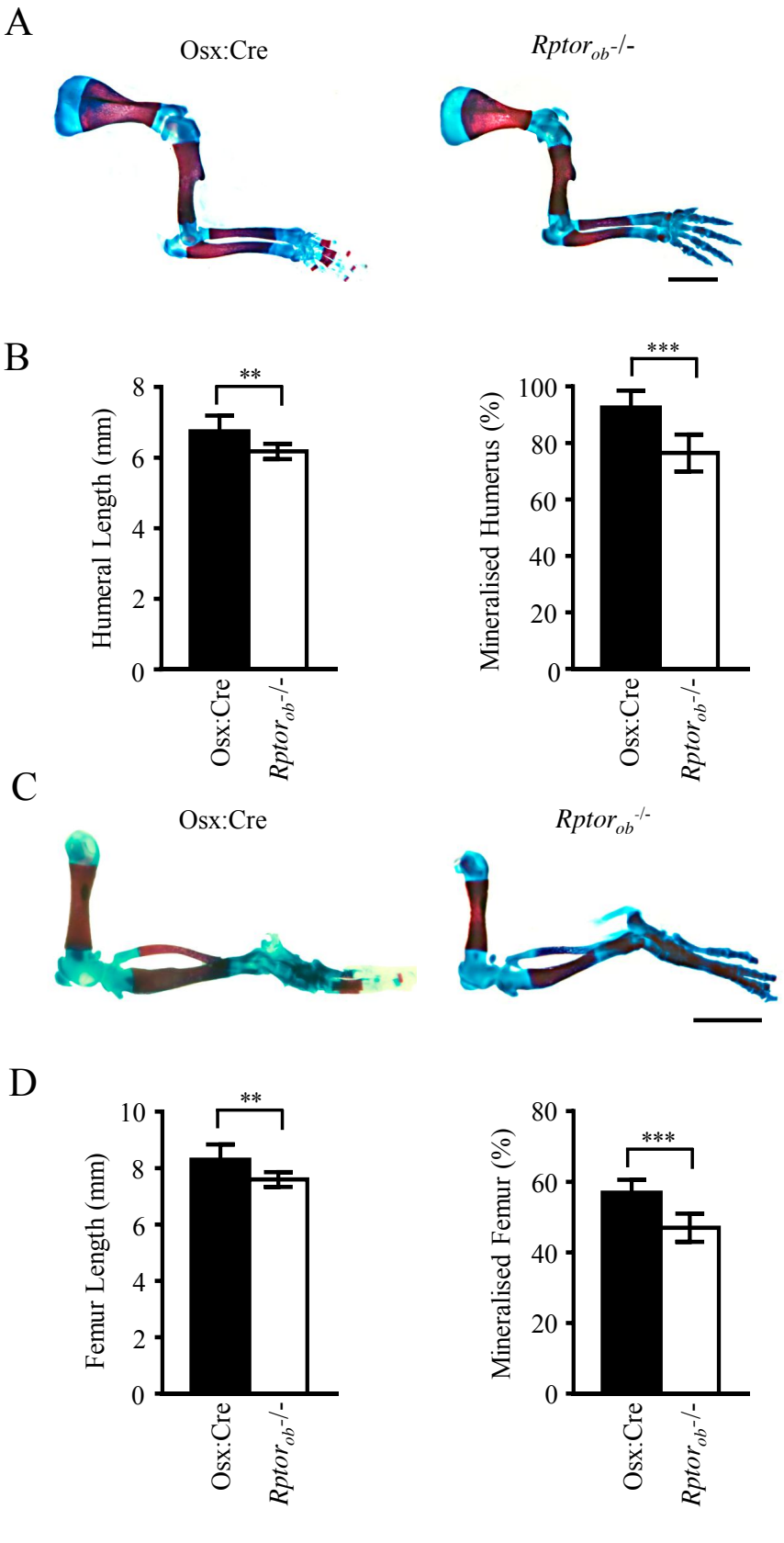
A
Osx:Cre
Rptor$_{ob}$-/-
B
Humeral Length (mm)
**
Osx:Cre
Rptor$_{ob}$-/-
Mineralised Humerus (%)
***
Osx:Cre
Rptor$_{ob}$-/-
C
Osx:Cre
Rptor$_{ob}$-/-
D
Femur Length (mm)
**
Osx:Cre
Rptor$_{ob}$-/-
Mineralised Femur (%)
***
Osx:Cre
Rptor$_{ob}$-/-

each of these time points, Osx:Cre, *Rptor*$_{ob}^{-/+}$ and *Rptor*$_{ob}^{-/-}$ animals were weighed and, as shown in Figure 4.7B, *Rptor*$_{ob}^{-/-}$ animals were found to have a significantly lower body weight compared to Osx:Cre animals at both 4 and 12 weeks of age (mean decrease 22.9±7.8% and 15.2±2.12%, respectively), whereas the *Rptor*$_{ob}^{-/+}$ animals did not exhibit any changes in body weight at these time points. Additionally, *Rptor*$_{ob}^{-/-}$ animals weighed significantly less than *Rptor*$_{ob}^{-/+}$ animals at 8 and 12 weeks of age (mean decrease 24.5±6.5% and 15.4±3.5%, respectively). However, somewhat surprisingly, *Rptor*$_{ob}^{-/+}$ animals displayed an increase in body weight at 8 weeks of age compared to Osx:Cre controls (mean increase 16.43±2.43) (Fig. 4.7B; Table 4.2).

4.2.7 Organ development in *Rptor*$_{ob}^{-/-}$ mice

To determine whether OB-specific *Rptor* deletion affects other organ systems, organ weights of the spleen, heart, liver and kidney were recorded for Osx:Cre controls, *Rptor*$_{ob}^{-/+}$ and *Rptor*$_{ob}^{-/-}$ mice at 4, 8 and 12 weeks of age. Given that body weight is a key determinant of organ size, all organ weight measurements were normalised to total body weight. When normalised to body weight, *Rptor*$_{ob}^{-/-}$ mice were found to have a significantly smaller liver than Osx:Cre controls at 4 weeks of age (mean decrease 24.7±9%), but not at 8 and 12 weeks of age. In contrast, *Rptor* deletion had no effect on the spleen, heart or kidney weights at any of the time points examined (Fig. 4.8; Table 4.3).

4.2.8 Spinal and tibial length are reduced in Rptor$_{ob}^{-/-}$ mice

To further evaluate the macroscopic effects of OB-specific mTORC1 deletion on skeletal development, mice were x-rayed and spinal lengths (defined by the distance from C1 to L5 vertebrae) quantitated using ImageJ. A significant reduction in spinal length was observed in *Rptor*$_{ob}^{-/-}$ animals at 4 and 12 weeks of age compared to *Rptor*$_{ob}^{-/+}$ (mean decrease 11±2.8% and 10.8±2.3%, respectively) and Osx:Cre animals (mean decrease 16.8±2.5% and 14.4±2.5%, respectively). In contrast, no significant difference in spinal length were observed between any of the animal groups at 8 weeks of age (Fig. 4.9A; Table 4.2).

Figure 4.7 - *$Rptor_{ob}^{-/-}$* mice display reduced postnatal weight: (A) Representative images of male Osx:Cre, *$Rptor_{ob}^{-/+}$* and *$Rptor_{ob}^{-/-}$* animals (L-R) at 4, 8, and 12 weeks of age. Bar = 10mm. (B) Weights of Osx:Cre, *$Rptor_{ob}^{-/+}$* and *$Rptor_{ob}^{-/-}$* animals were recorded at 4, 8, and 12 weeks of age. Data are presented as mean ± SD, n≥8 per group. *$p<0.05$ and **$p<0.01$, two-way ANOVA with Tukey's post-hoc test.

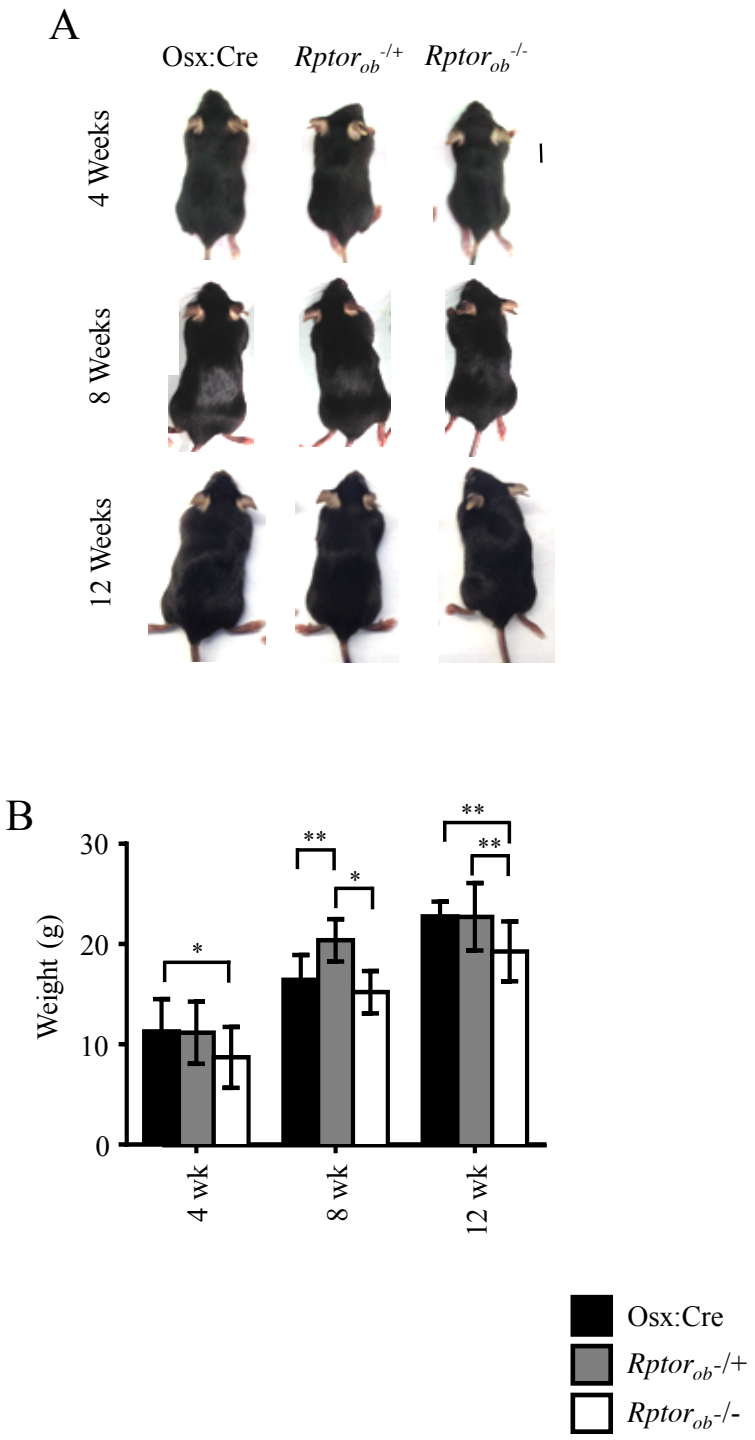
A
Osx:Cre
Rptor_ob-/+
Rptor_ob-/-
4 Weeks
8 Weeks
12 Weeks
B
Weight (g)
30
20
10
0
4 wk
8 wk
12 wk
Osx:Cre
Rptor_ob-/+
Rptor_ob-/-

Table 4.2: Postnatal Organ Weights (relative to total body weight)

	Osx:Cre		*Rptor*$_{ob}^{-/+}$		*Rptor*$_{ob}^{-/-}$		Osx:Cre vs *Rptor*$_{ob}^{-/+}$		Osx:Cre vs *Rptor*$_{ob}^{-/-}$		*Rptor*$_{ob}^{-/+}$ vs *Rptor*$_{ob}^{-/-}$	
	Mean	**St Dev[1]**	**Mean**	**St Dev**	**Mean**	**St Dev**	**Sig.[2]**	**P value[3]**	**Sig.**	**P value**	**Sig.**	**P value**
Spleen (g/g body weight)												
4 wk	0.0055	±0.0014	0.0042	±0.0013	0.0053	±0.0019	ns	0.12	ns	0.97	ns	0.23
8 wk	0.0033	±0.0005	0.0035	±0.0007	0.0047	±0.0015	ns	0.00	ns	0.10	ns	0.13
12 wk	0.0040	±0.0010	0.0032	±0.0006	0.0032	±0.0003	ns	0.67	ns	0.62	ns	1.00
Heart (g/g body weight)												
4 wk	0.0062	±0.0004	0.0058	±0.0017	0.0053	±0.0019	ns	0.96	ns	0.95	ns	0.98
8 wk	0.0059	±0.0013	0.0062	±0.0010	0.0047	±0.0015	ns	0.97	ns	0.20	ns	0.78
12 wk	0.0061	±0.0011	0.0045	±0.0010	0.0032	±0.0003	ns	0.66	ns	0.83	ns	0.67
Liver (g/g body weight)												
4 wk	0.0586	±0.0074	0.0485	±0.0059	0.0066	±0.0018	ns	0.19	*	0.04	ns	0.77
8 wk	0.0493	±0.0051	0.0525	±0.0100	0.0057	±0.0012	ns	0.92	ns	0.81	ns	0.99
12 wk	0.0564	±0.0073	0.0500	±0.0091	0.0054	±0.0008	ns	0.65	ns	0.97	ns	0.89
Kidney (g/g body weight)												
4 wk	0.0153	±0.0012	0.0142	±0.0031	0.0441	±0.0066	ns	0.73	ns	> 0.9999	ns	0.67
8 wk	0.0151	±0.0014	0.0141	±0.0018	0.0539	±0.0081	ns	0.80	ns	0.98	ns	0.95
12 wk	0.0141	±0.0016	0.0133	±0.0003	0.0539	±0.0077	ns	0.91	ns	0.98	ns	0.71

[1]St Dev = Standard deviation
[2]Sig. = Significance
[3]P value = Values determined using ANOVA with Tukey's post-hoc test

Figure 4.8 - *Rptor*$_{ob}^{-/-}$ mice display reduced liver weight: Following careful dissection of the major organs from the surrounding tissues, the weights of the (A) spleen, (B) liver, (C) heart, and (D) kidney were recorded for Osx:Cre, *Rptor*$_{ob}^{-/+}$ and *Rptor*$_{ob}^{-/-}$ animals at 4, 8 and 12 weeks of age, and normalised to total body weight. Data are presented as mean ± SD, n≥8 per group. *p<0.05, two-way ANOVA with Tukey's post-hoc test.

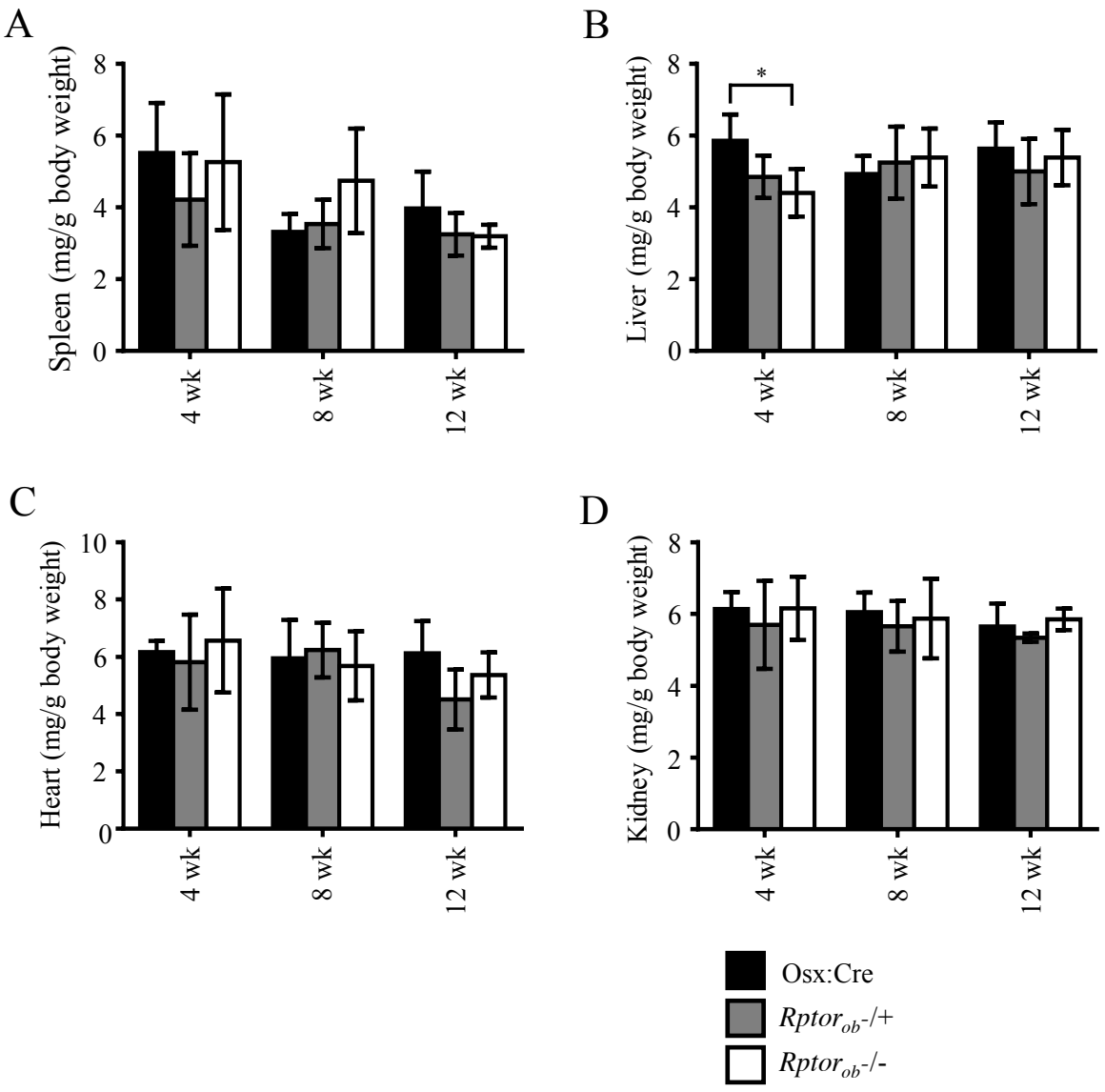
A
Spleen (mg/g body weight)
0
2
4
6
8
4 wk
8 wk
12 wk
B
Liver (mg/g body weight)
*
0
2
4
6
8
4 wk
8 wk
12 wk
C
Heart (mg/g body weight)
0
2
4
6
8
10
4 wk
8 wk
12 wk
D
Kidney (mg/g body weight)
0
2
4
6
8
4 wk
8 wk
12 wk
Osx:Cre
Rptor_ob-/+
Rptor_ob-/-

Table 4.3: Postnatal Body Measurements

	Osx:Cre		*Rptor*$_{ob}^{-/+}$		*Rptor*$_{ob}^{-/-}$		Osx:Cre vs *Rptor*$_{ob}^{-/+}$		Osx:Cre vs *Rptor*$_{ob}^{-/-}$		*Rptor*$_{ob}^{-/+}$ vs *Rptor*$_{ob}^{-/-}$	
	Mean	**St Dev[1]**	**Mean**	**St Dev**	**Mean**	**St Dev**	**Sig.[2]**	**P value[3]**	**Sig.**	**P value**	**Sig.**	**P value**
Weight (g)												
4 weeks	11.52	±3.23	11.17	±3.11	8.70	±3.04	ns	0.9994	*	0.0314	ns	0.0747
8 weeks	16.43	±2.47	20.38	±2.11	15.20	±2.12	*	0.0331	ns	0.8347	***	0.0008
12 weeks	22.76	±1.47	22.72	±3.37	19.27	±2.99	ns	> 0.9999	**	0.0047	**	0.0082
Spinal Length (cm)												
4 weeks	8.88	±0.55	8.30	±0.67	7.39	±0.46	ns	0.0507	****	< 0.0001	***	0.0010
8 weeks	8.57	±0.43	8.89	±0.30	8.39	±0.42	ns	0.8911	ns	0.9936	ns	0.5796
12 weeks	10.17	±0.35	9.76	±0.38	8.71	±0.39	ns	0.5124	****	< 0.0001	***	0.0002
Tibial Length (mm)												
4 weeks	9.04	±0.50	9.06	±0.70	7.68	±0.62	ns	0.6642	****	< 0.0001	****	< 0.0001
8 weeks	10.60	±0.50	10.65	±0.71	9.84	±0.86	ns	0.9984	ns	0.0748	*	0.0304
12 weeks	10.57	±0.49	10.74	±0.43	10.40	±0.46	ns	0.8804	ns	0.8945	ns	0.5114

[1]St Dev = Standard deviation
[2]Sig. = Significance
[3]P value = Values determined using ANOVA with Tukey's post-hoc test

To complement these findings, electronic calipers were used to measure the length of the tibia (from the proximal head to the fibular notch) in Osx:Cre, $Rptor_{ob}^{-/+}$ and $Rptor_{ob}^{-/-}$ animals at 4, 8 and 12 weeks of age. As shown in Figure 4.9B, a significant decrease in tibial length was observed in $Rptor_{ob}^{-/-}$ animals at 4 weeks of age compared to both Osx:Cre and $Rptor_{ob}^{-/+}$ animals (mean decrease 12.8±2.6% and 15.4±2.2% respectively). Additionally, at 8 weeks $Rptor_{ob}^{-/-}$ animals had a significantly shorter tibia than $Rptor_{ob}^{-/+}$ animals (mean decrease 7.2±2.9%), and although also reduced compared to Osx:Cre animals, this was not statistically significant. Despite the reduced weight and spinal length of $Rptor_{ob}^{-/-}$ animals in comparison to the $Rptor_{ob}^{-/+}$ and Osx:Cre animals, the stunted tibial growth was overcome by 12 weeks of age (Fig. 4.9 B; Table 4.3).

4.2.9 Growth plate thickness is reduced in $Rptor_{ob}^{-/-}$ mice

Numerous studies suggest that epiphyseal growth plate activity determines long bone growth [307]. To determine if the reduced tibial length observed in $Rptor_{ob}^{-/-}$ mice was associated with a reduction in tibial growth plate thickness, tibiae collected from Osx:Cre, $Rptor_{ob}^{-/+}$ and $Rptor_{ob}^{-/-}$ animals at 4, 8 and 12 weeks of age were analysed using high resolution mCT imaging. From 3-dimensional (3D) re-constructions of these μCT data, measurements of growth plate thickness were taken at 20 equidistant points across the central section of the proximal growth plate, and an average growth plate thickness calculated. At 4 weeks of age, a significant decrease in the thickness of the growth plate in both $Rptor_{ob}^{-/+}$ and $Rptor_{ob}^{-/-}$ animals compared to Osx:Cre controls was observed (mean decrease 16.4±4.5% and 25.9±3.2%, respectively, Fig. 4.10C). In contrast, no significant difference in growth plate thickness was observed between any of the animal cohorts at 8 and 12 weeks of age (Fig. 4.10C; Table 4.4).

4.2.10 Analysis of the trabecular bone micro-architecture in mice

To assess the effects of OB-specific *Rptor* deletion on the micro-architecture of trabecular bone, mCT analysis was performed on tibiae from Osx:Cre, $Rptor_{ob}^{-/+}$ and $Rptor_{ob}^{-/-}$ animals at 4, 8 and 12 weeks of age. For these studies, 150 slices (~0.97mm) were analysed in

Figure 4.9 - *$Rptor_{ob}^{-/-}$* mice display reduced postnatal spinal and tibial length: (A) The spinal lengths (defined by the distance from C1 to L5 vertebrae) of Osx:Cre, *$Rptor_{ob}^{-/+}$* and *$Rptor_{ob}^{-/-}$* mice were measured from X-ray images taken at 4, 8 and 12 weeks of age using ImageJ. (B) The tibial lengths (as determined by an average of three measurements taken from the proximal tibial head to the fibular notch using electronic calipers) of Osx:Cre, *$Rptor_{ob}^{-/+}$* and *$Rptor_{ob}^{-/-}$* mice were measured at 4, 8 and 12 weeks of age. Data are presented as mean ± SD, n≥8 per group. *p<0.05, **p<0.01, ***p<0.001 and ****p<0.0001, two-way ANOVA with Tukey's post-hoc test.

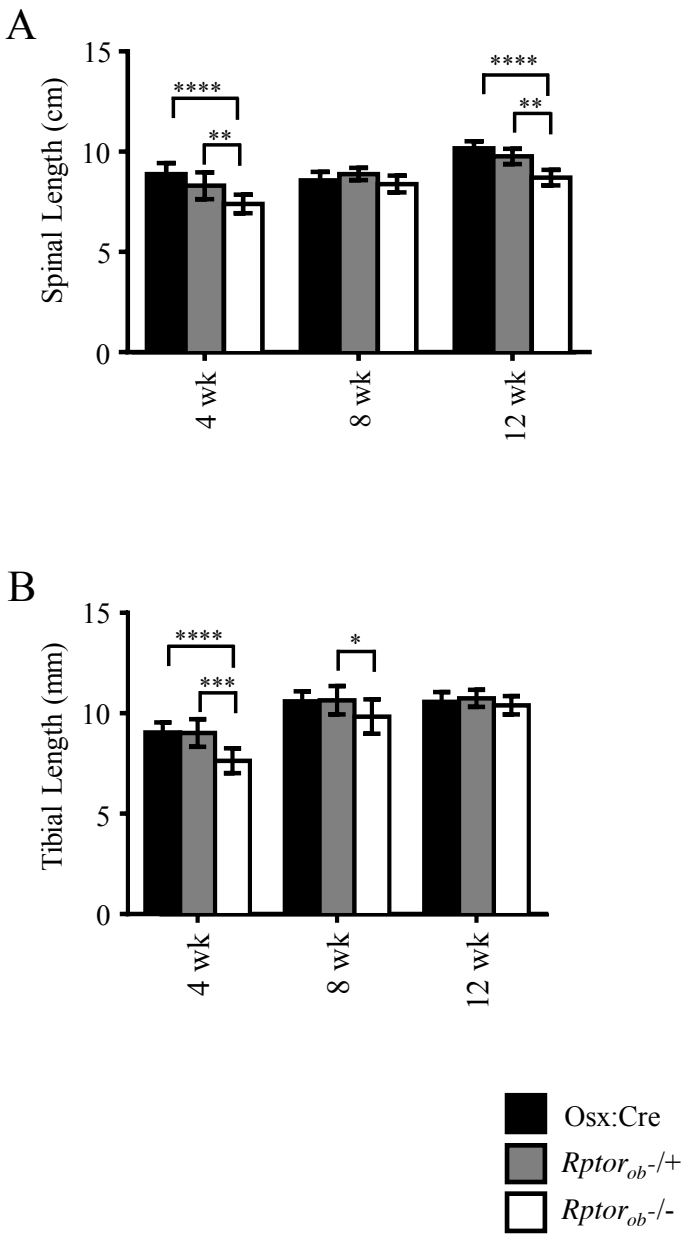
A
Spinal Length (cm)
15
10
5
0
****
**
****
**
4 wk
8 wk
12 wk
B
Tibial Length (mm)
15
10
5
0
****
***
*
4 wk
8 wk
12 wk
Osx:Cre
Rptor_ob-/+
Rptor_ob-/-

Figure 4.10 - *Rptor*$_{ob}^{-/-}$ mice display reduced growth plate thickness: The growth plate width in the proximal tibial head was analysed in male Osx:Cre, *Rptor*$_{ob}^{-/+}$ and *Rptor*$_{ob}^{-/-}$ animals at 4, 8 and 12 weeks of age from high resolution mCT images. (A) A schematic depiction of the proximal tibial growth plate. (B) A representative mCT image of the proximal tibial head of a male Osx:Cre, *Rptor*$_{ob}^{-/+}$ and *Rptor*$_{ob}^{-/-}$ animal at 4 weeks of age. In these images, the growth plate is identified by the unmineralised area, between the indicated arrows). (C) Mean growth plate thickness was determined by an average of 20 measurements taken across the growth plate. Data are presented as mean ± SD, n≥8 per group. **p<0.01, ****p<0.0001, two-way ANOVA with Tukey's post-hoc test.

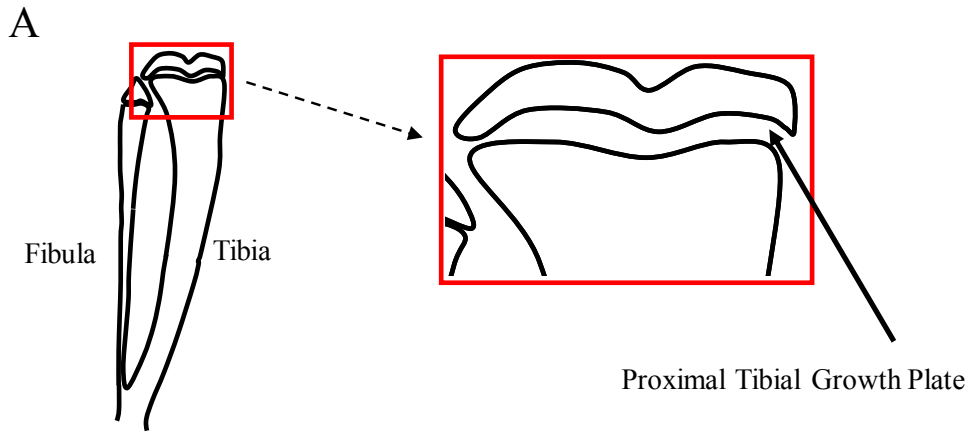
A
Fibula
Tibia
Proximal Tibial Growth Plate

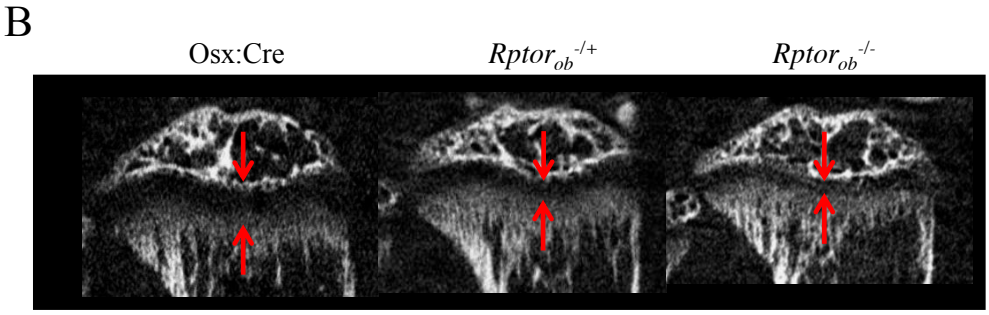
B
Osx:Cre
Rptor ob -/+
Rptor ob -/-

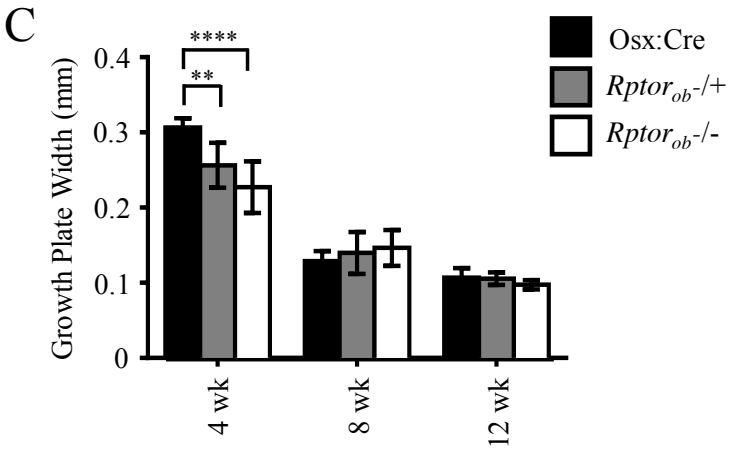
C
****
**
Growth Plate Width (mm)
0.4
0.3
0.2
0.1
0
4 wk
8 wk
12 wk
Osx:Cre
Rptor ob -/+
Rptor ob -/-

Table 4.4: Growth Plate Width

	Osx:Cre		*Rptor*$_{ob}^{-/+}$		*Rptor*$_{ob}^{-/-}$		Osx:Cre vs *Rptor*$_{ob}^{-/+}$		Osx:Cre vs *Rptor*$_{ob}^{-/-}$		*Rptor*$_{ob}^{-/+}$ vs *Rptor*$_{ob}^{-/-}$	
	Mean	**St Dev[1]**	**Mean**	**St Dev**	**Mean**	**St Dev**	**Sig.[2]**	**P value[3]**	**Sig.**	**P value**	**Sig.**	**P value**
GP[4] Width (μm)												
4 wk	306.6	±12.4	256.3	±30.0	227.2	±34.2	**	0.0039	****	< 0.0001	ns	0.17
8 wks	128.8	±13.5	139.7	±27.9	146.4	±23.9	ns	0.86	ns	0.59	ns	0.96
12 wk	106.7	±13.0	105.5	±8.2	97.3	±6.0	ns	0.9998	ns	0.91	ns	0.94

[1]St Dev = Standard deviation
[2]Sig. = Significance
[3]P value = Values determined using ANOVA with Tukey's post-hoc test
[4]GP = Growth Plate

a region of trabecular bone commencing 20 slices distal to the growth plate. Importantly, considering the differences observed in tibial length between animal cohorts (Fig. 4.9), an algorithm was devised to ensure the trabecular bone analyses were conducted in regions of the proximal tibiae in each animal. As summarised in Figure 4.11A, this algorithm ensures that (i) the distance from the growth plate, and (ii) the area of the region of interest (ROI) analysed for each animal was normalised to the length of the tibia (distance from growth plate = tibial length/11*20; length of ROI = tibial length/11*150).

4.2.11 Trabecular bone volume is decreased $Rptor_{ob}^{-/-}$ mice

High resolution mCT analysis of the secondary spongiosa within the proximal tibia revealed a visible reduction in the amount of trabecular bone in $Rptor_{ob}^{-/-}$ mice, compared to Osx:Cre controls, at 4, 8 and 12 weeks of age (Fig. 4.11B). Upon quantitation of these data, a significant decrease in trabecular bone volume, as a percentage of the total volume analysed (BV/TV), was observed in $Rptor_{ob}^{-/-}$ mice compared to Osx:Cre controls at 4, 8 and 12 weeks of age (mean decrease 29±3.5%, 31.8±11%, and 45±7%, respectively). At 12 weeks of age, a significant decrease in BV/TV was also observed in $Rptor_{ob}^{-/+}$ mice relative to Osx:Cre controls (mean decrease 31±5.2%). In addition, $Rptor_{ob}^{-/-}$ mice displayed a significant decrease in BV/TV compared to $Rptor_{ob}^{-/+}$ mice at 8 weeks of age (mean decrease 33.4±11.8%) (Fig. 4.11C; Table 4.5)

4.2.12 Trabecular number, but not thickness, is decreased in $Rptor_{ob}^{-/-}$ mice

Trabecular bone volume is largely determined by the number, thickness and/or spacing between the individual trabeculae [308, 309]. To further characterise the trabecular morphology of Osx:Cre, $Rptor_{ob}^{-/+}$ and $Rptor_{ob}^{-/-}$ mice, the following parameters were also measured from high resolution mCT reconstructions: (i) trabecular number (Tb.N), which analyses the number of individual trabeculae in the ROI, (ii) trabecular spacing (Tb.Sp), which calculates the average distance between each trabeculae, and (iii) trabecular thickness (Tb.Th), which calculates the average width of the individual trabeculae.

Figure 4.11 - *$Rptor_{ob}^{-/-}$* mice display reduced trabecular bone volume: Tibiae were isolated from male Osx:Cre, *$Rptor_{ob}^{-/+}$* and *$Rptor_{ob}^{-/-}$* animals at 4, 8 and 12 weeks of age and μCT analysis was performed on a region of trabecular bone distal to the proximal tibial growth plate. (A) A schematic depicting the defined region of the proximal tibia that was analysed. To account for differences in tibial length between genotypes, the region of interest (ROI) was normalised to the length of the bone for each animal, and the number of slices from the growth plate and number of slices included in the ROI were calculated as follows:distance from the growth plate = tibial length (mm)/11*20 and the ROI = tibial length(mm)/11*150). (B) Representative 3D μCT reconstructions showing a section of the trabeculae and cortices on the sagittal plane distal to the proxial tibial growth plate in the ROI of Osx:Cre, *$Rptor_{ob}^{-/+}$* and *$Rptor_{ob}^{-/-}$* animals at 4, 8 and 12 weeks of age. (C) Quantitation of the bone volume to total volume ratio (BV/TV) in the ROI of Osx:Cre, *$Rptor_{ob}^{-/+}$* and *$Rptor_{ob}^{-/-}$* animals at 4, 8 and 12 weeks of age. Data are presented as mean ± SD, n≥8 per group. *p<0.05, **p<0.01, ****p<0.0001, two-way ANOVA with Tukey's post–hoc test.

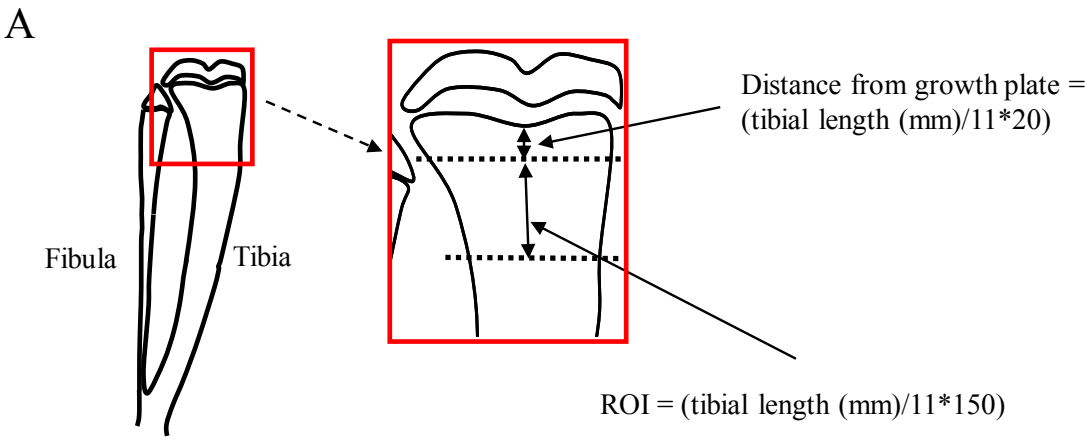
A
Distance from growth plate =
(tibial length (mm)/11*20)
Fibula
Tibia
ROI = (tibial length (mm)/11*150)

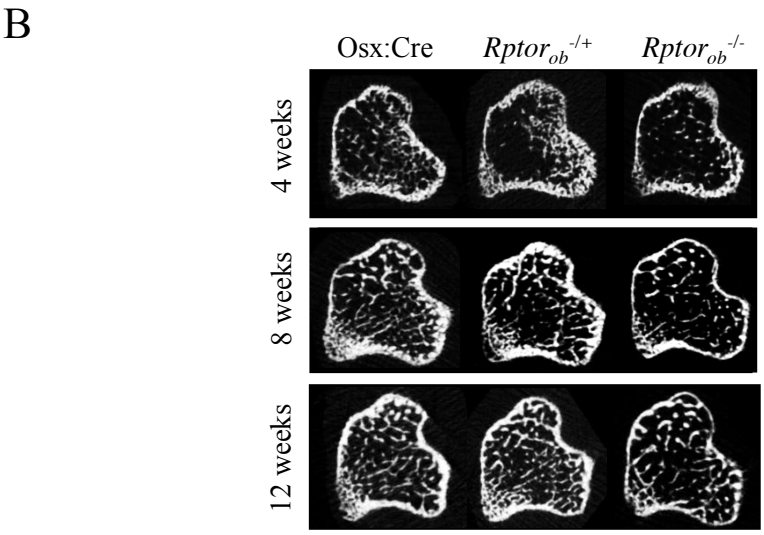
B
Osx:Cre
Rptor ob -/+
Rptor ob -/-
4 weeks
8 weeks
12 weeks

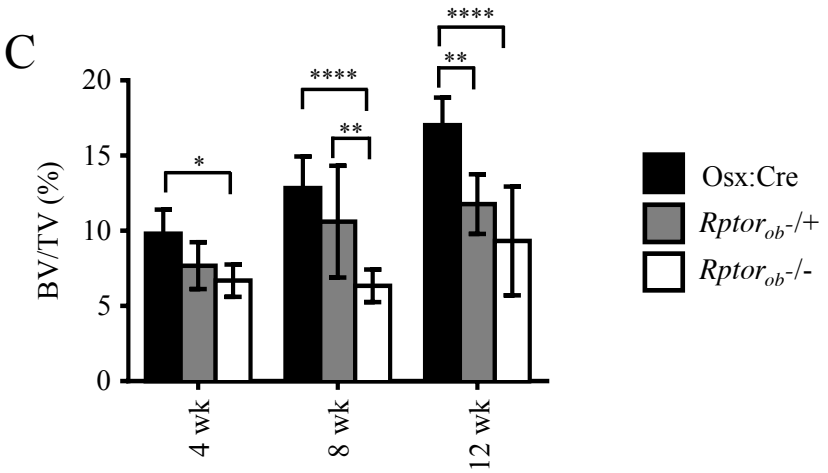
C
BV/TV (%)
20
15
10
5
0
*
****
**
****
**
4 wk
8 wk
12 wk
Osx:Cre
Rptor ob -/+
Rptor ob -/-

Table 4.5: Trabecular Bone Analyses

	Osx:Cre		*Rptor*$_{ob}^{-/+}$		*Rptor*$_{ob}^{-/-}$		Osx:Cre vs *Rptor*$_{ob}^{-/+}$		Osx:Cre vs *Rptor*$_{ob}^{-/-}$		*Rptor*$_{ob}^{-/+}$ vs *Rptor*$_{ob}^{-/-}$	
	Mean	**St Dev[1]**	**Mean**	**St Dev**	**Mean**	**St Dev**	**Sig.[2]**	**P value[3]**	**Sig.**	**P value**	**Sig.**	**P value**
BV/TV[4] (%)												
4 wk	9.81	±1.60	7.68	±1.56	6.97	±1.18	ns	0.21	ns	0.062	ns	0.74
8 wk	12.83	±2.10	10.61	±3.71	6.34	±1.08	ns	0.22	****	< 0.0001	**	0.0032
12 wk	17.03	±1.83	11.78	±1.98	9.33	±3.61	**	0.0019	****	< 0.0001	ns	0.15
Tb.N[5] (mm^{-1})												
4 wk	2.41	±0.36	1.84	±0.35	1.70	±0.30	*	0.047	**	0.0098	ns	0.75
8 wk	2.53	±0.36	2.08	±0.46	1.65	±0.30	ns	0.17	**	0.0022	ns	0.13
12 wk	2.86	±0.91	2.11	±0.37	1.81	±0.43	*	0.018	****	< 0.0001	ns	0.44
Tb.Sp[6] (mm)												
4 wk	0.235	±0.034	0.34	±0.07	0.34	±0.076	**	0.0043	**	0.0027	ns	0.99
8 wk	0.214	±0.023	0.22	±0.06	0.25	±0.062	ns	0.99	ns	0.46	ns	0.43
12 wk	0.179	±0.009	0.23	±0.02	0.26	±0.051	ns	0.29	*	0.045	ns	0.76
Tb.Th[7] (mm)												
4 wk	0.0487	±0.0050	0.0419	±0.0029	0.0411	±0.0020	ns	0.13	ns	0.08	ns	0.93
8 wk	0.0506	±0.0013	0.0499	±0.0088	0.0451	±0.0081	ns	0.98	ns	0.25	ns	0.26
12 wk	0.0511	±0.0050	0.0552	±0.0029	0.0499	±0.0094	ns	0.50	ns	0.92	ns	0.26

[1]St Dev = Standard deviation
[2]Sig. = Significance
[3]P value = Values determined using ANOVA with Tukey's post-hoc
[4]BV/TV = bone volume/total volume
[5]Tb.N = trabecular number
[6]Tb.Sp = trabecular spacing
[7]Tb.Th = trabecular thickness

As shown in Figure 4.12A, a significant decrease in Tb.N was observed in *Rptor*$_{ob}^{-/-}$ animals compared to Osx:Cre controls at 4, 8 and 12 weeks of age (mean decrease 29.4±4.2%, 34.8±9.9%, and 35.5±5.1% at 4, 8 and 12 weeks, respectively). Whilst Tb.N was also decreased in *Rptor*$_{ob}^{-/+}$ animals compared to Osx:Cre at all time points examined, this was only statistically significant at 4 and 12 weeks of age (mean decrease 23.65±9.8% and 24.8±5.9%, respectively) (Fig. 4.12A; Table 4.5).

Further analysis revealed that the decrease in Tb.N in *Rptor*$_{ob}^{-/+}$ and *Rptor*$_{ob}^{-/-}$ animals was coupled with a significant increase in Tb.Sp at 4 weeks of age (mean increase 44.3±7.5% and 45.7±9.4%, respectively) (Fig. 4.13B). A significant increase in Tb.Sp was also observed in *Rptor*$_{ob}^{-/-}$ animals compared to Osx:Cre animals at 12 weeks (mean increase 45.25±18%), however at the 8 week time point no significant differences were observed between the animal cohorts (Fig. 4.12B; Table 4.5). In contrast to the Tb.N and Tb.Sp data, no significant difference in trabecular thickness (Tb.Th) was observed in Osx:Cre, *Rptor*$_{ob}^{-/+}$ and *Rptor*$_{ob}^{-/-}$ animals at any of the time points examined (Fig. 4.12C; Table 4.5).

4.2.13 Trabecular structure is altered in *Rptor*$_{ob}^{-/-}$ mice

Structural integrity is determined by the shape and connectivity of the individual trabeculae within the lattice network [309]. To measure differences in the connectivity of the trabecular network in knockout mice, trabecular pattern factor (Tb.Pf) was measured in Osx:Cre, *Rptor*$_{ob}^{-/+}$ and *Rptor*$_{ob}^{-/-}$ mice using high resolution μCT. Tb.Pf is a bone-specific parameter enumerating the connection of trabeculae in three dimensions and provides an indication of the structural integrity of the trabecular network. At 4 weeks of age, there was no significant change in the connectivity of the trabecular micro-architecture between any of the animal cohorts. However, at the later 8 and 12 week time points, there was a significant decrease in the connectivity of the trabeculae in the KO animals, as indicated by an increase in the trabecular pattern factor (Fig. 4.13A). This difference was statistically significant for both *Rptor*$_{ob}^{-/+}$ and *Rptor*$_{ob}^{-/-}$ KO animals at 8 weeks (mean increase 35.6±13.9% and 55.8±13.9%,

Figure 4.12 - *Rptor*$_{ob}^{-/-}$ mice display reduced trabecular number and increased trabecular spacing: Tibiae were isolated from male Osx:Cre, *Rptor*$_{ob}^{-/+}$ and *Rptor*$_{ob}^{-/-}$animals at 4, 8 and 12 weeks of age and high resolution μCT analysis was performed on a region of trabecular bone distal to the proximal tibial growth plate (normalised to the length of the bone). Quantitation of (A) trabecular number (Tb.N), (B) trabecular separation (Tb.Sp), and (C) trabecular thickness (Tb.Th) was performed using CTAn (SkyScan). Data are presented as mean ± SD, n≥8 per group. *p<0.05, **p<0.01, ****p<0.0001, two-way ANOVA with Tukey post-hoc test.

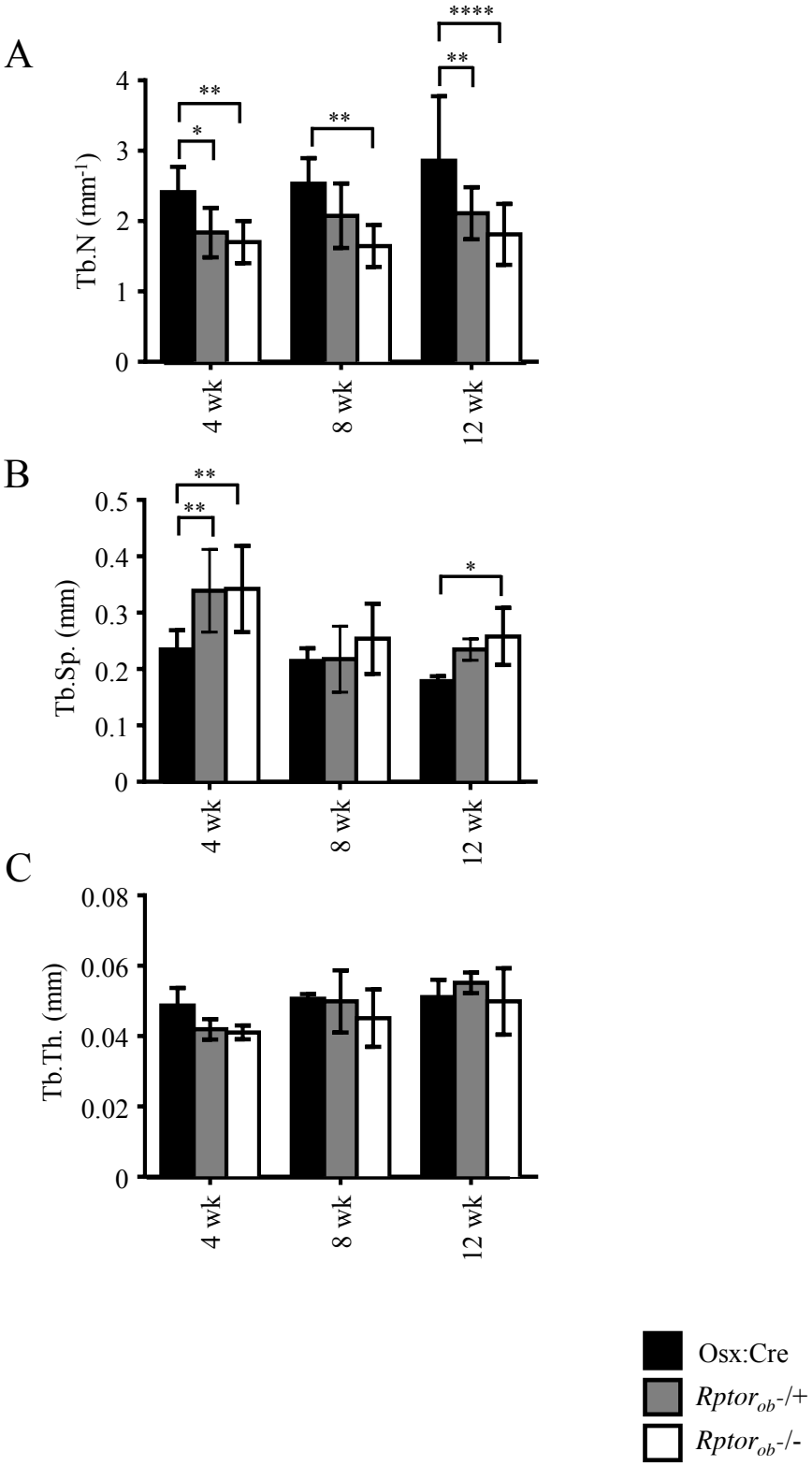
A
Tb.N (mm-1)
4
3
2
1
0
*
**
**
**
****
4 wk
8 wk
12 wk
B
Tb.Sp. (mm)
0.5
0.4
0.3
0.2
0.1
0
**
**
*
4 wk
8 wk
12 wk
C
Tb.Th. (mm)
0.08
0.06
0.04
0.02
0
4 wk
8 wk
12 wk
Osx:Cre
Rptor ob -/+
Rptor ob -/-

Figure 4.13 - *Rptor*$_{ob}^{-/-}$ mice display altered trabecular micro-architecture: Tibiae were isolated from male Osx:Cre, *Rptor*$_{ob}^{-/+}$ and *Rptor*$_{ob}^{-/-}$ animals at 4, 8 and 12 weeks of age and high resolution μCT analysis was performed on a region of trabecular bone distal to the proximal tibial growth plate. Quantitation of (A) trabecular pattern factor (Tb.Pf), and (B) structure model index (SMI) was performed using CTAn (SkyScan). Data are presented as mean ± SD, n≥8 per group. *p<0.05, **p<0.01 and ****p<0.001, two-way ANOVA with Tukey's post-hoc test.

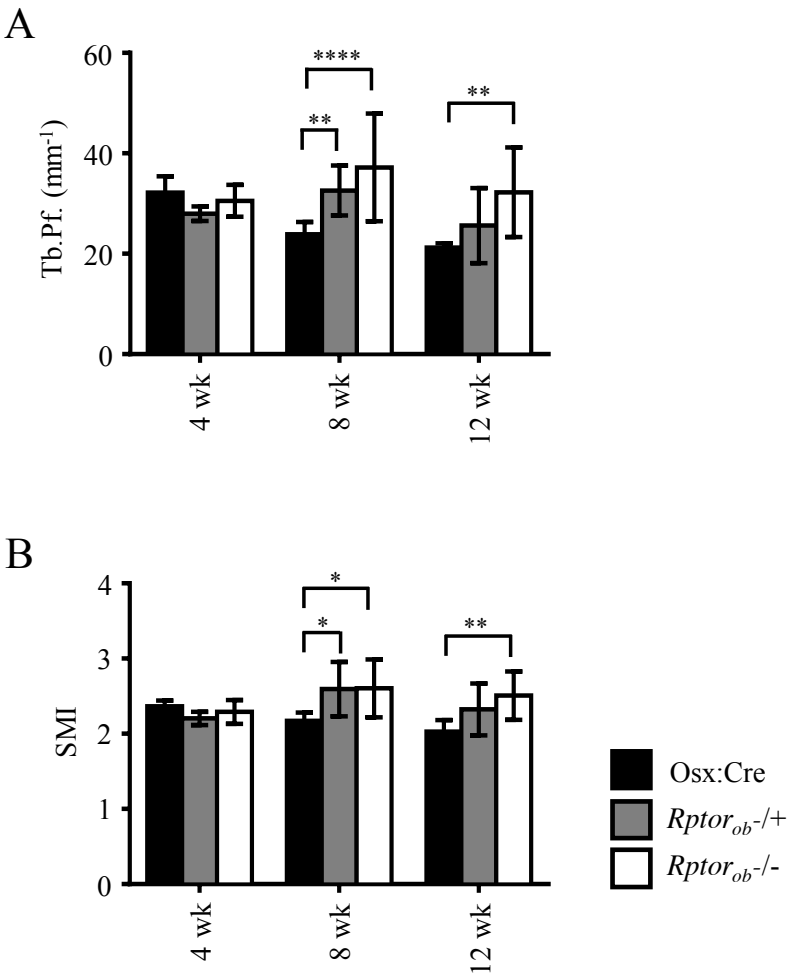
A
60
40
20
0
Tb.Pf. (mm-1)
****
**
**
4 wk
8 wk
12 wk
B
4
3
2
1
0
SMI
*
*
**
4 wk
8 wk
12 wk
Osx:Cre
Rptor_ob-/+
Rptor_ob-/-

Table 4.6: Trabecular Morphology Analyses

	Osx:Cre		*Rptor*$_{ob}^{-/+}$		*Rptor*$_{ob}^{-/-}$		Osx:Cre vs *Rptor*$_{ob}^{-/+}$		Osx:Cre vs *Rptor*$_{ob}^{-/-}$		*Rptor*$_{ob}^{-/+}$ vs *Rptor*$_{ob}^{-/-}$	
	Mean	**St Dev[1]**	**Mean**	**St Dev**	**Mean**	**St Dev**	**Sig.[2]**	**P value[3]**	**Sig.**	**P value**	**Sig.**	**P value**
Tb.Pf[4] (mm^{-1})												
4 wk	32.15	±3.26	27.99	±1.44	30.54	±3.16	ns	0.39	ns	0.86	ns	0.55
8 wks	23.87	±2.46	32.60	±4.99	37.20	±10.73	*	0.029	***	0.0005	ns	0.26
12 wk	21.24	±0.82	25.61	±7.48	32.24	±8.92	ns	0.437	**	0.002	ns	0.11
SMI[5]												
4 wk	2.37	±0.075	2.20	±0.09	2.29	±0.16	ns	0.46	ns	0.84	ns	0.70
8 wk	2.17	±0.11	2.59	±0.36	2.60	±0.39	*	0.012	*	0.010	ns	0.997
12 wk	2.03	±0.15	2.32	±0.34	2.51	±0.32	ns	0.14	**	0.0018	ns	0.40

[1]St Dev = Standard deviation
[2]Sig. = Significance
[3]P value = Values determined using ANOVA with Tukey's post-hoc
[4]Tb.Pf = trabecular pattern factor
[5]SMI = structure model index

respectively), and for *Rptor*$_{ob}^{-/-}$ animals at 12 weeks (mean increase 52±14%), compared to Osx:Cre controls (Fig. 4.13A; Table 4.6)

In addition to the changes in trabecular connectivity, the physical structure of the trabeculae was also examined. The structure model index (SMI) is used to describe the three-dimensional structure of the trabeculae, distinguishing between plate-like (SMI=0) and spherical (SMI=4) geometry [310]. At 4 weeks of age, there was no difference in the SMI between the three animal groups. However, at 8 weeks of age, a statistically significant increase in SMI was observed in *Rptor*$_{ob}^{-/+}$ and *Rptor*$_{ob}^{-/-}$ animals (mean increase 19.3±5.5% and 19.8±5.5%, respectively), suggesting a shift away from a plate-like trabecular morphology to a spherical morphology (Fig. 4.13B). A statistically significant difference in SMI was also seen in *Rptor*$_{ob}^{-/-}$ animals at 12 weeks of age, compared to Osx:Cre controls (mean change 23.6±5.3%) (Fig. 4.13B; Table 4.6).

4.2.14 Reduced cortical bone in *Rptor*$_{ob}^{-/-}$ mice

The shaft, or diaphyses of the long bones are composed of cortical bone surrounding the intramedullary cavity. To assess the effects of OB-specific *Rptor* deletion on the micro-architecture of cortical bone, mCT analysis was performed on tibiae from Osx:Cre, *Rptor*$_{ob}^{-/+}$ and *Rptor*$_{ob}^{-/-}$ animals at 4, 8 and 12 weeks of age. As previously described for the trabecular bone analyses (see Section 4.2.11), the ROI for cortical bone analysis was normalised to the length of the tibia for each animal, to account for differences in the tibiae lengths between animal groups (Fig. 4.11A).

As shown in Figure 4.14A, cross-sectional mCT images demonstrate a visible thinning of the cortical bone in *Rptor*$_{ob}^{-/-}$ animals compared to Osx:Cre controls. Quantitation of these data confirmed that the average thickness of the cortical bone (Ct.Th) was decreased at 4, 8 and 12 weeks in *Rptor*$_{ob}^{-/-}$ animals relative to both Osx:Cre controls (mean decrease 31±7.8%, 28.5±7.3% and 28.6±6%,respectively) and *Rptor*$_{ob}^{-/+}$ mice (mean decrease 25.8±8.6%, 28.6±6.9% and 23.08±7.8%, respectively) (Fig. 4.14B; Table 4.7). Furthermore, at 8 and 12

weeks of age, the average intramedullary diameter of the ROI analysed was significantly increased in $Rptor_{ob}^{-/-}$ animals compared to Osx:Cre controls (mean increase 18.2%±7.2 and 5.1%±4.4 respectively). $Rptor_{ob}^{-/+}$ animals also displayed a significant increase inintramedullary diameter compared to Osx:Cre controls at 12 weeks of age (mean increase 8.8%±4.8) (Fig. 4.14C; Table 4.7).

4.2.15 Reduced rigidity and strength of bone $Rptor_{ob}^{-/-}$ mice

In order to investigate changes in the mechanical properties of the long bones of OB-specific *Rptor* KO mice, dynamic three-point bending flexural tests were conducted on femurs isolated from 4 week old Osx:Cre, $Rptor_{ob}^{-/+}$ and $Rptor_{ob}^{-/-}$ animals. Three-point bending analyses test the stiffness and flexibility of the bones. Considering the association between body weight and the mechanical properties of bone, animal bodyweight was introduced as a covariate during statistical analyses (ANCOVA) of these data. The flexural rigidity (i.e. bending stiffness) was calculated from the load-displacement curves using basic beam theory [311]. As shown in Figure 4.15A (Table 4.8), a significant decrease in the flexural rigidity of long bones from $Rptor_{ob}^{-/+}$ and $Rptor_{ob}^{-/-}$ animals was observed, compared to Osx:Cre controls (mean decrease 71.9%±0.2 and 74.8%±10.1 respectively). Furthermore, a decrease in the amount of force the bone was able to withstand before breaking (ultimate load) was also observed in the long bones of $Rptor_{ob}^{-/-}$ animals compared to Osx:Cre controls (mean decrease 56.3%±10) (Fig. 4.15B; Table 4.8).

4.2.16 Altered cranial and facial morphology in $Rptor_{ob}^{-/-}$ mice

While tibial development is facilitated by endochondral ossification, intramembranous ossification facilitates the development of the flat bones including the cranial plates. To assess the effect of OB-specific *Rptor* deletion on intramembranous ossification, cranial mCT scans were performed on 4-week-old mice and 3D re-constructions of the data were generated using Avizo® Fire. As shown in Fig. 4.16B, the skulls of $Rptor_{ob}^{-/-}$ animals were visibly malformed compared to Osx:Cre controls. Regions of the skull of $Rptor_{ob}^{-/-}$ animals appeared incompletely

mineralised, especially in the frontal region adjacent to the coronal suture line and in the nasal region. Incomplete mineralization was also observed in the lambdoidal and sagittal sutures of *Rptor*$_{ob}^{-/-}$ animals. Lateral images derived from 3D reconstructions of the mCT data also indicated a change in morphology of the facial structure of *Rptor*$_{ob}^{-/-}$ animals compared to Osx:Cre controls (Fig. 4.16D). Of note, incomplete mineralization of the temporal and zygomatic bones was evident in *Rptor*$_{ob}^{-/-}$ animals compared to Osx:Cre controls, and their mandibles were smaller and displayed an altered morphology (Fig. 4.16 D).

Figure 4.14 - *Rptor*$_{ob}^{-/-}$ mice display reduced cortical thickness and increased intramedullary diameter: Tibiae were isolated from male Osx:Cre, *Rptor*$_{ob}^{-/+}$ and *Rptor*$_{ob}^{-/-}$ animals at 4, 8 and 12 weeks of age and μCT analysis of cortical bone distal was analysed in the ROI proximal tibial growth plate (ROI as outlined in Figure 4.11). (A) Representative 3D mCT reconstructions showing a section of the cortices on the sagittal plane distal to the proximal tibial growth plate in the ROI of Osx:Cre, *Rptor*$_{ob}^{-/+}$ and *Rptor*$_{ob}^{-/-}$animals at 4, 8 and 12 weeks of age. Quantitation of (B) cortical thickness (Ct.Th), and (C) intramedullary diameter (Im.Dm) was performed using CTAn (SkyScan). Data are presented as mean ± SD, n≥8 per group. *p<0.05, **p<0.01 and ***p<0.001, two-way ANOVA with Tukey's post-hoc test.

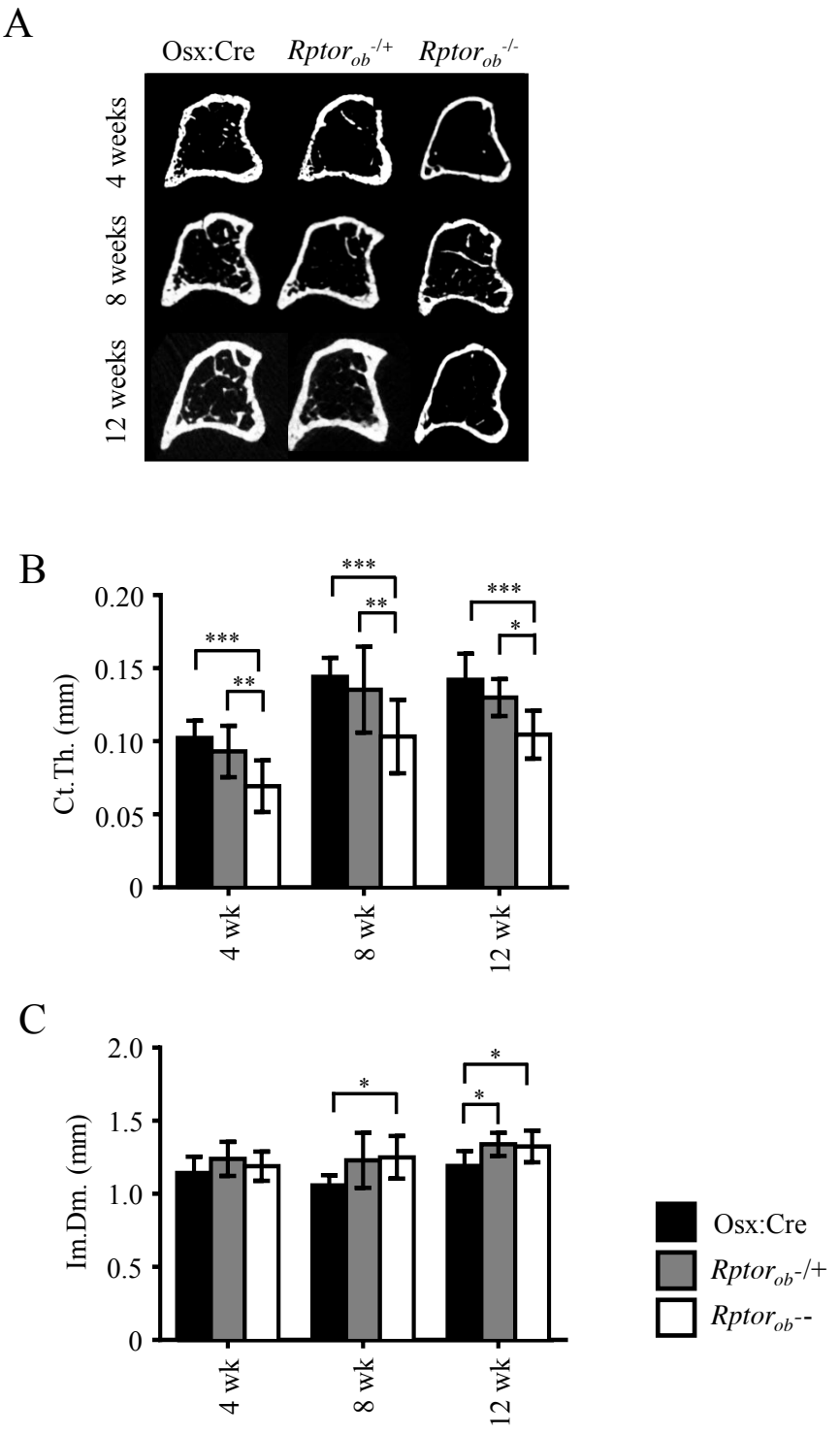
A
Osx:Cre
Rptor_ob-/+
Rptor_ob-/-
4 weeks
8 weeks
12 weeks
B
Ct.Th. (mm)
0.20
0.15
0.10
0.05
0
***
**
***
**
***
*
4 wk
8 wk
12 wk
C
Im.Dm. (mm)
2.0
1.5
1.0
0.5
0
*
*
*
4 wk
8 wk
12 wk
Osx:Cre
Rptor_ob-/+
Rptor_ob--

Table 4.7: Cortical Bone Analyses

	Osx:Cre		*Rptor*$_{ob}^{-/+}$		*Rptor*$_{ob}^{-/-}$		Osx:Cre vs *Rptor*$_{ob}^{-/+}$		Osx:Cre vs *Rptor*$_{ob}^{-/-}$		*Rptor*$_{ob}^{-/+}$ vs *Rptor*$_{ob}^{-/-}$	
	Mean	**St Dev[1]**	**Mean**	**St Dev**	**Mean**	**St Dev**	**Sig.[2]**	**P value[3]**	**Sig.**	**P value**	**Sig.**	**P value**
Ct.Th[4] (mm)												
4 wk	0.10	±0.012	0.093	±0.018	0.069	±0.018	ns	0.48	***	0.0001	*	0.011
8 wk	0.14	±0.013	0.14	±0.029	0.10	±0.025	ns	0.69	***	0.0008	**	0.0029
12 wk	0.14	±0.018	0.13	±0.013	0.10	±0.016	ns	0.40	***	0.0001	*	0.037
Im.D[5] (mm)												
4 wk	1.14	±0.11	1.24	±0.12	1.19	±0.10	ns	0.12	ns	0.57	ns	0.56
8 wk	1.13	±0.090	1.25	±0.12	1.28	±0.12	ns	0.069	*	0.037	ns	0.96
12 wk	1.19	±0.10	1.34	±0.079	1.32	±0.11	*	0.031	*	0.033	ns	0.97

[1]St Dev = Standard deviation
[2]Sig. = Significance
[3]P value = Values determined using ANOVA with Tukey's post-hoc
[4] Ct.Th = cortical thickness
[5] Im.D = intramedullary diameter

Figure 4.15 - Reduced long bone strength and flexibility in *Rptor*$_{ob}^{-/-}$ mice : Femurs were isolated from male Osx:Cre, *Rptor*$_{ob}^{-/+}$and *Rptor*$_{ob}^{-/-}$ animals at 4 weeks of age and subjected to 3-point load testing using using a materials testing machine (Model 800LE4; TestResources Inc, Shakopee MN, USA). Femurs were placed posterior side down on the test anvils, which where immersed in a bath of distilled water to keep the bones hydrated. The lower span of the anvils was 5.2 mm and the upper and lower contact radii were 1.0 mm. A pre-load of 0.5 N was applied to the bones before ramp loading to failure with a constant displacement rate of 0.017 mm/s. Compliance in the load-line and bend fixtures was removed from the displacement measurement by using a correction factor obtained from tests with an aluminium calibration specimen. (A) Flexural rigidity was calculated from the load-displacement curves using basic beam theory. (B) Ultimate load was taken directly as the peak load during the tests. Data are presented as mean ± SD, n≥5 per group. *p<0.05, ANCOVA normalised to body weight with Levene's post-hoc test.

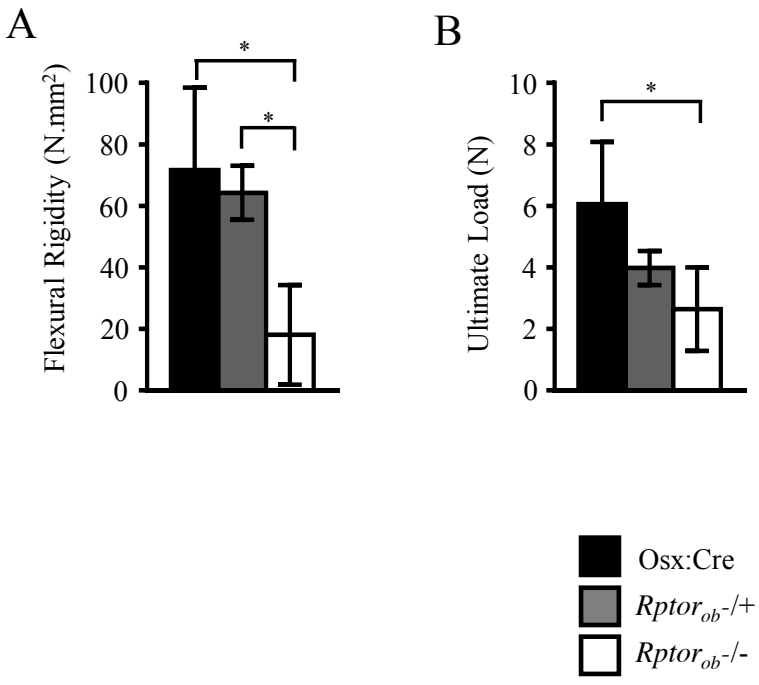
A
B
Flexural Rigidity (N.mm2)
100
80
60
40
20
0
*
*
Ultimate Load (N)
10
8
6
4
2
0
*
Osx:Cre
Rptorob-/+
Rptorob-/-

Table 4.8: Mechanical Testing of Long Bones

	Osx:Cre		*Rptor*$_{ob}^{-/+}$		*Rptor*$_{ob}^{-/-}$		Osx:Cre vs *Rptor*$_{ob}^{-/+}$		Osx:Cre vs *Rptor*$_{ob}^{-/-}$		*Rptor*$_{ob}^{-/+}$ vs *Rptor*$_{ob}^{-/-}$	
	Mean	**St Dev[1]**	**Mean**	**St Dev**	**Mean**	**St Dev**	**Sig.[2]**	**P value[3]**	**Sig.**	**P value**	**Sig.**	**P value**
N.FR[4]	71.6	±26.9	64.3	±8.8	18.1	±16.2	ns	0.84	**	0.003	*	0.012
N.UL[5]	6.1	±2.0	4.0	±0.55	2.6	±1.4	ns	0.14	*	0.011	ns	0.41

[1]St Dev = Standard deviation
[2]Sig. = Significance
[3]P value = Values determined using ANCOVA with Levene's post-hoc
[4]N.FR = Normalised flexural rigidity
[5]N.UL = Normalised ultimate load

Figure 4.16 - *Rptor*$_{ob}^{-/-}$ mice display altered craniofacial development: Three-dimensional reconstructions of the skull were generated for 4 week old *Rptor*$_{ob}^{-/-}$ and Osx:Cre animals using high resolution mCT imaging. (A) A schematic of the basic anatomy of the superior view of the skull. (B) Representative 3D mCT images of the skull (superior view) of a representative 4 week old Osx:Cre and *Rptor*$_{ob}^{-/-}$ mouse. (C) A schematic of the basic anatomy of the lateral view of the skull. (D) Representative 3D mCT images of the skull (lateral view) of a representative 4 week old Osx:Cre and *Rptor*$_{ob}^{-/-}$ mouse.

A

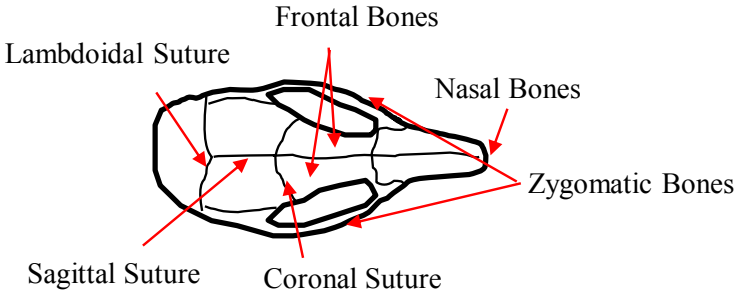
Frontal Bones
Lambdoidal Suture
Nasal Bones
Zygomatic Bones
Sagittal Suture
Coronal Suture

B

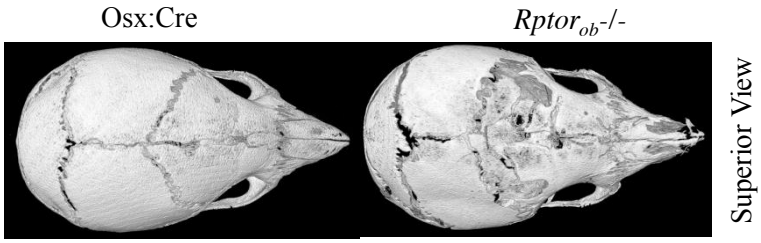
Osx:Cre
$Rptor_{ob}$-/-
Superior View

C

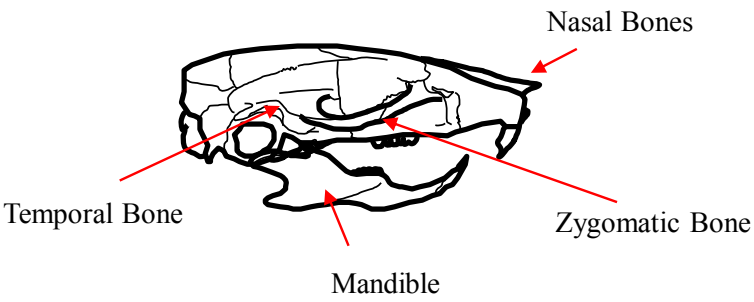
Nasal Bones
Temporal Bone
Zygomatic Bone
Mandible

D

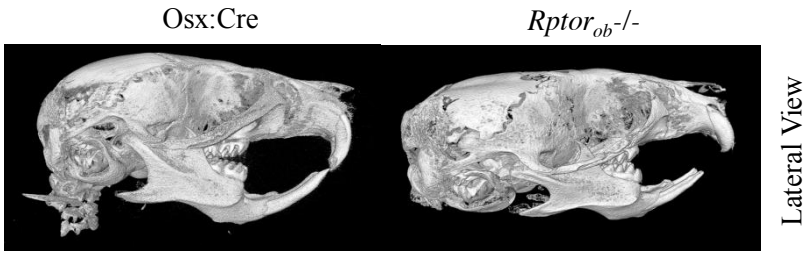
Osx:Cre
$Rptor_{ob}$-/-
Lateral View

4.3 Discussion

In this chapter, the role of mTORC1 in skeletal development was assessed by generating an OB-specific *Rptor* knockout mouse model. Following confirmation that the knockout of *Rptor* was specific to the skeleton in these animals, comparative analyses were performed to examine the whole body and skeletal consequences of OB-specific *Rptor* deletion *in vivo*.

While global deletion of *Rptor* confers embryonic lethality, OB-specific *Rptor* knockout mice were viable and born at the expected Mendelian ratios. However, the survival rates of both $Rptor_{ob}^{-/+}$ and $Rptor_{ob}^{-/-}$ mice were significantly lower than wild type littermates after 52 weeks. While the precise reasons this reduction in long term survival remain to be determined, abnormal OB function has been associated with a variety of pathological conditions in humans including osteogenesis imperfecta, van Buchem Disease and osteoporosis, which require therapeutic intervention for extended survival and disease management [312-314].

As the skeletal phenotype of Osx:Cre embryos has been reported as indistinguishable from wild type animals, wildtype littermates have been the standard comparative control in Osx:Cre-driven conditional knockout studies [33]. However, shortly after the commencement of this study, Davey et al. (2011) [315] published a contrasting study reporting that Osx:Cre mice have a decrease in body weight and reduced bone acquisition at 6 weeks of age, compared to wildtype littermate controls. Therefore, to investigate this further and ascertain which control group was the most suitable for this study, a series of comparative studies was performed between Osx:Cre mice and wild type controls. These analyses showed that Osx:Cre mice have significantly lower body weights than wild type animals at 4, 8 and 12 weeks of age and thinner cortical bone compared to wild type littermates at 4 weeks. While these findings were consistent with the study by Davey *et al* [315], intriguingly we did not observe the 'lag-phase' in Osx:Cre development that they described, whereby the significant differences present during early development (6 weeks of age) are overcome by adulthood (12 weeks of age). While the reason

for these discrepancies remain unclear, variations could be a result of differences in housing conditions and/or the respective breeding colonies.

More recently, additional studies have emerged detailing a defect in early craniofacial bone development [316], delayed calvarial ossification [317] and delayed fracture callus development [317] in Osx:Cre animals compared to wild type littermates. Collectively, these findings confirm the importance of using the correct control to eliminate inaccuracies when reporting the phenotype of knockout animals. As the presence of the tTA:OSX:Cre transgene clearly has an effect on skeletal development in mice, Osx:Cre animals were deemed to be the most suitable control group when characterising the skeletal phenotype of $Rptor_{ob}^{-/+}$ and $Rptor_{ob}^{-/-}$ mice and were used for all subsequent studies.

During normal murine embryonic development, the first evidence of skeletal formation appears at day E9.5. By day E14.5, the skeletal system has been fully formed and is primarily composed of cartilage. This cartilaginous skeleton then undergoes progressive mineralisation prior to birth at day E19 [35, 318]. Osterix expression is detected *in utero* at E12.5, immediately prior to mineralization of the limb buds [90]. At birth, whilst the gross morphology of Osx:Cre and $Rptor_{ob}^{-/-}$ mice were indistinguishable, the cartilage and mineral deposition in bones of newborn $Rptor_{ob}^{-/-}$ mice showed perturbed skeletal development as evidenced by incomplete mineralisation in the ilium and cranium. Furthermore, there was a decrease in both length and proportion of mineral in the long bones of newborn $Rptor_{ob}^{-/-}$ mice compared to Osx:Cre controls. While the exact mechanisms for this observation are currently unknown, IGF signalling upstream of mTORC1 may be a contributor. Mice with disruption of IGF1, IGF2 or IGF-1R exhibit a similar reduction in body weight and abnormal skeletal development consistent with the $Rptor_{ob}^{-/-}$ mice [251-253]. Furthermore, deletion of IGF-1R in pre-OBs using the Osx:Cre driver produced mice that exhibited the same low bone mass and reduced mineral deposition rates as seen in $Rptor_{ob}^{-/-}$ mice [319]. Finally, recent studies have shown that deletion of *Rptor* in mesenchymal progenitors results in a dramatic decrease in animal size and decreased long bone mineralization with a deficit in protein synthesis in chondrocytes leading to a

reduction in long bone length [286]. These results indicate that while mTORC1 activity in Osx-expressing cells is not necessary for embryonic survival, it is necessary for proper skeletal development *in utero*.

To characterise the postnatal skeletal phenotype of OB-specific knockout mice, $Rptor_{ob}^{-/+}$ and $Rptor_{ob}^{-/-}$ mice and Osx:Cre controls were examined at 4, 8 and 12 weeks of age in order to assess early, mid and late-stages of bone development and remodelling, respectively. A decrease in body weight was observed in $Rptor_{ob}^{-/-}$ mice compared to Osx:Cre mice at 4 and 12 weeks of age, and in $Rptor_{ob}^{-/+}$ mice at both 8 and 12 weeks of age. These data suggest the expression of a single *Rptor* allele in pre-OBs can overcome some of the systemic abnormalities associated with $Rptor_{ob}^{-/-}$ mice. However, it should be noted that $Rptor_{ob}^{-/+}$ mice have a significantly higher body weight compared to Osx:Cre mice at 8 weeks, with no difference observed at other time points. While mechanisms for this are unknown, the differences in $Rptor_{ob}^{-/+}$ mice could be attributed to phenotypic consequences associated with the gene dose effect and gene dosage compensation [320, 321]. To date, none of the published studies describing conditional *Rptor* knockouts have reported a heterozygous knockout animal phenotype and therefore further studies are required to determine the effects of heterozygous *Rptor* expression in other tissues [240, 241, 322].

To determine if conditional *Rptor* deletion caused any major systemic effects, major organs including heart, liver, kidneys and spleen were collected and weighed at 4, 8 and 12 week time points. The analysis of organ weight largely indicated no effects of conditional *Rptor* knockout. However, at 4 weeks $Rptor_{ob}^{-/-}$ animals had smaller livers, normalised to total body weight, compared to Osx:Cre mice. This reduction was seemingly rectified by 8 weeks and was most likely associated with the relative increase in $Rptor_{ob}^{-/-}$ animal weight at this time.

The rate of long bone growth is at its greatest during the period between weaning and sexual maturation (approximately week 4 in mice), with growth slowing thereafter and ceasing in early adulthood (approximately week 12 in mice) [306]. Long bone growth, which occurs via endochondral ossification, is facilitated via the chondrocyte-dense epiphyseal growth plates

which remain active throughout elongation prior to thinning and fusing following the cessation of growth. Previous studies have shown the major downstream mTORC1 substrate, p70S6K to be phosphorylated in growth plate chondrocytes suggesting mTORC1 activity during this process [286, 323]. Additionally, *Osx* expression in differentiating chondrocytes within the growth plate has been identified both pre-natally and post-natally in mice as early as E13.5 [324] and *Osx* expression has been shown to overlap with p70S6K activation within the growth plate in E16.5 – E18.5 embryos [323, 325]. As growth plate activity is the principle driving force of longitudinal bone growth, differences in thickness were examined in the proximal tibial growth plates of $Rptor_{ob}^{-/+}$ and $Rptor_{ob}^{-/-}$ mice. Analyses revealed the thickness of the tibial growth plate in $Rptor_{ob}^{-/-}$ mice was significantly thinner than that of both $Rptor_{ob}^{-/+}$ and Osx:Cre controls at 4 weeks. In similar studies, chondrocyte-specific deletion of the negative regulator of mTORC1, liver kinase b1 (*Lkb1*) led to an increase in growth plate thickness [323]. Therefore, loss of mTORC1 function reduces growth plate thickness which likely contributes to the reduced tibial length observed in $Rptor_{ob}^{-/-}$ mice relative to Osx:Cre controls. These findings also suggest that while the reduced long bone growth is evident at 4 and 8 weeks, this can be overcome by 12 weeks of age, suggesting an important role for anabolic mTORC1 signalling in rapid phases of endochondral ossification. While vertebral growth also occurs via endochondral ossification, the formation is less-rapid occurring over a longer period compared to long bone growth. The prolonged growth rate of the vertebrae may account for the decreased spinal length in $Rptor_{ob}^{-/-}$ mice, relative to both Osx:Cre and $Rptor_{ob}^{-/+}$ mice, that was evident at 12 weeks whereas tibial length had normalized by this time [326].

Recently, a study by Chen et. al., (2015) was published suggesting that genetic ablation of *Rptor* in osterix-expressing cells led to osteopenia in mice [327]. While this initial characterisation of OB-specific *Rptor*-null mice gives insight into a role of mTORC1 in the osteogenic program, the results presented are brief and are limited to the assessment of homozygous $Rptor_{ob}^{-/-}$ knockout mice (i.e. heterozygous *Rptor* KO mice were not examined), and data was presented for only one postnatal time point (i.e. 6 weeks of age). The studies

presented in this thesis describe a much more detailed investigation into the phenotypic characterizations of OB specific *Rptor* KO mice. These data presented here indicate that trabecular mineralisation in $Rptor_{ob}^{-/-}$ mice is reduced in the tibia, as indicated by a decrease in the percentage of bone volume (BV/TV), compared to Osx:Cre controls at 4, 8 and 12 weeks of age. Decreased BV/TV was also observed in $Rptor_{ob}^{-/+}$ mice in comparison to Osx:Cre at 12 weeks. Further investigations showed that the decrease in BV/TV in $Rptor_{ob}^{-/-}$ mice could be attributed to a decrease in the number of trabeculae (Tb.N), coupled with an increase in the spacing between the trabeculae (Tb.Sp). This reduction in Tb.N and increase in Tb.Sp is consistent with the 6 week findings from Chen *et al*., [327]. However, in contrast to the findings published by Chen *et al*., [327], decreased BV/TV observed at 4, 8 and 12 week time points was not attributable to a reduction trabecular thickness (Tb.Th). While trabecular structure was consistent between all genotypes at 4 weeks, there was a decrease in trabecular connectivity at 8 and 12 weeks, as indicated by (i) an increase in Tb.Pf, and (ii) a shift away from a plate-like morphology to a spherical morphology at 8 weeks in $Rptor_{ob}^{-/+}$ mice compared to Osx:Cre. These results suggest that in OBs, mTORC1 is involved in the formation and maintenance of structural integrity of the trabecular micro-architecture. An unexpected observation was made at 8 weeks of age, with a significant decrease in BV/TV observed in $Rptor_{ob}^{-/-}$ mice compared to $Rptor_{ob}^{-/+}$ mice, which was not associated with any differences in structural parameters. Furthermore, despite no differences in BV/TV, the structure of the trabeculae in $Rptor_{ob}^{-/+}$ mice differed to Osx:Cre mice represented as a decrease in Tb.N at 4 and 12 weeks and an increase in Tb.Sp at 4 weeks.

mCT analysis of the cortical bone within the proximal tibia also revealed a decrease in bone formation in $Rptor_{ob}^{-/-}$ mice. In addition to the reduced BV/TV of the trabeculae, tibiae of $Rptor_{ob}^{-/-}$ mice had significantly reduced cortical thickness at all time points examined, compared to both $Rptor_{ob}^{-/+}$ and Osx:Cre mice. This was accompanied by an increase in intramedullary diameter compared to Osx:Cre at 8 and 12 weeks and $Rptor_{ob}^{-/+}$ mice at 12 weeks. Riddle *et al*., (2014) showed that deletion of TSC2 (a negative regulator of mTORC1)

caused a progressive increase in postnatal cortical thickness. Furthermore, this excess bone phenotype was partially restored in compound mice in which one allele of mTOR was also deleted. These data suggest that mTORC1 function in osteoblasts is essential for the development and maintenance of long bone diaphyses. Ablation of one allele of *Rptor* resulted in less severe defects than those presented in the double mutation cohort. Nonetheless, the skeletal abnormalities in $Rptor_{ob}^{-/+}$ mice reflect the important role mTORC1 plays in these processes.

OB-specific *Rptor* knockout mice also displayed changes in the biomechanical dynamics of the long bones. Three-point bending analyses confirmed that $Rptor_{ob}^{-/+}$ and $Rptor_{ob}^{-/-}$ mice have more brittle and weak bones compared with Osx:Cre controls. These findings are characteristic of an osteoporotic phenotype found in humans which includes a decrease in bone mineral content as well as an increase in the rate of fracture caused by brittle and inflexible bones [328].

As indicated by representative 3D-reconstructions of mCT images of the skull, deletion of *Rptor* in pre-osteoblasts resulted in incomplete mineralization of the cranial plates, temporal and zygomatic bones and mandiles. Distinct from endochondral ossification, cranial bones develop through the process of intramembranous ossification arising without the production of a cartilage scaffold through the condensation and osteogenic differentiation of MSCs. OB clusters begin synthesizing osteoid which is subsequently mineralized forming spicules that grow and fuse to create interconnecting woven bone. Incomplete and reduced mineral was observed particularly around the calvarial sutures indicating mTORC1 activity is required for normal formation of bones during intramembranous ossification and proper suture fusion. In humans, it has been shown that increased IGF signalling in osteoblasts results in craniosynostosis, the premature fusion of the cranial plates [329, 330]. IGF is a potent activator of mTORC1 signalling in bone [319] suggesting the reduction in suture fusion in $Rptor_{ob}^{-/-}$ mice may be attributable to attenuated IGF-1 signalling in these processes. During the development of the jaw, Osx expression is evident in odontoblasts which are responsible for the formation of the

teeth [331]. While the incidence of malocclusion was similar in Osx:cre and *Rptor*$_{ob}^{-/-}$ mice (data not shown), further investigation onto the micro-architecture of the jaw may reveal a role for mTORC1 in tooth development..

Although results from Chapter 3 indicated that loss of mTORC1 function in primary MSCs had a pro-osteogenic effect, the deletion of *Rptor* in pre-OBs did not reflect this observation. Indeed, the low bone mass phenotype of *Rptor*$_{ob}^{-/-}$ mice suggests mTORC1 plays an important role in skeletal development. In support of this, mice harbouring a deletion of Pten, a negative regulator of PI3kinase, exhibit increased bone mineral density that is associated with constitutive mTORC1 activation. Furthermore, Osx:Cre-mediated deletion of Akt1 and Akt2 (proteins required for suppression of Tsc1/Tsc2, negative regulators of mTORC1) results in delayed bone ossification [166, 260] and shorter lone bones [259]. Additionally, OB-specific hyperactivity of mTORC1 via both Osx:Cre mediated TSC1 deletion and Ocn:Cre mediated TSC2 deletion presented increased bone production [300, 332]. Collectively, these studies indicate signalling via mTORC1 mediates skeletal formation and bone accrual. While the discrepancies between pro-osteogenic effect of *Rptor* deletion in MSC and the low bone mass phenotype in *Rptor*$_{ob}^{-/-}$ mice are not readily apparent, it is possible that this difference is due to mTORC1 activation during different stages of OB differentiation.

In summary, the data presented in this chapter shows that OB-specific deletion of *Rptor* in mice results in incomplete mineralisation and altered skeletal formation. Furthermore, a significant reduction in the length of long bones and in the level of mineralization in the long bones of newborn mice demonstrates an important role for mTORC1 in pre-natal skeletal development. Additionally, these data show that deletion of *Rptor* in pre-OBs leads to defective intramembranous and endochondral ossification and a low bone mass phenotype. Collectively, these findings highlight an important role for mTORC1 in pre- and post-natal skeletal development.

In the following chapter, changes in the cellular components of bone, which likely contribute to the morphological changes evident in *Rptor*$_{ob}^{-/+}$ and *Rptor*$_{ob}^{-/-}$ mice, were

examined. These studies were performed to ascertain whether the low bone mass phenotype of OB-specific *Rptor* knockout animals is due to (i) a decrease in the number of osteoblasts, (ii) a reduction in the synthetic potential of osteoblasts (iii) stalled differentiation of pre-osteoblasts or (iv) uncoupling of the balance between osteoblast-mediated bone-formation and osteoclast-mediated bone resorption.

Chapter 5 - Defining the mechanisms leading to reduced bone mass and limb length in *Rptor*$_{ob}^{-/-}$ mice

5.1 Introduction

A key determinant of skeletal integrity is the homeostatic balance between the actions of bone-resorbing OCs and bone-forming OBs. This tightly-coupled process is maintained by the coordinated actions and cross-talk between OBs and OCs. OBs secrete a number of proteins that regulate bone resorption activities of OCs, including M-CSF, RANKL and OPG while factors which activate OBs, including IGF-1, are sequestered in the bone matrix and released during OC-mediated bone resorption [55-58]. Uncoupling of normal bone remodelling results in pathological changes to the skeleton. In osteoporosis, bone mineral density is reduced as the result of an imbalance between the rate of resorption and the rate of formation and can be accounted for byreduced OB number and activity and increased OC number and activity [3, 4]. In Paget's disease, abnormal bone growth occurs as a result of increased bone resorption due to increased OC numbers [55, 59]. The increase in OC activity increases bone activating factors which signal the limited numbers of OBs to rapidly form bone and results in the synthesis of bone with poor structural integrity that lacks the strength and shape of normal bone [59].

In addition to the regulation of OC-mediated bone resorption, bone mass is determined by OB maturation and function. Multipotent MSCs within the BM undergo osteogenic differentiation in response to various local and systemic factors, which induce the expression of transcription factors promoting OB maturation. As discussed previously, osteogenesis requires the initial expression of the transcription factor Runx2 which in turn regulates the expression of Osterix (*Sp7*) [87, 90]. Furthermore, mature OBs are marked by their synthesis of integrin-binding sialoprotein (Ibsp), osteopontin (Spp1) and osteonectin (Sparc) and osteocalcin (Bglap) which collectively contribute to both the ECM and mineralised matrices of bone. The coordinated and temporal expression of these key markers can be used in the quantification of the different stages in OB differentiation.

mTORC1 is activated by several extracellular factors that control skeletal development. Insulin and IGF-1, activators of PI3K/Akt/mTOR signalling indirectly regulate Runx2 by down-regulating Twist1 and Twist2, negative regulators of Runx2 that bind and inhibit Runx2 activity [256, 333]. Additionally, insulin signalling inhibits Foxo1-mediated suppression of Runx2 [128, 334]. Deletion of the insulin receptor or insulin-like growth factor receptor 1 (*Igflr*) in OBs leads to the development of a post-natal low bone phenotype [319, 335]. Furthermore, studies indicate that these pro-osteogenic effects are mediated through mTORC1, as rapamycin administration *in vitro* has been shown to block IGF-1-stimulated osteogenesis [299, 335]. BMPs including BMP-2 and BMP-4 positively regulate both Runx2 and Osx expression and activity via activation of SMAD signalling molecules[7, 336, 337] Following stimulation by BMP-2 and BMP-7, PI3K/Akt/mTOR signalling is also activated in OBs during osteogenesis *in vitro* [338, 339].

As discussed previously, endochondral ossification facilitates longitudinal growth of the long bones via the proliferation and hypertrophy of chondrocytes within the growth plate [36, 47, 96, 318]. During this process, chondrocytes align in a vertical arrangement stratified into horizontal layers termed the resting, proliferative and hypertrophic zones [35, 318]. During growth, anabolic factors stimulate the resting chondrocytes to proliferate in an organised column formation in the direction of bone growth. Proliferating chondrocytes then mature into hypertrophic chondrocytes which undergo enlargement via both dry mass and liquid uptake. Chondrocyte maturation can be marked by the expression lineage specific genes including Col2A1, Sox9 as early lineage markers and Mmp13 and Col10A1 as mature markers. As osterix expression has been identified within the growth plate in differentiating chondrocytes [324], the potential deletion of *Rptor* in osterix expressing chondrocytes may account for the reduction in growth plate width as described in Chapter 4.

In Chapter 4, the characterisation of OB-specific raptor KO mice showed that mTORC1 plays an important role in pre- and post-natal skeletal development. These mice displayed perturbed intramembranous and endochondral ossification, skeletal fragility, and reduced long bone length. In this Chapter, the mechanisms by which this skeletal phenotype is caused were investigated by undertaking prospective histological and immunohistochemical analyses and analysis the effect of *Rptor* deletion in OB differentiation and function.

5.2 Results

As outlined in Chapter 4, $Rptor_{ob}^{-/+}$ and $Rptor_{ob}^{-/-}$ mice display reduced bone volume and increased skeletal fragility. As BMD is mediated by the relative contribution of OBs and OCs, this low bone mass phenotype is likely indicative of either: (i) a decrease in the number and/or activity of bone-forming OBs, or (ii) an increase in the number and/or activity of bone-resorbing OCs.

5.2.1 Deletion of *Rptor* in pre-OBs does not affect OB morphology or OB number.

To determine whether the low bone mass phenotype of $Rptor_{ob}^{-/+}$ and $Rptor_{ob}^{-/-}$ mice is due to a change in OB number, histomorphometric analyses were performed on tibiae isolated from Osx:Cre, $Rptor_{ob}^{-/+}$ and $Rptor_{ob}^{-/-}$ animals 4, 8 and 12 weeks of age. For this, undecalcified, formalin-fixed tibiae were embedded in methyl methacrylate and sections stained with Toluidine blue. OBs were identified based on their anatomical location on the bone surface and their distinct cuboidal morphology. As shown in Figure 5.1A, a visual assessment of OB morphology, in a defined region of the secondary spongiosa, revealed no distinct morphological differences in OBs in Osx:Cre, $Rptor_{ob}^{-/+}$ and $Rptor_{ob}^{-/-}$ mice. Quantitation of the number of OBs per bone perimeter (N.Ob/B.Pm) and the number of OBs per intramedullary area (N.Ob/M.Ar) was conducted using the OsteoMeasure XP (OsteoMetrics Inc) histomorphometric analysis system. These analyses revealed no significant difference in the number of OBs lining the bone surface (Fig. 5.1B; Table 5.1) or in the number of OBs per area of intramedullary bone surface analysed (Fig. 5.1C; Table 5.1) in $Rptor_{ob}^{-/+}$ and $Rptor_{ob}^{-/-}$ knockout mice compared to Osx:Cre controls at any of the time points examined.

5.2.2 Deletion of *Rptor* in pre-OBs does not affect OC morphology, OC number or OC activity

To determine whether the low bone mass phenotype of $Rptor_{ob}^{-/+}$ and $Rptor_{ob}^{-/-}$ mice is due to a change in OC number, histomorphometric analyses were performed to enumerate OCs

in tibial specimens from Osx:Cre, $Rptor_{ob}^{-/+}$ and $Rptor_{ob}^{-/-}$ animals 4, 8 and 12 weeks of age. OCs were identified in a defined region of secondary spongiosa, in toluidine blue-stained tibial sections, based on their anatomical location on the bone surface and their multi-nucleated morphology (Fig. 5.2A). Quantitative histomorphometric analyses revealed no significant difference in the number of OCs lining the bone perimeter (N.OC/B.Pm), nor any significant difference in the number of OCs present per intramedullary area (N.OC/M.Ar) in $Rptor_{ob}^{-/+}$ and $Rptor_{ob}^{-/-}$ mice, compared to Osx:Cre controls, at any of the time points examined (Fig.s 5.2B and C; Table 5.2).

To examine whether OC activity is altered in OB-specific *Rptor* knockout mice, serum levels of tartrate-resistant acid phosphatase (TRAcP5), an established biomarker of OC activity, were measured. For this, serum samples were collected from Osx:Cre, $Rptor_{ob}^{-/+}$ and $Rptor_{ob}^{-/-}$ mice at 4, 8 and 12 weeks of age by cardiac puncture and assayed using a commercial ELISA kit. As shown in Figure 5.2D, highly variable TRAcP5 levels were observed within each of the animal cohorts, and no statistically significant differences in TRAcP5 levels were observed $Rptor_{ob}^{-/+}$ and $Rptor_{ob}^{-/-}$ mice compared to Osx:Cre controls at any of the time points examined (Fig. 5.2 D).

5.2.3 OB activity is reduced in $Rptor_{ob}^{-/-}$ mice

As outlined in Sections 5.2.1 and 5.2.2, histological analyses suggest that the low bone mass of the OB-specific *Rptor* knockout animals was not attributable to a change in the number of OBs and OCs, nor a change in OC activity. These findings raised the possibility that the low bone mass phenotype of these animals was due to changes in OB activity.

5.2.3.1 The rate of bone formation is reduced $Rptor_{ob}^{-/-}$ mice

To measure OB activity and bone formation during rapid phases of bone growth, 4 week old Osx:Cre, $Rptor_{ob}^{-/+}$ and $Rptor_{ob}^{-/-}$ mice were subcutaneously injected with calcein

Figure 5.1 - OB-specific *Rptor* deletion does not affect OB numbers: Tibiae isolated from male Osx:Cre, $Rptor_{ob}^{-/+}$ and $Rptor_{ob}^{-/-}$ mice at 4, 8 and 12 weeks of age were embedded in methyl methacrylate and 5µm sections were stained with toluidine blue. Osteoblasts were identified based on their anatomical location on the bone surface and their distinct cuboidal morphology. (A) Representative images of toluidine blue-stained bone sections from 4 week old mice highlighting osteoblasts (red arrows) on a section of bone surface (green arrows). Bar = 50µm. (B) Number of osteoblasts per bone perimeter (N.OB/B.Pm). (C) Number of osteoblasts per intramedullary area (N.OB/M.Ar). Data represented as mean ± SD, n≥8 per group in duplicate. One-way ANOVA with Tukey's post-hoc test.

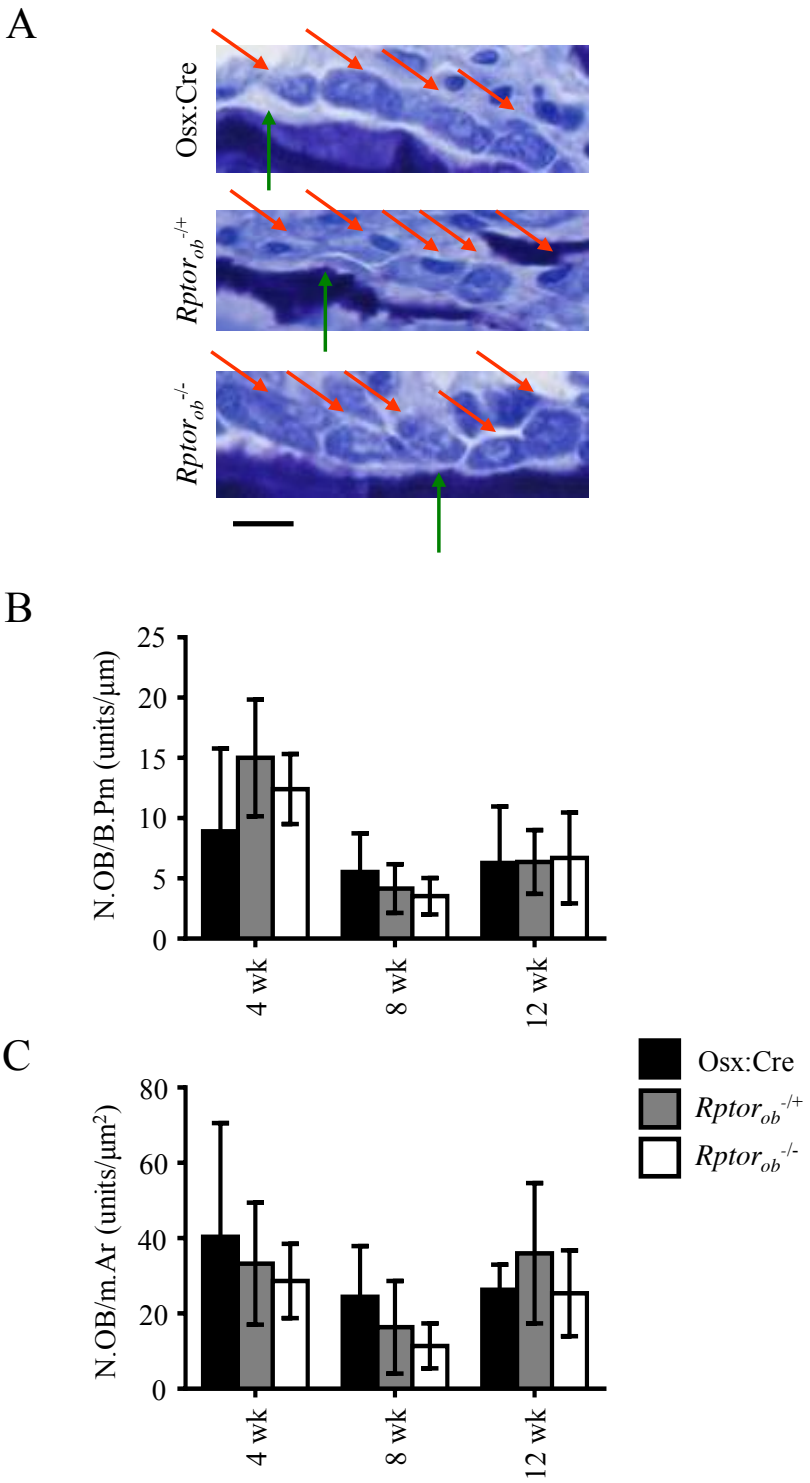
A
Osx:Cre
Rptor ob -/+
Rptor ob -/-
B
N.OB/B.Pm (units/µm)
25
20
15
10
5
0
4 wk
8 wk
12 wk
C
N.OB/m.Ar (units/µm²)
80
60
40
20
0
4 wk
8 wk
12 wk
Osx:Cre
Rptor ob -/+
Rptor ob -/-

Table 5.1: Histomorphological Assessment of Osteoblasts

	Osx:Cre		*Rptor*$_{ob}^{-/+}$		*Rptor*$_{ob}^{-/-}$		Osx:Cre vs *Rptor*$_{ob}^{-/+}$		Osx:Cre vs *Rptor*$_{ob}^{-/-}$		*Rptor*$_{ob}^{-/+}$ vs *Rptor*$_{ob}^{-/-}$	
	Mean	**St Dev[1]**	**Mean**	**St Dev**	**Mean**	**St Dev**	**Sig.[2]**	**P value[3]**	**Sig.**	**P value**	**Sig.**	**P value**
Ob.N[4]/B.Pm[5] (units/μm)												
4 wk	8.91	±6.87	13.50	±4.85	12.41	±2.90	ns	0.17	ns	0.27	ns	0.51
8 wk	5.54	±3.20	4.15	±2.03	3.53	±1.51	ns	0.85	ns	0.71	ns	0.97
12 wk	6.29	±4.68	6.36	±2.65	6.70	±3.77	ns	1.00	ns	0.98	ns	0.99
Ob.N/M.Ar[6] (units/μm^2)												
4 wk	40.39	±30.16	33.22	±16.21	28.66	±9.87	ns	0.73	ns	0.37	ns	0.87
8 wk	24.44	±13.45	16.34	±12.31	11.37	±5.97	ns	0.69	ns	0.38	ns	0.87
12 wk	26.27	±6.68	35.99	±18.63	25.36	±11.39	ns	0.50	ns	0.99	ns	0.47

[1]St Dev = Standard deviation
[2]Sig. = Significance
[3]P value = Values determined using ANOVA with Tukey's post-hoc test
[4] Ob.N = osteoblast number
[5]B.Pm = bone perimeter
[6]M.Ar = intramedullary area

Figure 5.2 - OB-specific *Rptor* deletion does not affect OC number or OC activity: Tibiae isolated from male Osx:Cre, $Rptor_{ob}^{-/+}$ and $Rptor_{ob}^{-/-}$ mice at 4, 8 and 12 weeks of age were embedded in methyl methacrylate and 5μm sections were stained with toluidine blue. Osteoclasts were identified based on their location on the bone surface and their morphology. (A) Representative images of toluidine blue-stained bone sections highlighting osteoclasts (red arrows) on a section of bone surface (green arrows). Bar = 50μm. (B) Number of osteoclasts per bone perimeter (N.OC/B.Pm). (C) Number of osteoclasts per intramedullary area (N.OC/M.Ar). Data represented as mean ± SD, n≥8 per group in duplicate. (D) Serum levels of the marker of osteoclast activity TRAcP5 (tartrate-resistant acid phosphatase) were measured in end-of-study blood samples collected at 4, 8 and 12 weeks of age. Data represented as mean ± SD, n≥3 per group.

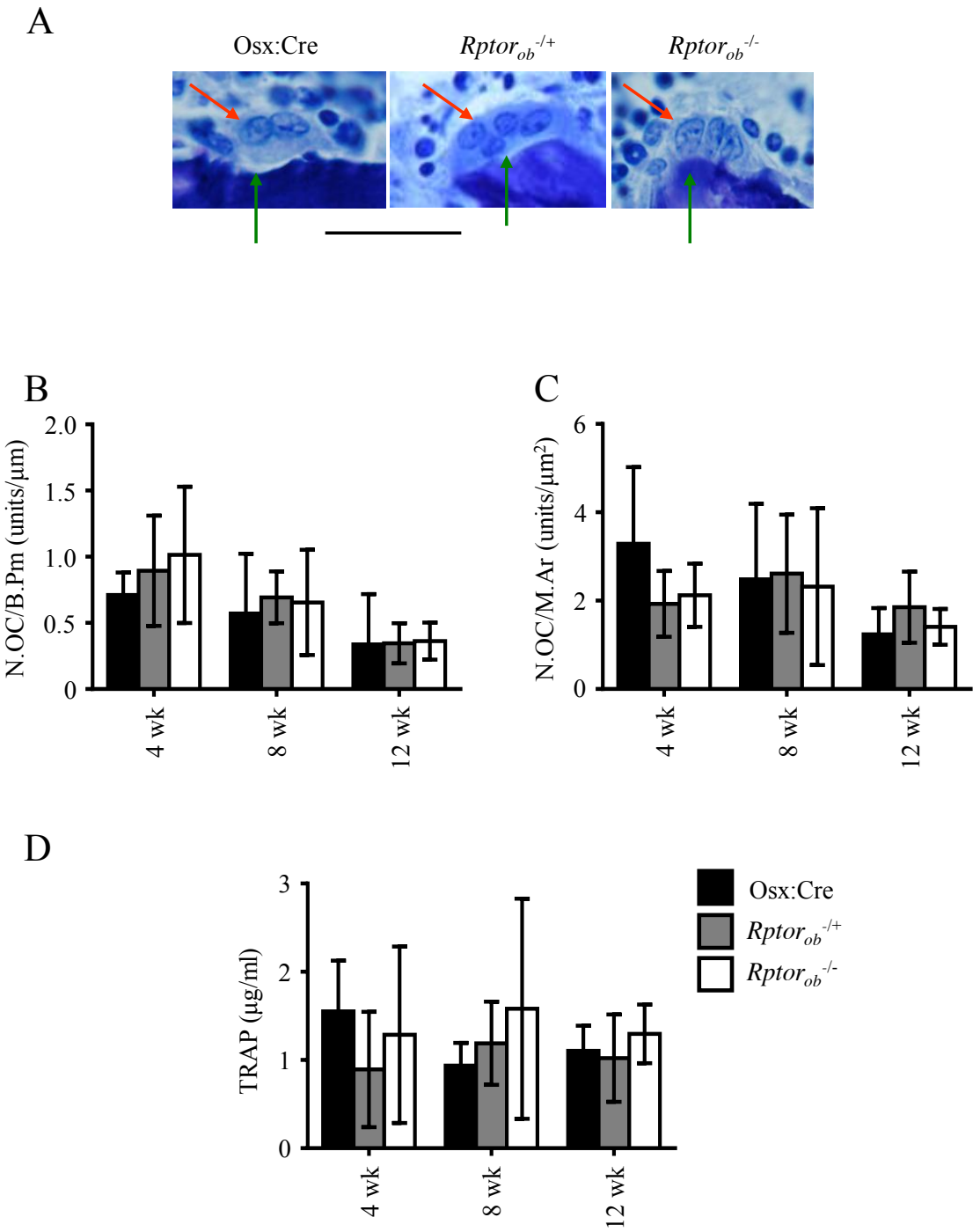
A
Osx:Cre
Rptor_ob-/+
Rptor_ob-/-
B
N.OC/B.Pm (units/µm)
2.0
1.5
1.0
0.5
0
4 wk
8 wk
12 wk
C
N.OC/M.Ar (units/µm²)
6
4
2
0
4 wk
8 wk
12 wk
D
TRAP (µg/ml)
3
2
1
0
4 wk
8 wk
12 wk
Osx:Cre
Rptor_ob-/+
Rptor_ob-/-

Table 5.2: Histomorphological Assessment of Osteoclasts

	Osx:Cre		*Rptor*$_{ob}^{-/+}$		*Rptor*$_{ob}^{-/-}$		Osx:Cre vs *Rptor*$_{ob}^{-/+}$		Osx:Cre vs *Rptor*$_{ob}^{-/-}$		*Rptor*$_{ob}^{-/+}$ vs *Rptor*$_{ob}^{-/-}$	
	Mean	**St Dev[1]**	**Mean**	**St Dev**	**Mean**	**St Dev**	**Sig.[2]**	**P value[3]**	**Sig.**	**P value**	**Sig.**	**P value**
Oc.N[4]/B.Pm[5] (units/μm)												
4 wk	0.71	±0.17	0.89	±0.42	1.01	±0.52	ns	0.66	ns	0.27	ns	0.82
8 wk	0.57	±0.45	0.69	±0.20	0.65	±0.40	ns	0.84	ns	0.92	ns	0.98
12 wk	0.34	±0.38	0.35	±0.15	0.36	±0.14	ns	0.999	ns	0.99	ns	0.996
Oc.N/M.Ar[6] (units/μm^2)												
4 wk	3.29	±1.73	1.93	±0.75	2.12	±0.71	ns	0.14	ns	0.18	ns	0.96
8 wk	2.48	±1.71	2.61	±1.34	2.32	±1.78	ns	0.98	ns	0.97	ns	0.92
12 wk	1.24	±0.59	1.85	±0.80	1.41	±0.40	ns	0.61	ns	0.96	ns	0.78

[1]St Dev = Standard deviation
[2]Sig. = Significance
[3]P value = Values determined using ANOVA with Tukey's post-hoc test
[4] Oc.N = osteoclast number
[5]B.Pm = bone perimeter
[6]M.Ar = intramedullary area

(20mg/gram body weight) at 4 days and 24 hours prior to harvest, to label the exposed bone surface. One day after the second injection, tibiae were collected, fixed in 10% formalin and embedded in methyl methacrylate. Dynamic measurements of bone formation were then conducted on a defined area of the secondary spongiosa using the Osteomeasure XP system.

As shown in Figure 5.3A, the calcein inter-label distance was visibly thinner in $Rptor_{ob}^{-/-}$ mice, compared to both $Rptor_{ob}^{-/+}$ and Osx:Cre controls (Fig. 5.3A). Mineral apposition rate (MAR), which provides an indication of OB activity, was calculated by quantitating the distance between the two calcein-labelled mineralisation fronts and dividing this by the time interval between calcein injections. A significant reduction in MAR was observed in $Rptor_{ob}^{-/-}$ mice compared to both $Rptor_{ob}^{-/+}$ and Osx:Cre controls at 4 weeks of age (mean decrease 38.8±8.1% and 36.3±8.3% respectively) (Fig. 5.3B; Table 5.3). The reduced MAR in $Rptor_{ob}^{-/-}$ mice was associated with a significant reduction in the bone formation rate (BFR), the volume of mineralized bone formed per unit time and per unit bone surface. BFR was significantly reduced in $Rptor_{ob}^{-/-}$ mice relative to both $Rptor_{ob}^{-/+}$ and Osx:Cre controls (36.9±5.9% and 39.3±5.7% respectively) at 4 weeks of age (Fig. 5.3C; Table 5.3). Newly mineralised bone surface to bone surface ratio (MS/BS) showed no significant difference between all genotypes (Fig. 5.3D; Table 5.3).

To examine the rate of activity of mature OBs in knockout mice, serum levels of established biomarkers of bone formation were assessed targeting the OB specific protein OCN and P1NP which indicates levels of collagen type 1 synthesis. Serum samples were collected from Osx:Cre, $Rptor_{ob}^{-/+}$ and $Rptor_{ob}^{-/-}$ mice at 4 weeks of age by cardiac puncture and assayed using commercial ELISA kits. As shown in Figure 5.3E, a significant reduction in serum OCN levels was observed in both $Rptor_{ob}^{-/+}$ and $Rptor_{ob}^{-/-}$ mice compared to Osx:Cre controls (mean decrease 49.7±18% and 56.5±16.7% respectively) (Fig. 5.3E). In contrast, no statistically significant difference in P1NP levels were observed in $Rptor_{ob}^{-/+}$ and $Rptor_{ob}^{-/-}$ mice compared to Osx:Cre controls (Fig. 5.3F).

Figure 5.3 OB-specific *Rptor* deletion reduces OB function

Osx:Cre, $Rptor_{ob}^{-/+}$ and $Rptor_{ob}^{-/-}$ animals were analysed for dynamic markers of bone formation at 4 weeks of age. Calcein was injected into mice 4 days and 24 hours prior to harvest. Undecalcified tibiae were embedded in methyl methacrylate and 5μm sections were analysed using fluorescence microscopy. (A) Representative images of calcein double labelling in Osx:Cre, $Rptor_{ob}^{-/+}$ and $Rptor_{ob}^{-/-}$ mice. The inter-label distance is indicated by red arrows. Bar = 30μm. (B) Mineral apposition rate was quantitated from the calcein inter-label distance relative to time. (C) Bone formation rate was quantitated from the calcein inter-label distance. (D) Mineralised surface to bone surface ratio was quantitated from the calcein inter-label distance. (E) Serum levels of total osteocalcin were measured in samples collected from 4 week old Osx:Cre, $Rptor_{ob}^{-/-}$ and $Rptor_{ob}^{-/+}$ mice using a commercial ELISA kit. (F) Serum levels of P1NP were measured in samples collected from Osx:Cre, $Rptor_{ob}^{-/-}$ and $Rptor_{ob}^{-/+}$ mice at 4 weeks of age using a commercial ELISA kit. Data are presented as mean ± SD, $n \geq 5$ per group. *$p<0.05$, **$p<0.01$, one-way ANOVA with Tukey's post-hoc test.

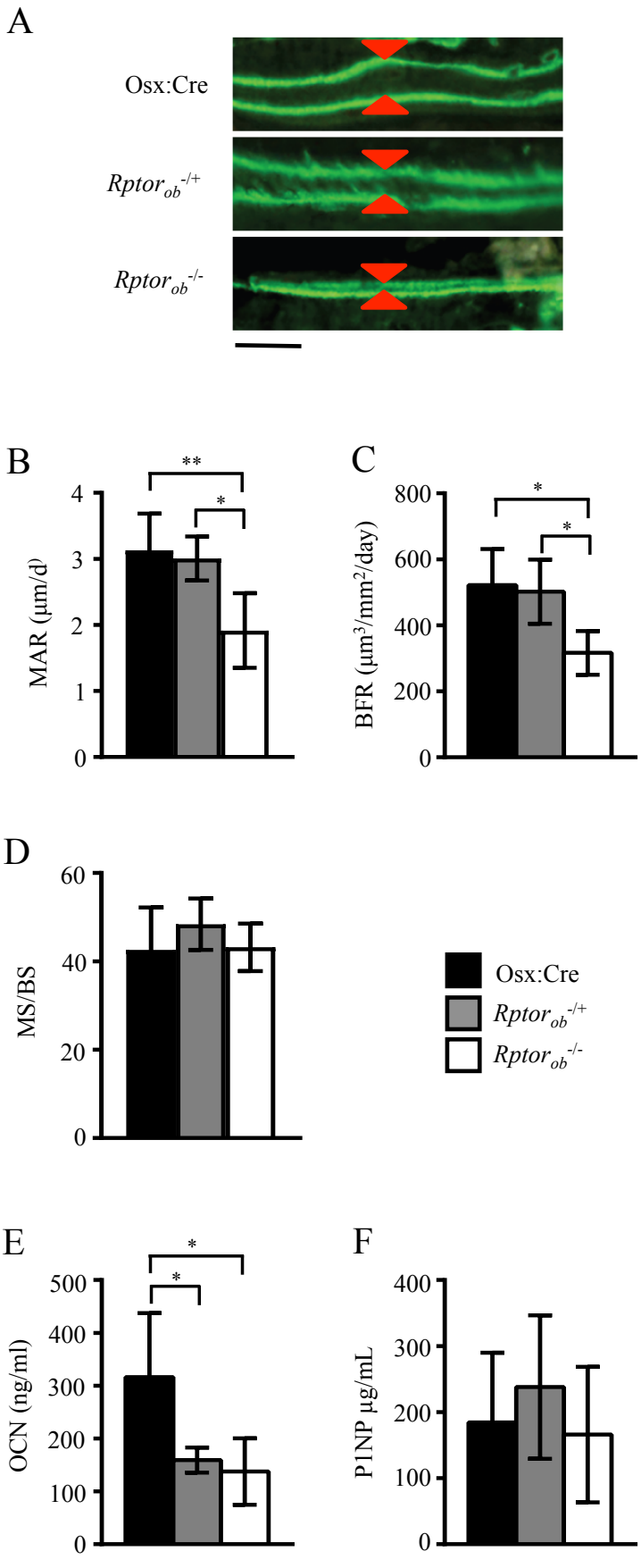
A
Osx:Cre
Rptor ob -/+
Rptor ob -/-
B
MAR (µm/d)
**
*
C
BFR (µm3/mm2/day)
*
*
D
MS/BS
Osx:Cre
Rptor ob -/+
Rptor ob -/-
E
OCN (ng/ml)
*
*
F
P1NP µg/mL

Table 5.3: Assessment of Dynamic Bone Formation

	Osx:Cre		*Rptor*$_{ob}^{-/+}$		*Rptor*$_{ob}^{-/-}$		Osx:Cre vs *Rptor*$_{ob}^{-/+}$		Osx:Cre vs *Rptor*$_{ob}^{-/-}$		*Rptor*$_{ob}^{-/+}$ vs *Rptor*$_{ob}^{-/-}$	
	Mean	**St Dev[1]**	**Mean**	**St Dev**	**Mean**	**St Dev**	**Sig.[2]**	**P value[3]**	**Sig.**	**P value**	**Sig.**	**P value**
MAR[4] (µm/d)	3.13	0.55	3.01	0.33	1.91	0.56	ns	0.92	**	0.0058	*	0.012
BFR[5] (µm3/mm2/day)	521.8	126.5	502.1	97.3	316.6	66.3	ns	0.96	*	0.016	*	0.021
MS/BS[6] (%)	42.57	9.63	48.4	5.81	43.18	5.37	ns	0.63	ns	0.99	ns	0.70

[1]St Dev = Standard deviation
[2]Sig. = Significance
[3]P value = Values determined using ANOVA with Tukey's post-hoc test
[4]MAR = mineral apposition rate
[5]BFR = bone formation rate
[6]MS/BS = mineral surface as a percentage of bone surface

5.2.3.2 OB differentiation marker expression is reduced in *Rptor*$_{ob}^{-/-}$ mouse tibia

To determine whether the reduction in OB function observed in *Rptor*$_{ob}^{-/-}$ mice was due to a block in OB differentiation, the expression of markers of OB differentiation was examined in tibial sections from Osx:Cre, *Rptor*$_{ob}^{-/+}$ and *Rptor*$_{ob}^{-/-}$ mice at 4 weeks of age. As shown in Figure 5.4A, osterix expression was clearly evident in cells of the primary spongiosa immediately adjacent to the zone of hypertrophic chondrocytes in the growth plate of Osx:Cre controls, but was not evident in *Rptor*$_{ob}^{-/-}$ sections (Fig. 5.4A). Similarly, osteocalcin expression, a marker of mature OBs, was evident in cells of the primary spongiosa in Osx:Cre controls but was absent in *Rptor*$_{ob}^{-/-}$ mice (Fig. 5.4A).

5.2.3.3 OBs derived form *Rptor*$_{ob}^{-/-}$ mice have an immature osteogenic transcriptional profile

To gain further insight into the osteoblastic phenotype of *Rptor* knockout cells, the transcript level of genes associated with different stages of osteogenesis was assessed in eYFP+ cells isolated from the long bones of eYFP-Osx:Cre and eYFP-*Rptor*$_{ob}^{-/-}$ mice using real time-PCR. Expression of *Runx2* and *Sp7* (osterix), transcription factors essential for the initial stages of osteogenesis, were significantly elevated in eYFP+ cells isolated from eYFP-*Rptor*$_{ob}^{-/-}$ mice relative to eYFP-Osx:Cre controls (mean fold increase 2.73±0.71 and 2.0±0.27, respectively) (Fig. 5.4B). In contrast, mRNA expression of late OB markers such as osteocalcin (*Bglap*), integrin-binding sialoprotein (*Ibsp*), osteopontin (*Spp1*), and osteonectin (*Sparc*) was significantly down-regulated in eYFP-*Rptor*$_{ob}^{-/-}$ mice relative to eYFP-Osx:Cre controls (mean decrease: *Bglap*: 79±1.5%, *Ibsp*: 81±4%, *Spp1*: 60.8± 1.8% and *Sparc*: 87.9±6%)(Fig. 5.4B).

5.2.3.4 OBs derived form *Rptor*$_{ob}^{-/-}$ mice have reduced osteogenic potential

To further assess OB function, calvarial MSCs isolated from Osx:Cre, *Rptor*$_{ob}^{-/+}$ and *Rptor*$_{ob}^{-/-}$ mice were cultured under osteogenic conditions and their ability to form a mineralised

matrix was assessed. As shown in Figure 5.5A, deletion of *Rptor* caused a significant reduction in mineralised matrix production, as evidenced by reduced alizarin red staining of calcium deposits in OBs from $Rptor_{ob}^{-/+}$ and $Rptor_{ob}^{-/-}$ mice compared to *Osx:Cre* controls. Furthermore, the level of acid-solubilised calcium and alizarin red staining of calcium deposits in OBs from $Rptor_{ob}^{-/+}$ and $Rptor_{ob}^{-/-}$ mice was decreased compared to *Osx:Cre* controls (mean decrease 41.5±8.5% and 72.8±4.1% respectively).

In order to gain further insight into the biochemical mechanisms by which mTORC1 facilitates OB maturation and function, the responsiveness of knockout and control calvarial OBs to anabolic factors known to activate mTORC1 [340] was assessed. Insulin signalling which stimulates osteogenesis, has been shown to signal upstream of mTORC1. Addition of insulin to osteogenic cultures of calvarial MSCs from Osx:Cre, $Rptor_{ob}^{-/+}$ and $Rptor_{ob}^{-/-}$ mice resulted in a significant increase in the amount of mineralised matrix production by Osx:Cre cells relative to unstimulated cultures (mean increase 35.8±2.7%). However, no significant differences were observed in response to insulin in cells isolated from $Rptor_{ob}^{-/+}$ and $Rptor_{ob}^{-/-}$ mice (Fig. 5.5B).

An organotypic culture system was also used to assess bone growth. In this assay, whole calvarias isolated from 4-day old control and knockout mice were cultured at the air-liquid interface *ex vivo* in the presence or absence of BMP-2, a potent anabolic factor. After 10 days of culture, calvarias were fixed in formalin, decalcified and embedded in paraffin. Quantitation of new bone growth in H&E-stained sections cut parallel to the midline suture showed that BMP-2 stimulated a significant increase in new bone formation in calvarias isolated from *Osx:Cre* controls (mean increase 37±7.7%), however, no significant anabolic effect was observed in calvarias isolated from $Rptor_{ob}^{-/+}$ and $Rptor_{ob}^{-/-}$ mice (Fig. 5.5C).

Figure 5.4 - *Rptor* null osteoblasts have an immature osteogenic transcriptional profile : (A) Tibiae were isolated from male Osx:Cre and $Rptor_{ob}^{-/-}$ mice at 4 weeks of age and immunohistological analyses performed on a region of primary spongiosa distal to the proximal growth plate. Formalin-fixed tibiae were decalcified, embedded in paraffin, and 5µm sections were stained with Haematoxylin and Eosin (H&E), and antibodies directed against osterix and osteocalcin. Bar = 50µm. (B) eYFP+ cells were isolated from 6 week old eYFP-Osx:cre and eYFP-$Rptor_{ob}^{-/-}$ mice (n=11 per genotype, pooled) and lysed for total RNA. qPCR analyses were performed to measure levels of Runx2, osterix (Sp7), osteocalcin (Bglap), integrin-binding sialoprotein (Ibsp), osteopontin (Spp1) and osteonectin (Sparc), and data were normalised to β-actin. Data are presented as mean ± SD. *$p<0.05$, **$p<0.01$, ***$p<0.001$, Student t-test.

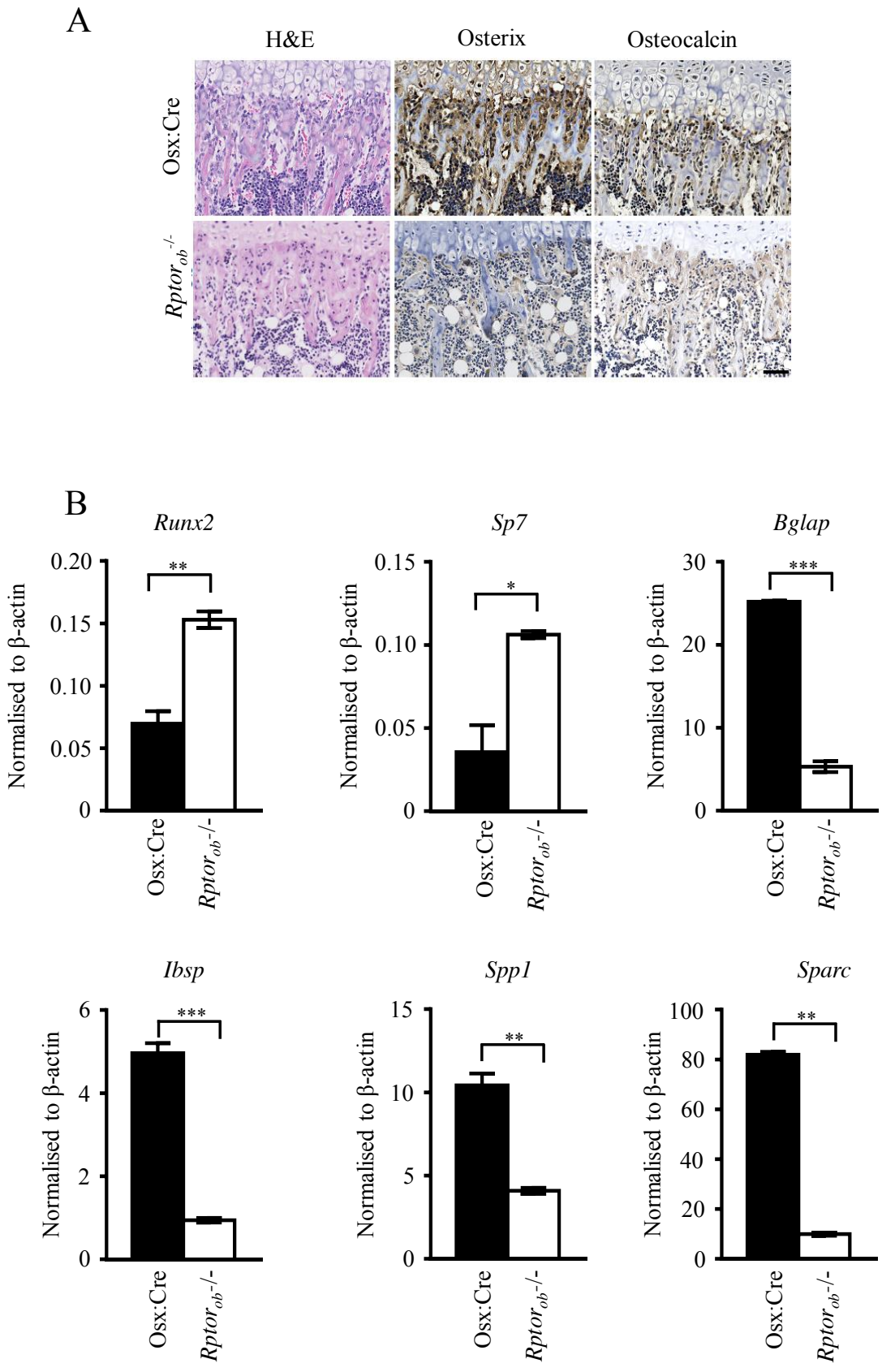
A
H&E
Osterix
Osteocalcin
Osx:Cre
Rptor_ob-/-
B
Runx2
Sp7
Bglap
Ibsp
Spp1
Sparc
Normalised to β-actin
Osx:Cre
Rptor_ob-/-

Figure 5.5 - *Rptor* null MSCs have a reduced osteogenic potential: (A) Calvarial MSCs isolated from 4 week old male Osx:Cre, $Rptor_{ob}^{-/+}$ and $Rptor_{ob}^{-/-}$ mice were cultured under osteogenic conditions for 21 days and the amount of acid-solubilised calcium was quantitated and normalised to cell number. Data are expressed as the mean ± SD of quadruplicate wells from a representative experiment of three. Representative images of Alizarin Red-stained wells are shown below the graph. *p<0.05; ***p<0.001, one-way ANOVA with Tukey's post-hoc test. (B) Cavarial MSCs isolated from Osx:Cre, $Rptor_{ob}^{-/+}$ and $Rptor_{ob}^{-/-}$ animals were cultured under osteogenic conditions for 21 days in the presence or absence of 10nM insulin, and the amount of acid-solubilised calcium was quantitated and normalised to cell number. Data are expressed as the mean ± SD of quadruplicate wells from a representative experiment of three. *p<0.05 ***p<0.001, one-way ANOVA with Tukey's post-hoc test. (C) Neonatal calvariae isolated from 4 day old Osx:Cre, $Rptor_{ob}^{-/+}$ and $Rptor_{ob}^{-/-}$ mice were cultured ex vivo in the presence or absence of recombinant human BMP-2 (50ng/mL) for 10 days. The width of newly-formed bone per bone perimeter (Ir.L.Th/B.Pm) was quantitated using histomorphometry. Data are presented as mean ± SD of three independent experiments each performed using four calvariae per genotype, *p<0.05, one-way ANOVA with Tukey's post-hoc test.

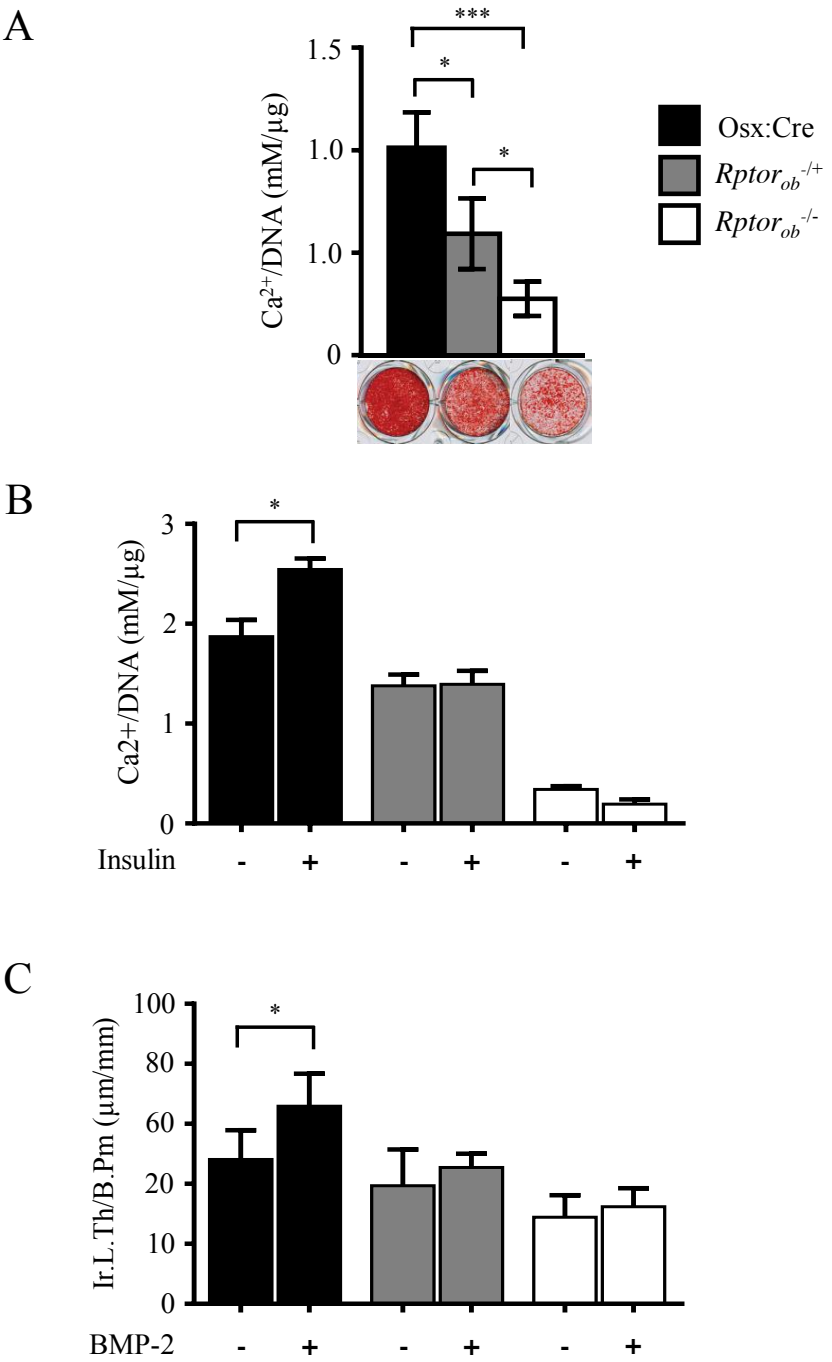
A
***
*
*
1.5
1.0
1.0
0
Ca2+/DNA (mM/µg)
Osx:Cre
Rptor ob -/+
Rptor ob -/-
B
*
3
2
1
0
Ca2+/DNA (mM/µg)
Insulin
- + - + - +
C
*
100
80
60
20
10
0
Ir.L.Th/B.Pm (µm/mm)
BMP-2
- + - + - +

5.2.4 Growth plate analysis

Longitudinal bone growth is primarily driven by the coordinated proliferation and differentiation of chondrocytes. At the growth plate, chondrogenic cells are arranged into vertical columns that can be stratified into horizontal layers (zones) corresponding to different phases of chondrocyte differentiation [35, 318]. These zones are termed the resting zone (RZ), proliferative zone (PZ) and hypertropic zone (HZ).

5.2.4.1 Osx is expressed in growth plate chondrocytes

Osterix expression has previously been observed in pre-hypertrophic chondrocytes of the embryonic [90, 341] and postnatal [342] skeleton. Therefore, the reduction in both growth plate thickness and long bone growth could be associated with *Rptor* deletion in Osx expressing chondrocytes. To confirm OSX expression in chondrocytes of the growth plate, tibiae from R26eYFP-Osx:Cre and R26eYFP-$Rptor_{ob}^{-/-}$ mice were analysed using confocal microscopy. Osx expression was assessed using the ROSA26eYFP reporter gene, whereby eYFP expression is activated through Cre mediated deletion of an upstream floxed STOP cassette[303]. As shown in Figure 5.6A, eYFP-labelled chondrogenic cells were detected within the proximal tibial growth plate in both eYFP-Osx:Cre control and eYFP-$Rptor_{ob}^{-/-}$ mice.

5.2.4.2 Proliferative- and hypertrophic- zones are smaller in the growth plate of $Rptor_{ob}^{-/-}$ mice

To investigate whether the deletion of *Rptor* in chondrogenic cells could contribute to the reduction in limb length observed in $Rptor_{ob}^{-/-}$ mice, the morphology of the tibial growth plate was analysed using sections in which acidic proteoglycan, present in cartilage tissues, was stained red with Safranin O (Fig. 5.6B). In $Rptor_{ob}^{-/-}$ mice, chondrocytes within the proliferating zone were disorganised with fewer cells arranged into vertical columns relative to Osx:Cre controls (Fig. 5.6B). To quantitate any changes in the growth plate of OB-specific KO mice, the width of the three chondrocyte zones within the growth plate were measured using

Figure 5.6 - OB-specific *Rptor* deletion results in decreased thickness of the proliferative zone in the growth plate: Tibiae from male Osx:Cre, $Rptor_{ob}^{-/+}$ and $Rptor_{ob}^{-/-}$ animals were isolated at 4 weeks of age for analysis of the proximal growth plate. (A) Formalin-fixed tibiae from eYFP-Osx-cre and eYFP- $Rptor_{ob}^{-/-}$ mice were embedded in OCT compound and 5µm sections stained with an anti-eYFP antibody. Cell nuclei were stained with DAPI. Confocal microscopy was used to detect eYFP expression in the growth plate. Representative images of eYFP-labelled cells (green) within the proliferative zone (PZ), hypertrophic zone (HZ), and primary spongiosa (PS) of the epiphyseal growth plate are shown. Bar = 50mm. (B) Tibiae from male Osx:Cre, $Rptor_{ob}^{-/+}$ and $Rptor_{ob}^{-/-}$ mice at 4, 8 and 12 weeks of age were embedded in methyl methacrylate and stained with Safranin O and Fast Green. Representative images of the growth plate of 4 week old Osx:Cre, $Rptor_{ob}^{-/+}$ and $Rptor_{ob}^{-/-}$ mice indicating the resting zone (RZ), proliferative zone (PZ), hypertrophic zone (HZ),. Bar = 200mm. The widths of the (C) proliferative zone, (D) resting zone and (E) hypertrophic zone of the growth plate were quantitated using histomorphometry, based on chondrocyte morphology Data are presented as mean ± S.D, n≥6 per group. *p<0.05; **p<0.01; ****p<0.001. One-way ANOVA with Tukey's post-hoc test.

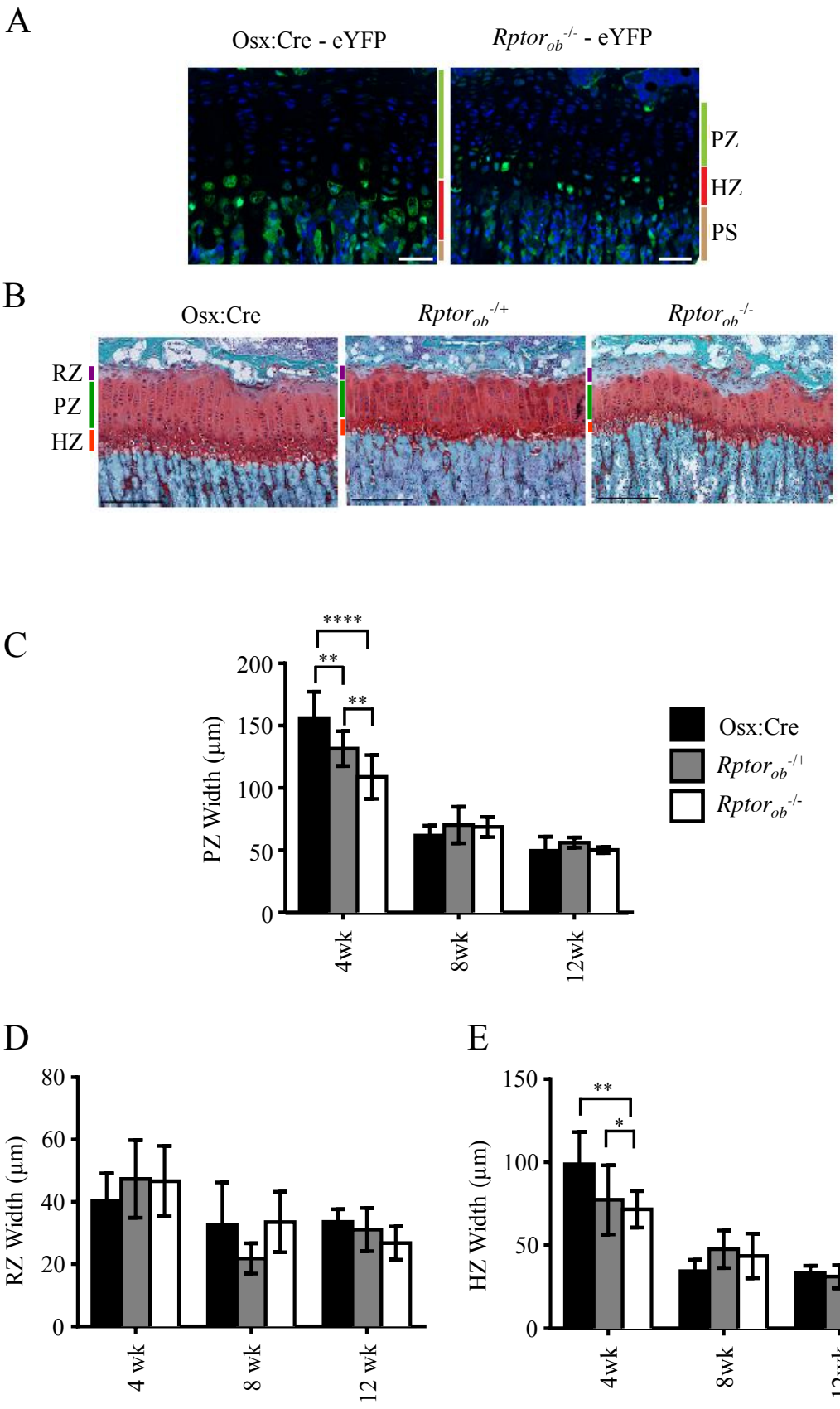
A
Osx:Cre - eYFP
Rptor_ob-/- - eYFP
PZ
HZ
PS
B
Osx:Cre
Rptor_ob-/+
Rptor_ob-/-
RZ
PZ
HZ
C
****
**
**
PZ Width (µm)
200
150
100
50
0
4wk
8wk
12wk
Osx:Cre
Rptor_ob-/+
Rptor_ob-/-
D
RZ Width (µm)
80
60
40
20
0
4 wk
8 wk
12 wk
E
**
*
HZ Width (µm)
150
100
50
0
4wk
8wk
12wk

histomorphometric analysis. At 4 weeks of age, the width of the proliferating zone was significantly reduced in both $Rptor_{ob}^{-/+}$ and $Rptor_{ob}^{-/-}$ mice (mean decrease 15.7±4% and 30.3±5% respectively) compared to Osx:Cre controls, however no statistically significant differences were observed at the 8 and 12 week time points (Fig. 5.6C; Table 5.4). Furthermore, no significant difference in the width of the resting zone (which contains precursor cells which, when activated, proliferate and synthesise a cartilagenous matrix) was observed at any of the time points examined (Fig. 5.6D). Whilst the width of the hypertrophic zone was significantly reduced in both $Rptor_{ob}^{-/+}$ and $Rptor_{ob}^{-/-}$ mice (mean decrease 21.6±9.4% and 27.4±5% respectively) compared to Osx:Cre controls at 4 weeks of age, no significant differences were observed at the 8 and 12 week time points (Fig. 5.6E).

5.2.4.3 Deletion of *Rptor* reduces the proliferation and maturation of growth plate chondrocytes in $Rptor_{ob}^{-/-}$ mice

To examine whether the marked reduction in the width of the proliferating and hypertrophic zones of the growth plate was attributable to a decrease in chondrocyte proliferation, PCNA expression, a nuclear marker of proliferating cells [343] was assessed in 4 week old $Rptor_{ob}^{-/-}$ mice. As shown in Figure 5.7A, PCNA expression was clearly evident in chondrocytes within the growth plate of Osx:Cre controls but was otherwise absent in chondrocytes in the growth plate of $Rptor_{ob}^{-/-}$ mice.

To determine if *Rptor* deletion in osterix-expressing chondrocytes affects chondrocyte differentiation, transcript levels of immature and mature chondrocyte markers were assessed in RNA isolated from eYFP+ cells recovered from the long bones of control *eYFP-Osx:Cre* and knockout *eYFP-*$Rptor_{ob}^{-/-}$ mice. As shown in Figure 5.7B, no significant difference in the expression of early chondrocyte markers *Sox9* and *Col2a1* (isoform 2) was observed in $Rptor_{ob}^{-/-}$ mice relative to Osx:Cre controls. However, transcript levels of *Mmp13* and *Col10a1*, markers of mature and terminally differentiated chondrocytes, were significantly reduced in $Rptor_{ob}^{-/-}$

Figure 5.7 - OB-specific *Rptor* deletion reduces chondrocyte proliferation and maturation: Tibiae from age-matched male Osx:Cre and $Rptor_{ob}^{-/-}$ mice at 4 weeks of age were isolated for immunohistological and histological analysis of the chondrocytes within the proximal growth plate. (A) Representative image of immune-histochemical staining of proliferating cell nuclear antigen (PCNA) in the growth plates of Osx:Cre and $Rptor_{ob}^{-/-}$ mice. The proliferative zone (PZ), hypertrophic zone (HZ), and primary spongiosa (PS) of the epiphyseal growth plate are shown. Bar = 50mm. (B) qPCR was performed on RNA extracted from eYFP+ cells isolated from control eYFP-Osx:cre and eYFP- $Rptor_{ob}^{-/-}$ mice at 4 weeks of age using primers specific to the indicated genes. Relative transcript levels were normalised to β-actin. *$p<0.05$, one-way ANOVA with Tukey's post-hoc test. (C) Osx:Cre, $Rptor_{ob}^{-/+}$ and $Rptor_{ob}^{-/-}$ animals were injected with calcein 4 days and 24 hours prior to harvest at 4 weeks of age. Tibiae were embedded in methyl methacrylate and 5μm sections were analysed using fluorescence microscopy. The rate of endochondral bone growth was quantitated from the average distance between the growth plate and newly-deposited mineral. Data are presented as mean ± S.D, $n\geq6$ per group. *$p<0.05$, one-way ANOVA with Tukey's post-hoc test.

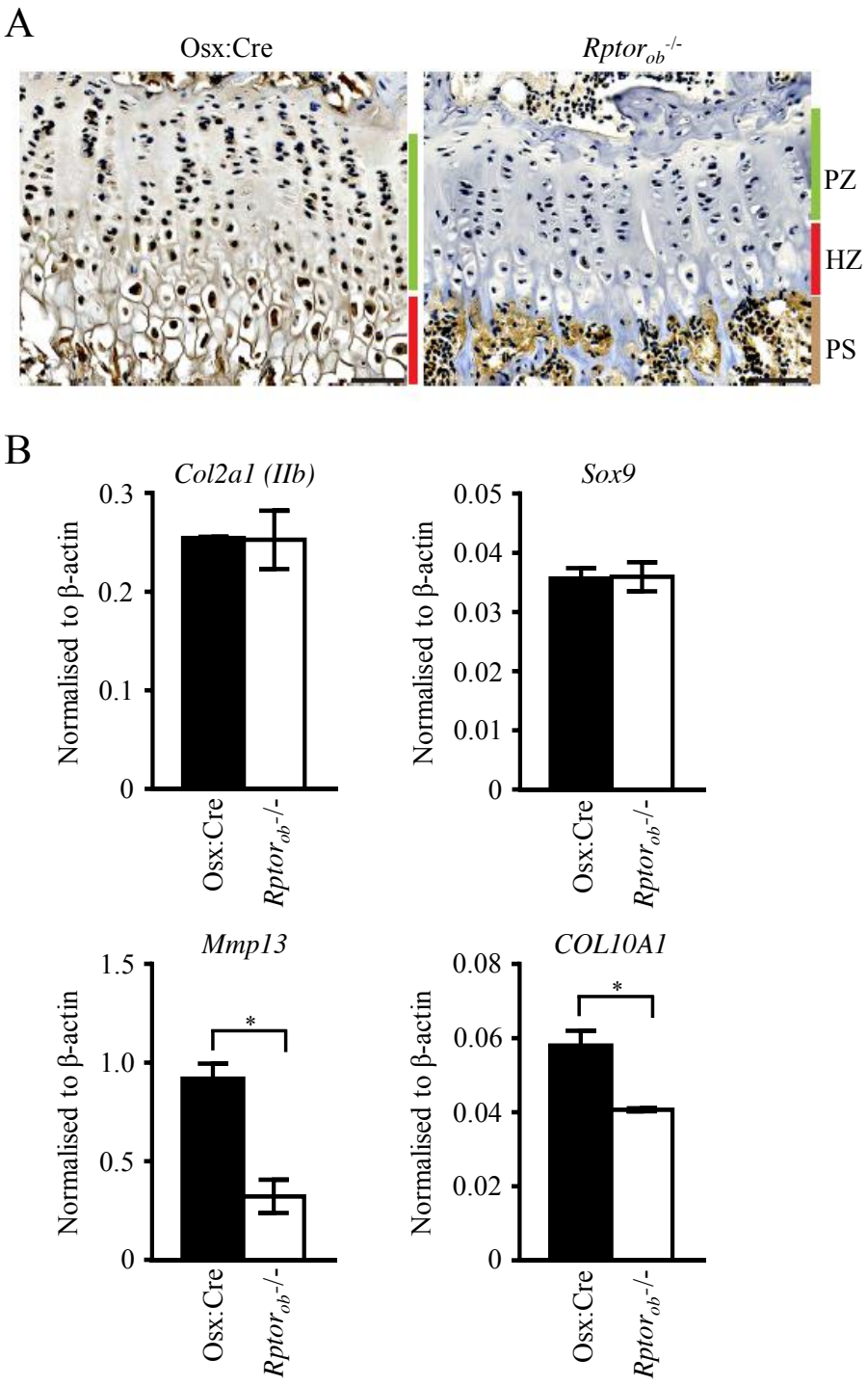
A
Osx:Cre
Rptor_ob-/-
PZ
HZ
PS
B
Col2a1 (IIb)
Sox9
Mmp13
COL10A1
Normalised to β-actin
Osx:Cre
Rptor_ob-/-
C
Distal Growth (µm/d)
Osx:Cre
Rptor_ob-/+
Rptor_ob-/-

Table 5.5: Endochondral Growth Analysis

	Osx:Cre		*Rptor*$_{ob}^{-/+}$		*Rptor*$_{ob}^{-/-}$		Osx:Cre vs *Rptor*$_{ob}^{-/+}$		Osx:Cre vs *Rptor*$_{ob}^{-/-}$		*Rptor*$_{ob}^{-/+}$ vs *Rptor*$_{ob}^{-/-}$	
	Mean	**St Dev[1]**	**Mean**	**St Dev**	**Mean**	**St Dev**	**Sig.[2]**	**P value[3]**	**Sig.**	**P value**	**Sig.**	**P value**
Endochondral Growth (µm/d)	122.6	±17.4	116.8	40.3	69.5	22.4	ns	0.94	*	0.031	ns	0.054

[1]St Dev = Standard deviation
[2]Sig. = Significance
[3]P value = Values determined using ANOVA with Tukey's post-hoc test

mice compared to Osx:Cre controls (fold decrease: *Mmp13*, 3.0±0.55; *Col10a1*, 1.4±0.07) (Fig. 5.7B).

Given the decreased proliferative zone width in the proximal tibial growth plate, the effect of OB-specific *Rptor* deletion on the rate of long bone growth was next assessed in 4 week old mice. To achieve this, Osx:Cre, $Rptor_{ob}^{-/+}$ and $Rptor_{ob}^{-/-}$ mice were subcutaneously injected with calcein (20μg/gram body weight) at 4 days and 24 hours prior to harvest at 4 weeks of age, to label the exposed bone surface. Using histomorphometric analysis, the rate of longitudinal growth per day was determined by measuring the average width of the newly-formed primary and secondary spongiosa, identified as unstained mineral, distal to the growth plate. As shown in Figure 5.7C, a significant reduction in longitudinal growth per day was observed in $Rptor_{ob}^{-/-}$ mice compared to Osx:Cre controls (mean decrease 43.3±15.4%; Table 5.5).

5.2.5 Intramedullary adiposity is increased in $Rptor_{ob}^{-/-}$ mice

During histological assessments of the tibia and femur of $Rptor_{ob}^{-/-}$ mice, it was noted that long bones of $Rptor_{ob}^{-/-}$ mice contain high levels of intramedullary adipose (as defined by the circular, unstained spaces within the intramedullary space) (Fig. 5.8A). To examine this further, histological analyses were carried out to quantitate AdC numbers and adipose volume in Osx:Cre, $Rptor_{ob}^{-/+}$ and $Rptor_{ob}^{-/-}$ mice. For these studies, the number of AdCs as a percentage of the intramedullary area (N.AdC/M.Ar) and the area of adipose tissue as a percentage of the intramedullary area (AdC.Ar/M.Ar) were quantified in a defined region of secondary spongiosa in toluidine blue-stained tibial sections from male Osx:Cre, $Rptor_{ob}^{-/+}$ and $Rptor_{ob}^{-/-}$ animals at 4, 8 and 12 weeks of age. As shown in Figure 5.8B, the number of AdCs as a percentage of the intramedullary area was significantly higher in $Rptor_{ob}^{-/-}$ mice relative to both $Rptor_{ob}^{-/+}$ and Osx:Cre controls at 4 weeks of age (mean fold increase 1.18±0.46 and 6.64±1.52, respectively) (Fig. 5.8B; Table 5.6). Whilst there was a trend towards a higher N.AdC/M.Ar in $Rptor_{ob}^{-/+}$ and

Figure 5.8 - OB-specific *Rptor* deletion is associated with increased intramedullary adipose: Tibiae isolated from male Osx:Cre, $Rptor_{ob}^{-/+}$ and $Rptor_{ob}^{-/-}$ mice at 4, 8 and 12 weeks of age were embedded in methyl methacrylate and 5μm sections were stained with toluidine blue. Adipocytes were identified based on their morphology. (A) Representative images of toluidine blue-stained bone sections from 4 week old mice highlighting the unstained zones representing lipid vacuoles of adipocytes cleared during the fixation process (red arrows). Bar = 250mm. (B) The number of adipocytes per area of intramedullary space (N.Adc/M.Ar), (C) the area occupied by adipocyes per number of adipocytes (AdC.Ar/N.AdC), and (D) the average adipocyte area (AdC.Ar/AdC.N) was quantified. Data are presented as mean ± S.D, n≥8 per group in duplicate. *p<0.05; **p<0.01 and ****p<0.0001, one-way ANOVA with Tukey's post-hoc test.

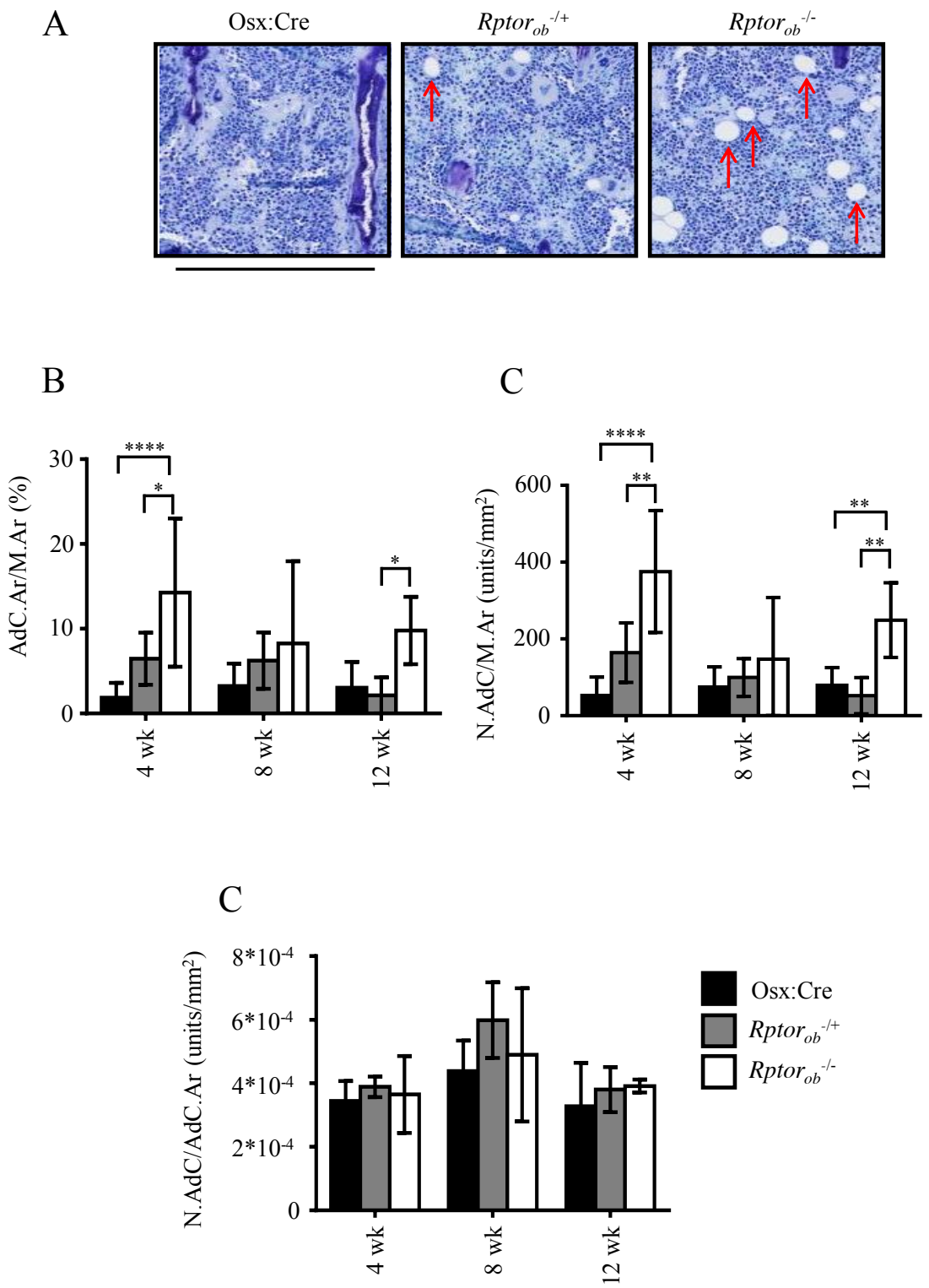
A
Osx:Cre
Rptor_ob-/+
Rptor_ob-/-
B
AdC.Ar/M.Ar (%)
30
20
10
0
****
*
*
4 wk
8 wk
12 wk
C
N.AdC/M.Ar (units/mm2)
600
400
200
0
****
**
**
**
4 wk
8 wk
12 wk
C
N.AdC/AdC.Ar (units/mm2)
8*10-4
6*10-4
4*10-4
2*10-4
0
4 wk
8 wk
12 wk
Osx:Cre
Rptor_ob-/+
Rptor_ob-/-

Table 5.6: Histomorphological Assessment of Medullary Adipose

	Osx:Cre		*Rptor*$_{ob}^{-/+}$		*Rptor*$_{ob}^{-/-}$		Osx:Cre vs *Rptor*$_{ob}^{-/+}$		Osx:Cre vs *Rptor*$_{ob}^{-/-}$		*Rptor*$_{ob}^{-/+}$ vs *Rptor*$_{ob}^{-/-}$	
	Mean	**St Dev[1]**	**Mean**	**St Dev**	**Mean**	**St Dev**	**Sig.[2]**	**P value[3]**	**Sig.**	**P value**	**Sig.**	**P value**
AdC.Ar/M.Ar (%)												
4 wk	1.87	±1.75	6.46	±3.07	14.26	±8.74	ns	0.31	***	0.0002	*	0.032
8 wk	3.23	±2.65	6.24	±3.32	8.27	±9.68	ns	0.62	ns	0.27	ns	0.80
12 wk	3.03	±3.07	2.13	±2.14	9.78	±3.97	ns	0.95	*	0.032	*	0.033
AdC.N/M.Ar (units/μm^2)												
4 wk	53.0	±47.7	164.3	±77.3	375.5	±158.9	ns	0.14	****	< 0.0001	**	0.0012
8 wk	74.9	±52.2	99.5	±49.3	147.2	±160.5	ns	0.91	ns	0.45	ns	0.71
12 wk	79.2	±46.1	52.0	±47.3	248.8	±97.3	ns	0.86	**	0.0065	**	0.0022
AdC.Ar/AdC.N (μm^2/units)												
4 wk	$3.44x10^{-4}$	$6.28x10^{-5}$	$3.89x10^{-4}$	$3.22x10^{-5}$	$3.65x10^{-4}$	$1.21x10^{-4}$	ns	0.78	ns	0.94	ns	0.93
8 wk	$4.39x10^{-4}$	$9.58x10^{-5}$	$5.99x10^{-4}$	$1.19x10^{-4}$	$4.89x10^{-4}$	$2.10x10^{-4}$	ns	0.06	ns	0.74	ns	0.26
12 wk	$3.28x10^{-4}$	$1.36x10^{-4}$	$3.80x10^{-4}$	$7.09x10^{-5}$	$3.91x10^{-4}$	$2.00x10^{-5}$	ns	0.65	ns	0.55	ns	0.98

[1]St Dev = Standard deviation
[2]Sig. = Significance
[3]P value = Values determined using ANOVA with Tukey's post-hoc test
[4] AdC.N = adipocyte number
[5] M.Ar = intramedullary area
[6] AdC.Ar = adipose area

Rptor$_{ob}^{-/-}$ animals compared to Osx:Cre controls at 8 weeks, this was not statistically significant (Table 5.4). However, at 12 weeks, there was significantly more AdCs in *Rptor*$_{ob}^{-/-}$ animals relative to *Rptor*$_{ob}^{-/+}$ mice (mean fold increase 3.59±1.38) (Fig. 5.8B; Table 5.6). Similarly, the area of adipose tissue as a percentage of the intramedullary area was significantly higher in *Rptor*$_{ob}^{-/-}$ mice relative to *Rptor*$_{ob}^{-/+}$ and Osx:Cre controls at both 4 weeks (mean fold increase 1.29±0.34 and 6.09±0.99, respectively) and 12 weeks of age (mean fold increase 3.78±1.05 and 2.14±0.66 respectively) (Fig. 5.8C; Table 5.6).

To examine whether the increase in intramedullary adiposity was due to an increase in the relative size of the AdCs present, the average AdC size was calculated by dividing the total AdC area measured by the number of AdCs enumerated (AdC.Ar/AdC.N). As shown in Figure 5.8D, there was no difference in relative AdC size observed at any of the time points examined Intramedullary AdCs in *Rptor*$_{ob}^{-/-}$ mice are not derived from *rptor* null pre-OBs

The observed increase in intramedullary adipose in *Rptor*$_{ob}^{-/-}$ mice suggests that OB-specific deletion of *Rptor* either (i) affects the differentiation potential of the MSC pool toward the adipogenic lineage, or (ii) that the AdCs arose from trans- or de-differentiation of *Rptor* knock-out cells. To investigate the latter, the origin of the intramedullary AdCs was examined using mice bred with the eYFP reporter. Tibial sections from control *eYFP-Osx:Cre* and *eYFP-Rptor*$_{ob}^{-/-}$ mice were stained for eYFP and perilipin (an adipocyte integral membrane protein) and overlapping signals assessed using 2-colour confocal microscopy. As shown in Figure 5.9A, only a small proportion of AdCs in the bone marrow of eYFP-*Rptor*$_{ob}^{-/-}$ mice were eYFP+perilipin+, suggesting that most of the AdCs did not arise from trans- or de-differentiation of *Rptor* null cells. Of note, eYFP+perilipin+ AdCs were also evident in eYFP-Osx:Cre controls (data not shown) suggesting osterix expression in an AdC precursor may account for the dual labelling [344, 345].

The effect of OB-specific *Rptor* deletion on the intramedullary MSC pool was next assessed by measuring the number of colony unit-fibroblastic (CFU-F) in cell populations isolated from the long bones of 4 week old $Rptor_{ob}^{-/+}$, $Rptor_{ob}^{-/-}$ and Osx:Cre control mice. CFU-F assays asses the number of clonogenic cells as an indirect measure of the size of the pool of immature MSCs. As shown in Figure 5.9B, there was a visible increase in the number of fibroblastic colonies formed from $Rptor_{ob}^{-/-}$ MSCs, and enumeration of the number of morphologically discreet fibroblastic colonies in serially-diluted cell populations revealed a significant increase in CFU-F in $Rptor_{ob}^{-/-}$ mice relative to Osx:Cre controls and $Rptor_{ob}^{-/+}$ mice (mean fold increase 9.6±4.8 and 5.2±9, respectively)(Fig. 5.9C).

Figure 5.9 - Increased intramedullary adipose is not caused by transdifferentiation of *Rptor* null pre-osteoblasts: (A) Two-colour confocal microscopy was used to detect overlapping eYFP (green) and perilipin (red) staining in frozen tibial sections isolated from 4-week-old eYFP- $Rptor_{ob}^{-/-}$ mice. Nuclei were stained with DAPI . Bar = 20mm. (B) Compact bone MSCs were isolated from the long bones of 4 week old Osx:Cre, $Rptor_{ob}^{-/+}$ and $Rptor_{ob}^{-/-}$ mice and plated at concentrations of 1, 3 and 6 x 105 cells/well in duplicate in 6 well plates for CFU-F assays. After 9 days, colonies were stained with toluidine blue. Representative images of toluidine blue-stained colonies are shown. (C) The frequency of CFU-F colonies per 105 cells plated was enumerated. Data are presented as mean ± S.D. n≥6 per group ****p<0.0001. one-way ANOVA with Tukey's post-hoc test.

A

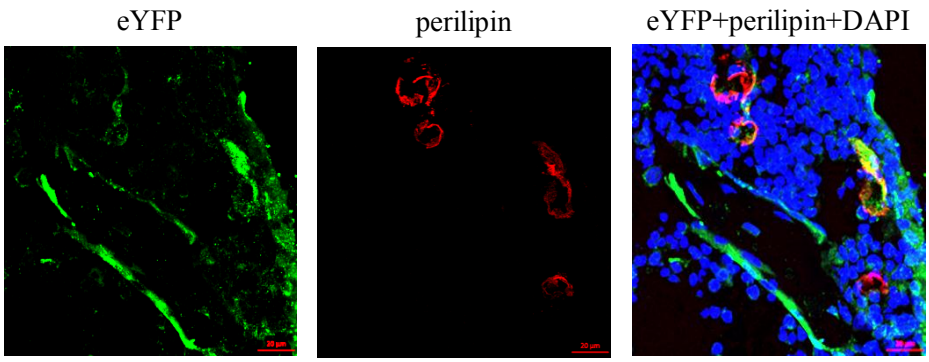
eYFP
perilipin
eYFP+perilipin+DAPI

B

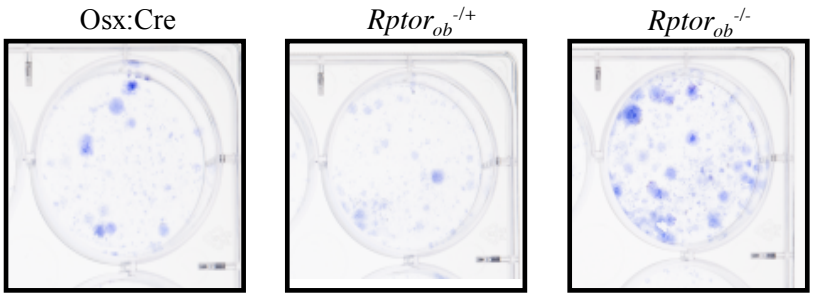
Osx:Cre
Rptor_ob -/+
Rptor_ob -/-

C

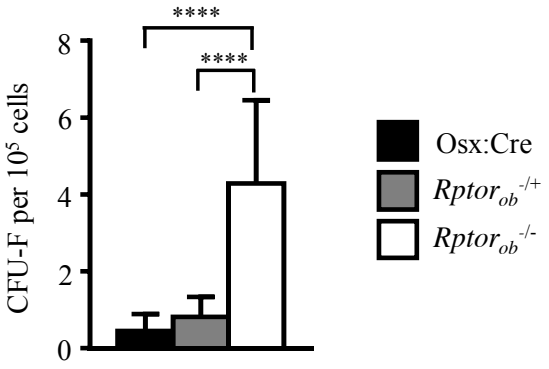
****
****
8
6
4
2
0
CFU-F per 10^5 cells
Osx:Cre
Rptor_ob -/+
Rptor_ob -/-

5.1 Discussion

As previously discussed, bone remodelling is tightly-coupled process mediated by two specialised cell types; OCs which resorb mineralized bone, and OBs which synthesise new bone [30]. In diseases, such as osteoporosis, which are characterised by a low bone mass phenotype and increased skeletal fragility, this tightly-coupled balance between OBs and OCs becomes skewed to favour bone resorption over bone synthesis. Somewhat surprisingly, when the number of OBs and OCs were enumerated in the long bones of Osx:Cre, $Rptor_{ob}^{-/+}$ and $Rptor_{ob}^{-/-}$ mice at 4, 8 and 12 weeks of age, no statistically significant differences were observed. Thus, the low bone mass phenotype of OB-specific *Rptor* KO mice was not attributable to a change in the number of OBs or OCs.

Further examinations also revealed no significant difference in OC activity, as evidenced by unchanged TRAcP5 serum levels, suggesting that the low bone mass phenotype of OB-specific *Rptor* KO mice was not caused by an increase in OC-mediated bone resorption. In contrast, calcein labelling studies showed that both the mineral apposition rate (MAR) and bone formation rate (BFR) were significantly reduced in $Rptor_{ob}^{-/-}$ mice relative to both Osx:Cre controls and heterozygous KO mice while the percentage of newly mineralised surface (MS/BS) was unaffected, demonstrating that deletion of *Rptor* in pre-OB cells had no effect on OB numbers, but significantly affected OB function. This could be associated with either a functional defect in the mineralisation capacity of mature OBs and/or a defect in the osteogenic differentiation program hindering maturation and subsequent bone synthesis. While circulating levels of the early marker of bone formation P1NP [346], a measure of OB-produced circulating type 1 collagen, were unchanged between the KO mice and Osx:Cre controls, both $Rptor_{ob}^{-/+}$ and $Rptor_{ob}^{-/-}$ mice had reduced serum levels of OCN [347]. This suggests *Rptor* null OBs can synthesize the osteoid matrix essential for bone formation but

have a reduced capacity for the deposition of hydroxyapatite which manifests as a low bone mass phenotype due to a stall in OB lineage progression.

While the precise mechanism leading to the decrease in bone accrual in *Rptor*$_{ob}^{-/-}$ mice remains to be determined, suppression of insulin and IGF-1 signalling is likely to play an important role. IGF-1 activates the PI3kinase/Akt/mTOR pathway and induces osteogenic differentiation in Sca-1^{+} MSC progenitor cells, which is blocked by rapamycin [319]. This suggests that the low bone mass phenotype in *Rptor*$_{ob}^{-/-}$ mice could be due in part to impaired IGF-1 signalling. In support of this view, addition of insulin to osteogenic cultures derived from the calvaria of *Rptor*$_{ob}^{-/-}$ mice failed to promote osteogenesis suggesting that *Rptor*-deletion leads to impaired insulin signalling. Similarly, mice in which the insulin receptor is deleted in OBs using *Ocn:Cre* fail to accumulate trabecular bone, however, unlike the present study this was due in part to a reduction in OB number and not OB function [256]. In addition, mice in which the insulin-like growth factor receptor (Igf1r) is deleted in OBs using Osx:Cre also have a low bone mass phenotype [319]. This low bone mass was not attributable to reduced OB numbers but rather a failure of Igf1r null OBs to fully differentiate into mature osteocalcin-positive cells.

In *Rptor*$_{ob}^{-/-}$ mice, OB differentiation appears to be stalled at an early stage of the osteogenic program, as evidenced by decreased expression of late OB markers and increased expression of *Runx2* and *Sp7* in eYFP+ cells isolated from eYFP-*Rptor*$_{ob}^{-/-}$ mice compared to controls. Runx2 controls OB differentiation by regulating the expression of key OB genes including osterix (*Sp7*) [90], integrin-binding saloprotein (*Ibsp*), osteopontin (*Spp1*), osteonectin (*Sparc*) and osteocalcin (*Bglap*) [91, 92]. How the OB differentiation pathway is stalled is currently unclear, however, it is likely related to the role played by mTORC1 in controlling important cellular functions such as protein translation [348]. Suppression of translation in OBs from *Rptor*$_{ob}^{-/-}$ mice is likely to limit the capacity of pre-OBs to proceed with the osteogenic

program after osterix expression is initiated by Runx2. In support of this, the significant reduction in protein synthesis observed in chondrocytes lacking *Rptor* is thought to account for the severe prenatal skeletal phenotype of *Prx-1-cre*:*mTOR* and *Prx-1-cre*:*Rptor* knockout animals [286].

Recent evidence suggests that correct regulation of mTORC1 activity during chondrogenesis is essential for the normal progression of pre-hypertrophic chondrocytes to a terminal hypertrophic fate. Deletion of *Lkb1*, a negative regulator of mTORC1 [349], in immature chondrocytes using *Col2α1-Cre,* caused a rapamycin-sensitive expansion of immature chondrocytes and formation of enchondroma-like tumors [323]. Deletion of *mTOR* or *Rptor* in the developing head and limb mesenchyme at E9.0, prior to skeletogenesis, using *Prx-1-cre* mice has also been shown to profoundly affect chondrogenesis [286]. Most notably, mTORC1 is important for the transition of chondrocytes to the hypertrophic program and may be involved in the phases of hypertrophy that drive the increase in dry cell mass [50, 286]. Given the importance of mTORC1 activity in chondrogenesis, deletion of *Rptor* in osterix-expressing prehypertrophic chondrocytes may have affected chondrocyte differentiation by prematurely terminating mTORC1 activity. *Col10a1* and *Mmp13* expression was reduced in eYFP+ chondrocytes isolated from the long bones of *eYFP-Rptor*$_{ob}^{-/-}$ mice, suggesting fewer terminally differentiated chondrocytes are present in *Rptor*$_{ob}^{-/-}$ mice. It was also evident that deletion of *Rptor* in osterix-expressing hypertrophic chondrocytes caused an overall reduction in chondrocyte proliferation as measured by a decrease in PCNA expression. Further investigation of the role of mTORC1 in chondrogenesis, following the deletion of *Rptor* in immature chondrocytes using *Col2α1-Cre* mice, would provide important insight into the role of Rptor in chondrogenesis.

Somewhat surprisingly, pre-OB-specific deletion of *Rptor* caused a significant increase in intramedullary AdCs, which appeared to be specific to bone, as no appreciable

increase in fat deposits was observed at other sites (data not shown). Histological analyses revealed an increase in both the of area of adipose tissue and an increase in the number of AdCs per intramedullary area in $Rptor_{ob}^{-/-}$ mice compared to both Osx:Cre and $Rptor_{ob}^{-/+}$ at 4 weeks and 12 weeks. Studies have demonstrated factors secreted from AdCs, such as adiponectin, leptin and fatty acids, modify the function and proliferation of neighbouring cells [350-352]. It has previously been suggested that the increase in medullary adiposity within the osteoporotic skeleton is due to adipogenic factors limiting the commitment of MSC to the OB lineage [353]. However, due to the stall in OB maturation observed in $Rptor_{ob}^{-/-}$ mice, it is also probable that these same adipogenic factors result in trans-differentiation of *Rptor* null pre-OBs to the adipogenic lineage [354, 355]. Immunofluorescence staining of intramedullary AdCs in long bone sections from *eYFP-*$Rptor_{ob}^{-/-}$ mice revealed eYFP labelling of only a small proportion of AdCs, suggesting that the majority of the AdCs did not arise from trans-differentiation of eYFP+ cells. Furthermore, eYFP+perilipin+ AdCs were also evident in *eYFP-Osx:Cre* controls (data not shown), suggesting that osterix expression in an AdC precursor may account for the dual labelling [344, 345]. Furthermore, the frequency of CFU-F was increased in the long bones of $Rptor_{ob}^{-/-}$ mice, which suggests that loss of mTORC1 function in pre-OBs affects the MSC pool. While it remains to be determined, these MSCs maybe a source of the increased bone marrow AdCs seen in the $Rptor_{ob}^{-/-}$ mice.

Taken together, these findings suggest that mTORC1 signalling is essential for proper skeletal development by driving the differentiation and maturation of OBs. Whilst the exact mechanisms by which this occurs remain to be determined, IGF signalling through mTORC1 is a likely contributor to the maturation and function of both OBs and chondrocytes. Thus, the loss of mTORC1 reduces the capacity for these cells to undergo differentiation to become mature functioning OBs.

Chapter 6 - Discussion

6.1 General discussion

Ageing, genetics and environmental factors influence the development and homeostasis of bone. These factors contribute to numerous bone-related diseases and co-morbidities, such as osteoporosis and osteogeneis imperfecta (OI), resulting in detrimental effects on patient health and placing a heavy financial burden on the Australian healthcare system[1]. While numerous studies from the last half century have identified the processes which govern skeletal development and homeostasis, therapeutics for bone disease remain limited.

Commitment of MSCs to the OB lineage is the critical first step in bone formation, and is followed by the step-wise maturation of these committed pre-OBs into mature, bone-forming OBs. mTORC1 is a key intracellular regulator of skeletal formation and transduces signals from extracellular factors such as insulin[128, 256, 333], BMPs[7, 337] and Wnt ligands [33, 136] to regulate stem cell function[356-358], MSC commitment, OB differentiation and OB function[18, 24, 205, 359]. However, delineating how mTORC1 regulates these complicated cellular processes has remained poorly understood due to limitations in previous investigative methods. The studies presented in this thesis provides clear insight into the role of mTORC1 in these processes via the utilisation of a novel genetic approach to analyse the role of mTORC1 in MSC commitment *in vitro* as well as the role of mTORC1 in OB maturation and skeletal development *in vivo*.

Identifying the role of mTORC1 in MSC function and commitment was achieved via the generation of primary MSC populations harbouring deletion of the essential mTORC1 adaptor protein, raptor. As mTORC1 is a known mediator of cellular proliferation [189], it was not surprising that deletion of *Rptor* reduced *in vitro* proliferation of MSCs. When cultured under adipogenic conditions, RapKO MSCs showed reduced adipogenic potential and reduced expression of the essential AdC transcription factor, PPARγ[108, 110]. These findings support previous *in vitro* studies showing that mTORC1 is essential for adipogenic MSC differentiation [21, 23, 203, 293]. Conversely, RapKO MSCs cultured under osteogenic conditions displayed

increased osteogenic capacity and an upregulation of both Runx2 and osterix, both essential transcription factors in OB commitment of MSCs. While the pro-osteogenic effect of mTORC1 inhibition presented in this thesis is supported by several studies [17, 18, 205], over the past two decades, evidence has emerged to suggest that inhibition of mTORC1 has an anti-osteogenic effect [24, 25, 27]. However, the novel *in vitro* approach applied in this study, via the genetic deletion of *Rptor* in primary MSC populations, overcome many of the deficiencies in the methodologies used in previous studies. For the first time, this study provides compelling evidence that inhibition of mTORC1 signalling promotes osteogenic MSC commitment, a theory previously considered inconclusive (Figure 6.1).

In keeping with the long-standing theory of a mutually exclusive relationship between OB and AdC commitment [121, 123, 360] studies presented in Chapter 3 of this thesis show that mTORC1 plays a role in MSC lineage commitment. As shown in this study, and confirmed by others, loss of mTORC1 reduces expression of PPARγ in MSC under adipogenic conditions [21, 23, 203, 293]. As expression of PPARγ has been shown to inhibit Runx2 expression and OB differentiation [108, 121-123], reduced PPARγ expression, due to loss of mTORC1, could allow for upregulation of Runx2-mediated commitment of MSCs toward the osteogenic lineage (Fig. 6.1).

In addition, age-related metabolic changes in MSCs are known to negatively influence their osteogenic differentiation potential. Previous studies have demonstrated that mTORC1 inhibition attenuates stem cell aging and mTORC1 activation promotes MSC proliferation and cell cycle progression [119, 356-358]. Increased cell cycle progression and proliferation results in loss of MSC quiescence and stem-ness, which reduces their osteogenic potential [117]. Therefore, it is likely that loss of mTORC1 serves to retain MSC quiescence, and serves to prime the MSC to be responsive to osteogenic induction (Fig 6.1).

Figure 6.1 - mTORC1 regulates MSC lineage commitment: (A) Activation of mTORC1 in MSCs sitmulates the upregulation of PPARg driving adipogenic commitment at the expense of osteogenic commitment. mTORC1 stimulation promotes cell cycle progression and loss of MSC quiescence. (B) Inhibition of mTORC1 in MSCs increases osteogenic commitment through downregulation of PPARg resulting in the upregulation of RUNX2. Inhibition of mTORC1 possibly increases quiescence and stem-ness of MSCs reducing age-related loss of osteogenic potential.

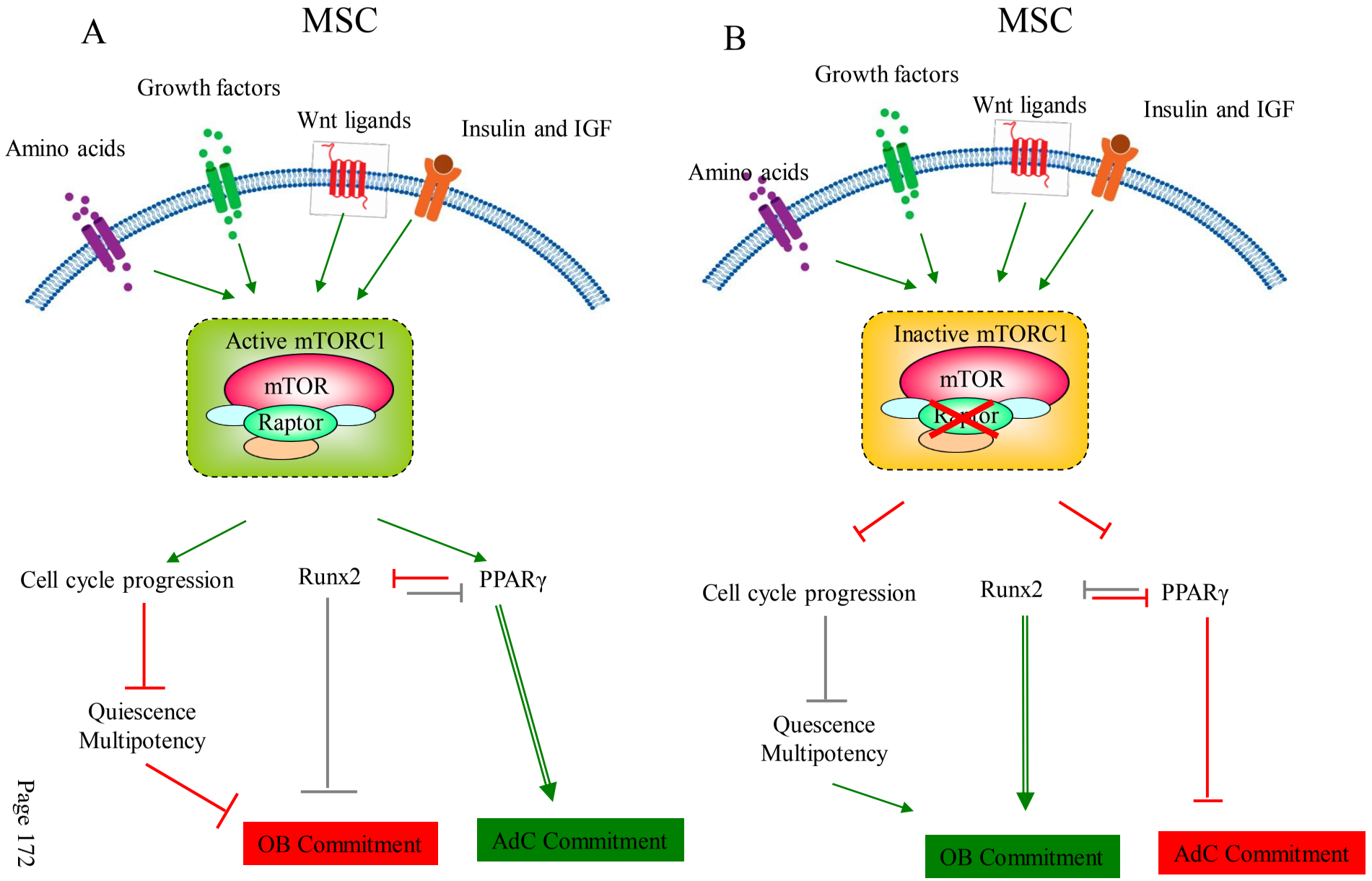
A
MSC
Growth factors
Wnt ligands
Insulin and IGF
Amino acids
Active mTORC1
mTOR
Raptor
Cell cycle progression
Runx2
PPARγ
Quiescence
Multipotency
OB Commitment
AdC Commitment
B
MSC
Growth factors
Wnt ligands
Insulin and IGF
Amino acids
Inactive mTORC1
mTOR
Cell cycle progression
Runx2
PPARγ
Quescence
Multipotency
OB Commitment
AdC Commitment

Based on the results from Chapter 3, which showed that loss of mTORC1 in primary MSCs mediates an increase in osteogenesis *in vitro*, it was expected that the OB-specific deletion of mTORC1 in a conditional knockout mouse model would show increased mineralised bone accrual. However, somewhat surprisingly, the number of mature OBs in $Rptor_{ob}^{-/-}$ mice was indistinguishable from controls and bone accrual was significantly reduced. Consistent with the pro-osteogenic transcriptional profile of RapKO MSCs presented in Chapter 3, the levels of Runx2 and Osx expression were elevated in *Rptor* knockout OBs isolated from $Rptor_{ob}^{-/-}$ mice. However, these OBs had reduced expression of late stage osteogenic markers (including Col1a1, BSP, OPN and OCN), indicating that the reduction in bone accrual was due to a stall in OB differentiation and maturation. Mechanistically, mTORC1 regulates translation and ribosomal biogenesis, therefore it is likely that suppression of translation prevents the translation of essential stage-dependant OB genes stalling pre-OB maturation following Osx expression (Figure 6.2).

Insulin and IGF-1 are established as regulators of OB differentiation via activation of the PI3K/AKT/mTOR signalling cascade [164, 198, 256, 340]. In established *in vitro* assays, OBs isolated from $Rptor_{ob}^{-/-}$ mice failed to respond to insulin, which suggests that disruption of this signalling pathway is a likely contributor to the low bone mass phenotype observed in $Rptor_{ob}^{-/-}$ mice. In support of this theory, mice harbouring a bone-specific deletion of the insulin receptor (OB-ΔIR) [319] or global deletion of insulin like growth factor receptor ($Igflr^{-/-}$)[252] also display a low bone mass phenotype. While this phenotype was attributed to reduced OB numbers in OB-ΔIR mice, the low bone phenotype observed in $Igflr^{-/-}$ mice was attributed to an inhibition of OB maturation. Furthermore, *in vitro* analyses indicate that IGF-1-induced osteogenesis is lost in MSCs with the addition of rapamycin. These findings indicate the loss of mTORC1 disrupts extracellular insulin and IGF-1 cues, which activate the PI3K/AKT/mTOR signalling cascade, resulting in an immature OB phenotype and reduced

bone accrual. Collectively, these findings highlight the essential role of mTORC1 in transducing bone-anabolic signals for the progression of pre-OBs to mature OBs.

Since the commencement of this study, additional insight into the role of mTORC1 during OB differentiation has emerged from mTORC1 gain-of-function mouse models in both pre- OBs[332] and mature OBs[300]. Huang et al.[332] employed Osx:Cre mediated deletion of the upstream negative regulator of mTORC1, TSC1 (ΔTSC1), which resulted in the hyperactivation of mTORC1. Interestingly, the reduced body weight and immature OB phenotype observed in $Rptor_{ob}^{-/-}$ mice was also present in ΔTSC1 mice. However, several key differences between the activation and inhibition models indicate mTORC1 serves to modulate the progression of osteogenic differentiation. In support of findings from this thesis, Huang et al. concluded that mTORC1 is activated during proliferation in pre-OBs and is suppressed during their differentiation. The increase in proliferative capacity was also reflected in ΔTSC1 mice, which had increased numbers of OB progenitors, however they lacked the proper morphology of mature OBs. Expression of Osx was also reduced, which was attributed to the activation of Notch signalling, a negative regulator of Runx2. As mentioned previously in Section 1.4.1, commitment of OB progenitors coincides with the upregulation of Runx2 and Osx and a conformational progression from the long, thin MSC morphology, to the cuboidal OB morphology regardless of functionality. Together, these data suggest that mTORC1 remains inactive in early OB differentiation promoting OB lineage commitment of MSCs through to the morphological change towards the pre-OB phenotype (Fig 6.3).

As outlined in Chapter 4, a stunted skeletal phenotype and improper skeletal patterning was observed in $Rptor_{ob}^{-/-}$ mice, compared to controls. This manifested as a reduction in trabecular number, which has been subsequently reported by Chen et al [327,] and reduced cortical thickness. Notably a reduction in OCN levels, the necessary component of mineral matrix synthesis, was also observed in $Rptor_{ob}^{-/-}$ mice. However, in contrast to

Figure 6.2 - mTORC1 regulates pre-OB maturation and function: (A) Activation of mTORC1 through stimulation of PI3K/Akt signaling cascade regulates the translation of osteogenic proteins driving the differential stages required for the maturation of pre-OBs to mature, mineral matrix forming OBs. (B) inhibition of mTORC1 in pre-OBs stalls OB maturation, osteoid synthesis and bone mineral synthesis.

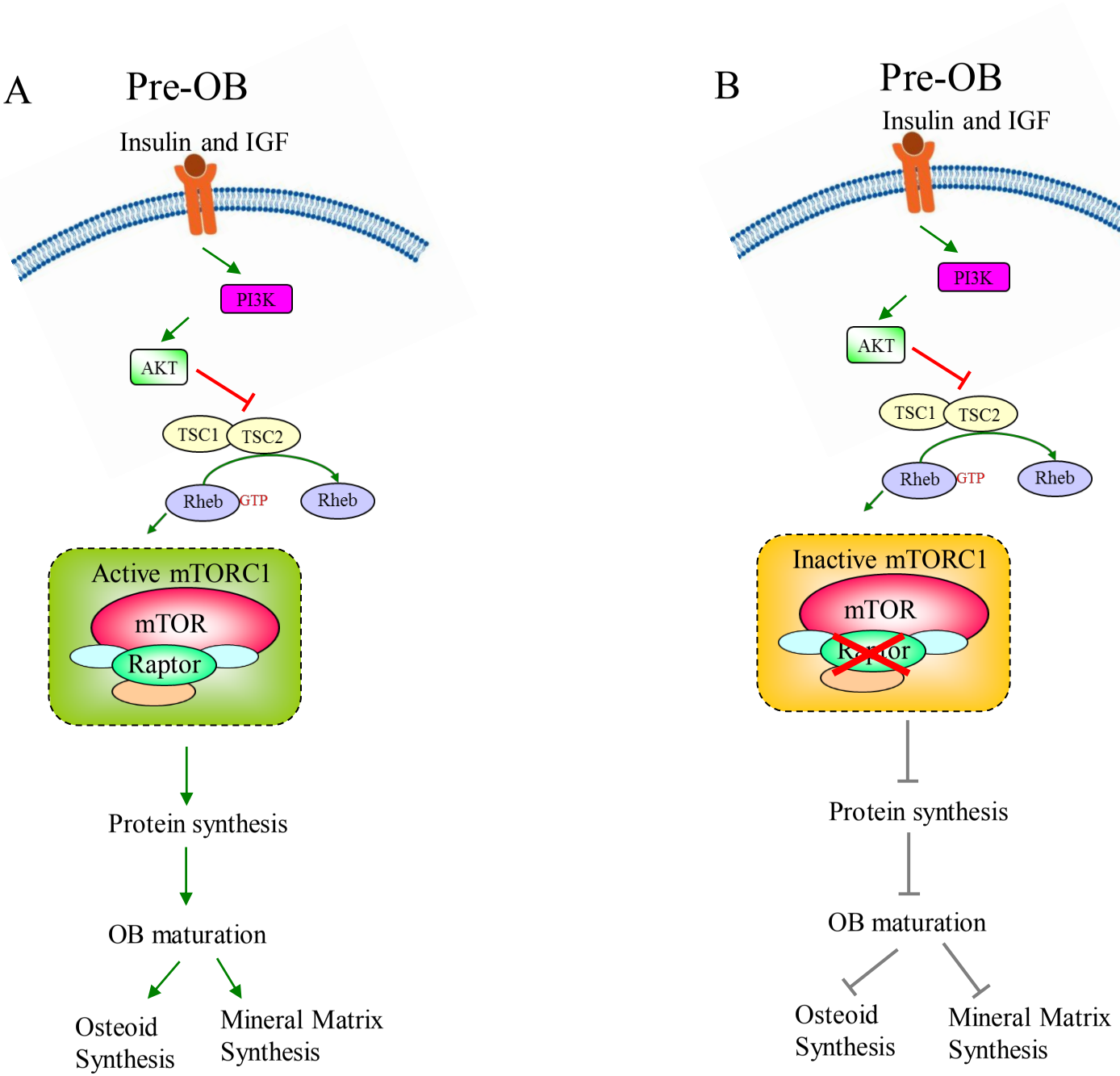
A
Pre-OB
Insulin and IGF
PI3K
AKT
TSC1
TSC2
Rheb
GTP
Rheb
Active mTORC1
mTOR
Raptor
Protein synthesis
OB maturation
Osteoid Synthesis
Mineral Matrix Synthesis
B
Pre-OB
Insulin and IGF
PI3K
AKT
TSC1
TSC2
Rheb
GTP
Rheb
Inactive mTORC1
mTOR
Raptor
Protein synthesis
OB maturation
Osteoid Synthesis
Mineral Matrix Synthesis

Rptor$_{ob}^{-/-}$ mice, observations in ΔTSC1 mice suggest that while displaying low levels of OCN, these mice display increased cortical thickness and trabecular number, which was attributed to stalled OB maturity. Additionally, while not defined in this study, ΔTSC1 mice showed hyperactivation of mTORC1 resulted in more porous bone of poor quality attributed to the marked increase in osteoid thickness [332]. While not investigated in this study, it is possible that mTORC1 is an essential regulator of osteoid synthesis by OBs. Following pre-OB maturation and prior to mineral matrix deposition, both pre-OBs and mature OBs synthesise osteoid providing the scaffold for which bone mineral is formed. Reduced osteoid synthesis reduces appositional bone growth of the cortices and reduces trabecular number as thinner trabeculae are more readily resorbed by osteoclasts. However, determination of the requirement for mTORC1 function in relation to osteoid synthesis remains to be elucidated.

Due to the prevalence of cells of an immature OB phenotype, the findings from this study cannot draw definitive conclusions for the exact role of mTORC1 in mineralised bone accrual by mature OBs. However, additional studies published during the course of the PhD studies described herein, suggest that mTORC1 is essential for both proper bone formation by mature OBs. Notably, deletion of TSC2 (Δ*TSC2*) in mature osteoblasts (using OCN:Cre), which leads to hyperactivation of mTORC1, resulted in increased post-natal cortical thickness and trabecular number[300] similar to ΔTSC1 mice. Δ*TSC2* mice also displayed an accumulation of disorganised bone, attributable to increased OB numbers and increased osteoid synthesis. However, while the bone formation rate and OCN levels were elevated, mineral apposition was not affected in Δ*TSC2* mice. Rapamycin administration to Δ*TSC1* and Δ*TSC2* OBs *in vitro* and to Δ*TSC1* mice were shown to rescue impaired OB function, suggesting that mTORC1 activation can lead to increased bone accrual. In contrast, Riddle et al. showed that mice

Figure 6.3 - mTORC1 activity during osteogenesis: mTORC1 activity is reduced in MSC resulting in increased RUNX2 expression resulting in commitment to the OB lineage. mTORC1 remains inactive during early OB differentiation increasing OSX and ALPL expression and facilitating conformational changes resulting in cuboidal OB morphology. Activation of mTORC1 is required for the maturation of pre-OBs capable of synthesising osteoid coinciding with upregulation of BSP and COL1A1. The role of mTORC1 in mature OB function and mineralised matrix synthesis remains to be determined.

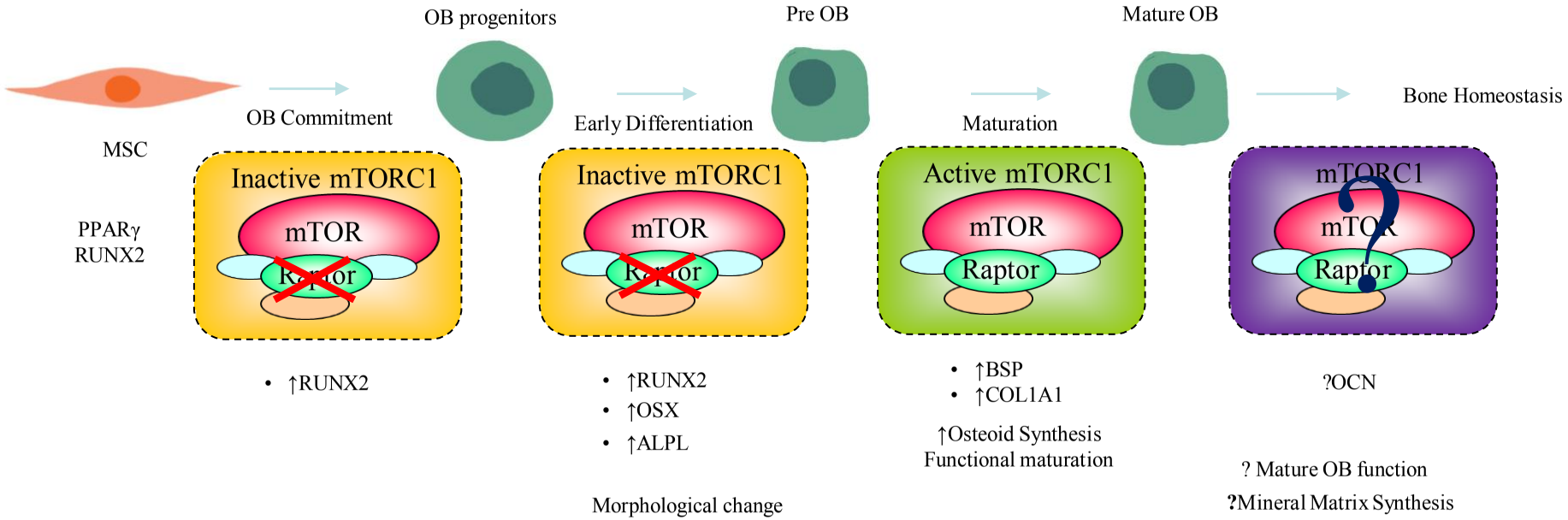
OB progenitors
Pre OB
Mature OB
MSC
OB Commitment
Early Differentiation
Maturation
Bone Homeostasis
PPARγ
RUNX2
Inactive mTORC1
mTOR
Raptor
Inactive mTORC1
mTOR
Raptor
Active mTORC1
mTOR
Raptor
mTORC1
mTOR
Raptor
• ↑RUNX2
• ↑RUNX2
• ↑OSX
• ↑ALPL
Morphological change
• ↑BSP
• ↑COL1A1
↑Osteoid Synthesis
Functional maturation
?OCN
? Mature OB function
?Mineral Matrix Synthesis

harbouring loss of *mTOR* in mature OBs (Δ*mTOR*), through OCN:Cre mediated deletion, have reduced trabecular number and bone volume, similar to $Rptor_{ob}^{-/-}$ mice[300]. While Δ*mTOR* targets both mTORC1 and mTORC2, the trabecular bone phenotype of Δ*mTOR* mice can be attributed directly to mTORC1, as subsequent studies have shown that deletion of *Rictor* in mature OBs does not contribute to the tibial bone phenotype [361]. Taken together, these findings suggest that mTORC1 is essential in normal skeletal development, most likely via regulation of osteoid synthesis; while the mechanisms that regulate bone mineralisation remain to be elucidated.

As mentioned in section 1.4, osteocytes are the terminal differentiation stage of OBs and play an integral role in the mediation of cues governing bone development and remodelling [62-65]. While not investigated in this study, stalled pre-OB maturation likely affects the presence and activity of osteocytes contributing to the distinct $Rptor_{ob}^{-/-}$ phenotype. Histological assessment of mineral-sequestered osteocytes[372] and analyses of markers of mature osteocytes (including Dentin matrix protein 1 (DMP-1)[373], sclerostin[374] and matrix extracellular phosphoglycoprotein[375]) would give further insight into the role of mTORC1 in pre-OB maturation contributing to observations presented in $Rptor_{ob}^{-/-}$ mice. Furthermore, recent studies by Joeng et al (2017)[376] have revealed a role for mTORC1 in osteocyte activity via Wnt signaling. Utilising Cre-mediated targeting of osteocytes, via Dentin matrix acidic protein 1 (Dmp-1:Cre), over-expression of *Wnt1* stimulated bone formation and an increase in mature OB numbers. These findings were attributed to activation of mTORC1, as rapamycin administration was able to reverse this effect. Furthermore, as mTORC1 regulates protein translation, Osx:Cre mediated *Rptor* deletion may affect the production of osteocyte-derived factors, such as IGF-1 and nitric oxide, during bone growth and homeostasis[62-65]. These findings highlight the complex role of mTORC1 in multiple aspects of skeletal development and homeostasis and warrants further studies to better understand these processes.

It should also be noted Osx expression was detected in growth plate chondrocytes of *Rptor*$_{ob}^{-/-}$ mice. As a regulator of endochondral ossification, it was concluded that the reduced longitudinal tibial growth in *Rptor*$_{ob}^{-/-}$ mice is attributed to the loss of mTORC1 through reduced growth plate chondrocyte proliferation. Additionally, reduced MMP13 levels and hypertrophic zone width were observed in *Rptor*$_{ob}^{-/-}$ mice, indicating that mTORC1 is essential in the normal progression of pre-hypertrophic chondrocytes to a terminal hypertrophic fate. In support of these findings, deletion of *Lkb1*, a negative regulator of mTORC1 [349], in immature chondrocytes using *Col2α1-Cre* causes a rapamycin-sensitive overgrowth of the proliferative zone [323]. Additionally, using *Prx-1-cre* mice to delete *mTOR* or *Rptor* in the developing head and limb mesenchyme at E9.0, prior to skeletogenesis, results in severe delays chondrocyte hypertrophy [286]. In addition to mediating chondrocyte proliferation and hypertrophy, evidence shows mTORC1 is essential for the synthesis of cartilage matrices. In chapter 5, transcriptional profiling indicated that collagen synthesis was reduced in *Rptor*$_{ob}^{-/-}$ cells cultured *ex vivo.* Notably, a low collagen matrix phenotype was also reported by Chen et al. (2014) [286]. Moreover, while the growth plate was not specifically examined, recent studies examining the effects of chondrocyte-specific deletion of TSC1 in the ΔTSC1 mouse model[362], showed that mTORC1 activity is necessary for type 1 collagen expression in chondrocytes. Yan et. al (2016) showed that hyperactivation of mTORC1 in chondrocytes, via Col2a1-cre deletion *TSC1 in vivo*, resulted in the uncoupling of normal chondrocyte proliferation and differentiation. Taken together, these findings indicate that mTORC1 is essential in the regulation of chondrocyte activity during endochondral growth.

Findings from this study, together with others detailed above, indicate that mTORC1 is essential in the synthesis of type I collagen. While still speculative, these data provide evidence that the low bone mass phenotype is as a result of the requirement for mTORC1 during osteoid synthesis. While further confirmation is required, this could contribute to the disparate findings presented between the *in vitro* and *in vivo* results presented in Chapters 3

and 4 of this thesis. *In vivo* findings from this study show mTORC1 deletion in pre-OBs reduces both trabecular bone formation and cortical thickness. These processes require the three-dimensional synthesis of osteoid and mineral accrual which are regulated by systemic cues during both development and remodelling. Conversely, *in vitro* loss of mTORC1 in multipotent MSCs promotes osteogenic commitment and increased mineral matrix production However, *in vitro* mineralisation assays are unable to mimic both three-dimensional nature of the *in vivo* environment, or the various systemic cues. Additionally, the adherent nature of MSCs and OBs to *in vitro* culture plates, could negate the necessity for osteoid synthesis. The disparities between the *in vitro* and *in vivo* results in this thesis, contrast the results of Riddle et al[300] who showed that deletion of *TSC2,* reduced the osteogenic potential of MSCs *in vitro* while deletion of TSC2 (Δ*TSC2*) in mature OBs (using OCN:Cre) resulted in increased post-natal bone formation, but not mineral apposition[300]. Riddle *et. al* concluded that while activation of mTORC1 caused increased proliferation, a stall in OB maturation led to a reduction in mineralised matrix production *in vitro*. Collectively, these findings suggest that the skeletal phenotype presented in $Rptor_{ob}^{-/-}$ mice is a result of mTORC1 activity in the synthesis of osteoid. In support of this theory, several subtypes OI in humans, and their corresponding mouse models, present a similar bone phenotype to that of $Rptor_{ob}^{-/-}$ mice caused by mutations to collagen genes[313, 363, 364]. While this theory remains speculative and awaits further investigation, it is tempting to speculate that mTORC1 is an essential component in the formation and regulation of osteoid through the synthesis of essential collagens.

6.2 Clinical Significance

MSC therapies have emerged at the forefront of regenerative medicine, with numerous clinical studies described examining their efficacy in the therapies directed at repairing bone [365], cartilage [366] and for the treatment of autoimmune diseases [367]. However, to date, the

clinical standards and government regulations required for their use in regenerative medicine, remain ill-defined and this in some way due to limitations in current knowledge of biochemical regulators that maintain stem-ness and/or promote tissue-specific differentiation. The identification of mTORC1 as a regulator of MSC proliferation and differentiation is invaluable to developing established protocols for manipulation of MSC populations *ex vivo*.

As discussed previously, diseases of the skeleton have detrimental impacts on a patient's physical and mental health and are a significant burden on healthcare systems globally. While there are countless effectors of skeletal health, including genetics, age and lifestyle; therapies aimed at improving skeletal health are limited. Identifying the role of mTORC1 in mediating skeletal formation and health may provide novel drug targets for skeletal-related therapies. Furthermore, by identifying mechanisms by which mTORC1 regulates extracellular signals, insight into mechanisms regulating current bone therapies, such as IGF-1 utilised for treatment of paediatric growth failure [368], will allow for further regulation of dosage, efficacy and patient suitability for current therapies.

The identification of mTORC1 as a regulator of both OB and chondrocyte function in this study highlights the requirement for caution in the administration of mTORC1 inhibitors. Currently, rapamycin (Sirolimus) and the related analogue (Everolimus) are used clinically in the treatment of a variety of cancers and as an immunosuppressant to prevent organ transplant rejection[369]. While studies have identified bone sparing effects in rapamycin administration, this has been attributed to a reduction in OC bone resorption as opposed to increased bone formation[236, 370]. Nevertheless, additional care should be taken when administering mTORC1 inhibitors due to the possible bone-related side effects.

6.3 Future directions

These studies show that mTORC1 is an essential regulator of MSC lineage commitment and functions to regulate MSC proliferation and translation of essential differentiation-

associated transcription factors and lineage-restricted proteins. More recently, mTORC1 has been identified in the regulation of stem cell quiescence and aging [356-358]. Loss of MSC stemness, due to aging, results in a reduced capacity for osteogenesis, a known contributor to age-related bone loss and osteoporosis [3, 4]. To examine whether mTORC1 is involved in this process and how it regulates MSC commitment by modulating stem cell aging, will require the establishment of long-term culture studies in which MSC self-renewal and multi-lineage differentiation potential could be measured as a function of the age of the cell.

Findings presented in this thesis, together with studies that have been published during the course of these studies, demonstrate that mTORC1 is a key regulator of collagen synthesis [286, 371]. As speculated in section 6.1, the bone phenotype of *Rptor*$_{ob}^{-/-}$ mice may be attributable to the abnormal synthesis of collagens during both endochondral growth and osteoid synthesis[313, 363, 364]. Genetic disorders such, as OI, manifest in abnormal skeletal phenotypes in patients. The classification of genetic mutations in COL1A1 are known to attribute to improper collagen synthesis in several OI subtypes. Patients harbouring these mutations, and the corresponding mouse models, present similar skeletal phenotypes to that seen in the *Rptor*$_{ob}^{-/-}$ mice. However, the contribution of genetic mutations in several subtypes of OI have yet to be established. This raises the possibility that mutations in mTORC1-related genes may contribute to these disorders. Genomic profiling of OI patients would reveal whether the skeletal phenotype of OI can, in some way, be attributed to genetic mutations in mTORC1-related components. Together these findings could provide valuable insight into the diagnoses and treatment of OI.

It remains to be determined whether the low bone mass phenotype observed in *Rptor*$_{ob}^{-/-}$ mice is the result of the contribution that mTORC1 makes during mineral matrix synthesis and/or related to the stall in OB maturation. Recent gain of function studies [300, 332], are yet to resolve whether stalled OB maturation and/or OB function is the cause the low bone mass phenotype seen in the *Rptor*$_{ob}^{-/-}$ mice. To determine the contribution of mTORC1 signalling

during mineral matrix synthesis, future studies utilising OCN-Cre-mediated deletion of Raptor (ie. in which deletion of *Rptor* is restricted to *mature* OBs only) would provide vital insight into these outstanding questions. Furthermore, future studies utilising Dmp1-Cre-mediated deletion of Raptor (ie. in which deletion of *Rptor* is restricted to differentiated osteocytes only) to determine the role of mTORC1 in osteocyte-stimulated osteogenesis.

6.4 Concluding Remarks

In summary, this study has revealed a novel role for mTORC1 in both MSC fate determination and osteogenesis, in that mTORC1 function must be switched off to allow for MSC commitment to the osteogenic lineage but is subsequently required for the progression of the osteogenic program from the pre-osteoblast stage to the mature osteoblast stage. As outlined in Figure 6.1, loss of mTORC1 signalling in MSC increases OB differentiation potential, at the expense of AdC differentiation, via both suppression of PPARγ expression and maintenance of MSC stem-like properties. Furthermore, while deletion of *Rptor* in pre-OBs allows for a shift in the OB morphology, OBs are unable to mature and function resulting in abnormal skeletal development (fig 6.3).

Together, these findings give new insight into the role of mTORC1 in MSCs and skeletal development. This knowledge will assist in the development of future therapeutic strategies and diagnostic approaches to improve patient outcome through the identification of new drug targets and the understanding of possible side effects of current mTORC1 inhibition therapies.

Chapter 7 - References

1. Watts, J.J., J. Abimanyi-Ochom, and K.M. Sanders, *Osteoporosis costing all Australian: a new burden of disease analysis-2012 to 2022.* 2013.
2. Elabd, C., et al., *Oxytocin controls differentiation of human mesenchymal stem cells and reverses osteoporosis.* Stem Cells, 2008. **26**(9): p. 2399-407.
3. Rodriguez, J.P., et al., *Abnormal osteogenesis in osteoporotic patients is reflected by altered mesenchymal stem cells dynamics.* J Cell Biochem, 1999. **75**(3): p. 414-23.
4. D'Ippolito, G., et al., *Age-related osteogenic potential of mesenchymal stromal stem cells from human vertebral bone marrow.* J Bone Miner Res, 1999. **14**(7): p. 1115-22.
5. Stevens, J.R., et al., *Wnt10b deficiency results in age-dependent loss of bone mass and progressive reduction of mesenchymal progenitor cells.* J Bone Miner Res, 2010. **25**(10): p. 2138-47.
6. Yuan, Z., et al., *PPARgamma and Wnt Signaling in Adipogenic and Osteogenic Differentiation of Mesenchymal Stem Cells.* Current stem cell research & therapy, 2016. **11**(3): p. 216-25.
7. Matsubara, T., et al., *BMP2 regulates Osterix through Msx2 and Runx2 during osteoblast differentiation.* J Biol Chem, 2008. **283**(43): p. 29119-25.
8. Kang, Q., et al., *A comprehensive analysis of the dual roles of BMPs in regulating adipogenic and osteogenic differentiation of mesenchymal progenitor cells.* Stem Cells Dev, 2009. **18**(4): p. 545-59.
9. Kim, W.K., et al., *Hedgehog signaling and osteogenic differentiation in multipotent bone marrow stromal cells are inhibited by oxidative stress.* J Cell Biochem, 2010. **111**(5): p. 1199-209.

10. James, A.W., et al., *Additive effects of sonic hedgehog and Nell-1 signaling in osteogenic versus adipogenic differentiation of human adipose-derived stromal cells.* Stem Cells Dev, 2012. **21**(12): p. 2170-8.

11. Li, L., et al., *Hedgehog signaling is involved in the BMP9-induced osteogenic differentiation of mesenchymal stem cells.* Int J Mol Med, 2015. **35**(6): p. 1641-50.

12. Greenblatt, M.B., J.H. Shim, and L.H. Glimcher, *Mitogen-activated protein kinase pathways in osteoblasts.* Annual review of cell and developmental biology, 2013. **29**: p. 63-79.

13. Vinals, F., et al., *Inhibition of PI3K/p70 S6K and p38 MAPK cascades increases osteoblastic differentiation induced by BMP-2.* FEBS Lett, 2002. **510**(1-2): p. 99-104.

14. Giustina, A., G. Mazziotti, and E. Canalis, *Growth hormone, insulin-like growth factors, and the skeleton.* Endocrine reviews, 2008. **29**(5): p. 535-59.

15. Tahimic, C.G., Y. Wang, and D.D. Bikle, *Anabolic effects of IGF-1 signaling on the skeleton.* Frontiers in endocrinology, 2013. **4**: p. 6.

16. Lee, K.W., et al., *Rapamycin promotes the osteoblastic differentiation of human embryonic stem cells by blocking the mTOR pathway and stimulating the BMP/Smad pathway.* Stem Cells Dev, 2010. **19**(4): p. 557-68.

17. Ogawa, T., et al., *Osteoblastic Differentiation Is Enhanced by Rapamycin in Rat Osteoblast-like Osteosarcoma (ROS 17/2.8) Cells.* Biochemical and Biophysical Research Communications, 1998. **249**: p. 226-230.

18. Martin, S.K., et al., *NVP-BEZ235, A Dual Pan Class I PI3 Kinase and mTOR Inhibitor, Promotes Osteogenic Differentiation in Human Mesenchymal*

Stromal Cells. journal of Bone and Mineral Research, 2010. **25**(10): p. 2126-2137.

19. Bell, A., L. Grunder, and A. Sorisky, *Rapamycin Inhibits Human Adipocyte Differentiation in Primary Culture.* Obesity Research, 2000. **8**(3): p. 249-254.
20. Cho, H.J., et al., *Regulation of adipocyte differentiation and insulin action with rapamycin.* Biochem Biophys Res Commun, 2004. **321**(4): p. 942-8.
21. El-Chaar, D., A. Gagnon, and A. Sorisky, *Inhibition of insulin signaling and adipogenesis by rapamycin: effect on phosphorylation of p70 S6 kinase vs eIF4E-BP1.* Int J Obes Relat Metab Disord, 2004. **28**(2): p. 191-8.
22. Yeh, W.C., B.E. Bierer, and S.L. McKnight, *Rapamycin inhibits clonal expansion and adipogenic differentiation of 3T3-L1 cells.* Proc Natl Acad Sci U S A, 1995. **92**(24): p. 11086-90.
23. Zhang, H.H., et al., *Insulin stimulates adipogenesis through the Akt-TSC2-mTORC1 pathway.* PLoS One, 2009. **4**(7): p. e6189.
24. Isomoto, S., et al., *Rapamycin as an inhibitor of osteogenic differentiation in bone marrow-derived mesenchymal stem cells.* J Orthop Sci, 2007. **12**(1): p. 83-8.
25. Singha, U.K., et al., *Rapamycin inhibits osteoblast proliferation and differentiation in MC3T3-E1 cells and primary mouse bone marrow stromal cells.* J Cell Biochem, 2008. **103**(2): p. 434-46.
26. Tang, L., et al., *FK506 enhanced osteoblastic differentiation in mesenchymal cells.* Cell Biol Int, 2002. **26**(1): p. 75-84.
27. Shoba, L.N. and J.C. Lee, *Inhibition of phosphatidylinositol 3-kinase and p70S6 kinase blocks osteogenic protein-1 induction of alkaline phosphatase activity in fetal rat calvaria cells.* J Cell Biochem, 2003. **88**(6): p. 1247-55.

28. Phornphutkul, C., et al., *The effect of rapamycin on bone growth in rabbits.* J Orthop Res, 2009. **27**(9): p. 1157-61.

29. Alvarez-Garcia, O., et al., *Rapamycin retards growth and causes marked alterations in the growth plate of young rats.* Pediatr Nephrol, 2007. **22**(7): p. 954-61.

30. Harada, S.-i. and G.A. Rodan, *Control of Osteoblast Function and Regulation of Bone Mass.* Nature, 2003. **423**: p. 349-355.

31. Gaalen, S.c., et al., *Tissue Engineering of Bone*, in *Tissue Engineering*, C.v. Blitterswijk, Editor 2008, Academic Press: London.

32. Blair, H.C., M. Zaidi, and P.H. Schlesinger, *Mechanisms balancing skeletal matrix synthesis and degradation.* Biochem J, 2002. **364**(Pt 2): p. 329-41.

33. Rodda, S.J. and A.P. McMahon, *Distinct roles for Hedgehog and canonical Wnt signaling in specification, differentiation and maintenance of osteoblast progenitors.* Development, 2006. **133**: p. 3231-3244.

34. Abboud, S.L., et al., *Rescue of the osteopetrotic defect in op/op mice by osteoblast-specific targeting of soluble colony-stimulating factor-1.* Endocrinology, 2002. **143**(5): p. 1942-9.

35. Kronenberg, H.M., *Developmental regulation of the growth plate.* Nature, 2003. **423**(6937): p. 332-6.

36. Olsen, B.R., A.M. Reginato, and W. Wang, *Bone development.* Annual review of cell and developmental biology, 2000. **16**: p. 191-220.

37. Vortkamp, A., *Skeleton morphogenesis: Defining the skeletal elements.* Current Biology, 1997. **7**(2): p. R104-R107.

38. Buchdunger, E., et al., *Inhibition of the Abl protein-tyrosine kinase in vitro and in vivo by a 2-phenylaminopyrimidine derivative.* Cancer Res, 1996. **56**(1): p. 100-4.

39. Horton, W.A., et al., *Immunohistochemistry of types I and II collagen in undecalcified skeletal tissues.* The journal of histochemistry and cytochemistry : official journal of the Histochemistry Society, 1983. **31**(3): p. 417-25.

40. Hardingham, T.E. and A.J. Fosang, *Proteoglycans: many forms and many functions.* FASEB J, 1992. **6**(3): p. 861-70.

41. Park, K.W., D.S. Halperin, and P. Tontonoz, *Before they were fat: Adipocyte Progenitors.* Cell Metabolism, 2008. **8**: p. 454-457.

42. Dodds, G., *Osteoclasts and cartilage removal in endochondral ossification of certain mammals.* American Journal of Anatomy, 1932. **50**(1): p. 97-127.

43. Dodds, C., *Row formation and other types of arrangement of cartilage cells in endochondral ossification.* The Anatomical Record, 1930. **46**(4): p. 385-399.

44. Kember, N. and H. Sissons, *Quantitative histology of the human growth plate.* J Bone Joint Surg Br., 1976. **58-B**(4): p. 433-437.

45. Sissons, H. and N. Kember, *Longitudinal bone growth of the human femur.* Postgrad Med J., 1977. **53**(622): p. 433-437.

46. Wilsman, N., et al., *Differential growth by growth plates as a function of multiple parameters of chondrocytic kinetics.* J Orthop Res., 1996. **14**(6): p. 927-936.

47. Villemure, I. and I.A. Stokes, *Growth plate mechanics and mechanobiology. A survey of present understanding.* Journal of biomechanics, 2009. **42**(12): p. 1793-803.

48. Parfitt, A.M., *Misconceptions (1): epiphyseal fusion causes cessation of growth.* Bone, 2002. **30**(2): p. 337-9.

49. Hunziker, E. and R. Schenk, *Physiological mechanisms adopted by chondrocytes in*

regulating longitudinal bone growth in rats. J Physiol, 1989. **414**: p. 55-71.

50. Cooper, K.L., et al., *Multiple phases of chondrocyte enlargement underlie differences in skeletal proportions.* Nature, 2013. **495**(7441): p. 375-8.

51. Dudley, H.R. and D. Spiro, *The Fine Structure of Bone Cells.* The Journal of biophysical and biochemical cytology, 1961. **11**(3): p. 627-49.

52. Seeman, E., *Modelling and Remodelling: The Cellular Machinery Responsible for the Gain and Loss of Bone's Material and Structural Strength*, in *Principles of Bone Biology (Third Edition)*, J.P. Bilezikian, L. Raisz, and T.J. Martin, Editors. 2008, Academic Press. p. 1-28.

53. Zhao, C., et al., *Bidirectional ephrinB2-EphB4 signaling controls bone homeostasis.* Cell Metab, 2006. **4**(2): p. 111-21.

54. MacIntyre, I., et al., *Osteoclastic inhibition: an action of nitric oxide not mediated by cyclic GMP.* Proc Natl Acad Sci U S A, 1991. **88**(7): p. 2936-40.

55. Zaidi, M., *Skeletal Remodelling in Health and Disease.* Nature Medicine, 2007. **13**(7): p. 791-801.

56. Yasuda, H., et al., *Osteoclast differentiation factor is a ligand for osteoprotegerin/osteoclastogenesis-inhibitory factor and is identical to TRANCE/RANKL.* Proc Natl Acad Sci U S A, 1998. **95**(7): p. 3597-602.

57. Lacey, D.L., et al., *Osteoprotegerin ligand is a cytokine that regulates osteoclast differentiation and activation.* Cell, 1998. **93**(2): p. 165-76.

58. Simonet, W.S., et al., *Osteoprotegerin: a novel secreted protein involved in the regulation of bone density.* Cell, 1997. **89**(2): p. 309-19.

59. Reddy, S.V., *Etiology of Paget's disease and osteoclast abnormalities.* J Cell Biochem, 2004. **93**(4): p. 688-96.

60. Manolagas, S.C., *Cell Number Versus Cell Vigor - What Really Matters to a Regenerating Skeleton.* Endocrinology, 1999. **140**: p. 4377-4381.

61. Kogianni, G. and B.S. Noble, *The biology of osteocytes.* Current osteoporosis reports, 2007. **5**(2): p. 81-6.

62. Klein-Nulend, J., et al., *Pulsating fluid flow increases nitric oxide (NO) synthesis by osteocytes but not periosteal fibroblasts--correlation with prostaglandin upregulation.* Biochem Biophys Res Commun, 1995. **217**(2): p. 640-8.

63. Lean, J.M., et al., *Increased insulin-like growth factor I mRNA expression in rat osteocytes in response to mechanical stimulation.* The American journal of physiology, 1995. **268**(2 Pt 1): p. E318-27.

64. Pitsillides, A.A., et al., *Mechanical strain-induced NO production by bone cells: a possible role in adaptive bone (re)modeling?* FASEB J, 1995. **9**(15): p. 1614-22.

65. Klein-Nulend, J., et al., *Sensitivity of osteocytes to biomechanical stress in vitro.* FASEB J, 1995. **9**(5): p. 441-5.

66. Fischman, D.A. and E.D. Hay, *Origin of osteoclasts from mononuclear leucocytes in regenerating newt limbs.* The Anatomical Record, 1962. **143**: p. 329-37.

67. Tinkler, S.M., et al., *Formation of osteoclasts from blood monocytes during 1 alpha-OH Vit D-stimulated bone resorption in mice.* Journal of anatomy, 1981. **133**(Pt 3): p. 389-96.

68. Scheven, B.A., J.W. Visser, and P.J. Nijweide, *In vitro osteoclast generation from different bone marrow fractions, including a highly enriched haematopoietic stem cell population.* Nature, 1986. **321**(6065): p. 79-81.

69. King, G.J. and M.E. Holtrop, *Actin-like filaments in bone cells of cultured mouse calvaria as demonstrated by binding to heavy meromyosin.* J Cell Biol, 1975. **66**(2): p. 445-51.

70. Scott, B.L. and D.C. Pease, *Electron microscopy of the epiphyseal apparatus.* The Anatomical Record, 1956. **126**(4): p. 465-95.

71. Ross, S.R., R.A. Graves, and B.M. Spiegelman, *Targeted expression of a toxin gene to adipose tissue: transgenic mice resistant to obesity.* Genes Dev, 1993. **7**(7B): p. 1318-24.

72. Gonzales, F. and M.J. Karnovsky, *Electron microscopy of osteoclasts in healing fracturees of rat bone.* The Journal of biophysical and biochemical cytology, 1961. **9**: p. 299-316.

73. Minkin, C. and J.M. Jennings, *Carbonic anhydrase and bone remodeling: sulfonamide inhibition of bone resorption in organ culture.* Science, 1972. **176**(4038): p. 1031-3.

74. Laitala, T. and H.K. Vaananen, *Inhibition of bone resorption in vitro by antisense RNA and DNA molecules targeted against carbonic anhydrase II or two subunits of vacuolar H(+)-ATPase.* J Clin Invest, 1994. **93**(6): p. 2311-8.

75. Lehenkari, P., et al., *Carbonic anhydrase II plays a major role in osteoclast differentiation and bone resorption by effecting the steady state intracellular pH and Ca2+*. Exp Cell Res, 1998. **242**(1): p. 128-37.

76. Rousselle, A.V. and D. Heymann, *Osteoclastic acidification pathways during bone resorption.* Bone, 2002. **30**(4): p. 533-40.

77. Baron, R., et al., *Cell-mediated extracellular acidification and bone resorption: evidence for a low pH in resorbing lacunae and localization of a 100-kD lysosomal membrane protein at the osteoclast ruffled border.* J Cell Biol, 1985. **101**(6): p. 2210-22.

78. Saftig, P., et al., *Impaired osteoclastic bone resorption leads to osteopetrosis in cathepsin-K-deficient mice.* Proc Natl Acad Sci U S A, 1998. **95**(23): p. 13453-8.

79. Nesbitt, S.A. and M.A. Horton, *Trafficking of matrix collagens through bone-resorbing osteoclasts.* Science, 1997. **276**(5310): p. 266-9.

80. Salo, J., et al., *Removal of osteoclast bone resorption products by transcytosis.* Science, 1997. **276**(5310): p. 270-3.

81. Pittenger, M.F., et al., *Multilineage Potential of Adult Human Mesenchymal Stem Cells.* Science, 1999. **284**: p. 143-147.

82. Pountos, I., et al., *Mesenchymal Stem Cell Tissue Engineering: Techniques for Isolation, Expansion and Application.* Injury, 2007. **38**(4): p. 23-33.

83. Jaiswal, N., et al., *Osteogenic Differentiation of Purified Culture-Expanded Human Mesenchymal Stem Cells In Vitro.* Journal of Cellular Biochemisrty, 1997. **64**: p. 295-312.

84. Zuk, P.A., et al., *Human adipose tissue is a source of multipotent stem cells.* Molecular biology of the cell, 2002. **13**(12): p. 4279-95.

85. Huang, A.H., et al., *Isolation and characterization of dental pulp stem cells from a supernumerary tooth.* Journal of oral pathology & medicine : official publication of the International Association of Oral Pathologists and the American Academy of Oral Pathology, 2008. **37**(9): p. 571-4.

86. Kuroda, R., et al., *Cartilage repair using bone morphogenetic protein 4 and muscle-derived stem cells.* Arthritis Rheum, 2006. **54**(2): p. 433-42.

87. Nakashima, K. and B. de Crombrugghe, *Transcriptional mechanisms in osteoblast differentiation and bone formation.* Trends Genet, 2003. **19**(8): p. 458-66.

88. Rosen, E.D., et al., *Transcriptional regulation of adipogenesis.* Genes Dev, 2000. **14**(11): p. 1293-307.

89. Komori, T., et al., *Targeted disruption of Cbfa1 results in a complete lack of bone formation owing to maturational arrest of osteoblasts.* Cell, 1997. **89**(5): p. 755-64.

90. Nakashima, K., et al., *The novel zinc finger-containing transcription factor osterix is required for osteoblast differentiation and bone formation.* Cell, 2002. **108**(1): p. 17-29.

91. Ducy, P., et al., *Osf2/Cbfa1: a transcriptional activator of osteoblast differentiation.* Cell, 1997. **89**(5): p. 747-54.

92. Karsenty, G., *The genetic transformation of bone biology.* Genes Dev, 1999. **13**(23): p. 3037-51.

93. Yoshida, C.A., et al., *Runx2 and Runx3 are essential for chondrocyte maturation, and Runx2 regulates limb growth through induction of Indian hedgehog.* Genes Dev, 2004. **18**(8): p. 952-63.

94. Lian, J.B., et al., *Networks and hubs for the transcriptional control of osteoblastogenesis.* Reviews in Endocrine and Metabolic DIsorders, 2006. **7**: p. 1-16.

95. Mackie, E.J., *Osteoblasts: novel roles in orchestration of skeletal architecture.* Int J Biochem Cell Biol, 2003. **35**(9): p. 1301-5.

96. Muir, H., *The chondrocyte, architect of cartilage. Biomechanics, structure, function and molecular biology of cartilage matrix macromolecules.* BioEssays : news and reviews in molecular, cellular and developmental biology, 1995. **17**(12): p. 1039-48.

97. Lefebvre, V., et al., *SOX9 is a potent activator of the chondrocyte-specific enhancer of the pro alpha1(II) collagen gene.* Mol Cell Biol, 1997. **17**(4): p. 2336-46.

98. Bi, W., et al., *Sox9 is required for cartilage formation.* Nature genetics, 1999. **22**(1): p. 85-9.

99. Bridgewater, L.C., V. Lefebvre, and B. de Crombrugghe, *Chondrocyte-specific enhancer elements in the Col11a2 gene resemble the Col2a1 tissue-specific enhancer.* J Biol Chem, 1998. **273**(24): p. 14998-5006.

100. Takeda, S., et al., *Continuous expression of Cbfa1 in nonhypertrophic chondrocytes uncovers its ability to induce hypertrophic chondrocyte differentiation and partially rescues Cbfa1-deficient mice.* Genes Dev, 2001. **15**(4): p. 467-81.

101. Inada, M., et al., *Maturational disturbance of chondrocytes in Cbfa1-deficient mice.* Dev Dyn, 1999. **214**(4): p. 279-90.

102. Ueta, C., et al., *Skeletal malformations caused by overexpression of Cbfa1 or its dominant negative form in chondrocytes.* J Cell Biol, 2001. **153**(1): p. 87-100.

103. Park, H.I., et al., *The intermediate S1' pocket of the endometase/matrilysin-2 active site revealed by enzyme inhibition kinetic studies, protein sequence analyses, and homology modeling.* J Biol Chem, 2003. **278**(51): p. 51646-53.

104. Rosen, E.D. and O.A. MacDougald, *Adipocyte differentiation from the inside out.* Nat Rev Mol Cell Biol, 2006. **7**(12): p. 885-96.

105. Rosen, E.D. and O.A. MacDougald, *Adipocyte differentiation from the inside out.* Molecular Cell Biology, 2006. **7**: p. 885-896.

106. Cao, Z., R.M. Umek, and S.L. McKnight, *Regulated expression of three C/EBP isoforms during adipose conversion of 3T3-L1 cells.* Genes Dev, 1991. **5**(9): p. 1538-52.

107. Yeh, W.C., et al., *Cascade regulation of terminal adipocyte differentiation by three members of the C/EBP family of leucine zipper proteins.* Genes Dev, 1995. **9**(2): p. 168-81.

108. Rosen, E.D., et al., *C/EBPa induces adipogenesis through PPARy: a unified pathway.* Genes and Development, 2002. **16**: p. 22-26.

109. Hwang, C.S., et al., *Transcriptional activation of the mouse obese (ob) gene by CCAAT/enhancer binding protein alpha.* Proc Natl Acad Sci U S A, 1996. **93**(2): p. 873-7.

110. Darlington, G.J., S.E. Ross, and O.A. MacDougald, *The role of C/EBP genes in adipocyte differentiation.* J Biol Chem, 1998. **273**(46): p. 30057-60.

111. Zhou, S., et al., *Age-related intrinsic changes in human bone-marrow-derived mesenchymal stem cells and their differentiation to osteoblasts.* Aging Cell, 2008. **7**(3): p. 335-43.

112. Caplan, A.I., *Mesenchymal stem cells.* J Orthop Res, 1991. **9**(5): p. 641-50.

113. Caplan, A.I., *The mesengenic process.* Clin Plast Surg, 1994. **21**(3): p. 429-35.

114. Young, H.E., et al., *Mesenchymal stem cells reside within the connective tissues of many organs.* Dev Dyn, 1995. **202**(2): p. 137-44.

115. Yu, Z.K., J.T. Wright, and G.J. Hausman, *Preadipocyte recruitment in stromal vascular cultures after depletion of committed preadipocytes by immunocytotoxicity.* Obes Res, 1997. **5**(1): p. 9-15.

116. Qiu, W., et al., *Patients with high bone mass phenotype exhibit enhanced osteoblast differentiation and inhibition of adipogenesis of human mesenchymal stem cells.* J Bone Miner Res, 2007. **22**(11): p. 1720-31.

117. Moerman, E.J., et al., *Aging activates adipogenic and suppresses osteogenic programs in mesenchymal marrow stroma/stem cells: the role of PPAR-gamma2 transcription factor and TGF-beta/BMP signaling pathways.* Aging Cell, 2004. **3**(6): p. 379-89.

118. Aubin, J.E., *Mesenchymal Stem Cells and Osteoblast Differentiation*, in *Principles of Bone Biology Third Edition*2008, Academic Press.

119. Stenderup, K., et al., *Aging is associated with decreased maximal life span and accelerated senescence of bone marrow stromal cells.* Bone, 2003. **33**: p. 919-926.

120. Zhang, X., et al., *Runx2 overexpression enhances osteoblastic differentiation and mineralization in adipose--derived stem cells in vitro and in vivo.* Calcif Tissue Int, 2006. **79**(3): p. 169-78.

121. Beresford, J.N., et al., *Evidence for an inverse relationship between the differentiation of adipocytic and osteogenic cells in rat marrow stromal cell cultures.* Journal of Cell Science, 1992. **102**: p. 341-351.

122. Gimble, J.M., et al., *Bone morphogenetic proteins inhibit adipocyte differentiation by bone marrow stromal cells.* Journal of Cellular Biochemistry, 1995. **58**: p. 393-402.

123. Gimble, J.M., et al., *Playing With Bone and Fat.* Journal of Cellular Biochemistry, 2006. **98**: p. 251-266.

124. Hu, H., et al., *Sequential roles of Hedgehog and Wnt signaling in osteoblast development.* Development, 2005. **132**(1): p. 49-60.

125. Kang, S., et al., *Wnt signaling stimulates osteoblastogenesis of mesenchymal precursors by suppressing CCAAT/enhancer-binding protein alpha and peroxisome proliferator-activated receptor gamma.* J Biol Chem, 2007. **282**(19): p. 14515-24.

126. Long, F., et al., *Ihh signaling is directly required for the osteoblast lineage in the endochondral skeleton.* Development, 2004. **131**(6): p. 1309-18.

127. Nakae, J., et al., *The forkhead transcription factor Foxo1 regulates adipocyte differentiation.* Dev Cell, 2003. **4**(1): p. 119-29.

128. Yang, S., et al., *Foxo1 mediates insulin-like growth factor 1 (IGF1)/insulin regulation of osteocalcin expression by antagonizing Runx2 in osteoblasts.* J Biol Chem, 2011. **286**(21): p. 19149-58.

129. Klemm, D.J., et al., *Insulin-induced adipocyte differentiation. Activation of CREB rescues adipogenesis from the arrest caused by inhibition of prenylation.* J Biol Chem, 2001. **276**(30): p. 28430-5.

130. Uehara, T., Y. Tokumitsu, and Y. Nomura, *Wortmannin inhibits insulin-induced Ras and mitogen-activated protein kinase activation related to adipocyte differentiation in 3T3-L1 fibroblasts.* Biochem Biophys Res Commun, 1995. **210**(2): p. 574-80.

131. Kato, M., et al., *Cbfa1-independent decrease in osteoblast proliferation, osteopenia, and persistent embryonic eye vascularization in mice deficient in Lrp5, a Wnt coreceptor.* J Cell Biol, 2002. **157**(2): p. 303-14.

132. Bodine, P.V., et al., *The Wnt antagonist secreted frizzled-related protein-1 controls osteoblast and osteocyte apoptosis.* J Cell Biochem, 2005. **96**(6): p. 1212-30.

133. Bodine, P.V., et al., *The Wnt antagonist secreted frizzled-related protein-1 is a negative regulator of trabecular bone formation in adult mice.* Mol Endocrinol, 2004. **18**(5): p. 1222-37.

134. Tamai, K., et al., *A mechanism for Wnt coreceptor activation.* Mol Cell, 2004. **13**(1): p. 149-56.

135. Pinson, K.I., et al., *An LDL-receptor-related protein mediates Wnt signalling in mice.* Nature, 2000. **407**(6803): p. 535-8.

136. Day, T.F., et al., *Wnt/beta-catenin signaling in mesenchymal progenitors controls osteoblast and chondrocyte differentiation during vertebrate skeletogenesis.* Dev Cell, 2005. **8**(5): p. 739-50.

137. Takada, I., A.P. Kouzmenko, and S. Kato, *Wnt and PPARgamma signaling in osteoblastogenesis and adipogenesis.* Nat Rev Rheumatol, 2009. **5**(8): p. 442-7.

138. Hemmati-Brivanlou, A. and G.H. Thomsen, *Ventral mesodermal patterning in Xenopus embryos: expression patterns and activities of BMP-2 and BMP-4.* Dev Genet, 1995. **17**(1): p. 78-89.

139. Kobayashi, T., et al., *BMP signaling stimulates cellular differentiation at multiple steps during cartilage development.* Proc Natl Acad Sci U S A, 2005. **102**(50): p. 18023-7.

140. Bobacz, K., et al., *Expression of bone morphogenetic protein 6 in healthy and osteoarthritic human articular chondrocytes and stimulation of matrix synthesis in vitro.* Arthritis Rheum, 2003. **48**(9): p. 2501-8.

141. Wagner, D.O., et al., *BMPs: from bone to body morphogenetic proteins.* Sci Signal, 2010. **3**(107): p. mr1.

142. Noel, D., et al., *Short-term BMP-2 expression is sufficient for in vivo osteochondral differentiation of mesenchymal stem cells.* Stem Cells, 2004. **22**(1): p. 74-85.

143. Huang, Z., et al., *Modulating osteogenesis of mesenchymal stem cells by modifying growth factor availability.* Cytokine, 2010. **51**(3): p. 305-10.

144. Rosen, V., *BMP2 signaling in bone development and repair.* Cytokine & growth factor reviews, 2009. **20**(5-6): p. 475-80.

145. Jensen, E.D., R. Gopalakrishnan, and J.J. Westendorf, *Regulation of gene expression in osteoblasts.* BioFactors, 2010. **36**(1): p. 25-32.

146. Lian, J.B., et al., *Regulatory controls for osteoblast growth and differentiation: role of Runx/Cbfa/AML factors.* Critical reviews in eukaryotic gene expression, 2004. **14**(1-2): p. 1-41.

147. Javed, A., et al., *Structural coupling of Smad and Runx2 for execution of the BMP2 osteogenic signal.* J Biol Chem, 2008. **283**(13): p. 8412-22.

148. Sabatini, D.M., et al., *RAFT1: a mammalian protein that binds to FKBP12 in a rapamycin-dependent fashion and is homologous to yeast TORs.* Cell, 1994. **78**(1): p. 35-43.

149. Kim, S.G., G.R. Buel, and J. Blenis, *Nutrient regulation of the mTOR complex 1 signaling pathway.* Molecules and cells, 2013. **35**(6): p. 463-73.

150. Kim, D.H., et al., *mTOR interacts with raptor to form a nutrient-sensitive complex that signals to the cell growth machinery.* Cell, 2002. **110**(2): p. 163-75.

151. Brugarolas, J., et al., *Regulation of mTOR function in response to hypoxia by REDD1 and the TSC1/TSC2 tumor suppressor complex.* Genes Dev, 2004. **18**(23): p. 2893-904.

152. Sancak, Y., et al., *The Rag GTPases bind raptor and mediate amino acid signaling to mTORC1.* Science, 2008. **320**(5882): p. 1496-501.

153. Heitman, J., N.R. Movva, and M.N. Hall, *Targets for cell cycle arrest by the immunosuppressant rapamycin in yeast.* Science, 1991. **253**(5022): p. 905-9.

154. Loewith, R., et al., *Two TOR complexes, only one of which is rapamycin sensitive, have distinct roles in cell growth control.* Mol Cell, 2002. **10**(3): p. 457-68.

155. Jacinto, E., et al., *Mammalian TOR complex 2 controls the actin cytoskeleton and is rapamycin insensitive.* Nat Cell Biol, 2004. **6**(11): p. 1122-8.

156. Sarbassov, D.D., et al., *Rictor, a Novel Binding Partner of mTOR, Defines a Rapamycin-Insensitive and Raptor-Independent Pathway that Regulates the Cytoskeleton.* Current Biology, 2004. **14**: p. 1296-1302.

157. Sarbassov, D.D., et al., *Rictor, a novel binding partner of mTOR, defines a rapamycin-insensitive and raptor-independent pathway that regulates the cytoskeleton.* Curr Biol, 2004. **14**(14): p. 1296-302.

158. Kim, H.K., et al., *Inhibition of endothelial cell proliferation by the recombinant kringle domain of tissue-type plasminogen activator.* Biochem Biophys Res Commun, 2003. **304**(4): p. 740-6.

159. Yang, H., et al., *mTOR kinase structure, mechanism and regulation.* Nature, 2013. **497**(7448): p. 217-23.

160. Benjamin, D., et al., *Rapamycin passes the torch: a new generation of mTOR inhibitors.* Nature reviews. Drug discovery, 2011. **10**(11): p. 868-80.

161. Thoreen, C.C., et al., *An ATP-competitive mammalian target of rapamycin inhibitor reveals rapamycin-resistant functions of mTORC1.* J Biol Chem, 2009. **284**(12): p. 8023-32.

162. Sarbassov, D.D., et al., *Prolonged rapamycin treatment inhibits mTORC2 assembly and Akt/PKB.* Mol Cell, 2006. **22**(2): p. 159-68.

163. Guertin, D.A. and D.M. Sabatini, *An expanding role for mTOR in cancer.* Trends Mol Med, 2005. **11**(8): p. 353-61.

164. Vander Haar, E., et al., *Insulin signalling to mTOR mediated by the Akt/PKB substrate PRAS40.* Nat Cell Biol, 2007. **9**(3): p. 316-23.

165. Wang, L., et al., *PRAS40 regulates mTORC1 kinase activity by functioning as a direct inhibitor of substrate binding.* J Biol Chem, 2007. **282**(27): p. 20036-44.

166. Rokutanda, S., et al., *Akt regulates skeletal development through GSK3, mTOR, and FoxOs.* Developmental biology, 2009. **328**(1): p. 78-93.

167. Inoki, K., et al., *TSC2 integrates Wnt and energy signals via a coordinated phosphorylation by AMPK and GSK3 to regulate cell growth.* Cell, 2006. **126**(5): p. 955-68.

168. Inoki, K., T. Zhu, and K.L. Guan, *TSC2 mediates cellular energy response to control cell growth and survival.* Cell, 2003. **115**(5): p. 577-90.

169. Gwinn, D.M., et al., *AMPK phosphorylation of raptor mediates a metabolic checkpoint.* Mol Cell, 2008. **30**(2): p. 214-26.

170. Lopez-Lluch, G., et al., *Mitochondrial biogenesis and healthy aging.* Exp Gerontol, 2008. **43**(9): p. 813-9.

171. Arsham, A.M., J.J. Howell, and M.C. Simon, *A novel hypoxia-inducible factor-independent hypoxic response regulating mammalian target of rapamycin and its targets.* J Biol Chem, 2003. **278**(32): p. 29655-60.

172. Liu, L., et al., *Hypoxia-induced energy stress regulates mRNA translation and cell growth.* Mol Cell, 2006. **21**(4): p. 521-31.

173. DeYoung, M.P., et al., *Hypoxia regulates TSC1/2-mTOR signaling and tumor suppression through REDD1-mediated 14-3-3 shuttling.* Genes Dev, 2008. **22**(2): p. 239-51.

174. Carriere, A., et al., *Oncogenic MAPK signaling stimulates mTORC1 activity by promoting RSK-mediated raptor phosphorylation.* Curr Biol, 2008. **18**(17): p. 1269-77.

175. Mendoza, M.C., E.E. Er, and J. Blenis, *The Ras-ERK and PI3K-mTOR pathways: cross-talk and compensation.* Trends Biochem Sci, 2011. **36**(6): p. 320-8.

176. Kim, E., et al., *Regulation of TORC1 by Rag GTPases in nutrient response.* Nat Cell Biol, 2008. **10**(8): p. 935-45.

177. Hay, N. and N. Sonenberg, *Upstream and downstream of mTOR.* Genes and Development, 2004. **18**: p. 1926-1945.

178. Jastrzebski, K., et al., *Coordinate regulation of ribosome biogenesis and function by the ribosomal protein S6 kinase, a key mediator of mTOR function.* Growth factors, 2007. **25**(4): p. 209-26.

179. Holz, M.K. and J. Blenis, *Identification of S6 kinase 1 as a novel mammalian target of rapamycin (mTOR)-phosphorylating kinase.* J Biol Chem, 2005. **280**(28): p. 26089-93.

180. Holz, M.K., et al., *mTOR and S6K1 mediate assembly of the translation preinitiation complex through dynamic protein interchange and ordered phosphorylation events.* Cell, 2005. **123**(4): p. 569-80.

181. Peterson, R.T. and S.L. Schreiber, *Translation control: connecting mitogens and the ribosome.* Curr Biol, 1998. **8**(7): p. R248-50.

182. Richter, J.D. and N. Sonenberg, *Regulation of cap-dependent translation by eIF4E inhibitory proteins.* Nature, 2005. **433**(7025): p. 477-80.

183. Ma, X.M. and J. Blenis, *Molecular mechanisms of mTOR-mediated translational control.* Nat Rev Mol Cell Biol, 2009. **10**(5): p. 307-18.

184. Ganley, I.G., et al., *ULK1.ATG13.FIP200 complex mediates mTOR signaling and is essential for autophagy.* J Biol Chem, 2009. **284**(18): p. 12297-305.

185. Codogno, P. and A.J. Meijer, *Autophagy and signaling: their role in cell survival and cell death.* Cell Death Differ, 2005. **12 Suppl 2**: p. 1509-18.

186. Hosokawa, N., et al., *Nutrient-dependent mTORC1 association with the ULK1-Atg13-FIP200 complex required for autophagy.* Molecular biology of the cell, 2009. **20**(7): p. 1981-91.

187. Jung, C.H., et al., *ULK-Atg13-FIP200 complexes mediate mTOR signaling to the autophagy machinery.* Molecular biology of the cell, 2009. **20**(7): p. 1992-2003.

188. Russell, R.C., et al., *ULK1 induces autophagy by phosphorylating Beclin-1 and activating VPS34 lipid kinase.* Nat Cell Biol, 2013. **15**(7): p. 741-50.

189. Laplante, M. and D.M. Sabatini, *mTOR signaling in growth control and disease.* Cell, 2012. **149**(2): p. 274-93.

190. Um, S.H., et al., *Absence of S6K1 protects against age- and diet-induced obesity while enhancing insulin sensitivity.* Nature, 2004. **431**(7005): p. 200-5.

191. Tzatsos, A. and K.V. Kandror, *Nutrients suppress phosphatidylinositol 3-kinase/Akt signaling via raptor-dependent mTOR-mediated insulin receptor substrate 1 phosphorylation.* Mol Cell Biol, 2006. **26**(1): p. 63-76.

192. Chiang, G.G. and R.T. Abraham, *Phosphorylation of mammalian target of rapamycin (mTOR) at Ser-2448 is mediated by p70S6 kinase.* J Biol Chem, 2005. **280**(27): p. 25485-90.

193. Hsu, P.P., et al., *The mTOR-regulated phosphoproteome reveals a mechanism of mTORC1-mediated inhibition of growth factor signaling.* Science, 2011. **332**(6035): p. 1317-22.

194. Liu, M., et al., *Grb10 promotes lipolysis and thermogenesis by phosphorylation-dependent feedback inhibition of mTORC1.* Cell Metab, 2014. **19**(6): p. 967-80.

195. Wullschleger, S., R. Loewith, and M.N. Hall, *TOR Signaling in Growth and Metabolism.* Cell, 2006. **124**: p. 471-484.

196. Guertin, D.A. and D.M. Sabatini, *Defining the role of mTOR in cancer.* Cancer Cell, 2007. **12**(1): p. 9-22.

197. Nojima, H., et al., *The mammalian target of rapamycin (mTOR) partner, raptor, binds the mTOR substrates p70 S6 kinase and 4E-BP1 through their TOR signaling (TOS) motif.* J Biol Chem, 2003. **278**(18): p. 15461-4.

198. Wang, L., C.J. Rhodes, and J.C. Lawrence, Jr., *Activation of mammalian target of rapamycin (mTOR) by insulin is associated with stimulation of 4EBP1 binding to dimeric mTOR complex 1.* J Biol Chem, 2006. **281**(34): p. 24293-303.

199. Schalm, S.S. and J. Blenis, *Identification of a conserved motif required for mTOR signaling.* Curr Biol, 2002. **12**(8): p. 632-9.

200. Schalm, S.S., et al., *TOS motif-mediated raptor binding regulates 4E-BP1 multisite phosphorylation and function.* Curr Biol, 2003. **13**(10): p. 797-806.

201. Long, X., et al., *Rheb binds and regulates the mTOR kinase.* Curr Biol, 2005. **15**(8): p. 702-13.

202. Guertin, D.A., et al., *Ablation in mice of the mTORC components raptor, rictor, or mLST8 reveals that mTORC2 is required for signaling to Akt-FOXO and PKCalpha, but not S6K1.* Dev Cell, 2006. **11**(6): p. 859-71.

203. Kim, J.E. and J. Chen, *regulation of peroxisome proliferator-activated receptor-gamma activity by mammalian target of rapamycin and amino acids in adipogenesis.* Diabetes, 2004. **53**(11): p. 2748-56.

204. Bell, A., L. Grunder, and A. Sorisky, *Rapamycin inhibits human adipocyte differentiation in primary culture.* Obes Res, 2000. **8**(3): p. 249-54.

205. Lee, K.W., et al., *Rapamycin promotes the osteoblastic differentiation of human embryonic stem cells by blocking the mTOR pathway and stimulating the BMP/Smad pathway.* Stem Cells Dev, 2009.

206. Wood, A.R., et al., *Defining the role of common variation in the genomic and biological architecture of adult human height.* Nature genetics, 2014. **46**(11): p. 1173-86.

207. Gong, Y., et al., *LDL receptor-related protein 5 (LRP5) affects bone accrual and eye development.* Cell, 2001. **107**(4): p. 513-23.

208. Boyden, L.M., et al., *High bone density due to a mutation in LDL-receptor-related protein 5.* N Engl J Med, 2002. **346**(20): p. 1513-21.

209. Little, R.D., et al., *A mutation in the LDL receptor-related protein 5 gene results in the autosomal dominant high-bone-mass trait.* Am J Hum Genet, 2002. **70**(1): p. 11-9.

210. Barron, R.P., et al., *Tuberous sclerosis: clinicopathologic features and review of the literature.* Journal of cranio-maxillo-facial surgery : official publication of the European Association for Cranio-Maxillo-Facial Surgery, 2002. **30**(6): p. 361-6.

211. Marie, P., *Growth factors and bone formation in osteoporosis: roles for IGF-I and TGF-beta.* Revue du rhumatisme, 1997. **64**(1): p. 44-53.

212. Yakar, S., et al., *Circulating levels of IGF-1 directly regulate bone growth and density.* J Clin Invest, 2002. **110**(6): p. 771-81.

213. Crowne, E.C., et al., *The role of IGF-binding proteins in mediating the effects of recombinant human IGF-I on insulin requirements in type 1 diabetes mellitus.* J Clin Endocrinol Metab, 2001. **86**(8): p. 3686-91.

214. Bereket, A., C.H. Lang, and T.A. Wilson, *Alterations in the growth hormone-insulin-like growth factor axis in insulin dependent diabetes mellitus.* Horm Metab Res, 1999. **31**(2-3): p. 172-81.

215. Grinspoon, S., et al., *Effects of recombinant human IGF-I and oral contraceptive administration on bone density in anorexia nervosa.* J Clin Endocrinol Metab, 2002. **87**(6): p. 2883-91.

216. Misra, M., et al., *Alterations in growth hormone secretory dynamics in adolescent girls with anorexia nervosa and effects on bone metabolism.* J Clin Endocrinol Metab, 2003. **88**(12): p. 5615-23.

217. Martel, R.R., J. Klicius, and S. Galet, *Inhibition of the immune response by rapamycin, a new antifungal antibiotic.* Canadian journal of physiology and pharmacology, 1977. **55**(1): p. 48-51.

218. Eng, C.P., S.N. Sehgal, and C. Vezina, *Activity of rapamycin (AY-22,989) against transplanted tumors.* J Antibiot (Tokyo), 1984. **37**(10): p. 1231-7.

219. Couriel, D.R., et al., *Sirolimus in combination with tacrolimus and corticosteroids for the treatment of resistant chronic graft-versus-host disease.* Br J Haematol, 2005. **130**(3): p. 409-17.

220. Johnston, L.J., et al., *Rapamycin (sirolimus) for treatment of chronic graft-versus-host disease.* Biology of blood and marrow transplantation : journal of the American Society for Blood and Marrow Transplantation, 2005. **11**(1): p. 47-55.

221. Nishida, S., et al., *Sirolimus (rapamycin)-based rescue treatment following chronic rejection after liver transplantation.* Transplantation proceedings, 2001. **33**(1-2): p. 1495.

222. Vezina, C., A. Kudelski, and S.N. Sehgal, *Rapamycin (AY-22,989), a new antifungal antibiotic. I. Taxonomy of the producing streptomycete and isolation of the active principle.* J Antibiot (Tokyo), 1975. **28**(10): p. 721-6.

223. Law, B.K., *Rapamycin: an anti-cancer immunosuppressant?* Crit Rev Oncol Hematol, 2005. **56**(1): p. 47-60.

224. Grewe, M., et al., *Regulation of cell growth and cyclin D1 expression by the constitutively active FRAP-p70s6K pathway in human pancreatic cancer cells.* Cancer Res, 1999. **59**(15): p. 3581-7.

225. Seufferlein, T. and E. Rozengurt, *Rapamycin inhibits constitutive p70s6k phosphorylation, cell proliferation, and colony formation in small cell lung cancer cells.* Cancer Res, 1996. **56**(17): p. 3895-7.

226. Moore, S.M., et al., *The presence of a constitutively active phosphoinositide 3-kinase in small cell lung cancer cells mediates anchorage-independent proliferation via a protein kinase B and p70s6k-dependent pathway.* Cancer Res, 1998. **58**(22): p. 5239-47.

227. Li, B.D., et al., *Overexpression of eukaryotic initiation factor 4E (eIF4E) in breast carcinoma.* Cancer, 1997. **79**(12): p. 2385-90.

228. Rosenwald, I.B., et al., *Upregulation of protein synthesis initiation factor eIF-4E is an early event during colon carcinogenesis.* Oncogene, 1999. **18**(15): p. 2507-17.

229. Li, B.D., et al., *Clinical outcome in stage I to III breast carcinoma and eIF4E overexpression.* Annals of surgery, 1998. **227**(5): p. 756-6l; discussion 761-3.

230. Nathan, C.O., et al., *Detection of the proto-oncogene eIF4E in surgical margins may predict recurrence in head and neck cancer.* Oncogene, 1997. **15**(5): p. 579-84.

231. Movsowitz, C., et al., *Cyclosporin-A in vivo produces severe osteopenia in the rat: effect of dose and duration of administration.* Endocrinology, 1988. **123**(5): p. 2571-7.

232. Cvetkovic, M., et al., *The deleterious effects of long-term cyclosporine A, cyclosporine G, and FK506 on bone mineral metabolism in vivo.* Transplantation, 1994. **57**(8): p. 1231-7.

233. Goodman, G.R., et al., *Immunosuppressant use without bone loss--implications for bone loss after transplantation.* J Bone Miner Res, 2001. **16**(1): p. 72-8.

234. Joffe, I., et al., *Lack of change of cancellous bone volume with short-term use of the new immunosuppressant rapamycin in rats.* Calcif Tissue Int, 1993. **53**(1): p. 45-52.

235. Romero, D.F., et al., *Rapamycin: a bone sparing immunosuppressant?* J Bone Miner Res, 1995. **10**(5): p. 760-8.

236. Hadji, P., R. Coleman, and M. Gnant, *Bone effects of mammalian target of rapamycin (mTOR) inhibition with everolimus.* Crit Rev Oncol Hematol, 2013. **87**(2): p. 101-11.

237. Gnant, M., et al., *Effect of everolimus on bone marker levels and progressive disease in bone in BOLERO-2.* Journal of the National Cancer Institute, 2013. **105**(9): p. 654-63.

238. Gangloff, Y.G., et al., *Disruption of the mouse mTOR gene leads to early postimplantation lethality and prohibits embryonic stem cell development.* Mol Cell Biol, 2004. **24**(21): p. 9508-16.

239. Murakami, M., et al., *mTOR is essential for growth and proliferation in early mouse embryos and embryonic stem cells.* Mol Cell Biol, 2004. **24**(15): p. 6710-8.

240. Polak, P., et al., *Adipose-Specific Knockout of raptor Results in Lean Mice with Enhanced Mitochondrial Respiration.* Cell Metabolism, 2008. **8**: p. 399-410.

241. Bentzinger, C.F., et al., *Skeletal Muscle-Specific Ablation of raptor, but Not of rictor, Causes Metabolic Changes and Results in Muscle Dystrophy.* Cell Metabolism, 2008. **8**(5): p. 411-424.

242. Sengupta, S., et al., *mTORC1 controls fasting-induced ketogenesis and its modulation by ageing.* Nature, 2010. **468**(7327): p. 1100-4.

243. Cloetta, D., et al., *Inactivation of mTORC1 in the developing brain causes microcephaly and affects gliogenesis.* J Neurosci, 2013. **33**(18): p. 7799-810.

244. Bercury, K.K., et al., *Conditional ablation of raptor or rictor has differential impact on oligodendrocyte differentiation and CNS myelination.* J Neurosci, 2014. **34**(13): p. 4466-80.

245. Zeng, H., et al., *mTORC1 couples immune signals and metabolic programming to establish T(reg)-cell function.* Nature, 2013. **499**(7459): p. 485-90.

246. Gorre, N., et al., *mTORC1 Signaling in oocytes is dispensable for the survival of primordial follicles and for female fertility.* PLoS One, 2014. **9**(10): p. e110491.

247. Sampson, L.L., et al., *mTOR disruption causes intestinal epithelial cell defects and intestinal atrophy postinjury in mice.* FASEB J, 2016. **30**(3): p. 1263-75.

248. Knight, Z.A., et al., *A critical role for mTORC1 in erythropoiesis and anemia.* eLife, 2014. **3**: p. e01913.

249. Logan, M., et al., *Expression of Cre Recombinase in the developing mouse limb bud driven by a Prxl enhancer.* Genesis, 2002. **33**(2): p. 77-80.

250. Zhang, M., et al., *Osteoblast-specific knockout of the insulin-like growth factor (IGF) receptor gene reveals an essential role of IGF signaling in bone matrix mineralization.* J Biol Chem, 2002. **277**(46): p. 44005-12.

251. Liu, J.P., et al., *Mice carrying null mutations of the genes encoding insulin-like growth factor I (Igf-1) and type 1 IGF receptor (Igf1r).* Cell, 1993. **75**(1): p. 59-72.

252. Baker, J., et al., *Role of insulin-like growth factors in embryonic and postnatal growth.* Cell, 1993. **75**(1): p. 73-82.

253. Long, F., et al., *Independent regulation of skeletal growth by Ihh and IGF signaling.* Developmental biology, 2006. **298**(1): p. 327-33.

254. He, J., et al., *Postnatal growth and bone mass in mice with IGF-I haploinsufficiency.* Bone, 2006. **38**(6): p. 826-35.

255. Govoni, K.E., et al., *Conditional deletion of insulin-like growth factor-I in collagen type 1alpha2-expressing cells results in postnatal lethality and a dramatic reduction in bone accretion.* Endocrinology, 2007. **148**(12): p. 5706-15.

256. Fulzele, K., et al., *Insulin receptor signaling in osteoblasts regulates postnatal bone acquisition and body composition.* Cell, 2010. **142**(2): p. 309-19.

257. Jiang, J., et al., *Transgenic mice with osteoblast-targeted insulin-like growth factor-I show increased bone remodeling.* Bone, 2006. **39**(3): p. 494-504.

258. Kawamura, N., et al., *Akt1 in osteoblasts and osteoclasts controls bone remodeling.* PLoS One, 2007. **2**(10): p. e1058.

259. Peng, X.D., et al., *Dwarfism, impaired skin development, skeletal muscle atrophy, delayed bone development, and impeded adipogenesis in mice lacking Akt1 and Akt2.* Genes Dev, 2003. **17**(11): p. 1352-65.

260. Ulici, V., et al., *The role of Akt1 in terminal stages of endochondral bone formation: angiogenesis and ossification.* Bone, 2009. **45**(6): p. 1133-45.

261. Ford-Hutchinson, A.F., et al., *Inactivation of Pten in osteo-chondroprogenitor cells leads to epiphyseal growth plate abnormalities and skeletal overgrowth.* J Bone Miner Res, 2007. **22**(8): p. 1245-59.

262. Liu, X., et al., *Lifelong accumulation of bone in mice lacking Pten in osteoblasts.* Proc Natl Acad Sci U S A, 2007. **104**(7): p. 2259-64.

263. Srinivas, S., et al., *Cre reporter strains produced by targeted insertion of EYFP and ECFP into the ROSA26 locus.* BMC developmental biology, 2001. **1**: p. 4.

264. Short, B.J., N. Brouard, and P.J. Simmons, *Prospective Isolation of Mesenchymal Stem Cells from Mouse Compact Bone*, in *Stem Cells in Regenerative Medicine*2009. p. 259-268.

265. Isenmann, S., et al., *TWIST family of basic helix-loop-helix transcription factors mediate human mesenchymal stem cell growth and commitment.* Stem Cells, 2009. **27**(10): p. 2457-68.

266. Dietmair, S., et al., *A multi-omics analysis of recombinant protein production in Hek293 cells.* PLoS One, 2012. **7**(8): p. e43394.

267. Galli, A., et al., *Sodium-dependent norepinephrine-induced currents in norepinephrine-transporter-transfected HEK-293 cells blocked by cocaine and antidepressants.* The Journal of experimental biology, 1995. **198**(Pt 10): p. 2197-212.

268. Rost, F.W. and J.M. Polak, *Fluorescence microscopy and microspectrofluorimetry of malignant melanomas, naevi and normal*

melanocytes. Virchows Archiv. A, Pathology. Pathologische Anatomie, 1969. **347**(4): p. 321-6.

269. Gronthos, S., et al., *Molecular and cellular characterisation of highly purified stromal stem cells derived from human bone marrow.* J Cell Sci, 2003. **116**(Pt 9): p. 1827-35.

270. Vandyke, K., et al., *The Tyrosine Kinase Inhibitor Dasatinib Dysregulates Bone Remodeling Through Inhibition of Osteoclasts In Vivo.* Journal of Bone and Mineral Research, 2010. **25**(8): p. 1759-1770.

271. Ovchinnikov, D., *Alcian blue/alizarin red staining of cartilage and bone in mouse.* Cold Spring Harbor protocols, 2009. **2009**(3): p. pdb prot5170.

272. Schneider, C.A., W.S. Rasband, and K.W. Eliceiri, *NIH Image to ImageJ: 25 years of image analysis.* Nature methods, 2012. **9**(7): p. 671-5.

273. Schriefer, J.L., et al., *A comparison of mechanical properties derived from multiple skeletal sites in mice.* Journal of biomechanics, 2005. **38**(3): p. 467-75.

274. Wakitani, S., T. Saito, and A.I. Caplan, *Myogenic cells derived from rat bone marrow mesenchymal stem cells exposed to 5-azacytidine.* Muscle & nerve, 1995. **18**(12): p. 1417-26.

275. Grigoriadis, A.E., J.N. Heersche, and J.E. Aubin, *Differentiation of muscle, fat, cartilage, and bone from progenitor cells present in a bone-derived clonal cell population: effect of dexamethasone.* J Cell Biol, 1988. **106**(6): p. 2139-51.

276. Yamaguchi, A., T. Komori, and T. Suda, *Regulation of osteoblast differentiation mediated by bone morphogenetic proteins, hedgehogs, and Cbfa1*. Endocrine reviews, 2000. **21**(4): p. 393-411.

277. Cao, Y., et al., *Osterix, a transcription factor for osteoblast differentiation, mediates antitumor activity in murine osteosarcoma.* Cancer Res, 2005. **65**(4): p. 1124-8.

278. Katagiri, T. and N. Takahashi, *Regulatory mechanisms of osteoblast and osteoclast differentiation.* Oral diseases, 2002. **8**(3): p. 147-59.

279. Chen, D., et al., *Bone morphogenetic protein 2 (BMP-2) enhances BMP-3, BMP-4, and bone cell differentiation marker gene expression during the induction of mineralized bone matrix formation in cultures of fetal rat calvarial osteoblasts.* Calcif Tissue Int, 1997. **60**(3): p. 283-90.

280. Feil, R., et al., *Ligand-activated site-specific recombination in mice.* Proc Natl Acad Sci U S A, 1996. **93**(20): p. 10887-90.

281. Konishi, T., et al., *Visualization of heavy ion tracks by labeling 3'-OH termini of induced DNA strand breaks.* J Radiat Res, 2011. **52**(4): p. 433-40.

282. Yoon, M.S., et al., *Mechanistic target of rapamycin controls homeostasis of adipogenesis.* Journal of lipid research, 2013. **54**(8): p. 2166-73.

283. Lamming, D.W., et al., *Rapamycin-induced insulin resistance is mediated by mTORC2 loss and uncoupled from longevity.* Science, 2012. **335**(6076): p. 1638-43.

284. Cybulski, N., V. Zinzalla, and M.N. Hall, *Inducible raptor and rictor knockout mouse embryonic fibroblasts.* Methods Mol Biol, 2012. **821**: p. 267-78.

285. Patursky-Polischuk, I., et al., *The TSC-mTOR pathway mediates translational activation of TOP mRNAs by insulin largely in a raptor- or rictor-independent manner.* Mol Cell Biol, 2009. **29**(3): p. 640-9.

286. Chen, J. and F. Long, *mTORC1 signaling controls mammalian skeletal growth through stimulation of protein synthesis.* Development, 2014.

287. Gundle, R., C.J. Joyner, and J.T. Triffitt, *Human bone tissue formation in diffusion chamber culture in vivo by bone-derived cells and marrow stromal fibroblastic cells.* Bone, 1995. **16**(6): p. 597-601.

288. Mogi, M. and A. Kondo, *Down-regulation of mTOR leads to up-regulation of osteoprotegerin in bone marrow cells.* Biochemical an Biophysical Research Communications, 2009. **384**: p. 82-86.

289. Wang, E.A., et al., *Bone morphogenetic protein-2 causes commitment and differentiation in C3H10T1/2 and 3T3 cells.* Growth factors, 1993. **9**(1): p. 57-71.

290. Chen, G., C. Deng, and Y.P. Li, *TGF-beta and BMP signaling in osteoblast differentiation and bone formation.* Int J Biol Sci, 2012. **8**(2): p. 272-88.

291. Yu, W., et al., *Critical role of phosphoinositide 3-kinase cascade in adipogenesis of human mesenchymal stem cells.* Mol Cell Biochem, 2008. **310**(1-2): p. 11-8.

292. Miki, H., et al., *Essential role of insulin receptor substrate 1 (IRS-1) and IRS-2 in adipocyte differentiation.* Mol Cell Biol, 2001. **21**(7): p. 2521-32.

293. Le Bacquer, O., et al., *Elevated sensitivity to diet-induced obesity and insulin resistance in mice lacking 4E-BP1 and 4E-BP2.* J Clin Invest, 2007. **117**(2): p. 387-96.

294. Konige, M., H. Wang, and C. Sztalryd, *Role of adipose specific lipid droplet proteins in maintaining whole body energy homeostasis.* Biochim Biophys Acta, 2014. **1842**(3): p. 393-401.

295. Kalaitzidis, D., et al., *mTOR complex 1 plays critical roles in hematopoiesis and Pten-loss-evoked leukemogenesis.* Cell Stem Cell, 2012. **11**(3): p. 429-39.

296. Kneissel, M., et al., *Everolimus suppresses cancellous bone loss, bone resorption, and cathepsin K expression by osteoclasts.* Bone, 2004. **35**(5): p. 1144-56.

297. Glantschnig, H., et al., *M-CSF, TNFalpha and RANK ligand promote osteoclast survival by signaling through mTOR/S6 kinase.* Cell Death Differ, 2003. **10**(10): p. 1165-77.

298. Oldham, S. and E. Hafen, *Insulin/IGF and target of rapamycin signaling: a TOR de force in growth control.* Trends in cell biology, 2003. **13**(2): p. 79-85.

299. Gao, J., et al., *The involvement of FoxO in cell survival and chemosensitivity mediated by Mirk/Dyrk1B in ovarian cancer.* Int J Oncol, 2012. **40**(4): p. 1203-9.

300. Riddle, R.C., et al., *Tsc2 is a molecular checkpoint controlling osteoblast development and glucose homeostasis.* Mol Cell Biol, 2014. **34**(10): p. 1850-62.

301. Yu, K., et al., *Conditional inactivation of FGF receptor 2 reveals an essential role for FGF signaling in the regulation of osteoblast function and bone growth.* Development, 2003. **130**(13): p. 3063-74.

302. Kim, J.E., K. Nakashima, and B. de Crombrugghe, *Transgenic mice expressing a ligand-inducible cre recombinase in osteoblasts and odontoblasts: a new tool to examine physiology and disease of postnatal bone and tooth.* The American journal of pathology, 2004. **165**(6): p. 1875-82.

303. Madisen, L., et al., *A robust and high-throughput Cre reporting and characterization system for the whole mouse brain.* Nature neuroscience, 2010. **13**(1): p. 133-40.

304. Tommasini, S.M., P. Nasser, and K.J. Jepsen, *Sexual dimorphism affects tibia size and shape but not tissue-level mechanical properties.* Bone, 2007. **40**(2): p. 498-505.

305. Callewaert, F., et al., *Skeletal sexual dimorphism: relative contribution of sex steroids, GH-IGF1, and mechanical loading.* J Endocrinol, 2010. **207**(2): p. 127-34.

306. Silbermann, M. and T. Kedar, *Observations on the growth of the normal male mouse.* Acta anatomica, 1977. **98**(3): p. 253-63.

307. Pines, M. and S. Hurwitz, *The role of the growth plate in longitudinal bone growth.* Poultry science, 1991. **70**(8): p. 1806-14.

308. Pauly, H.M., et al., *Assessment of cortical and trabecular bone changes in two models of post-traumatic osteoarthritis.* J Orthop Res, 2015. **33**(12): p. 1835-45.

309. Cohen, A., et al., *Assessment of trabecular and cortical architecture and mechanical competence of bone by high-resolution peripheral computed tomography: comparison with transiliac bone biopsy.* Osteoporos Int, 2010. **21**(2): p. 263-73.

310. Hildebrand, T. and P. Ruegsegger, *Quantification of Bone Microarchitecture with the Structure Model Index.* Computer methods in biomechanics and biomedical engineering, 1997. **1**(1): p. 15-23.

311. Arthur, A., et al., *EphB4 enhances the process of endochondral ossification and inhibits remodeling during bone fracture repair.* J Bone Miner Res, 2013. **28**(4): p. 926-35.

312. Saad, F., et al., *Pathologic fractures correlate with reduced survival in patients with malignant bone disease.* Cancer, 2007. **110**(8): p. 1860-7.

313. Forlino, A. and J.C. Marini, *Osteogenesis imperfecta.* Lancet, 2016. **387**(10028): p. 1657-71.

314. Russell, G., et al., *Clinical disorders of bone resorption.* Novartis Foundation symposium, 2001. **232**: p. 251-67; discussion 267-71.

315. Davey, R.A., et al., *Decreased body weight in young Osterix-Cre transgenic mice results in delayed cortical bone expansion and accrual.* Transgenic Research, 2011. **21**(4): p. 885-893.

316. Wang, L., Y. Mishina, and F. Liu, *Osterix-Cre transgene causes craniofacial bone development defect.* Calcif Tissue Int, 2015. **96**(2): p. 129-37.

317. Huang, W. and B.R. Olsen, *Skeletal defects in Osterix-Cre transgenic mice.* Transgenic research, 2015. **24**(1): p. 167-72.

318. Long, F. and D.M. Ornitz, *Development of the endochondral skeleton.* Cold Spring Harbor perspectives in biology, 2013. **5**(1): p. a008334.

319. Xian, L., et al., *Matrix IGF-1 maintains bone mass by activation of mTOR in mesenchymal stem cells.* Nat Med, 2012. **18**(7): p. 1095-101.

320. Veitia, R.A., S. Bottani, and J.A. Birchler, *Gene dosage effects: nonlinearities, genetic interactions, and dosage compensation.* Trends Genet, 2013. **29**(7): p. 385-93.

321. Brockdorff, N. and B.M. Turner, *Dosage compensation in mammals.* Cold Spring Harbor perspectives in biology, 2015. **7**(3): p. a019406.

322. Chen, J., et al., *WNT7B promotes bone formation in part through mTORC1.* PLoS Genet, 2014. **10**(1): p. e1004145.

323. Lai, L.P., et al., *Lkb1/Stk11 regulation of mTOR signaling controls the transition of chondrocyte fates and suppresses skeletal tumor formation.* Proc Natl Acad Sci U S A, 2013. **110**(48): p. 19450-5.

324. Yagi, K., et al., *Bone morphogenetic protein-2 enhances osterix gene expression in chondrocytes.* J Cell Biochem, 2003. **88**(6): p. 1077-83.

325. Chen, C., et al., *mTOR inhibition rescues osteopenia in mice with systemic sclerosis.* J Exp Med, 2015. **212**(1): p. 73-91.

326. Coffey, S.A. and L. Klein, *Comparison of long bones and vertebrae in growing male rats: rate of growth, mineralization, and uptake of 3H-tetracycline at the organ level.* Growth, development, and aging : GDA, 1988. **52**(3): p. 151-6.

327. Chen, J. and F. Long, *mTORC1 Signaling Promotes Osteoblast Differentiation from Preosteoblasts.* PLoS One, 2015. **10**(6): p. e0130627.

328. Kanis, J.A., et al., *Guidelines for diagnosis and management of osteoporosis. The European Foundation for Osteoporosis and Bone Disease.* Osteoporos Int, 1997. **7**(4): p. 390-406.

329. Bradley, J.P., et al., *Increased IGF-I and IGF-II mRNA and IGF-I peptide in fusing rat cranial sutures suggest evidence for a paracrine role of insulin-like growth factors in suture fusion.* Plastic and reconstructive surgery, 1999. **104**(1): p. 129-38.

330. Jacob, S., et al., *Expression of Indian Hedgehog, BMP-4 and Noggin in craniosynostosis induced by fetal constraint.* Annals of plastic surgery, 2007. **58**(2): p. 215-21.

331. Zheng, L., et al., *Runx3 negatively regulates Osterix expression in dental pulp cells.* Biochem J, 2007. **405**(1): p. 69-75.

332. Huang, B., et al., *mTORC1 Prevents Preosteoblast Differentiation through the Notch Signaling Pathway.* PLoS Genet, 2015. **11**(8): p. e1005426.

333. Bialek, P., et al., *A twist code determines the onset of osteoblast differentiation.* Dev Cell, 2004. **6**(3): p. 423-35.

334. Teixeira, C.C., et al., *Foxo1, a novel regulator of osteoblast differentiation and skeletogenesis.* J Biol Chem, 2010. **285**(40): p. 31055-65.

335. Fulzele, K., et al., *Disruption of the insulin-like growth factor type 1 receptor in osteoblasts enhances insulin signaling and action.* J Biol Chem, 2007. **282**(35): p. 25649-58.

336. Beamer, W.G., et al., *Spontaneous fracture (sfx): a mouse genetic model of defective peripubertal bone formation.* Bone, 2000. **27**(5): p. 619-26.

337. Tsuji, K., et al., *BMP2 activity, although dispensable for bone formation, is required for the initiation of fracture healing.* Nature genetics, 2006. **38**(12): p. 1424-9.

338. Ghosh-Choudhury, N., et al., *Requirement of BMP-2-induced phosphatidylinositol 3-kinase and Akt serine/threonine kinase in osteoblast differentiation and Smad-dependent BMP-2 gene transcription.* J Biol Chem, 2002. **277**(36): p. 33361-8.

339. Yeh, L.C., et al., *Rapamycin inhibits BMP-7-induced osteogenic and lipogenic marker expressions in fetal rat calvarial cells.* J Cell Biochem, 2013. **114**(8): p. 1760-71.

340. Ferron, M., et al., *Insulin signaling in osteoblasts integrates bone remodeling and energy metabolism.* Cell, 2010. **142**(2): p. 296-308.

341. Koyama, E., et al., *Conditional Kif3a ablation causes abnormal hedgehog signaling topography, growth plate dysfunction, and excessive bone and cartilage formation during mouse skeletogenesis.* Development, 2007. **134**(11): p. 2159-69.

342. Zhou, X., et al., *Multiple functions of Osterix are required for bone growth and homeostasis in postnatal mice.* Proc Natl Acad Sci U S A, 2010. **107**(29): p. 12919-24.

343. Kurki, P., K. Ogata, and E.M. Tan, *Monoclonal antibodies to proliferating cell nuclear antigen (PCNA)/cyclin as probes for proliferating cells by immunofluorescence microscopy and flow cytometry.* Journal of immunological methods, 1988. **109**(1): p. 49-59.

344. Liu, Y., et al., *Osterix-cre labeled progenitor cells contribute to the formation and maintenance of the bone marrow stroma.* PLoS One, 2013. **8**(8): p. e71318.

345. Chen, J., et al., *Osx-Cre targets multiple cell types besides osteoblast lineage in postnatal mice.* PLoS One, 2014. **9**(1): p. e85161.

346. Dacic, S., et al., *Col1a1-driven transgenic markers of osteoblast lineage progression.* J Bone Miner Res, 2001. **16**(7): p. 1228-36.

347. Hauschka, P.V. and F.H. Wians, Jr., *Osteocalcin-hydroxyapatite interaction in the extracellular organic matrix of bone.* The Anatomical Record, 1989. **224**(2): p. 180-8.

348. Thoreen, C.C., et al., *A unifying model for mTORC1-mediated regulation of mRNA translation.* Nature, 2012. **485**(7396): p. 109-13.

349. Corradetti, M.N., et al., *Regulation of the TSC pathway by LKB1: evidence of a molecular link between tuberous sclerosis complex and Peutz-Jeghers syndrome.* Genes Dev, 2004. **18**(13): p. 1533-8.

350. Maurin, A.C., et al., *Role of polyunsaturated fatty acids in the inhibitory effect of human adipocytes on osteoblastic proliferation.* Bone, 2002. **31**(1): p. 260-6.

351. Maurin, A.C., et al., *Influence of mature adipocytes on osteoblast proliferation in human primary cocultures.* Bone, 2000. **26**(5): p. 485-9.

352. Elbaz, A., et al., *Inhibition of fatty acid biosynthesis prevents adipocyte lipotoxicity on human osteoblasts in vitro.* J Cell Mol Med, 2010. **14**(4): p. 982-91.

353. Muruganandan, S., A.A. Roman, and C.J. Sinal, *Role of chemerin/CMKLR1 signaling in adipogenesis and osteoblastogenesis of bone marrow stem cells.* J Bone Miner Res, 2010. **25**(2): p. 222-34.

354. Berendsen, A.D. and B.R. Olsen, *Osteoblast-adipocyte lineage plasticity in tissue development, maintenance and pathology.* Cellular and molecular life sciences : CMLS, 2014. **71**(3): p. 493-7.

355. Clabaut, A., et al., *Human osteoblasts derived from mesenchymal stem cells express adipogenic markers upon coculture with bone marrow adipocytes.* Differentiation; research in biological diversity, 2010. **80**(1): p. 40-5.

356. Castilho, R.M., et al., *mTOR mediates Wnt-induced epidermal stem cell exhaustion and aging.* Cell Stem Cell, 2009. **5**(3): p. 279-89.

357. Chen, C., Y. Liu, and P. Zheng, *mTOR regulation and therapeutic rejuvenation of aging hematopoietic stem cells.* Sci Signal, 2009. **2**(98): p. ra75.

358. Gharibi, B., et al., *Inhibition of Akt/mTOR attenuates age-related changes in mesenchymal stem cells.* Stem Cells, 2014.

359. Xiang, X., et al., *mTOR and the differentiation of mesenchymal stem cells.* Acta Biochim Biophys Sin (Shanghai), 2011. **43**(7): p. 501-10.

360. Rosen, E.D., et al., *C/EBPalpha induces adipogenesis through PPARgamma: a unified pathway.* Genes Dev, 2002. **16**(1): p. 22-6.

361. Liu, D.M., et al., *Rictor/mTORC2 loss in osteoblasts impairs bone mass and strength.* Bone, 2016. **90**: p. 50-8.

362. Yan, B., et al., *mTORC1 regulates PTHrP to coordinate chondrocyte growth, proliferation and differentiation.* Nature communications, 2016. **7**: p. 11151.

363. Sillence, D.O., D.L. Rimoin, and D.M. Danks, *Clinical variability in osteogenesis imperfecta-variable expressivity or genetic heterogeneity.* Birth defects original article series, 1979. **15**(5B): p. 113-29.

364. Sillence, D.O., A. Senn, and D.M. Danks, *Genetic heterogeneity in osteogenesis imperfecta.* J Med Genet, 1979. **16**(2): p. 101-16.

365. Wang, S., et al., *Mesenchymal Stem Cells and Cell Therapy for Bone Repair.* Current molecular pharmacology, 2016. **9**(4): p. 289-299.

366. Munir, H. and H.M. McGettrick, *Mesenchymal Stem Cell Therapy for Autoimmune Disease: Risks and Rewards.* Stem Cells Dev, 2015. **24**(18): p. 2091-100.

367. Frisch, J., et al., *Current progress in stem cell-based gene therapy for articular cartilage repair.* Current stem cell research & therapy, 2015. **10**(2): p. 121-31.

368. Collett-Solberg, P.F. and M. Misra, *The role of recombinant human insulin-like growth factor-I in treating children with short stature.* J Clin Endocrinol Metab, 2008. **93**(1): p. 10-8.

369. Saran, U., M. Foti, and J.F. Dufour, *Cellular and molecular effects of the mTOR inhibitor everolimus.* Clinical science, 2015. **129**(10): p. 895-914.

370. Kotulska, K., et al., *Long-term effect of everolimus on epilepsy and growth in children under 3 years of age treated for subependymal giant cell astrocytoma associated with tuberous sclerosis complex.* European journal of paediatric

neurology : EJPN : official journal of the European Paediatric Neurology Society, 2013. **17**(5): p. 479-85.

371. Guan, Y., et al., *Mechanical activation of mammalian target of rapamycin pathway is required for cartilage development.* FASEB J, 2014. **28**(10): p. 4470-81.

372. Jilka, R.L. et al., *Dysapaoptosis of osteoblasts and osteocytes increases cancellous bone formation but exaggerates bone porosity with age*. *J Bone Miner Res*. 2014 January ; 29(1):

373. Toyosawa S., et al., *Dentin matrix protein 1 is predominantly expressed in chicken and rat osteocytes but not in osteoblasts*. J Bone Miner Res. 2001 Nov; **16**(11): p. 2017-26.

374. van Bezooijen, RL., et al., *Sclerostin is an osteocyte-expressed negative regulator of bone formation, but not a classical BMP antagonist.* J Exp Med. 2004. **199**(6): p. 805-14.

375. Nampei A, et al., *Matrix extracellular phosphoglycoprotein (MEPE) is highly expressed in osteocytes in human bone*. J Bone Miner Metab*, 2004,* **22**: p. 176–184

376. Joeng K.S. et al., *Osteocyte-specific WNT1 regulates osteoblast function during bone homeostasis.* J Clin Invest. 2017 Jun 30; **127**(7): p. 2678–2688.